A Computer Based Mathematical Method
for Predicting the Directional Response of
Trucks and Tractor-Trailers – Phase II
Technical Report
Michigan University, June, 1973

EDC Library Reference No. 1066

PB 221630
UM-HSRI-PF-73-1

A Computer Based Mathematical Method for Predicting the Directional Response of Trucks and Tractor-Trailers

PHASE II TECHNICAL REPORT

Motor Truck Braking and Handling Performance Study

by

James E. Bernard
Christopher B. Winkler
Paul S. Fancher

June 1, 1973

Highway Safety Research Institute / University of Michigan

TECHNICAL REPORT STANDARD TITLE PAGE

1. Report No. UM-HSRI-PF-73-1	2. Government Accession No.	3. Recipient's Catalog No. PB-221 630
4. Title and Subtitle A computer based mathematical method for predicting the directional response of trucks and tractor-trailers. Phase II technical report.		5. Report Date June 1, 1973
		6. Performing Organization Code
7. Author(s) James E. Bernard, Christopher B. Winkler, and Paul S. Fancher		8. Performing Organization Report No. UM-HSRI-PF-73-1
9. Performing Organization Name and Address Highway Safety Research Institute University of Michigan Huron Parkway & Baxter Road Ann Arbor, Michigan 48105		10. Work Unit No.
		11. Contract or Grant No.
12. Sponsoring Agency Name and Address Motor Vehicle Manufacturers Association, Inc. 320 New Center Building Detroit, Michigan 48202		13. Type of Report and Period Covered
		14. Sponsoring Agency Code

15. Supplementary Notes

16. Abstract

This report presents a detailed technical discussion of analytical and empirical work which has been completed to obtain a validated digital computer program for predicting the directional response of trucks and articulated vehicles.

17. Key Words TRUCKS TRACTOR-TRAILERS VEHICLE HANDLING VEHICLE BRAKING COMPUTER SIMULATION	18. Distribution Statement UNLIMITED

19. Security Classif. (of this report) UNCLASSIFIED	20. Security Classif. (of this page) UNCLASSIFIED	21. No. of Pages	22. Price

Form DOT F 1700.7 (8-69)

117

117

CONTENTS

CONTENTS (Continued)

CONTENTS (Continued)

FIGURES

Preceding page blank

FIGURES (Continued)

FIGURES (Continued)

TABLES

Preceding page blank

ACKNOWLEDGMENTS

The work described in this report was conducted at the Highway Safety Research Institute (HSRI) of The University of Michigan, under contract to the Motor Vehicle Manufacturers Association of the United States, Inc. (MVMA).

The authors wish to acknowledge that many individuals and organizations made significant contributions to the program, not only by supplying vehicles, but also by providing technical assistance. These include: Mr. P. Terrano, White Motors, Chairman of the Ad Hoc Advisory Panel of the MVMA Motor Truck Research Committee, and Panel members M. A. Bowen, Chrysler Corporation; J. W. Gurney, Ford Motor Company; E. Ottenhoff, Chrysler Corporation; T. E. Price, Diamond Reo Trucks; R. E. Rassmussen, General Motors Corporation; H. Western, G. M. Truck and Coach; and G. Whitcomb, International Harvester Company. Further technical assistance was provided by Mr. J. W. Marshall of Uniroyal and Mr. J. E. Getz of Fruehauf.

Vehicles were supplied for use in this program by White Motors, Diamond Reo Trucks, and the Fruehauf Corporation. Tires were supplied by Uniroyal.

Special credit is surely due to Mr. Jerome J. Boron, Manager, Motor Truck Technical Services Department of MVMA, for his patient and constant guidance in the administrative matters.

The extensive computer models were programmed by Ms. Linda Howe and Mr. Garrick Hu of HSRI. The test vehicles used in this study were prepared and initially outfitted under the direction of Mr. J. Boissonneault of HSRI.

Preceding page blank

1. INTRODUCTION

The puprose of this report is to present a detailed technical discussion of analytical and empirical work which has been completed to obtain a validated digital computer program for predicting the directional response of trucks and articulated vehicles.

The analytical work for this directional response program was preceded by the development of a computer based mathematical method for predicting the braking performance of trucks and tractor-trailers [1]. The new directional response program contains all of the brake, suspension, and tire modeling features which were included in the previous braking performance program. Thus it is now possible to use this new program to compute truck and tractor-trailer directional response during combined braking and turning maneuvers. A concise summary, encompassing all the features of both the braking performance and the directional response programs, is presented under separate cover [2].

The next section of this report contains (1) a description of the coordinate systems used to write the equations of motion and (2) a discussion of the equations for expressing (a) the displacements, velocities, and accelerations of pertinent points in the vehicle and (b) the angular orientations, velocities, and accelerations of the various sprung and unsprung masses which make up the vehicle.

Section 3 presents the mathematical models used to compute the forces and moments acting on the sprung and unsprung masses. Particular attention is paid to discussing (1) the lateral and longitudinal shear forces generated at tire-road interface, (2) the forces and moments coupled through the fifth wheel connection, (3) the gravitational force due to an inclined roadway, (4) the influence of the mechanics of the steering system, and (5) the influence of wind loading.

Section 4 contains a short technical summary of the size and other operational aspects of the digital computer simulation. The measurement of the vehicle parameters needed to operate the simulation is discussed in Section 5. Sections 6 and 7 contain comparisons between measured and computed truck and tractor-trailer maneuvers, including steady turns and braking in a turn. Measured and simulated results are given for a variety of loading and surface conditions, including empty and loaded vehicles on a dry surface and empty vehicles on a wet surface. The body of the report closes with a brief summary of the utility of this program.

A list of symbols is given in Appendix A. A detailed discussion of Euler angles is given in Appendix B, followed by the equations of motion in Appendix C. Details on the ordering of the input data are given in Appendix D followed by flow charts in Appendix E and the data used in the validation runs in Appendix F. An extensive list of measured tire data is given in Appendix G, and a short algorithm which may be used to compute tire parameters is given in Appendix H.

2.0 AXIS SYSTEMS AND KINEMATICS

2.1 INTRODUCTION

The vehicle to be simulated by the digital computer program may have up to thirty-two degrees of freedom, with calculations taking place in up to five coordinate systems. Section 2 gives an overview of the mathematical formulation, including some kinematic details necessary for the explanation of the various mathematical models. The coordinate systems and some explanation of the methods of computation of sprung mass and unsprung mass motion are given, but the details of the various suspension and steer models are left to Section 3 and Appendix C.

2.2 THE AXIS SYSTEMS

The large number of translational and rotational degrees of freedom required to represent a tractor-trailer precludes the use of only one coordinate system. In fact, the equations of motion may be most easily written if several systems are used. The purpose of this section is to identify the (1) orientation and purpose of the various axis systems, and (2) to identify the transformation variables used to relate the unit vectors in the various systems. The sets of axes to be described are the inertial axes, the body axes, and the unsprung mass axes. Most of the mathematical details will be found in Appendix B.

2.2.1 SYSTEM I. - THE INERTIAL AXES. Since Newton's laws are valid only for accelerations measured from an inertial reference, it is necessary to have one set of fixed axes. This set of axes, which shall be termed the [XN, YN, ZN] system, has its origin at the sprung mass center of the vehicle at time zero. The vehicle will always be assumed to start with the following orientation:

XN is out the front of the vehicle,

YN is out the right door,

ZN is vertically downward, normal to the plane of the road.

The set of unit vectors in the XN, YN, and ZN directions are defined as $\hat{x}n$, $\hat{y}n$, and $\hat{z}n$ respectively. The [XN, YN, ZN] system is, of course, fixed, and therefore the time derivatives of the unit vectors, $\hat{x}n$, $\hat{y}n$, and $\hat{z}n$ are identically zero. It should be noted that there is no requirement that $\hat{z}n$ be vertical (i.e., in the direction of gravitational forces). It will be shown in a subsequent section that non-vertical $\hat{z}n$ may be chosen to simulate an inclined roadway.

2.2.2 SYSTEM II. - THE BODY AXES. To facilitate the calculation of the location and velocity of points on the sprung mass, it is convenient to use a system of so-called body axes. This set of axes, which shall be termed the [XB, YB, ZB] system, is coincident with [XN, YN, ZN] at time zero, but remains fixed in the sprung mass. The transformation from this set of axes to the inertial set may be defined as

$$[\hat{x}n\ \hat{y}n\ \hat{z}n] = [\hat{x}b\ \hat{y}b\ \hat{z}b](a_{ij}) \tag{2-1a}$$

$$[\hat{x}b\ \hat{y}b\ \hat{z}b] = [\hat{x}n\ \hat{y}n\ \hat{z}n](a_{ji}) \tag{2-1b}$$

where the a_{ij} are functions of the roll angle, ϕ, the pitch angle, θ, and the yaw angle, ψ. These so-called Euler angles and the transformation equation (2-1), are considered in detail in Appendix B.

In the case of an articulated vehicle, there will be two sets of body axes; one for the tractor and one for the trailer. The trailer body axes, which shall be termed the [TXB, TYB, TZB] system, have unit vectors $t\hat{x}b$, $t\hat{y}b$, and $t\hat{z}b$ initially in the direction of $\hat{x}n$, $\hat{y}n$, and $\hat{z}n$, respectively. These axes remain fixed

Preceding page blank

in the trailer sprung mass. The transformation from this set of axes to the inertial set may be defined as:

$$[\hat{x}n, \hat{y}n, \hat{z}n] = [t\hat{x}b, t\hat{y}b, t\hat{z}b](ta_{ij}) \tag{2-2a}$$

$$[t\hat{x}b, t\hat{y}b, t\hat{z}b] = [\hat{x}n, \hat{y}n, \hat{z}n](ta_{ji}) \tag{2-2b}$$

2.2.3 SYSTEM III. - THE UNSPRUNG MASS AXES. To facilitate the calculation of shear forces at the tire/road interface, it is convenient to define one more set of axes. This set of axes, which shall be termed the [X1, Y1, Z1] system, has its origin at the road level on a line in the $\hat{z}n$ direction through the sprung mass center. It is required that

$$\hat{z}1 \equiv \hat{z}n \tag{2-3}$$

Since $\hat{z}1$ is normal to the road, $\hat{x}1$ and $\hat{y}1$ are in the plane of the road, and the origin of [X1, Y1, Z1] must translate with the component of the sprung mass velocity which is in the road plane.

This set of axes is constrained to yaw with the vehicle sprung mass. The transformation from this set of axes to the inertial set is

$$[\hat{x}1, \hat{y}1, \hat{z}1] = [\hat{x}n, \hat{y}n, \hat{z}n] \begin{pmatrix} \cos\psi & -\sin\psi & 0 \\ \sin\psi & \cos\psi & 0 \\ 0 & 0 & 1 \end{pmatrix} \tag{2-4a}$$

where ψ is the yaw angle. In addition, it may be shown that

$$[\hat{x}n, \hat{y}n, \hat{z}n] = [\hat{x}1, \hat{y}1, \hat{z}1] \begin{pmatrix} \cos\psi & \sin\psi & 0 \\ -\sin\psi & \cos\psi & 0 \\ 0 & 0 & 1 \end{pmatrix} \tag{2-4b}$$

The transformation between the unsprung mass axes and the body axes may be written

$$[\hat{x}1, \hat{y}1, \hat{z}1] = [\hat{x}b, \hat{y}b, \hat{z}b](b_{ij}) \tag{2-5a}$$

$$[\hat{x}b, \hat{y}b, \hat{z}b] = [\hat{x}1, \hat{y}1, \hat{z}1](b_{ji}) \tag{2-5b}$$

where

$$b_{ij} = a_{ij}\Big|_{\psi = 0} \tag{2-5c}$$

In the case of an articulated vehicle, there will be two sets of unsprung mass axes; one for the tractor and one for the trailer. The trailer unsprung mass system, which shall be termed the [TX1, TY1, TZ1] system, has its origin on the road level on a line in the $\hat{z}n$ direction through the trailer sprung mass center. It will be required that

$$t\hat{z}1 \equiv \hat{z}n \tag{2-6}$$

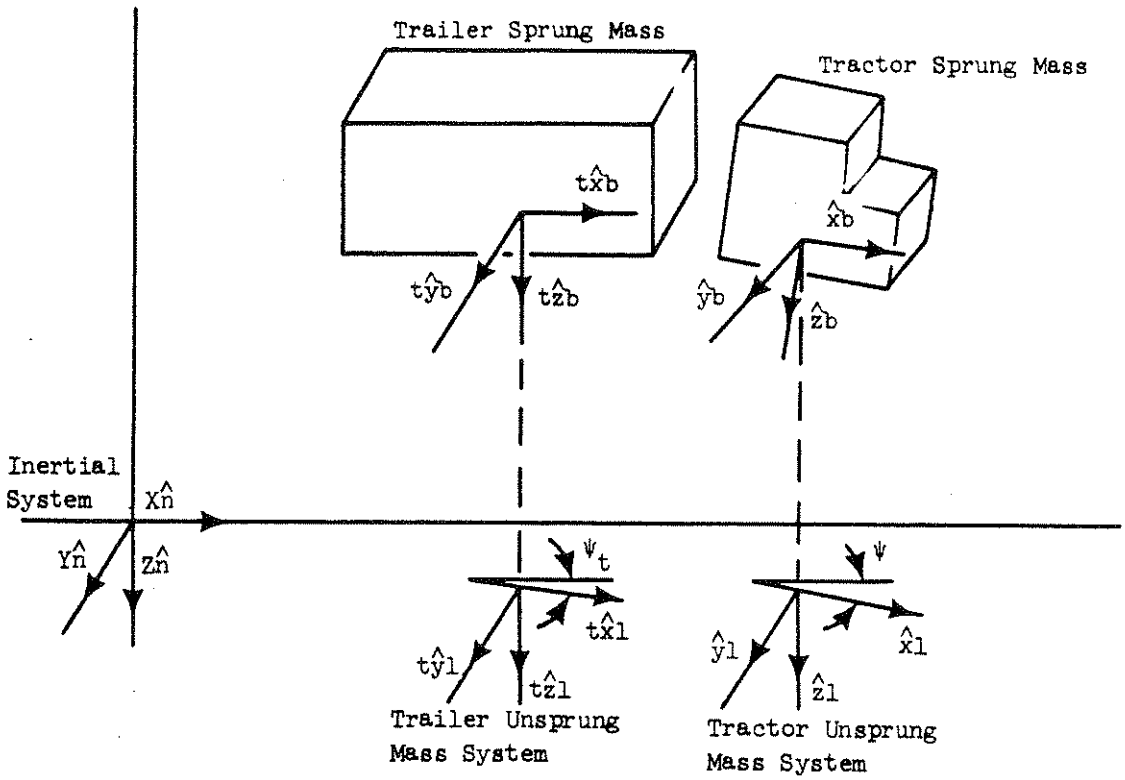

Figure 2-1. Schematic diagram of the articulated venicle

Thus, $t\hat{x}1$ and $t\hat{y}1$ are in the plane of the road, and the origin of [TX1, TY1, TZ1] must translate with the component of the sprung mass center velocity which is in the road plane.

This set of axes is constrained to yaw with the trailer sprung mass. The transformation from this set of axes to the inertial set is

$$[t\hat{x}1,\ t\hat{y}1,\ t\hat{z}1] = [\hat{x}n,\ \hat{y}n,\ \hat{z}n]\begin{pmatrix}\cos\psi t & -\sin\psi t & 0\\ \sin\psi t & \cos\psi t & 0\\ 0 & 0 & 1\end{pmatrix} \tag{2-7a}$$

where ψt is the trailer yaw angle. It may be shown that

$$[xn,\ yn,\ zn] = [tx1,\ ty1,\ tz1]\begin{pmatrix}\cos\psi t & \sin\psi t & 0\\ -\sin\psi t & \cos\psi t & 0\\ 0 & 0 & 1\end{pmatrix} \tag{2-7b}$$

It will be shown in Section 3 that there is no geometric constraint between tractor and trailer in the mathematical model; both the tractor and the trailer sprung mass are considered to have six independent degrees of freedom. Therefore, no transformation equation between the body axis systems has been written. A schematic diagram of an articulated vehicle in an arbitrary orientation is shown in Figure 2-1.

2.3 THE KINEMATICS OF THE SPRUNG MASS

This section will be concerned both with definitions of variables and with certain algebraic manipulations chosen to lay the groundwork for the equations of motion. Since no geometric constraint between tractor and trailer has been assumed in this model, all the kinematic arguments will be made for a unit vehicle sprung mass. Analogous arguments apply to the trailer in the case of an articulated vehicle.

The velocity of the sprung mass center can be written as

$$\overline{V} = u\,\hat{x}b + v\,\hat{y}b + w\,\hat{z}b \tag{2-8a}$$

where u is called the longitudinal velocity, v the lateral velocity, and w the vertical velocity of the sprung mass center. Use of Equation (2-1) in Equation (2-8a) allows the velocity to be expressed with respect to the inertial system, viz.

$$\overline{V} = (XNDOT)\hat{x}n + (YNDOT)\hat{y}n + (ZNDOT)\hat{z}n \tag{2-8b}$$

The components of $\overline{V}$ given in Equation (2-8b) can be integrated to obtain the inertial coordinate positions XN, YN, and ZN of the sprung mass center.

It becomes necessary to compute the position of other points on the sprung mass to find the suspension forces. This computation may be facilitated by considering a point p on the vehicle sprung mass. Assume a vector $\overline{\rho}$ from the mass center to the point p where

$$\overline{\rho} = XS\,\hat{x}b + YS\,\hat{y}b + ZS\,\hat{z}b \tag{2-9a}$$

In terms of inertial unit vectors, $\overline{\rho}$ may be written

$$\begin{aligned}\overline{\rho} = {} & (XS\,a_{11} + YS\,a_{21} + ZS\,a_{31})\hat{x}n \\ & + (XS\,a_{12} + YS\,a_{22} + ZS\,a_{32})\hat{y}n \\ & + (XS\,a_{13} + YS\,a_{23} + ZS\,a_{33})\hat{z}n\end{aligned} \tag{2-9b}$$

The distance of any sprung mass point below static equilibrium position of the sprung mass center is

$$h = ZN + (\overline{\rho} \cdot \hat{z}n) \tag{2-10}$$

Equation (2-10) will be used in the suspension model.

It is also necessary to calculate the velocity of the arbitrary sprung mass point. Since the vector to the point p from the origin of [XN, YN, ZN] is

$$\overline{P} = XN\,\hat{x}n + YN\,\hat{y}n + ZN\,\hat{z}n + \overline{\rho}, \tag{2-11}$$

the velocity is

$$\dot{\overline{P}} = (XNDOT)\hat{x}n + (YNDOT)\hat{y}n + (ZNDOT)\hat{z}n + \overline{\omega} \times \overline{\rho} \tag{2-12}$$

where the [XB, YB, ZB] system rotates with angular velocity, $\overline{\omega}$. Equation (2-12) may be written

$$\dot{\overline{P}} = u\,\hat{x}b + v\,\hat{y}b + w\,\hat{z}b + \overline{\omega} \times \overline{\rho} \tag{2-13}$$

where u, v, and w are the components of the velocity of the sprung mass center along the directions of the body axes. The angular rotation vector $\overline{\omega}$ may be defined as

$$\overline{\omega} = p\hat{x}b + q\hat{y}b + r\hat{z}b \tag{2-14}$$

where p, q, and r are the rotation rates in roll, pitch, and yaw, respectively. Using $\bar{\rho}$ from Equation (2-9a) we have

$$\bar{\omega} \times \bar{\rho} = (qZS - rYS)\hat{x}b + (rXS - pZS)\hat{y}b + (pYS - qXS)\hat{z}b \qquad (2\text{-}15)$$

Thus, in body axis notation, the velocity of the sprung mass point is

$$\dot{\bar{P}} = (u + qZS - rYS)\hat{x}b + (v + rXS - pZS)\hat{y}b + (w + pXS - qXS)\hat{z}b \qquad (2\text{-}16)$$

which may be rewritten

$$\dot{\bar{P}} = (uu)\hat{x}b + (vv)\hat{y}b + (ww)\hat{z}b \qquad (2\text{-}17)$$

Using Equation (2-1), the right-hand side of Equation (2-17) may be expressed in terms of fixed vectors.

$$\begin{aligned}\dot{\bar{P}} = {} & (uu\, a_{11} + vv\, a_{21} + ww\, a_{31})\hat{x}n \\ & + (uu\, a_{12} + vv\, a_{22} + ww\, a_{32})\hat{y}n \\ & + (uu\, a_{13} + vv\, a_{23} + ww\, a_{33})\hat{z}n\end{aligned} \qquad (2\text{-}18)$$

(The $\hat{z}n$ component of the right-hand side of Equation (2-18) will be useful in the calculation of the suspension velocity, a quantity needed for the coulomb friction model.)

At this stage, it is appropriate to define the acceleration of the sprung mass center. Differentiation of the sprung mass velocity vector given in Equation (2-8a) leads to

$$\dot{\bar{V}} = \dot{u}\hat{x}b + \dot{v}\hat{y}b + \dot{w}\hat{z}b + \bar{\omega} \times (u\hat{x}b + v\hat{y}b + w\hat{z}b) \qquad (2\text{-}19)$$

which after carrying out the cross product produces the following result:

$$\dot{\bar{V}} = (\dot{u} + qw - rv)\hat{x}b + (\dot{v} - pw + ru)\hat{y}b + (\dot{w} + pv - qu)\hat{z}b \qquad (2\text{-}20)$$

Application of Newton's law yields

$$M\dot{\bar{V}} = \bar{F} \qquad (2\text{-}21)$$

where M is the sprung mass and $\bar{F}$ is the total force applied to the sprung mass. It is convenient to set the scalar components of Equation (2-20) equal to the appropriate components of the external forces on the sprung mass in order to find $\dot{u}$, $\dot{v}$, and $\dot{w}$. (The velocity components, u, v, and w, are found by integrating $\dot{u}$, $\dot{v}$, and $\dot{w}$, respectively.)

Next, consider the rate of change of angular momentum of the sprung mass about the sprung mass center. This may be written

$$\begin{aligned}\dot{\bar{H}} = {} & \{I_{xx}\dot{p} + qr(I_{zz} - I_{yy}) - I_{xz}(\dot{r} + pq)\}\hat{x}b \\ & + \{I_{yy}q - pr(I_{xx} - I_{zz}) - I_{xz}(r^2 - p^2)\}\hat{y}b \\ & + \{I_{zz}r + pq(I_{yy} - I_{xx}) + I_{xz}(qr - p)\}\hat{z}b\end{aligned} \qquad (2\text{-}22)$$

where

I_{xx} is the roll moment of inertia

I_{yy} is the pitch moment of inertia

I_{zz} is the yaw moment of inertia

$I_{xz} = \int xz \, dm$

Lateral symmetry has been assumed (i.e., I_{xy} and I_{yz} are assumed to be zero).

The rate of change of angular momentum, $\dot{\overline{H}}$, is used in the equation

$$\overline{T} = \dot{\overline{H}} \tag{2-23}$$

where $\overline{T}$ is the total moment applied to the sprung mass. The scalar components of Equation (2-22) are set equal to the appropriate applied moments in order to find $\dot{p}$, $\dot{q}$, and $\dot{r}$. (The angular velocity components, p, q, and r are found by integrating $\dot{p}$, $\dot{q}$, and $\dot{r}$, respectively.)

These equations of the sprung mass, in scalar form, permit us to:

(1) Integrate the accelerations to obtain the angular and translational velocity components of the sprung mass.

(2) Perform the appropriate transformations to allow integration of the angular and translational velocity to find the angular and translational position of the sprung mass. (The details of the transformations required to integrate the angular velocity are given in Appendix B, whereas the transformations required to integrate translational velocity are given by a straightforward application of Equation (2-1).)

To evaluate the forces and moments appearing in Equations (2-21) and (2-23), it is required that the location and velocity of the axles be known. This topic is considered below.

2.4 KINEMATICS OF THE UNSPRUNG MASSES

In order to compute the reactions at the tire-road interface and the suspension forces, the locations and velocities of the axles relative to the sprung mass must be determined. Consideration of the articulated vehicle doubles the size of the problem but not the difficulty; for each calculation of the velocity and position of the axles on the tractor there is a directly analogous calculation for the trailer. Therefore, in this section, we shall consider only the kinematics of the unsprung masses associated with the truck or tractor. The equations applicable to the trailer axles are given in Appendix C.

Consider an arbitrary point, p', in the unsprung mass system. Assume a vector $\overline{\rho}$ from the origin of the unsprung mass system to the point p' where

$$\overline{\rho} = (XU)\hat{x}1 + (YU)\hat{y}1 + (ZU)\hat{z}1 \tag{2-24}$$

For all points on the unsprung mass, XU and YU are assumed fixed; ZU, however, is variable. A vector from the origin of the inertial system to p' may be written

$$\overline{PP} = \overline{R} + h\hat{z}1 + \overline{\rho} \tag{2-25}$$

where h is the perpendicular distance from the sprung mass center to the road and $\overline{R}$ is a vector from the origin of the inertial system to the sprung mass center. Thus, the velocity of the point p' (with respect to the inertial reference) is

$$\dot{\overline{PP}} = \overline{V} + \dot{h}\hat{z}1 + \left.\frac{d\overline{\rho}}{dt}\right|_{[X1\ Y1\ Z1]} + (\dot{\psi}\hat{z}1) \times (\overline{\rho}) \tag{2-26}$$

where

$\overline{V}$ is defined in Equation (2-8)

$\dot{h}$ is the negative of the $\hat{z}1$ component of $\overline{V}$ (Note: $\hat{z}1 \equiv \hat{z}n$)

$\dot{\psi}$ is the rate of rotation of the unsprung mass axis system [X1, Y1, Z1].

Equation (2-26) may be expanded into a more useful form. First, the sprung mass velocity $\overline{V}$ may be written in terms of the unit vectors $\hat{x}1$, $\hat{y}1$, and $\hat{z}1$.

$$\overline{V} = U1\hat{x}1 + V1\hat{y}1 + W1\hat{z}1 \tag{2-27}$$

Expansion of the cross product in Equation (2-26) yields

$$\dot{\psi}\hat{z}1 \times \overline{\rho} = \dot{\psi}(-YU\hat{x}1 + XU\hat{y}1) \tag{2-28}$$

Substitution of Equations (2-27) and (2-28) into (2-26) leads to the following result:

$$\dot{\overline{PP}} = (U1 - \dot{\psi}YU)\hat{x}1 + (V1 + \dot{\psi}XU)\hat{y}1 + \left.\frac{d\overline{\rho}}{dt}\right|_{[X1,\ Y1,\ Z1]} \tag{2-29}$$

Since XU and YU have been assumed to be constant, $\left.\frac{d\overline{\rho}}{dt}\right|_{[X1,\ Y1,\ Z1]}$ may only be in the $\hat{z}1$ direction.

$$\left.\frac{d\overline{\rho}}{dt}\right|_{[X1,\ Y1,\ Z1]} = Z\dot{U}\ \hat{z}1 \tag{2-30}$$

The above assumption may be restated in the following way: The track and wheelbase, when viewed from the $\hat{z}1$ direction, remain constant. This may be expected to be very accurate in the presence of the magnitude roll and pitch angles encountered in even very severe maneuvers of trucks and tractor-semitrailers.

In order to compute the forces of constraint between the unsprung masses and the sprung mass, it is necessary to express the acceleration of the unsprung mass point. Differentiation of Equation (2-26) leads to

$$\ddot{\overline{PP}} = \dot{\overline{V}} + (\ddot{h} + Z\ddot{U})\hat{z}1 + \ddot{\psi}\hat{z}1 \times \overline{\rho} + \dot{\psi}\hat{z}1 \times \frac{d\overline{\rho}}{dt} \tag{2-31}$$

Noting that

$$\frac{d\overline{\rho}}{dt} = Z\dot{U}\hat{z}1 + \dot{\psi}\hat{z}1 \times \overline{\rho} \tag{2-32}$$

and that $\dot{\overline{V}}$, which was given in Equation (2-20), may be rewritten

$$\dot{\overline{V}} = UD1\ \hat{x}1 + VD1\ \hat{y}1 + WD1\ \hat{z}1 \tag{2-33}$$

where

$$WD1 = -\ddot{h}, \tag{2-34}$$

a more useful form of Equation (2-31) is obtained, viz.,

$$\ddot{\overline{PP}} = [UD1 - (XU)\dot{\psi}^2 + (XU)\ddot{\psi}]\hat{x}1 + [VD1 - (YU)\dot{\psi}^2 + (XU)\ddot{\psi}]\hat{y}1 + \ddot{Z}U\hat{z}1 \qquad (2\text{-}35)$$

Equation (2-35) is used in calculating the forces of constraint between the sprung and unsprung masses.

2.5 SUMMARY

Since it is quite tedious just to keep track of the various reference systems, all of the reference systems are listed in Table 2-1.

TABLE 2-1
Reference Systems

Name	Notation	Rotation Vector	Use
Inertial	XN, YN, ZN	0	Location of the vehicle. Observation point for accelerations and velocities
Body, Tractor or Straight Truck	XB, YB, ZB	$p\hat{x}b + q\hat{y}b + r\hat{z}b$	Convenient for calculation of rotational equations of sprung mass
Semitrailer	TXB, TYB, TZB	$pt\cdot\hat{xt}b + qt\cdot\hat{yt}b + rt\cdot\hat{zt}b$	
Unsprung Mass Tractor or Straight Truck	X1, Y1, Z1	$\dot{\psi}\hat{z}1$	Convenient for calculation of shear forces at the tire/road interface
Semitrailer	TX1, TY1, TZ1	$\dot{\psi}t \cdot \hat{zt}1$	

The transformation equations, which are given briefly in Equation (2-1) and in detail in Appendix B, are used in the representation of the forces, moments, and velocities in the various coordinate systems. The equations of motion yielding the components of the translational acceleration and the components of the rate of change of angular momentum are derived from Equations (2-21) and (2-23), respectively. Equation (2-33) is used to compute the translational acceleration of the unsprung masses; these accelerations are used to calculate the constraint forces between the sprung and unsprung masses. It is assumed that the unsprung masses must yaw with the sprung mass, but they can roll as determined by the forces and moments applied to them.

Various other equations have been given for the positions and velocities of various points on the sprung or unsprung masses. These equations will be referred to below when discussing and explaining the various suspension models and the model used to represent the pneumatic tires.

3.0 THE MATHEMATICAL MODELS

3.1 INTRODUCTION

The simulation consists of a large number of interconnected algorithms, each one made up of equations derived to model some aspect of the motion of the vehicle. The purpose of this section is to list the pertinent assumptions and demonstrate the analytical basis for these models.

The tire model is discussed first, since the forces at the tire-road interface are a necessary part of the explanations of the other models. This discussion is divided into several sections dealing respectively with the forces generated at the tire-road interface, complications arising in the wheel rotational equations and in simulating low vehicle speeds, and the special effects of dual tires.

Next, the equations of motion of a single axle suspension are considered in considerable detail. The analysis of the tandem axle suspensions is then shown to follow from the single axle analysis and work detailed previously in Reference 1. The suspension analysis is followed by an explanation of the model of the steering system, including deflection steer and compliance steer, and an analysis of the constraint between tractor and semitrailer of an articulated vehicle. The last two parts of this section concern the equations of motion of the vehicle on an inclined roadway, and an explanation of the use of the program to simulate wind loading.

3.2 THE TIRE MODEL

3.2.1 NORMAL FORCES AT THE TIRE-ROAD INTERFACE. The normal force at the tire-road interface is assumed to be the sum of the static normal load on the tire plus (1) the product of the change in distance between the wheel center and the road and the tire spring rate, KT, and (2) the product of the vertical velocity of the wheel center and the tire dissipation constant, CT. In all cases, the normal force is in the $\hat{z}1$ direction, i.e., perpendicular to the road. As was pointed out in Section 2, the $\hat{z}1$ direction need not be aligned with the direction of the gravitational force. The unit vector is, however, a constant.

It should be noted that it is not assumed that the road surface is smooth. A road profile description, in functional or coordinate form, may be introduced into the programs. However, the direction of the normal force at the tire-road interface is assumed to be constant, thus the fore-aft or lateral forces that might be expected due only to the particular shape of road undulations will not be predicted by this model.

3.2.2 SHEAR FORCES AT THE TIRE-ROAD INTERFACE. The velocity of any wheel center (see Equation (2-29)), is repeated here for convenience.

$$\dot{\overline{PP}} = (U1 - \dot{\psi}YU)\hat{x}1 + (V1 + \dot{\psi}XU)\hat{y}1 + \dot{Z}U\hat{z}1 \qquad (3\text{-}1)$$

where

U1 is the velocity of the sprung mass center in the $\hat{x}1$ direction

$\dot{\psi}$ rate of change of vehicle yaw angle

YU is the half track

XU is the distance in the $\hat{x}1$ direction from the sprung mass center to the wheel center.

The velocity of the wheel center in the plane of the road is precisely the first two terms of Equation (3-1). Thus, the velocity components, ui and vi of the wheel center in the $\hat{x}1$ and $\hat{y}1$ directions, respectively, are:

$$ui = U1 - \dot{\psi} YU \tag{3-2a}$$

$$vi = V1 + \dot{\psi} XU \tag{3-2b}$$

It is also necessary to determine uw, the longitudinal velocity component in the wheel plane:

$$uw = ui \cdot \cos\delta + vi \cdot \sin\delta \tag{3-3}$$

where δ is the steer angle. Finally, the tire sideslip angle α is given by (see Figure 3-1)

$$\alpha = \tan^{-1} \frac{vi}{ui} - \delta \tag{3-4}$$

The components of the tire forces in the horizontal plane are computed with the aid of a comprehensive tire model developed in a previous HSRI study [3]. The longitudinal and lateral force components in the tire axis system (see Figure 3-2) are given by

$$FXW = -\frac{C_s(S)}{1-S} f(\lambda) \tag{3-5}$$

$$FYW = -\frac{C_\alpha \tan\alpha}{1-S} f(\lambda) \tag{3-6}$$

where

$$\lambda = (1/2)\mu\, Fx\, (1-S)\, [(C_s S)^2 + (C_\alpha \tan\alpha)^2]^{-1/2} \tag{3-7a}$$

$$f(\lambda) = (2 - \lambda)\lambda \text{ for } \lambda < 1 \tag{3-7b}$$

$$f(\lambda) = 1, \text{ for } \lambda \geqq 1 \tag{3-7c}$$

The above representation of the tire involves two* empirical complicance parameters: (1) the longitudinal stiffness, C_s, defined as the absolute value of the slope of the curve of longitudinal force versus longitudinal slip, S, evaluated at S = 0, with the sideslip angle α, equal to zero; and (2) the lateral stiffness C_α, defined as the absolute value of the rate of change of lateral force with respect to sideslip angle, evaluated at $\alpha = 0$ with S = 0. It can be shown (see Reference 3) that the non-dimensional variable λ represents the longitudinal coordinate (in the tire axis system) of the point on the tire carcass associated with the inception of sliding in the contact patch.

The tire sideslip angle, α, is a kinematic variable defined as indicated in Figure 3-2. The longitudinal slip ratio, S, is defined as

$$S = 1 - \frac{RR \cdot \Omega}{u_w} \tag{3-8}$$

*In the model given in Reference 3, camber was an important consideration. Thus there was an additional empirical parameter related to camber. Since the present work assumes suspensions with solid axles, camber effects have been neglected.

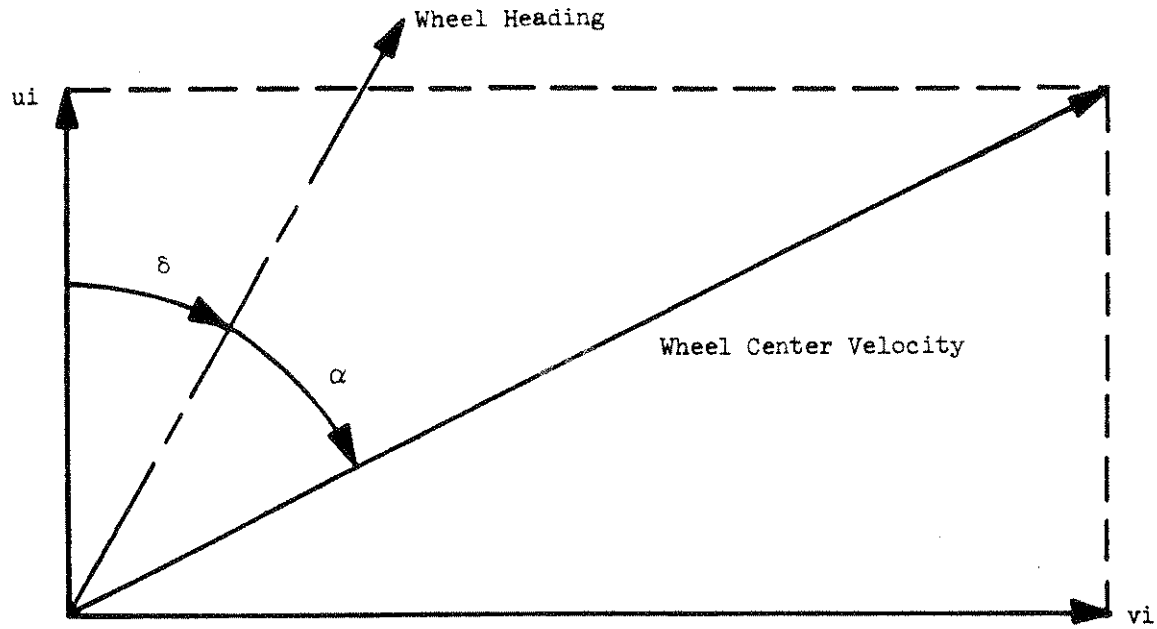

Figure 3-1. Tire-road interface kinematics

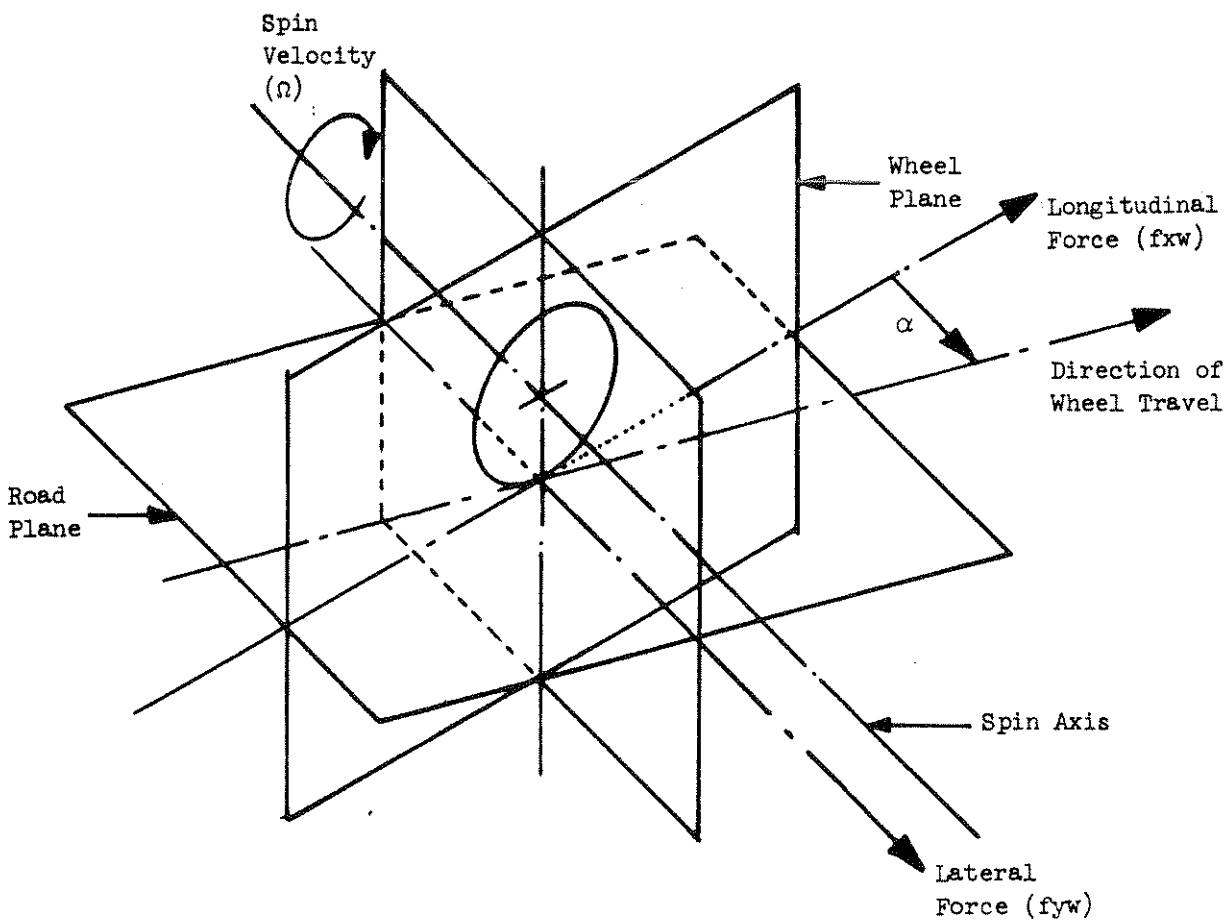

Figure 3-2. Longitudinal and lateral force components in the tire axis system

where Ω is the wheel spin velocity (see Figure 3-2), and RR is the effective rolling radius of the tire.

The coefficient of tire-road friction, μ, is computed from

$$\mu = \mu_o(1 - FA \cdot V_s) \tag{3-9}$$

where V_s, the effective sliding velocity, is given by

$$V_s = u_w[S^2 + (\tan \alpha)^2]^{1/2} \tag{3-10}$$

and μ_o and FA are characterizing parameters that must be evaluated empirically for a specific tire-pavement combination.

There is obviously significant interaction between longitudinal and lateral shear forces at the tire-road interface. This interaction is, of course, dependent on the empirical parameters C_α, C_s, μ_o, and FA. The parameters C_α and C_s have been determined for a wide variety of truck tires and load conditions and listed in Appendix G. Since very little experimental data exists from which FA and μ_o can be determined, it is presently necessary to use full-scale vehicle test results to estimate reasonable values. This procedure is explained further in Section 6.4, in which the method of choosing μ_o for the calculations performed to validate the overall model is discussed. (It should be noted that HSRI is currently designing a test device to alleviate this problem.)

Although the details of the tire model have been left to Reference 3, it is appropriate to discuss the application of this model and to outline, in detail, the methods used to model a tire and to perform simulations of the tire-vehicle system. In addition, some sample results from the tire model demonstrating the interaction between longitudinal and lateral force characteristics will be shown.

Consider the tire data given in Table 3-1 and shown in carpet plot form on Figure 3-3a. These data were obtained on the HSRI flat bed tire test device for a new 10 x 20F truck tire inflated to 85 psi. (This type of tire was used in the validation testing on the front axle of the tractor and on the tandem axles of the straight truck and the semitrailer.)

TABLE 3-1
Lateral Force vs. Steer Angle and Vertical Load

Tire: 10 x 20/F (new)
Rim: 20 x 7.5
Inflation Pressure: 85 psi

Vertical Load (lb)	Lateral Force (lb) at Indicated Steer Angle (deg)					
	1	2	4	8	12	16
1400	214	399	688	971	1050	1115
2800	364	693	1227	1829	2052	2213
4200	467	897	1612	2490	2881	3187
5430	523	1009	1830	2917	3458	3994
6700	550	1066	1962	3237	3994	4605
8100	558	1086	2044	3446	4328	5181
9200	557	1097	2044	3517	4459	--

*See Reference 4 for details of the test equipment.

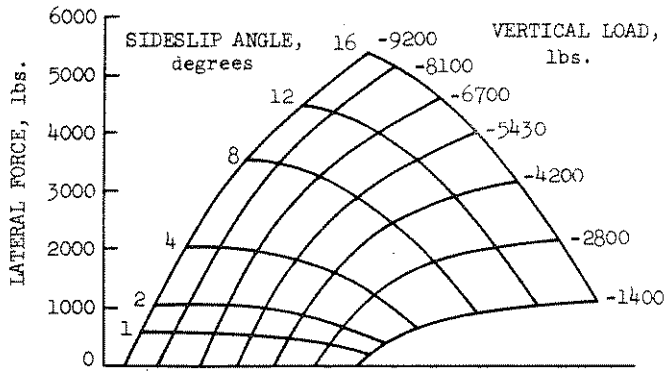

Figure 3-3a. Lateral force vs. sideslip angle at various vertical loads for a new 10 x 20 F tire at 85 psi

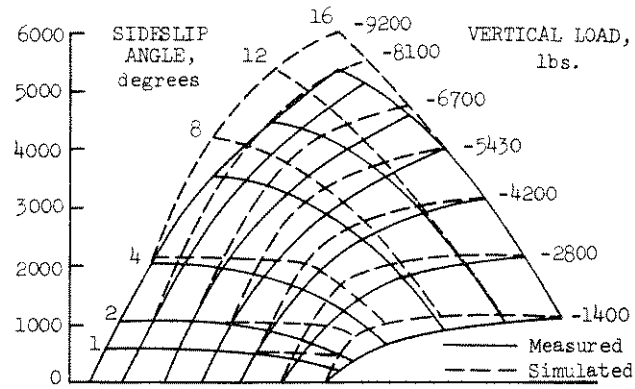

Figure 3-3b. Lateral force vs. sideslip angle. FA = 0, μ_o = .85, FA = 0, C_α = 523 pounds/degree

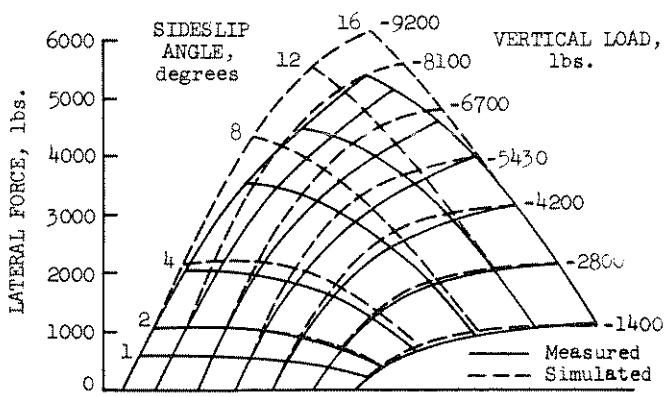

Figure 3-3c. Lateral force vs. sideslip angle. FA = 0, μ_o = .85, C_α from Table 3-2

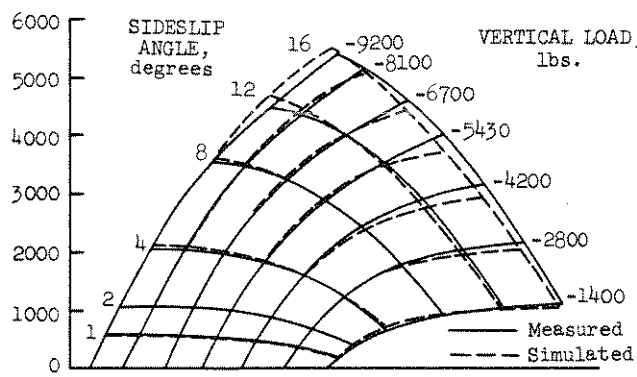

Figure 3-3d. Lateral force vs. sideslip angle. FA = 0, μ_o = .85, C_α from Table 3-2, KF = 1.2, $\bar{\alpha}$ = 9

In order to use the tire properties, as measured on the flat bed test device, in the simulation, it is necessary to match these data using the tire model. Since the speed effects on friction may be considered negligible in the flat bed test, the speed sensitivity parameter, FA, should be set to zero. Under this condition, the simulated carpet plot must approach $\mu_o \cdot F_z$ for large sideslip angles, thus an approximate value of μ_o may be determined from the sideforce data obtained at a vertical load of 1400 pounds. An estimate of 1190 pounds as the maximum F_y at 1400 pounds normal load leads to

$$\mu_o = \frac{1190}{1400} \cong .85 \tag{3-11}$$

The value of cornering stiffness may be chosen from any segment of the data. If the rated load of 5430 were considered to be the most important range of the data, the obvious choice for C_α is

$$C_\alpha = 523 \text{ lbs/degree} \tag{3-12}$$

This choice will result in the simulated values shown in the carpet plot of Figure 3-3b. Note that a fixed value of cornering stiffness only fits the tire data at small sideslip angles and large values of vertical load. Consequently, to simulate accurately a more widely varying load, the cornering stiffness, C_α, may be made a function of the normal load on the tire. When a -1 is entered in the usual C_α position in the input data, a table lookup of C_α vs. normal load will be read. (Programming details are in Appendix E.) For the example under consideration, the appropriate user-entered values are shown in Table 3-2. The simulation will then produce the data shown in carpet plot form in Figure 3-3c. Note that the results are quite acceptable for low slip angle at all loads, but that significant differences between the simulation and the empirical results are apparent for large slip angle and high loads. These differences are not unexpected since the tire model being employed in this simulation was not derived from curve fitting methods but was analytically derived based on the mechanics perceived at the tire-road interface. Thus the model, like all other mathematical analyses of real-world situations, entails certain assumptions. In this case, the validity of the assumptions is at least in part a function of sideslip angle and normal load. However, the tire model with variable C_α should be quite adequate for many users of the simulation if they are not concerned with maneuvers that involve large sideslip angles.

TABLE 3-2
Appropriate C_α Values for the 10 x 20F Tire

Normal Load	C_α
1400	214
2800	364
4200	467
5430	523
6700	550
8100	558
9200	557

To obtain a much more accurate fit of the tire data, curve fitting techniques have been combined with the analytical model. Specifically, the uses of the

simulations may specify as input, along with the table lookup of C_α vs. normal load, two more parameters, KF and $\bar{\alpha}$, such that

$$C'_\alpha = C_\alpha\left(1 - \frac{KF}{57.3} \cdot |\alpha|\right) \quad |\alpha| < \bar{\alpha} \tag{3-13a}$$

$$C'_\alpha = C_\alpha\left(1 - \frac{KF}{57.3} \cdot \bar{\alpha}\right) \quad |\alpha| \geq \bar{\alpha} \tag{3-13b}$$

where C'_α will be the value of cornering stiffness used in tire Equations (3-6) and (3-7). The values of KF and $\bar{\alpha}$ may easily be determined to match the simulation more closely to the measured data. (An algorithm to aid in the choice of KF and $\bar{\alpha}$ is presented in Appendix H.) For example, the values

$$KF = 1.7 \tag{3-14a}$$

$$\bar{\alpha} = 9 \tag{3-14b}$$

produce the simulated curves presented in Figure 3-3d. The values of C_α tabulated in Table 3-2 and the values of KF and $\bar{\alpha}$ given in Equation (3-14) were used for this tire in making the dry surface validation runs.

The selection of values μ_o and FA for use in the simulation runs must still be chosen. This selection will scale up or down the high slip angle portion of the simulated carpet plots with the low slip angle portion remaining unaffected. As an example, consider a carpet plot derived from values of C_α, KF and $\bar{\alpha}$, as given above, but with $\mu_o = .65$. These parameters produce the carpet plot representing the 10 x 20F tire on a wet surface and is shown in Figure 3-4, superimposed on the dry surface plot given in Figure 3-4.

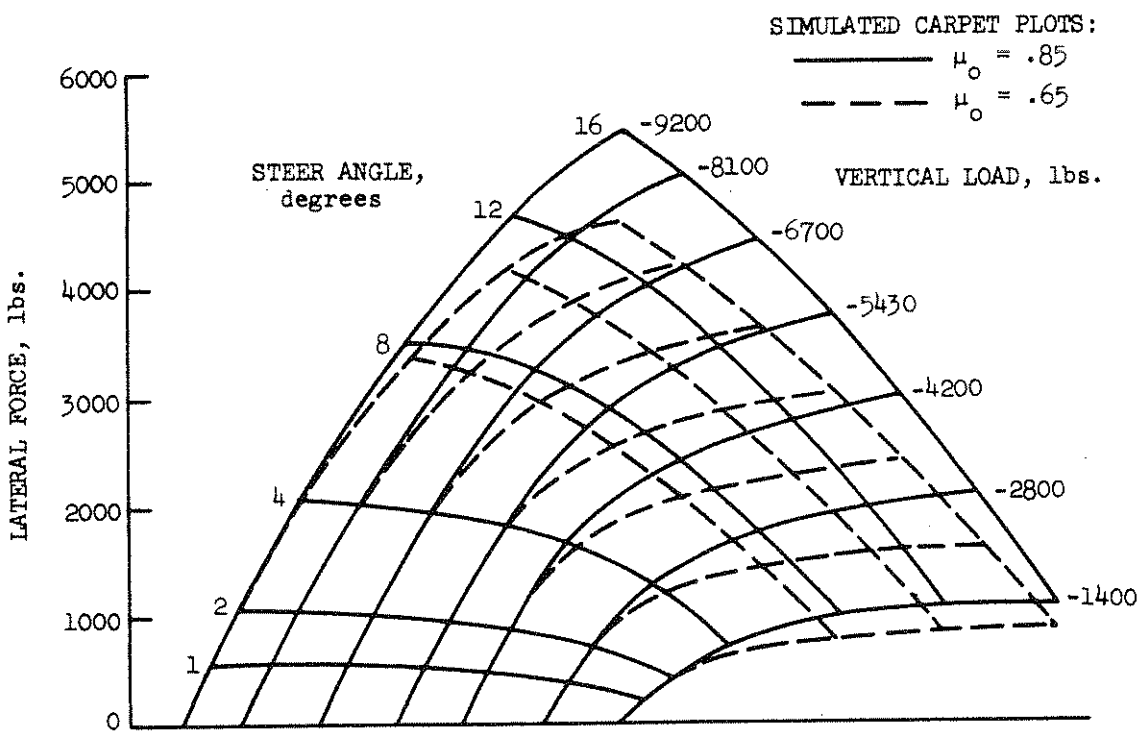

Figure 3-4. Lateral force vs. sideslip angle. FA = 0, C_α from Table 3-2, KF = 1.2, $\bar{\alpha}$ = 9

To complete the list of parameters needed to use the tire model, a value for C_S must be entered. To account for the variation of C_S with normal load, a -1 may be entered in the C_S position in the input data, allowing table lookup of C_S vs. normal load. (Programming details are in Appendix E.)

Figures 3-5a and b present typical results produced by the tire model showing the nonlinear interaction of the sideslip angle, α, and the longitudinal slip, S. In Figure 3-5a, cornering force vs. sideslip angle is plotted for various longitudinal slip values; in Figure 3-5b, brake force vs. longitudinal slip is plotted for various sideslip angles. The tire parameters used to produce these figures are those used to simulate the 10 x 20F truck tire on the dry surface at 5430 lbs. vertical load.

3.2.3 ALIGNING TORQUE. In Table 3-3, values of aligning torque for the 10 x 20F tire are given for various loads and slip angles. The method for entering the aligning torque data and some comments on the use of the aligning torque algorithm are given below.

TABLE 3-3
Aligning Torque vs. Steer Angle and Vertical Load

Tire: 10 x 20/F (new)
Rim: 20 x 7.5
Inflation Pressure: 85 psi

Vertical Load (lb)	Aligning Torque (lb-ft) at Indicated Steer Angle (deg)					
	1	2	4	8	12	16
1400	18	30	36	20	7	4
2800	47	80	108	81	47	24
4200	77	136	194	170	115	67
5430	101	182	274	263	193	132
6700	126	229	358	372	313	205
8100	153	281	458	504	439	318
9200	173	323	533	618	561	--

Preceding the steer tables, aligning torque data will be read. (Programming details are in Appendix E.) The user must enter this data in the following way—first a normal load, then the aligning torque vs. slip angle data corresponding to that load. The following important details should be noted:

(1) If the normal load on the tire is below the lowest normal load entered in the data, the aligning torque on that tire will be set to zero.

(2) If the normal load on the tire is above the highest normal load entered in the data, the aligning torque on that tire will be set to the aligning torque corresponding to the highest normal load entered in the data.

(3) The simulation calculates the aligning torque in a manner which is <u>independent</u> of the surface. Thus the user should consider the differences between the surface presented to the tire by the test device surface and the surface to be simulated when entering the aligning torque data. (Note that in the choice of the parameters used to model the lateral forces, the user can usually end up with a sensible interpretation of empirical data by a proper choice of μ_o. It might be argued that the aligning torque should be modified by the ratio of μ_o characterizing the simulated surface to μ_o characterizing the tire test device. This

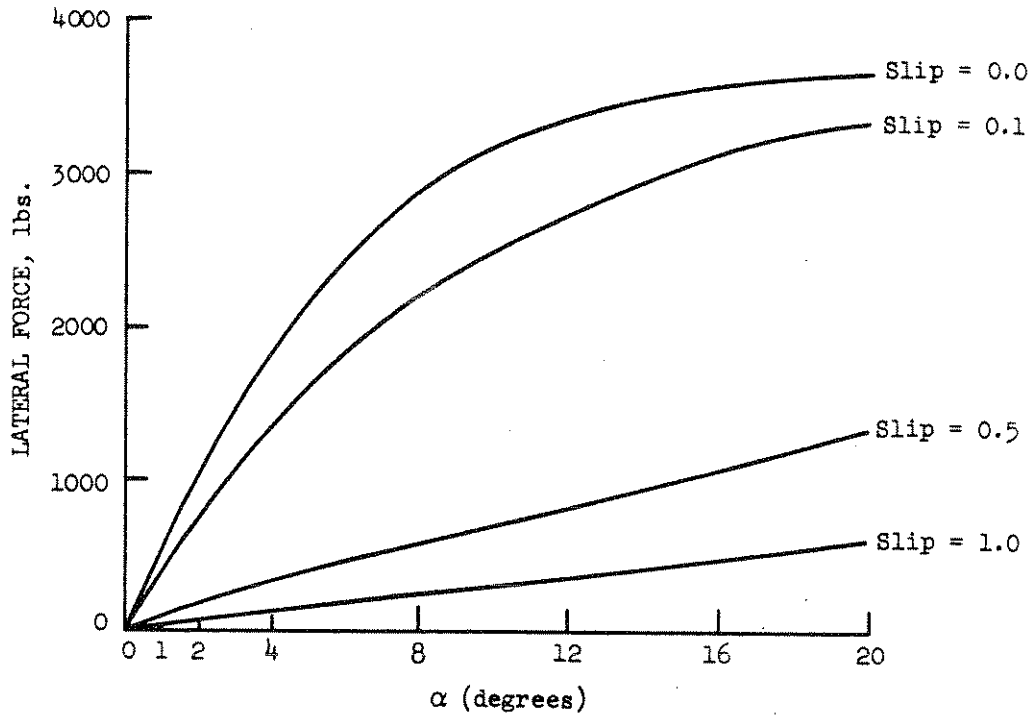

Figure 3-5a. Cornering force vs. sideslip angle for various longitudinal slip values

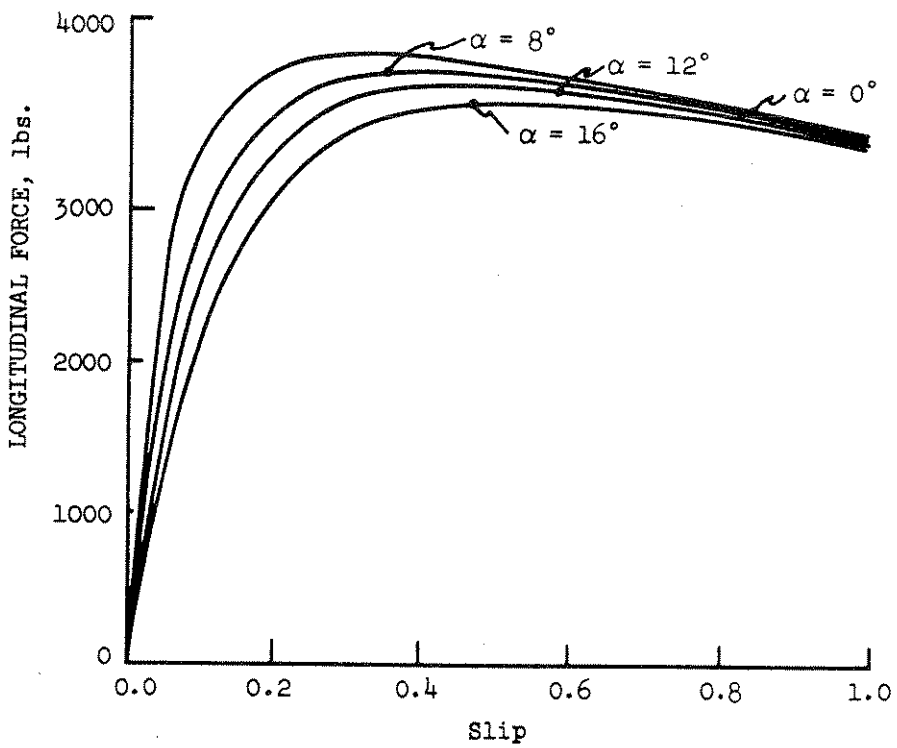

Figure 3-5b. Brake force vs. longitudinal slip for various sideslip angles

approach may easily be added if it is desired by the user; however, any manipulation of the aligning torque data must be considered very speculative.

The aligning torque data used in the validation runs for the 10 x 20F tire on the dry surface is given in Table 3-4.

TABLE 3-4
Data Used for Aligning Torque Simulation

Tire: 10 x 20F
Rim: 20 x 7.5
Inflation Pressure: 85 psi

Vertical Load (lb)	Aligning Torque (lb-ft) at Indicated Steer Angle (deg)					
	1	2	4	8	12	16
2800	--	80	108	81	--	24
5430	--	182	274	263	--	132
9200	--	323	533	618	561	--

3.2.4 WHEEL ROTATIONAL DYNAMICS. As was pointed out in [5], there is sufficient reason to include the wheel rotational degree of freedom in a straight line braking simulation; namely, the control devices presently used in antiskid devices require explicit or implicit information about the rotation of the wheels. Furthermore, in developing a simulation of braking and handling maneuvers, one finds that wheel rotation rate must be calculated if the interaction between longitudinal slip and sideslip is to be taken with account.

Figure 3-6 is a free body diagram of a rotating wheel. The equation of rotational motion is

$$JS(\dot{\Omega}) = -TT - FXW \cdot RR \tag{3-15}$$

where

FXW is the longitudinal force at the tire/road interface

JS is the polar moment of inertia

RR is the effective tire radius

TT is the applied brake torque

$\dot{\Omega}$ is the wheel angular acceleration

Since longitudinal slip S is defined as

$$S = 1 - \frac{RR \cdot \Omega}{uw} \tag{3-16}$$

Equation (3-15) can be written as

$$\frac{dS}{dt} = \frac{-RR}{uw \cdot JS}[-TT - FXW \cdot RR] + \frac{XDD(1-S)}{uw} \tag{3-17}$$

where

N is the normal force at the tire-road interface

uw is the longitudinal velocity of the wheel center

XDD is longitudinal acceleration of the wheel center

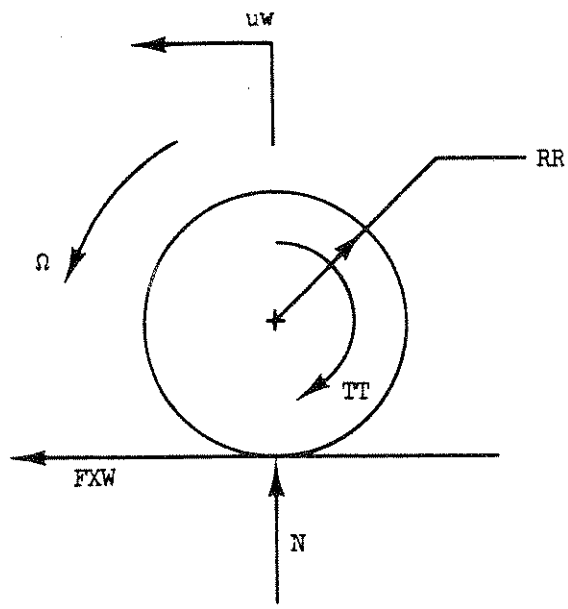

Figure 3-6. Free body diagram: wheel with braking

The assumption may be made that, for a short time lapse Δt, (in this case, the integration time step of .0025 sec), all variables with the exception of FXW on the right side of Equation (3-17) may be approximated by a constant value. Furthermore, it may be assumed that during the time interval Δt, FXW is a linear function of S only. The other variables affecting FXW, such as load, velocity and slip angle, are held constant during Δt. This leads to a particularly convenient and economical formulation which allows calculation of S rather than integration of Equation (3-15). Details may be found in [1] or [5].

3.2.5 THE LOW SPEED APPROXIMATIONS. The calculation of the tire sideslip angle, α, given in Equation (3-4), depends on the ratio $\frac{vi}{ui}$. For small ui, small errors in ui produce large errors in sideslip angle, resulting in inaccurate calculations of lateral force. Rather than shorten the integration time step Δt to preserve necessary accuracy in ui, the shear forces at the tire-road interface are assumed to remain constant when ui becomes small. Since any ui cannot be greatly different from the longitudinal speed of the sprung mass center, U1, the following procedure is used. (See Equation (3-2a). Note $|\dot{\psi}|$ may be expected to be significantly less than 1, $|YU|$ is normally about 3 ft.) If U1 falls below 5 ft/sec, all the FXW and FYW values will be assumed to remain "frozen" to the value calculated at the last time when U1 was greater than 5 ft/sec. Normally this phenomenon will only be seen in a maneuver in which the vehicle is braked to a stop, as in a violent spin.

3.2.6 THE EFFECTS OF DUAL TIRES. Since the cornering stiffness C_α and the longitudinal stiffness C_s are functions of the normal load, the assumption that

the dual tires may be modeled as one tire at the sum of the normal loads on the duals may not be appropriate. Thus, in the following analysis, the dual tires are considered separately.

Consider the axle in Figure 3-7, which has static position ZA = 0 and $\phi A = 0$. The normal loads are:

$$N(1,1) = N(1,1)\text{Static} + KT(ZA - (TRA+DT)\phi A) + CT(\dot{Z}A - (TRA+DT)\dot{\phi}A) \quad (3\text{-}18a)$$

$$N(1,2) = N(1,2)\text{Static} + KT(ZA - (TRA-DT)\phi A) + CT(\dot{Z}A - (TRA-DT)\dot{\phi}A) \quad (3\text{-}18b)$$

$$N(2,1) = N(2,1)\text{Static} + KT(ZA - (TRA-DT)\phi A) + CT(\dot{Z}A - (TRA-DT)\dot{\phi}A) \quad (3\text{-}18c)$$

$$N(2,2) = N(2,2)\text{Static} + KT(ZA + (TRA+DT)\phi A) + CT(\dot{Z}A + (TRA+DT)\dot{\phi}A) \quad (3\text{-}18d)$$

where

TRA measures from the axle center to the mid point between the duals

DT is half the distance between the duals

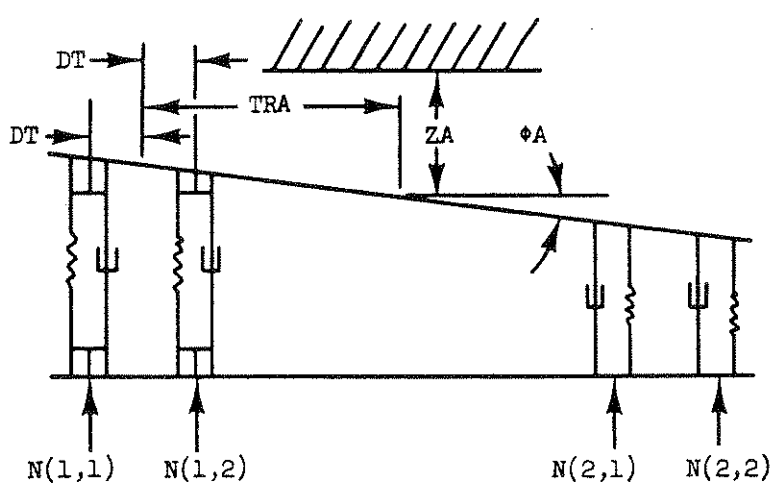

Figure 3-7. Axle with dual tires

Since the half distance between duals, DT, is quite small compared to the half-track, TRA, it is a good approximation to use the average value for the normal forces rather than calculate them separately. Thus,

$$N(1,1) = N(1,2) = \frac{1}{2}[(N(1,1) + N(1,2)_{Static} + 2KT(\dot{Z}A - TRA \cdot \dot{\phi}A) + 2CT(\dot{Z}A - TRA \cdot \dot{\phi}A)] \quad (3\text{-}19a)$$

$$N(2,1) = N(2,2) = \frac{1}{2}[(N(2,1) + N(2,2)_{Static} + 2KT(\dot{Z}A + TRA \cdot \dot{\phi}A) + 2CT(\dot{Z}A + TRA \cdot \dot{\phi}A)] \quad (3\text{-}19b)$$

The dual tires on one side of the vehicle are modeled with identical C_α values. The C_α values for the left side and the right side of the vehicle will, of course, be quite different in the presence of appreciable lateral load transfer.

The normal forces on all tires except those on the front axle are calculated with equations similar to (3-19). Should the user wish to designate single tires on any axle, he need only enter DT = 0 in the input data, and appropriate adjustments will be made.

In addition to the different normal force acting on the inside and outside dual tires, it should be recognized that the sideslip angle on the outside dual may differ from the sideslip angle on the inside dual. Consider the plan view of the unsprung masses given in Figure 3-8. The sideslip angle of the left outside dual is (neglecting any roll steer)

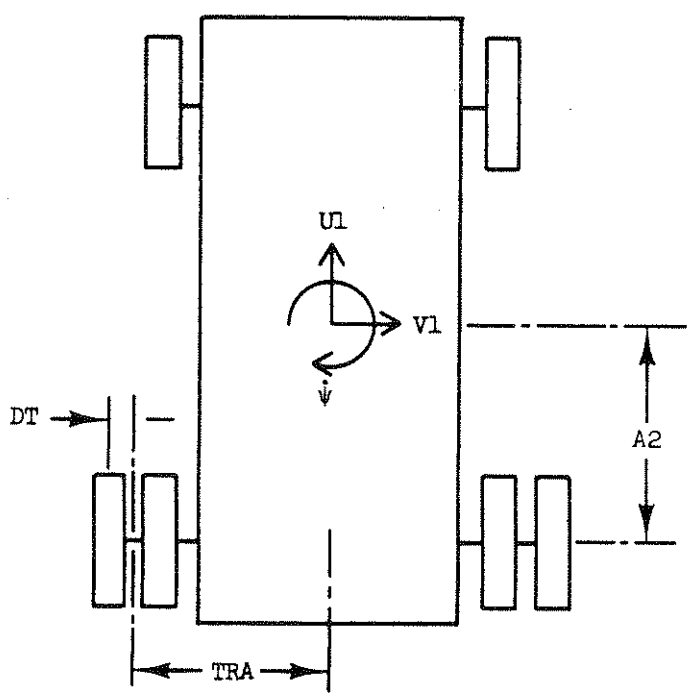

Figure 3-8. Unsprung masses, plan view

$$\alpha_o = \tan^{-1}\left(\frac{V1 - A2\,\dot{\psi}}{U1 + \dot{\psi}(TRA + DT)}\right) \tag{3-20a}$$

and for inside tire,

$$\alpha_i = \tan^{-1}\left(\frac{V1 - A2\,\dot{\psi}}{U1 + \dot{\psi}(TRA - DT)}\right) \tag{3-20b}$$

Since DT may be expected to be much smaller than TRA, it is a good approximation to use the average sideslip angle to compute the cornering force.

$$\text{Total } F_y = 2F_y\Big|_{\text{ave } \alpha,\text{ave } N} \tag{3-21}$$

Naturally, it is most convenient that the normal forces and sideslip angles for a set of duals may be averaged for use in the tire model insofar as the writing of the force equations is concerned, and insofar as lower computer costs are achieved than would be the case with individual calculations. In the case of the spin velocity Ω, there is no question of an average value, since dual tires are constrained to have the same spin rate. This constraint, however, results in a differential longitudinal slip between the dual tires when traversing a curved path. While it may be shown through arguments similar to those given for sideslip angle that an average slip value is adequate for the calculation of the total brake force on the set of dual tires, the differential longitudinal slip between duals can cause an appreciable aligning torque.

The longitudinal velocity of the left outside dual is (neglecting any roll steer considerations)

$$U_o = U1 + \dot{\psi}(TRA + DT) \tag{3-22a}$$

Thus the longitudinal slip of that tire is

$$S_o = 1 - \frac{RR \cdot \Omega}{U1 + \dot{\psi}(TRA + DT)} \tag{3-22b}$$

where Ω is the rotation rate of both duals and RR is the rolling radius.

On the other hand, for the inside dual, we have

$$U_i = U1 + \dot{\psi}(TRA - DT) \tag{3-23a}$$

and

$$S_i = 1 - \frac{RR \cdot \Omega}{U1 + \dot{\psi}(TRA - DT)} \tag{3-23b}$$

where an equal rolling radius, RR, has been assumed for the inside and outside dual.

Consider now positive $\dot{\psi}$. A comparison of Equations (3-22b) and (3-23b) shows that

$$S_i < S_o \tag{3-24}$$

Thus, there must be a differential longitudinal force on the duals such that, in this case, a negative yaw moment (i.e., an understeer contribution) results. (A similar understeer result also applies to the right hand set of duals.)

The above defined moment is calculated using the procedure outlined below. The value of longitudinal slip used in the brake force calculations, S(I), is an average value calculated on the basis of the longitudinal velocity of the mid point between the duals. The slope of the μ-slip curve at this point is (see Figure 3-9) given by

$$\text{SLOPE (I)} = \left.\frac{\partial\mu}{\partial S}\right|_{S=S(I)} = \frac{-1}{N}\left.\frac{\partial F_x}{\partial S}\right|_{S=S(I)} \tag{3-25}$$

where N is the normal force on each dual tire. The slip of the outside and inside dual may be written

$$S_o = S(I) + \frac{S_o - S_i}{2} \tag{3-26a}$$

$$S_i = S(I) - \frac{S_o - S_i}{2} \tag{3-26b}$$

Expanding the μ-slip curve about the point S = S(I) in a Taylor series and, since $S_o - S_i$ may be expected to be very small, dropping higher order terms yields

$$FX_o = \frac{FX_{ave}}{2} - N\frac{\partial\mu}{\partial S}\left(\frac{S_o - S_i}{2}\right) \tag{3-27a}$$

$$FX_i = \frac{FX_{ave}}{2} + N\frac{\partial\mu}{\partial S}\left(\frac{S_o - S_i}{2}\right) \tag{3-27b}$$

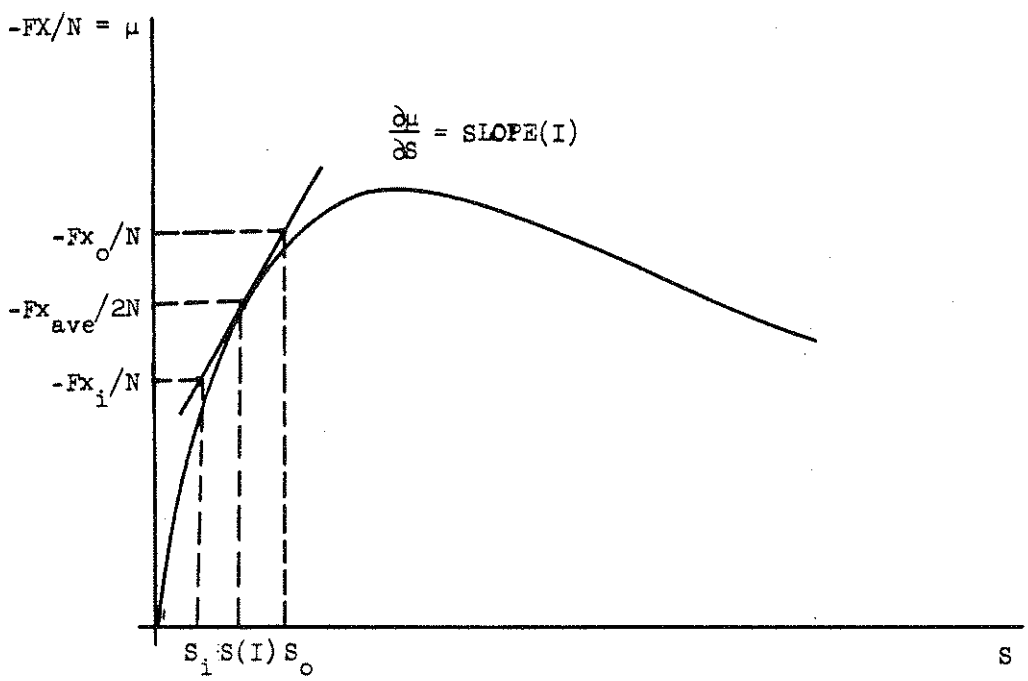

Figure 3-9. A μ-slip curve

where $FX_{ave} = FX_o + FX_i$.

Thus this system may be written as a force FX_{ave} and a couple $\overline{MZ}$ where

$$MZ = -[N \frac{\partial \mu}{\partial S} (S_o - S_i)]DT \hat{2}1 \qquad (3\text{-}28)$$

Since $\left|\frac{\partial \mu}{\partial S}\right|$ can be very large, especially at small longitudinal slip values, the aligning torque deriving from the differential slip of dual tires is an important effect and has been included in the model.

3.3 THE SUSPENSION MODELS

Any one of three possible suspension configurations may be simulated at each axle location other than at the front axle, as in the pitch-plane simulation documented in [1]. Initially, the simplest configuration viz., the single axle, will be treated with the walking-beam and four-spring configurations to follow.

3.3.1 THE SINGLE AXLE SUSPENSION.

3.3.2.1 Derivation of the Equations. A sketch of the single axle is given in Figure 3-10. The forces at the tire-road interface and the forces between the sprung and unsprung mass must be calculated at the beginning of each new integration time step, these forces being used to calculate the accelerations of the sprung mass. The forces at the tire-road interface and the suspension forces, SF, (the number 1 denotes the left side and 2 denotes the right side) are functions only of the positions and velocities of the sprung and unsprung masses, and may therefore be calculated in a straightforward manner. However, the longitudinal and lateral constraint forces between the sprung mass and the unsprung masses also depend on the acceleration of the unsprung masses, and thus computational complications arise.

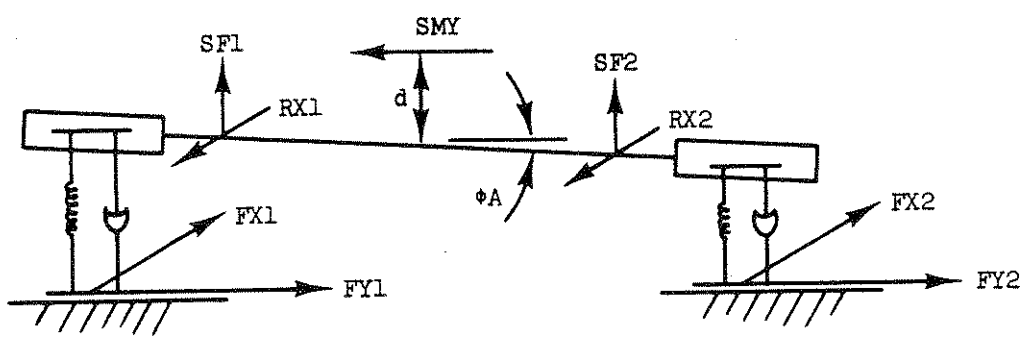

Figure 3-10. Schematic diagram: single axle model

Consideration of a free body diagram of a wheel and of the axle will be of assistance in the analysis of this system. Consider the wheel diagrammed in Figure 3-11, in which xw, yw, and zw axles are fixed with the origin at the axle center. At the instant of interest, $\hat{z}w$ is in the $\hat{z}1$ direction, and $\hat{x}w$ is in the plane of the wheel. The axis system rotates at angular velocity $\omega 1$ where

$$\overline{\omega 1} = \dot{\phi}A\ \hat{x}w + \dot{\psi}\ \hat{z}w \tag{3-29}$$

where

$\dot{\phi}A$ is the roll rate of the axle

$\dot{\psi}$ is the rotation rate of $\hat{x}1$, $\hat{y}1$, $\hat{z}1$; the yaw rate of the unsprung mass system.

Since the solid axle may reasonably be assumed to deviate only slightly from the $\hat{y}1$ direction,* it will be assumed in the following analysis that

$$\hat{y}w = \hat{y}1 \tag{3-30}$$

The reaction forces and moments from the axle on the wheel are AFX, AFY, AFZ, and AMX, ANY, and AMZ, respectively. The forces at the tire-road interface are FXW, FYW, and FZW; MX, MY, and MZ are the moments. Application of Newton's laws leads to (see Equation (2-35)):

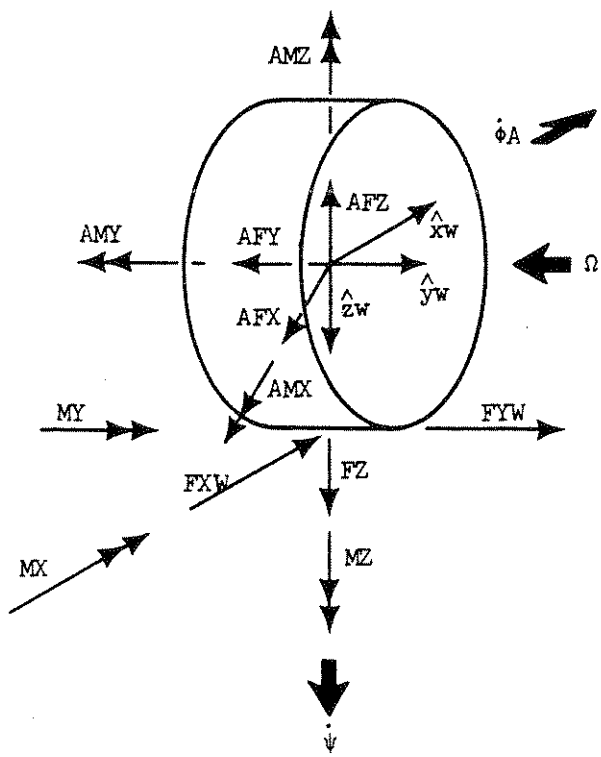

Figure 3-11. Free body diagram: rolling wheel

*The possible deviations are those due to roll steer and to roll angle ϕA of the axle assembly.

$$(FX-AFX)\hat{x}1 + (FY-AFY)\hat{y}1 + (FZ-AFZ)\hat{z}1$$

$$= M_w([UD1 - \dot{\psi}^2(XU) - \ddot{\psi}(YU)]\hat{x}1$$

$$+ [VD1 - \dot{\psi}^2(YU) + \ddot{\psi}(XU)]\hat{y}1 + \ddot{ZU}_w\hat{z}1) \qquad (3\text{-}31)$$

where

XU is the half track

YU is the distance in the $\hat{x}1$ direction from the sprung mass center to the mass center of the wheel

UD1 is the acceleration of the sprung mass center in the $\hat{x}1$ direction

VD1 is the acceleration of the sprung mass center in the $\hat{y}1$ direction

$\ddot{ZU}$ is the vertical acceleration of the wheel mass center

M_w is the mass of the wheel

Now using the same free body diagram, we can write the equations of rotational motion. Assuming that the polar moments of inertia of the tire about the xw, yw, zw axes are principal moments (i.e., wheel imbalance is neglected), the rotational equations for the wheel become

$$MX-AMX = JT \cdot \ddot{\phi}A + JS \cdot \dot{\psi} \cdot \Omega \qquad (3\text{-}32a)$$

$$+FX(RR) + MY-AMY = -JS\,\dot{\Omega} \qquad (3\text{-}32b)$$

$$MZ-AMZ = JT \cdot \ddot{\psi} - JS \cdot \Omega \cdot \dot{\phi}A \qquad (3\text{-}32c)$$

where JT, JS, JT are the polar moments of the wheel about xw, yw, and zw, respectively.

Now consider the free body diagram of the axle in Figure 3-12. (The number 1 in a force or couple indicates the left-hand side, the number 2, the right.) The reaction forces from the sprung mass on the axle are RX1 and RX2, SMY, and SF1 and SF2. The moment applied from the frame to the axle is assumed to be only the brake torque TT1 and TT2. The force summation in the $\hat{x}1$ direction leads to

$$RX1 + RX2 = AFX1 + AFX2 - MAX[UD1 - \dot{\psi}^2 \cdot \dot{XU}] \qquad (3\text{-}33)$$

where MAX is the mass of the axle, and the axle mass center is assumed to be located such that

$$YU = 0 \qquad (3\text{-}34)$$

From Equation (3-34), we have

$$AFX1 + AFX2 = FX1 + FX2 - 2M_w[UD1 - \dot{\psi}^2 \cdot XU] \qquad (3\text{-}35)$$

But the unsprung mass is defined as the mass of the axle plus the mass of the wheels, i.e.,

$$MS = MAX + 2M_w \qquad (3\text{-}36)$$

Thus, the $\hat{x}1$ component of Equation (3-33) may be written

$$RX1 + RX2 = FX1 + FX2 - MS[UD1 - \dot{\psi}^2\, XU] \qquad (3\text{-}37a)$$

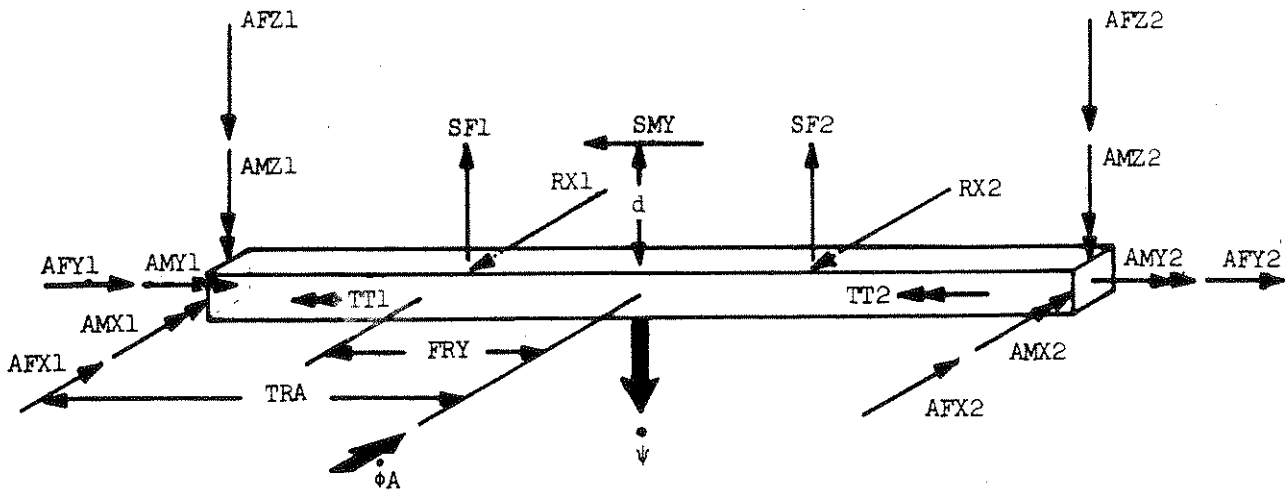

Figure 3-12. Free body diagram: single axle

In the same way, it can be shown that

$$SMY = FY1 + FY2 - MS[VD1 + \ddot{\psi}\, XU] \qquad (3\text{-}37b)$$

$$-SF1 - SF2 + FZ1 + FZ2 = MS \cdot \ddot{ZA} \qquad (3\text{-}38c)$$

where ZA is the vertical position of the mid point of the axle. Now, under the assumption that the principle moments of inertia of the axle are Ja, 0, Ja, about axes in the $\hat{x}1$, $\hat{y}1$, $\hat{z}1$ directions with origin at the axle center (i.e., the dynamics of axle "wrap up" are neglected), the Euler equations may be written for the axle.

$$(SF1-SF2)FRY + (AFZ2-AFZ1)TRA - SMY\,(d) + AMX1 + AMX2 = J_a\ddot{\phi}A \qquad (3\text{-}38a)$$

$$AMY1 + AMY2 - TT1 - TT2 = 0 \qquad (3\text{-}38b)$$

$$AMZ1 + AMZ2 + (AFX1 - AFX2)TRA + (RX2-RX1)FRY = J_a\ddot{\psi} \qquad (3\text{-}38c)$$

By combination of Equations (3-38c) and (3-32c) we can eliminate AMZ1 and AMZ2, yielding

$$MZ1 + MZ2 + (AFX1-AFX2)TRA + (RX2-RX1)FRY$$

$$= 2(JT)\ddot{\psi} + -Js(\dot{\phi}A)[\Omega_1 + \Omega_2] + J_a\ddot{\psi} \qquad (3\text{-}39)$$

But from the $\hat{x}1$ component of Equation (3-31) we have

$$FX1 - AFX1 = M_w[UD1 - \dot{\psi}^2 XU + \ddot{\psi}(TRA)] \qquad (3\text{-}40a)$$

$$FX2 - AFX2 = M_w[UD1 - \dot{\psi}^2 XU - \ddot{\psi}(TRA)] \qquad (3\text{-}40b)$$

Thus,

$$AFX1 - AFX2 = FX1 - FX2 - 2M_w \cdot \ddot{\psi} \cdot TRA \tag{3-41}$$

Substitution of Equation (3-41) in (3-38) yields

$$\begin{aligned} &MZ1 + MZ2 + (FX1-FX2)TRA - 2M_w\ \psi(TRA)^2 + (RX2-RX1)FRY \\ &= 2(JT)\ddot{\psi} - J_s\dot{\phi}A[\Omega_1 + \Omega_2] + J_a\ddot{\psi} \end{aligned} \tag{3-42}$$

But the polar moment of inertia of the axle wheel assembly may be written as

$$JA = J_a + 2JT + 2M_w(TRA)^2 \tag{3-43}$$

Thus,

$$MZ1 + MZ2 + (FX1-FX2)TRA + (RX2-RX1)FRY + (JS)\ (\dot{\phi}A)[\Omega_1 + \Omega_2] = JA(\ddot{\psi}) \tag{3-44}$$

Both equations (3-37a) and (3-44) contain the unknown constraint forces RX1 and RX2. However, there is a major complication to using these two equations to solve for RX1 and RX2; namely, the sprung mass acceleration, UD1, and the unsprung mass angular acceleration, $\ddot{\psi}$ are unknown at this stage of this development. A rigorous solution would require the added consideration of the sprung mass equations of motion in order to solve the system of equations for the constraint forces and the accelerations.

Since we have not constrained the suspensions to remain perpendicular to the sprung mass, and since added complications result from the variety of suspension options, a rigorous approach is very tedious and numerically quite time consuming, requiring a matrix inversion to solve for the accelerations at each time step. We have elected instead to apply an alternate, approximate method. In this method, it is assumed that the unknown accelerations of the unsprung masses may be successfully estimated based on the assumption that the entire vehicle is moving as a single rigid body in the yaw plane.

The acceleration of the mass center of the entire vehicle is assumed to be

$$\bar{A} = \frac{GVW}{g} \sum (FXI\ \hat{x}1 + FYI\ \hat{y}1) \tag{3-45}$$

where the summation sign indicates a sum over all the tires. The yaw acceleration may be written

$$\ddot{\psi}\hat{z}1 = \frac{1}{IZ} \sum_i \bar{r}_i X(FXI\ \hat{x}1 + FYI\ \hat{y}1) \tag{3-46}$$

where IZ is the yaw moment of the entire vehicle (assuming no roll or pitch), the $\bar{r}_i$ are the appropriate moment arms and the sum is again over all of the tires. The yaw plane components of the individual unsprung masses may now be found from Equations (3-45) and (3-46).

$$\bar{a}_i = \bar{A} - \dot{\psi}^2\ \bar{r}_i + \ddot{\psi}(\hat{z}1 \times \bar{r}_i) \tag{3-47}$$

Thus, given the forces at the tire-road interface, the $\bar{a}_i$ may be used in Equations (3-37a) and (3-47) to calculate the forces on the sprung mass from the unsprung mass. A schematic diagram of this process is shown in Figure 3-13.

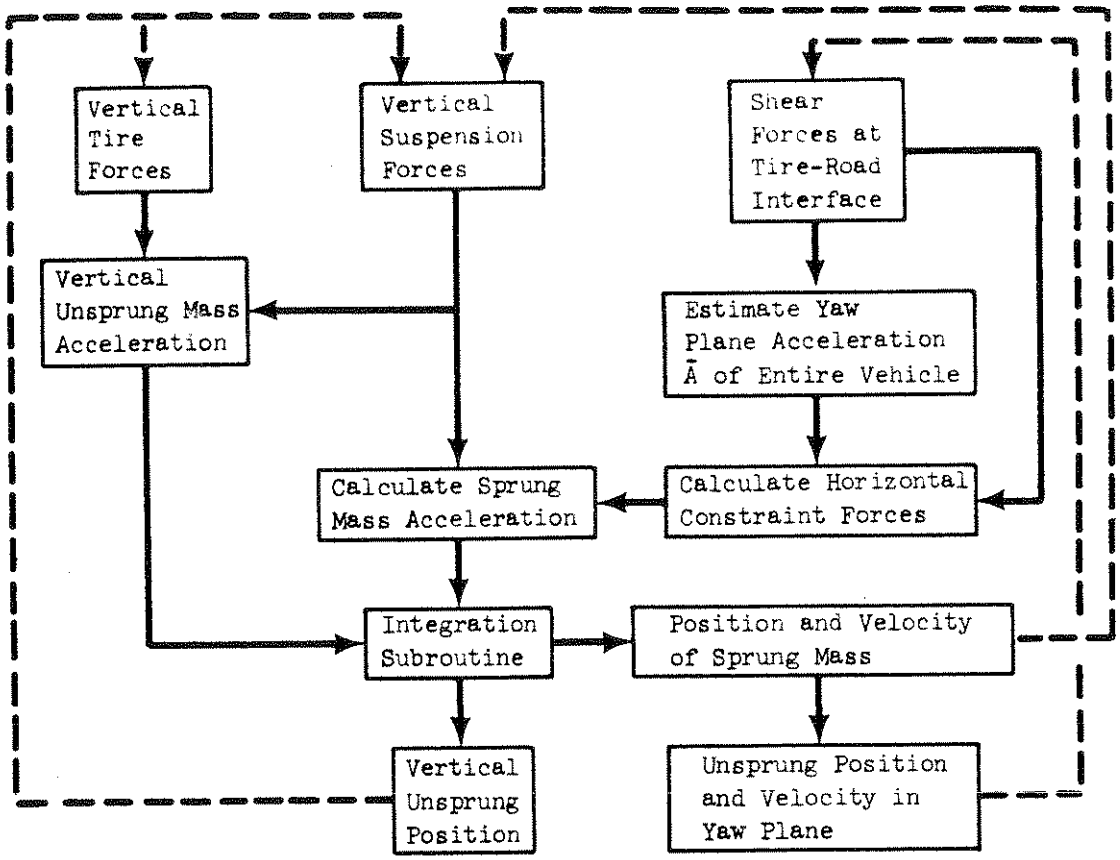

Figure 3-13. Flow diagram: method of computation of the constraint forces

Similar equations will now be derived combining the force equations in the $\hat{z}1$ directions and moments about the $\hat{x}1$ axis.

By combining Equations (3-38a) and (3-32a), AMX1 and AMX2 are eliminated, yielding

$$(SF1-SF2)FRY - SMY \cdot d + MX1 + MX2 + (AFZ2-AFZ1)TRA$$
$$= (J_a + 2JT)\ddot{\phi}\ddot{A} + (JS)\dot{\psi}[\Omega_1 + \Omega_2] \tag{3-48}$$

But from the $\hat{z}1$ component of Equation (3-31) we have

$$FZ1 - AFZ1 = M_{w1}\ddot{ZU}_{w1}$$
$$FZ2 - AFZ2 = M_{w2}\ddot{ZU}_{w2} \tag{3-49}$$

Thus,

$$AFZ2-AFZ1 = FZ2-FZ1 + M_{w1}\ddot{ZU}_{w1} - M_{wz}\ddot{ZU}_{wz} \tag{3-50}$$

The acceleration terms on the right-hand side of Equation (3-50) may be written as

$$M_{w1}[\ddot{ZA} - TRA\cdot\ddot{\phi}A] - M_{w2}[\ddot{ZA} + TRA\cdot\ddot{\phi}A] \tag{3-51}$$

where ZA is the vertical position of the axle center. The use of Equations (3-41) and (3-50) in Equation (3-48) leads to

$$MX1 + MX2 + (SF1-SF2)FRY - SMY(d) + [FZ2-FZ1-2M_w(TRA)\ddot{\phi}A]TRA$$
$$= (J_a + 2JT)\ddot{\phi}\ddot{A} + (JS)\dot{\psi}(\Omega_1 + \Omega_2) \tag{3-52}$$

But

$$J_a + 2JT - 2M_w(TRA)^2 = JA \qquad (3\text{-}53)$$

where JA is the total moment of inertia of the axle and wheels around an axis in the $\hat{x}1$ direction through the axle center. Thus,

$$MX1 + MX2 - JS \cdot \dot{\psi} \cdot (\Omega_1 + \Omega_2) + (FZ2-FZ1)TRA$$

$$+ (S1-S2)FRY - SMY(d) = JA(\ddot{\Phi}A) \qquad (3\text{-}54)$$

Equations (3-37c) and (3-54) are used to calculate the accelerations of the axle, the former equation yielding the "bounce" acceleration of the axle center, the latter yielding the roll acceleration of the axle. The lateral constraint force SMY may be calculated using Equation (3-37b) and the methods of Figure 3-13.

3.3.2.2 A Summary of the Assumptions Used in the Single Axle Model. A number of simplifying assumptions were made in the derivation of the equations of motion of the single axle in the preceding section. These are listed below.

1. Deviations of the axle from the $\hat{y}1$ direction were ignored since axle steer displacements and axle roll angle, ΦA, are expected to be small. (Note, the effects of roll steer and axle roll on tire slip angles are not neglected; rather, the effects of roll steer and axle roll angle on the orientation of the wheel axis system are neglected. The means for computing the steer of the axle, assumed to be a linear function of suspension deflection, are discussed in Chapter 5.)
2. The wheels are balanced. Thus the mass center of the wheel is assumed to be at the axle center, and the polar moments about the xw, yw, zw axes are assumed to be principal moments.
3. Axle rotation about an axis in the $\hat{y}1$ direction (i.e., wrap up) is neglected.
4. Various assumptions have been made concerning the forces between the sprung and unsprung masses.
   a. The reactions in the $\hat{x}1$ direction are applied at the height of the axle center, and the torque about the axle is the brake torque. (Anti-pitch geometry is not considered.)
   b. The constraint in the $\hat{y}1$ direction is assumed to be a point force applied at constant distance d above the axle. (In the simulation, the input variable is the distance of RCH above the ground, i.e., the roll center height.)
   c. The suspension forces SF are assumed to act in the $\hat{z}1$ direction.

These assumptions lead to equations which predict the forces on the sprung mass only if the acceleration of the unsprung mass is known. These accelerations are found through an approximate method which assumes motion in the yaw plan. A diagram of the procedure is given in Figure 3-13. Using this procedure, the constraint forces RX and SMY may be computed and then used to find the acceleration of the sprung mass.

In spite of the many assumptions made, the equations given are quite detailed. Since for each added feature of the simulation the user must pay the price in both the tedium of dealing with the added input variables as well as increasing computation costs, it was decided to drop from the equations certain terms which may be considered negligibly small. Among these are overturning moments at the tire-road interface and the gyroscopic effects caused by the yaw velocity of the axis of tire rotation. These terms may easily be added by the user should they be considered significant.

3.3.2 THE FOUR SPRING SUSPENSION. The four spring suspension is a four degree of freedom system coupled longitudinally by the load levelers and laterally by the solid axles. Thus the system will admit an axle tramp mode as well as brake hop. This level of sophistication is possible since the frame may correctly be assumed not to apply significant roll moments to the springs at the load leveler or the contact points between the leaf springs and the frame. The equations of the four spring suspension are therefore quite similar to the pitch plane equations given in [1] and [5]. The added complications resulting from the yaw and roll freedom will be summarized here, but that part of the derivation previously published will not be repeated. Thus, it is assumed in the following analysis that the reader is familiar with the pitch plane derivation.

A schematic and free-body diagram of the suspension viewed from the left side is given in Figure 3-14. With two changes in nomenclature, the schematic diagram given in Figure 3-10 becomes valid for either of the tandem axles. These changes are indicated in Figure 3-15 and listed below:

(a) In place of the longitudinal constraint forces, RX1 and RX2, we have the horizontal components of the forces in the torque rods. For example, for the left side of the lead axle,

$$(TR2 \cdot \cos AA7)_1 = RX1 \qquad (3\text{-}55)$$

(b) In place of the suspension forces, SF1 and SF2, are the leaf-frame contact forces, TN, plus the vertical component of the torque rod force. For example, for the left side of a lead axle,

$$TR2 \sin AA7 - TN1 - TN2 = SF1 \qquad (3\text{-}56)$$

The longitudinal constraint forces, RX, may be found from Equations (3-37a) and (3-47) and thus the torque rod forces are known. From this point the equations for the TN forces are exactly those given in [1] and [5]. Since there is a direct relationship between the TN and the SF, the motion of the axles may be found from a straightforward application of Equations (3-37c) and (3-54).

3.3.3 THE WALKING BEAM SUSPENSION. The walking beam suspension which is shown in side view in Figure 3-16, is a four degree of freedom system with the wheels on each side coupled to each other longitudinally by the walking beam. Side-to-side coupling due to the solid axle connection has been neglected due to the significant complexity* this would add to the simulation. Thus, dynamics of the mass center on the left side are coupled to the dynamics of the mass center on the right side only through the motion of the frame. A schematic view of this simplified model is shown in Figure 3-17.

While this simplification is major in its implications, it is not believed to be important with respect to smooth, level road operations since, in most cases, axle tramp in the walking beam suspension is not a significant problem. Nevertheless, if brake hop** is to be simulated or if operation on a rough road with

*In contrast to the four spring suspensions, in which no geometric constraint is imposed by the suspension, the load levelling device in the walking beam suspension provides a geometric constraint on the position of the axles. To model the combination of constraints (the side-to-side constraint of each axle plus the longitudinal constraint of each walking beam) is indeed a formidable task.

**It should be noted that brake hop did not occur during the testing of the straight truck with the walking beam suspension, even during very severe braking runs.

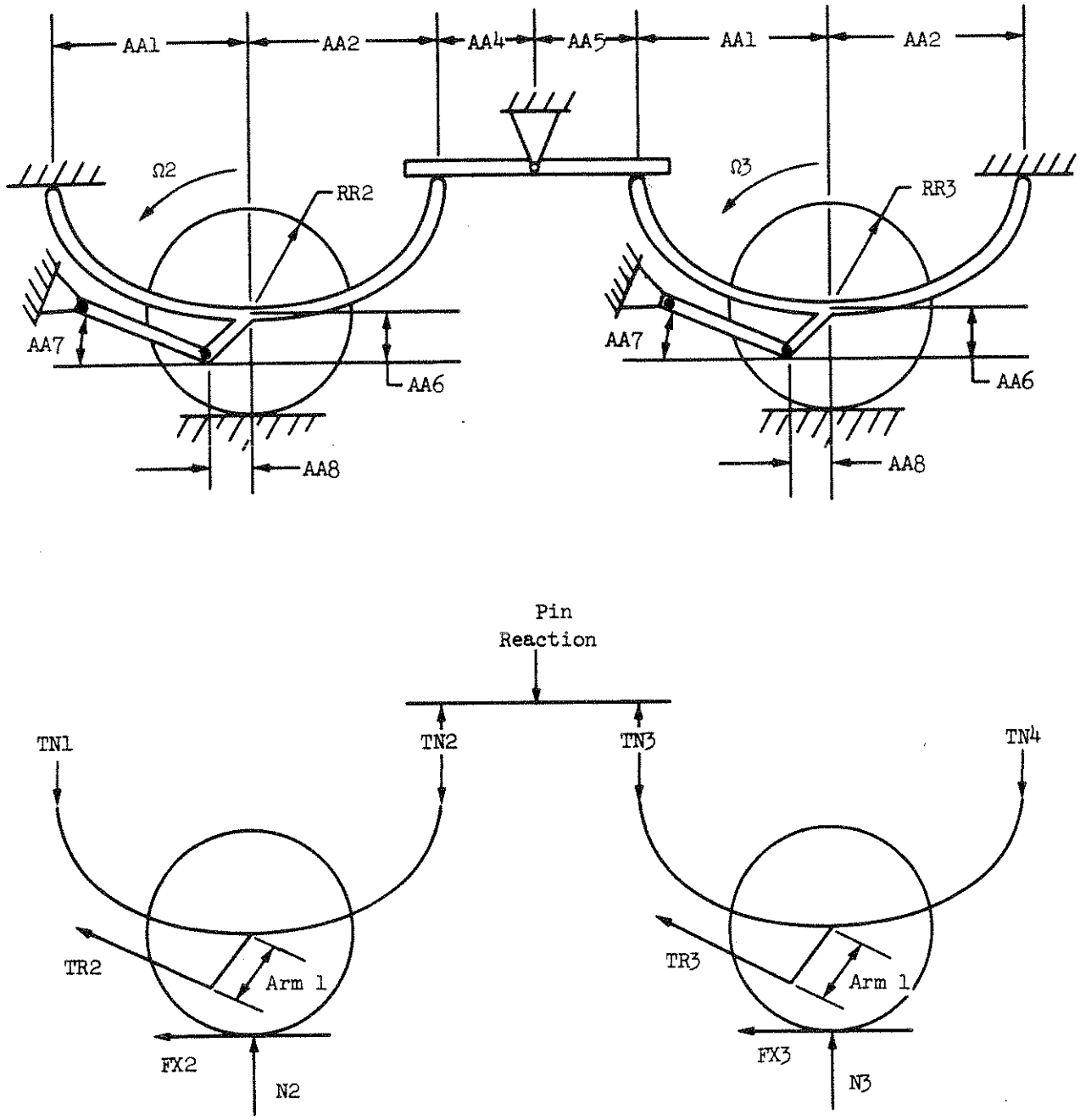

Figure 3-14. Free body diagram: four spring suspension

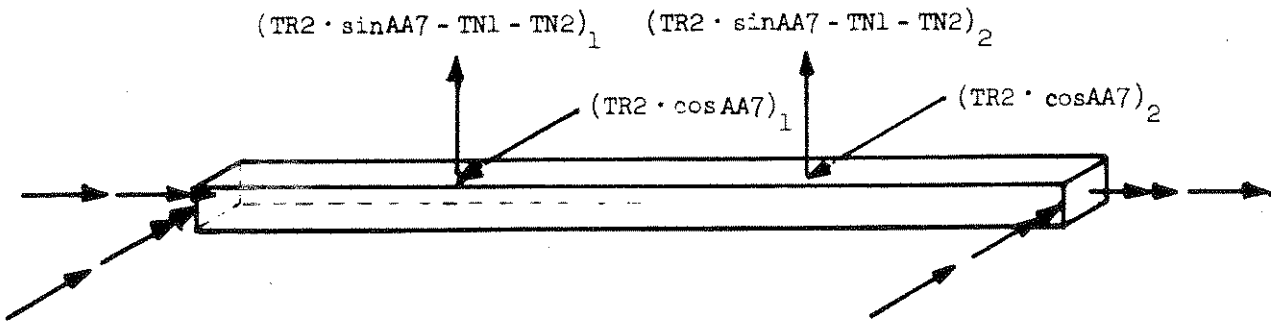

Figure 3-15. Free body diagram: axle of a four spring suspension

side-to-side variations in road profile is assumed, the elimination of the side-to-side coupling through the axles is likely to be a serious deficiency.

The following analysis summarizes the extension of the pitch-plane model of the walking beam suspension to the three-dimensional case. It is assumed that the reader is familiar with the pitch plane derivation. Only the rear wheel of the left side of suspension 2 (tractor or straight truck rear suspension) is treated; the free body diagram of this wheel is shown in Figure 3-18. The motions of the other three wheels will be described by similar equations.

It is assumed that the mass MS2(3) of the wheel and axle shown in Figure 3-18 is one-half the mass of the rear axle assembly, plus the mass of the wheel. The longitudinal and vertical forces on the frame and the pitch moment applied to the frame have been given in [1] and [5]. Only the horizontal force, SMY, and the roll and yaw moments, TX and TZ, will be considered here.

A summation of forces yields

$$SMY = FYW - MS2(3) \cdot YDD(3) \qquad (3\text{-}57)$$

where

SMY is the lateral force transmitted to the frame. Note that, since the axle itself is neglected, the dimension h is irrelevant. We choose the height of the frame rail for convenience only.

YDD(3) is the lateral acceleration of the assumed mass center point, the wheel center.

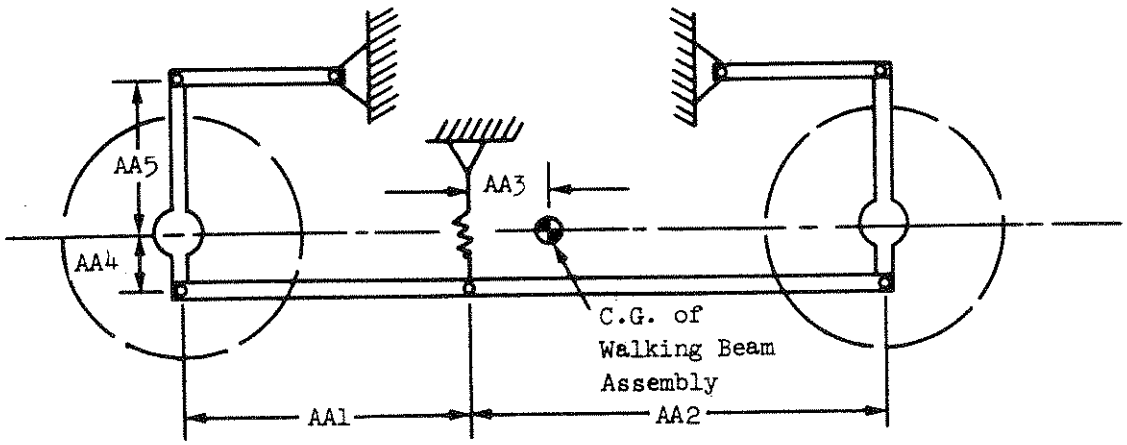

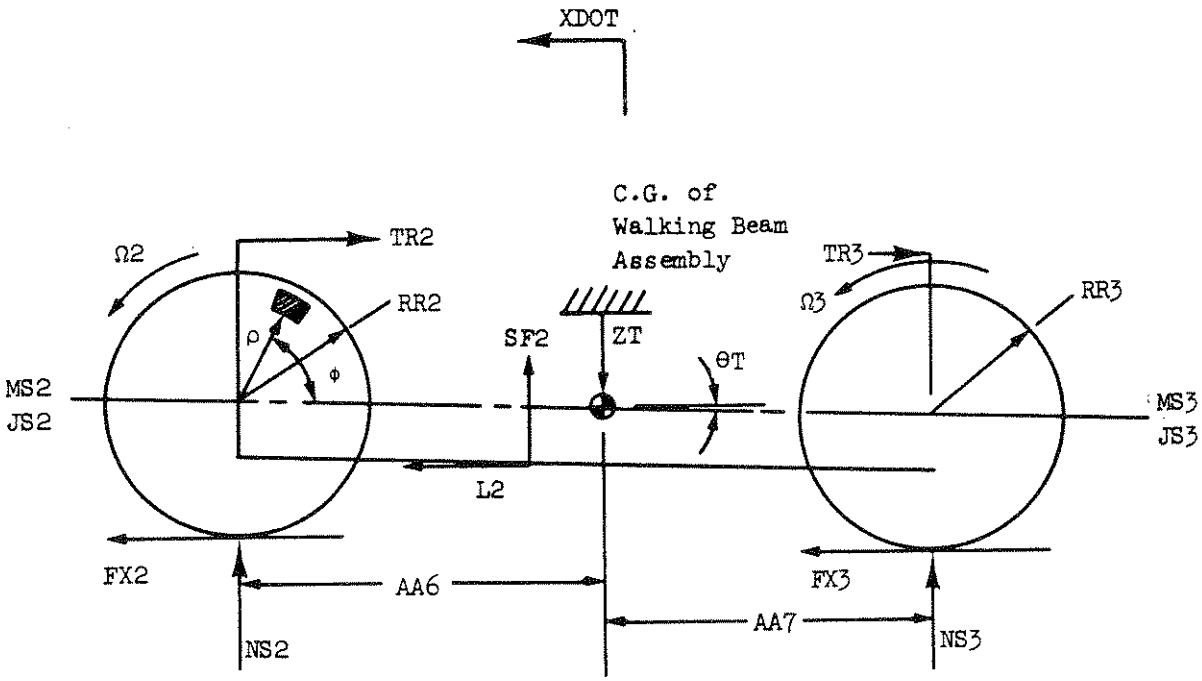

Figure 3-16. Free body diagram: free body diagram: walking beam suspension

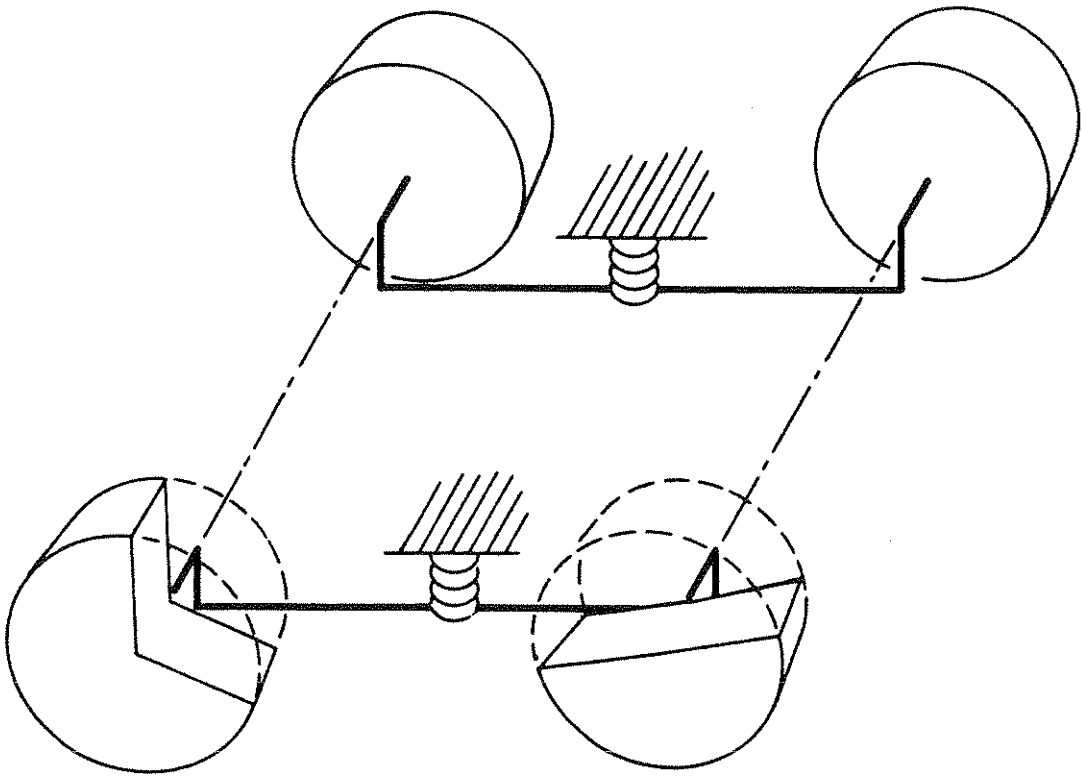

Figure 3-17. Schematic diagram: walking beam suspension

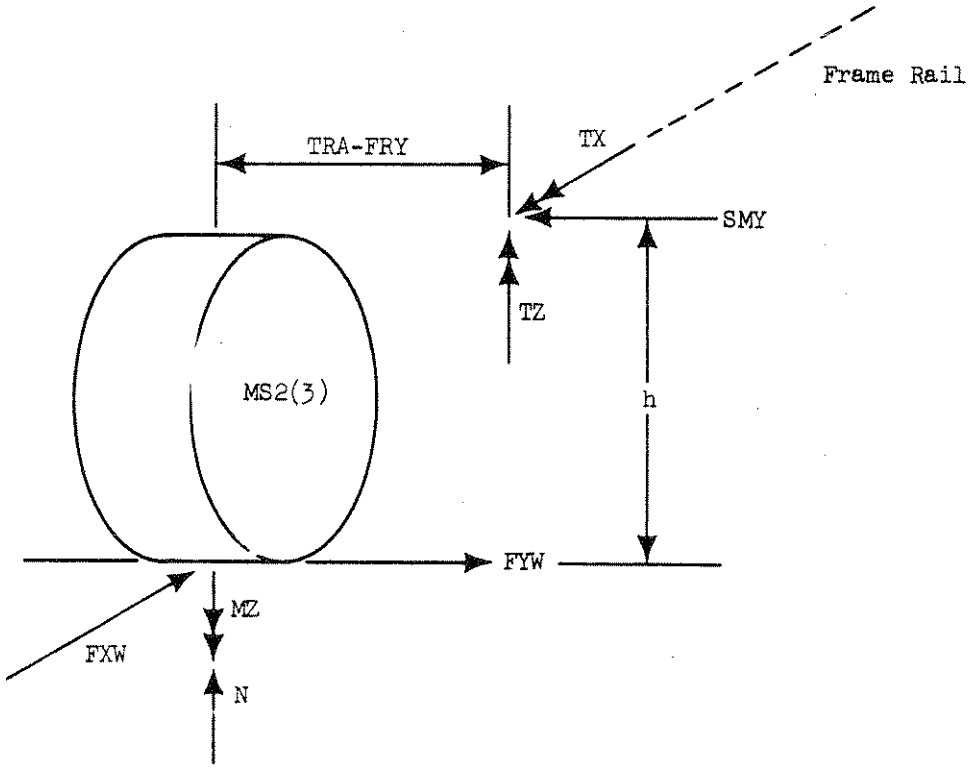

Figure 3-18. Free body diagram: left rear wheel of walking beam suspension

A summation of moments at the frame rail yields

$$TX = N(TRA - FRY) - FYW(h) \tag{3-58}$$

$$TZ = MZ - FXW(TRA - FRY) \tag{3-59}$$

where

(TRA-FRY) is the horizontal distance from the normal force N to the frame rail

MZ is the aligning torque.

Through the use of Equations (3-56) to (3-59) and the pitch moment and suspension force previously given in [1] and [5], all forces and moments applied to the frame through the walking beam suspension are calculated.

3.4 STEERING SYSTEM

Heavy highway vehicles typically employ beam type front axles and a steering system that can be characterized as a series type, i.e., the left-hand steering knuckle is steered through the action of a drag link connected to the pitman arm of the steering gear. The right-hand steering knuckle is, in turn, controlled by a tie rod connected between the left and right knuckles (see Figure 3-19). As is true for most steering systems, the actual steer angles of the front wheels are not simply a function of the driver's steering input. Changes in the geometry of the steering mechanism caused by suspension movement result in small steer angle displacements of the front wheels about their nominal position. Compliances of the various members of the steering system also lead to small differential motions. In contrast to the treatment of the steering mechanism given in [6] and [7], certain geometric and compliance steer effects are considered here.

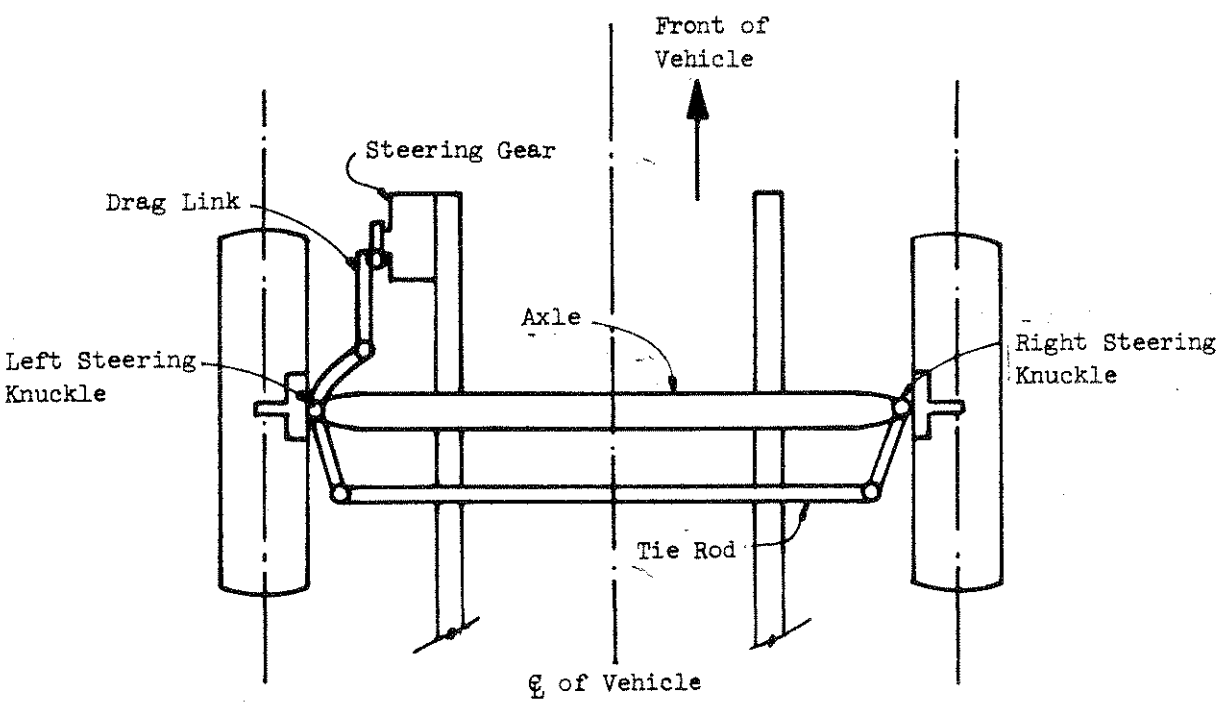

Figure 3-19. Typical heavy truck steering system

3.4.1 STEERING SYSTEM OPTIONS. In order to maximize the utility of the simulation program, a variety of steering system models have been made available to the user. If providing the additional input necessary to simulate a complex steering system is considered undesirable, a very simple steering system model may be used. On the other hand, the effects of small changes in steer angle due to suspension movement and system compliance may be simulated through the use of the more complex options.

The following paragraphs review the steering system options, starting with the simplest model and proceeding in order of complexity. Specific program instructions and examples of the use of various options are given in Appendix D.

3.4.2 SINGLE TABLE STEER ANGLE INPUT. The simplest available steering system input is a single tabular input of steer angle versus time. During the course of a simulation run, this table is called by subroutine FCT, and a linear interpolation is performed on the tabular data to determine the value of the steer angle. This steer angle is assumed to be applied to both left and right front wheels of the vehicle. Any effects of geometry or compliance in the system are neglected.

3.4.3 TWO TABLE STEER ANGLE INPUT. Just as in the case of an automobile, a side-to-side steer angle difference is designed into the steering systems of trucks. In addition, further differences may result from compliance of the various steering-suspension system members. In order to account for the side-to-side difference in steer angle, a two-table input option is available. Program operation is similar to that described for the single table option above; however, one table for each of the left and right front wheels must be entered.

In the steady turn analysis conducted in this study, we found that the use of an average steer angle in the single table rather than the measured left and right side values resulted in as much as five percent increase in the predicted lateral acceleration.

3.4.4 AXLE ROLL STEER OPTIONS. A property common to most suspension systems is "roll steer." In particular, for the beam-type front suspension used on heavy vehicles, the locating function of the leaf springs causes the axle to move through a curved path (as viewed from the side) rather than vertically during jounce and rebound. As the vehicle rolls, this action imparts some steer angle to the axle (see Figure 3-20). Thus, the actual steer angle of either front wheel may be expressed as the sum of the steer angle of the axle plus the steer angle of the wheel relative to the axle. If the simulation is being used in conjunction with a test program, the steer angle of the wheels relative to the axle is comparatively easy to measure and can be made available as input. For accurate simulation this input should then be modified by the addition of the steer angle caused by axle roll relative to the frame.

To implement this approach, either the single table or the two table input option discussed above is utilized to input the steer angle of the wheels relative to the axle. In addition, a linearized roll steer coefficient (whose units are degrees axle steer/degree roll with positive values implying front axle roll steer in the understeer direction) must be input to the program. During a simulation run, the program calculates roll angle of the vehicle relative to the front axle (note that the axle itself will roll slightly due to vertical tire deflection) and, with this information and the roll steer coefficient, the program will calculate the roll steer of the front axle. The equations of interest are:

$$\delta 1 = \delta T1 + (\phi - \phi A1)RSC1 \qquad (3\text{-}60)$$

$$\delta 2 = \delta T2 + (\phi - \phi A1)RSC1 \qquad (3\text{-}61)$$

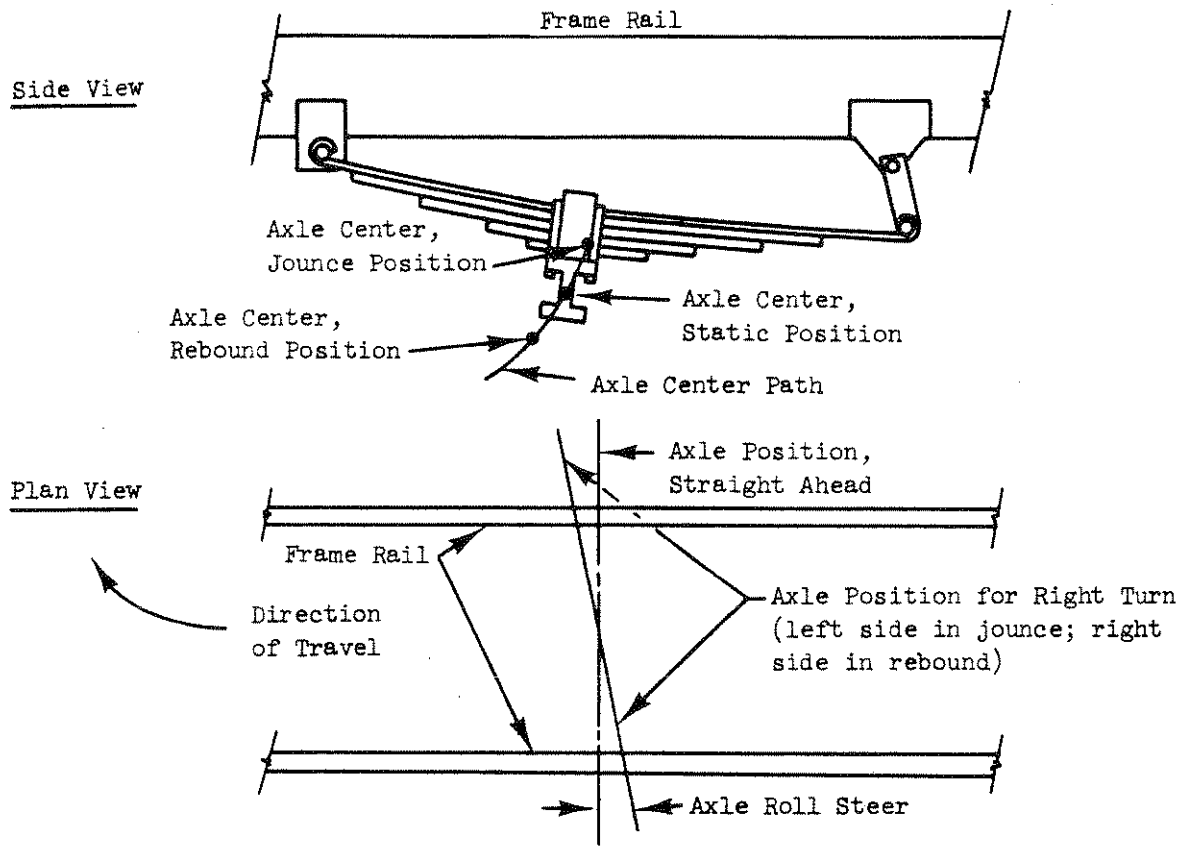

Figure 3-20. Schematic diagram: axle roll steer

where

δI is the front wheel steer angle; I = 1 left; I = 2, right

δTI is the front wheel steer angle from table input; I = 1, left; I = 2, right

ϕ is the body roll angle

$\phi A1$ is the front axle roll angle

RSC1 is the front axle roll steer coefficient.

Although it is permissible to use the roll steer option with the single table steer angle input, this practice is not recommended. The approximation accepted by using an average front wheel steer angle would tend to negate any increase accuracy gained by considering axle roll steer.

A description of a test method suitable for measuring the roll steer coefficient of a specific axle is given in Section 5.3.1.

3.4.5 COMBINED ROLL, PITCH AND BOUNCE STEER OPTION. In addition to axle steer, pitch, bounce, and roll motions of the chassis can cause small steer angle displacements of the left- and right-front wheels. If, as was discussed in Section 3.4.5 steer angles, as measured relative to the axle are used as input, then these additional effects are automatically accounted for in the input. If, however, the user wishes to input a nominal driver-attempted steer angle and then compute the actual front wheel steer angles, it is necessary to include the effects of the motion of the vehicle on the steer angles.

An exact prediction of the effects of suspension motion on steering angles would involve the solution of a complex linkage problem in three dimensions. The

computational expense of such a solution was not felt to be warranted within the context of a total vehicle simulation. Consequently, a simplified model, based on a variety of assumptions, was developed. It is felt that this model reduces the complexity of the problem to a level commensurate with its role within the total simulation program.

The basic assumptions which were made in developing this model are:

(1) Axle location is dependent on the deflection and locating properties of the leaf springs under vertical loading only. Spring displacements due to horizontal and torsional loads are ignored.

(2) Differential steer angles about the nominal driver-commanded steer angles are equal for both the left and right wheels. The driver-input steer angles, however, may be different side-to-side.

(3) All components of the steering-suspension system, other than the leaf springs, are rigid. (Certain effects of steering compliance will be treated independently in Section 3.4.7.)

For the sake of clarity, the fitures employed in the following discussion shown the nominal driver-commanded steer angles as zero. However, the arguments apply for any steer angle input. The nomenclature employed below is defined in Table 3-5.

TABLE 3-5

Steering System Nomenclature: Deflection Steer

δI	Front wheel steer angle; I = 1, left; I = 2, right
δTI	Attempted wheel steer angle from tabular input; I = 1, left; I = 2, right
$\Delta\delta I$	Differential steer angle due to roll, pitch and bounce; I = 1, left; I = 2, right
$\bar{b}$	Differential position vector of point B in sprung mass axis system
$\bar{c}$	Differential position vector of point C in sprung mass axis system
Xc	The component of $\bar{c}$ in the x direction
Zc	The component of $\bar{c}$ in the z direction
YKP	Lateral distance from front axle centerline to steering system king pin (point C)
YFR	Lateral distance from front axle centerline to spring attachment points

Consider Figure 3-21 in which the reference axis system is fixed to the vehicle. From the geometry of the figure, the differential steer angle of the left knuckle which would result from any suspension deflection can be defined as some function of the differential motion vectors, $\bar{b}$ and $\bar{c}$, of points B and C, respectively. That is

$$\Delta\delta 1 = f_1(\bar{b},\bar{c}) \tag{3-62}$$

Assumption (3), above, states that

$$\Delta\delta 1 = \Delta\delta 2 = f_1(\bar{b},\bar{c}) \tag{3-63}$$

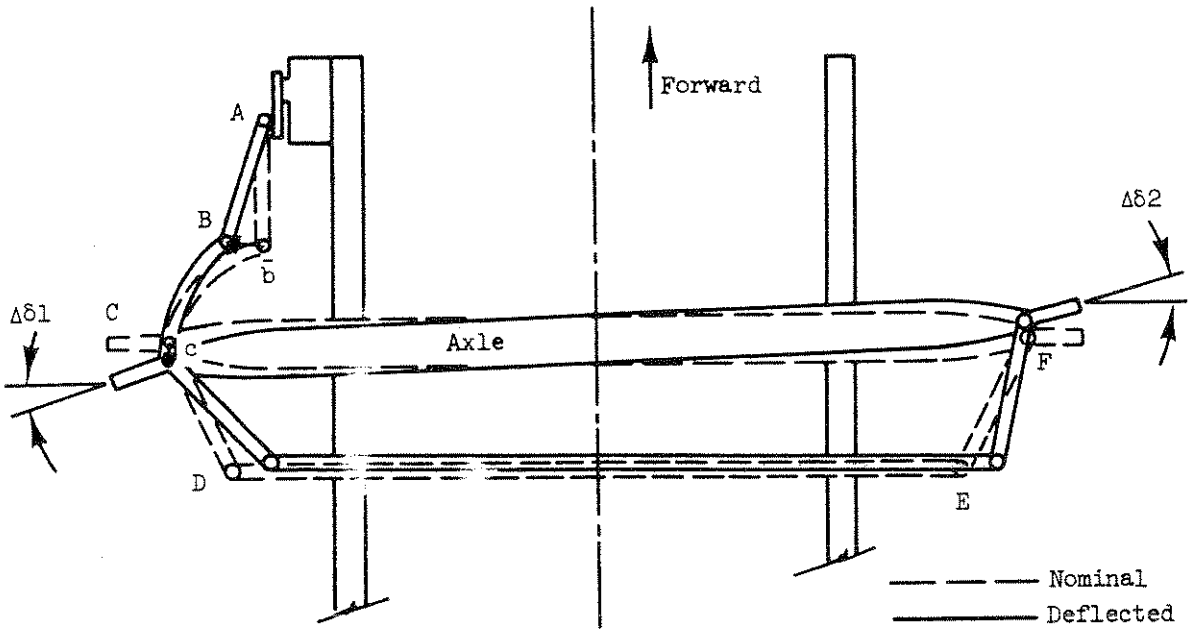

Figure 3-21. Differential steer angles due to suspension deflection

An intuitive feel for the accuracy of assumption (3) and, consequently, of Equation (3-63) can be gained by noting that assumption (3) implies that the four bar linkage composed of the front axle, the left and right steering knuckles, and the tie rod is a parallelogram. As illustrated in Figure 3-22, Equation (3-63) holds exactly for such a system, regardless of the angular position assumed by the front axle. To the extent that this linkage is not a parallelogram, Equation (3-63) is an approximation.

Equation (3-63) indicates that both the left and right differential steer angles are a function of displacements, $\bar{b}$ and $\bar{c}$, of points B and C from their nominal position. Consider the displacement $\bar{b}$. Point B is constrained by the drag link AB to move on a spherical surface of radius $\overline{AB}$ with center at A. The position of point B on this surface is a function of the position of point C relative to the vehicle frame and the roll angle of the front axle relative to the vehicle frame. (Note that effects due to spring wrap-up or lateral motion of the axle are ignored as per the first assumption.) For any given steering system, length $\overline{AB}$ is fixed, and since the location of point A is a function only of the desired left wheel steer angle, $\delta T1$, the displacement $\bar{b}$ can be considered a function of $\bar{c}$, $\delta T1$, and the roll angle of the front axle relative to the vehicle frame. Due to the close proximity in the y direction of point B to point C and the small roll angles attained by the front axle relative to the vehicle, this latter effect, i.e., front axle roll, is ignored. (Note that the most important effect of front axle roll is the vertical deflection of point C, which is included in the analysis. It is the slight additional effect of the change in orientation of the axle at point C which is ignored.) Then,

$$\bar{b} = f_2(\bar{c}, \delta T1) \qquad (3\text{-}64)$$

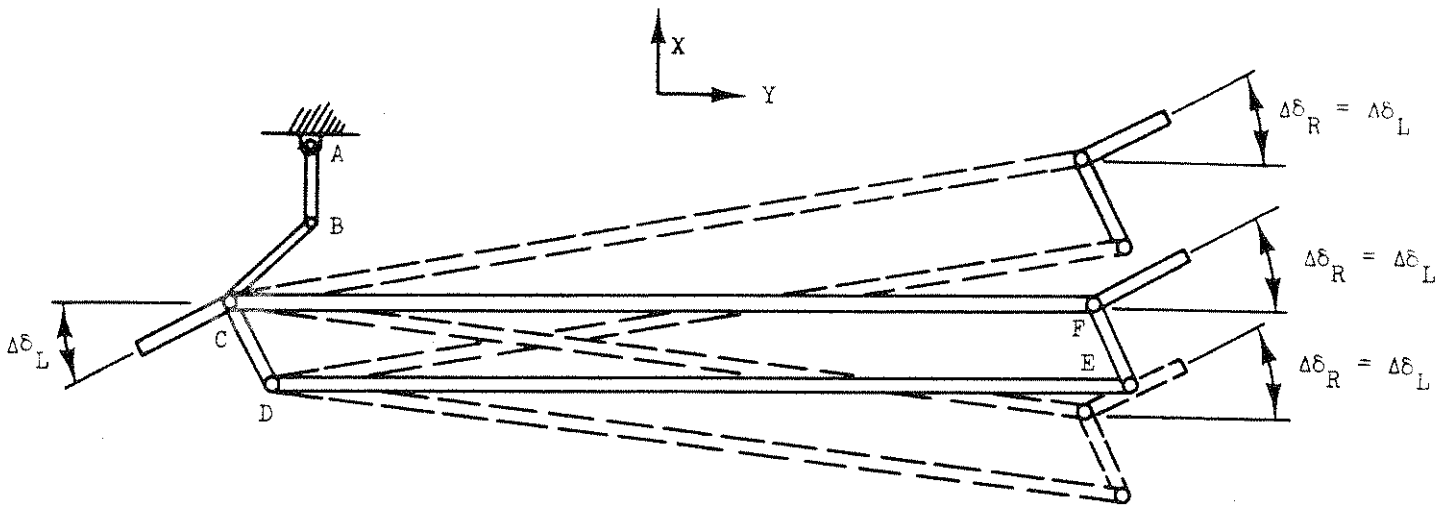

Figure 3-22. Parallelogram steering linkage

Combining Equations (3-63) and (3-64)

$$\Delta\delta 1 = \Delta\delta 2 = f_1[\bar{c}, f_2(\bar{c}, \delta T1)] = f_3(\bar{c}, \delta T1) \tag{3-65}$$

Consider now the schematic of the front axle diagrammed in Figure 3-23. From the geometry of the figure, we find that

$$z_c = \frac{YKP}{2}\left[\frac{Z_{S\ell} + Z_{SR}}{YKP} + \frac{Z_{S\ell} - Z_{SR}}{YFR}\right] \tag{3-66}$$

$$x_c = \frac{YKP}{2}\left[\frac{Z_{S\ell} + X_{SP}}{YKP} + \frac{X_{S\ell} - X_{SR}}{YFR}\right] \tag{3-67}$$

It has been assumed that axle location is dependent on the deflection and locating properties of the leaf springs under vertical loading only, i.e., that $X_{S\ell}$ and X_{SR} are functions of $Z_{S\ell}$ and Z_{SR}, respectively. Measurements performed on the two vehicles tested in this study indicates that it is reasonable to assume that this relationship is linear, i.e.,

$$X_{S\ell} = C_{XZ}\, Z_{S\ell} \tag{3-68}$$

$$X_{SR} = C_{XZ}\, Z_{SR} \tag{3-69}$$

Substituting Equations (3-68) and (3-69) into (3-67) yields

$$X_c = C_{XZ}\,\frac{YKP}{2}\left[\frac{Z_{S\ell} + Z_{SP}}{YKP} + \frac{Z_{S\ell} - Z_{SR}}{YFR}\right] \tag{3-70}$$

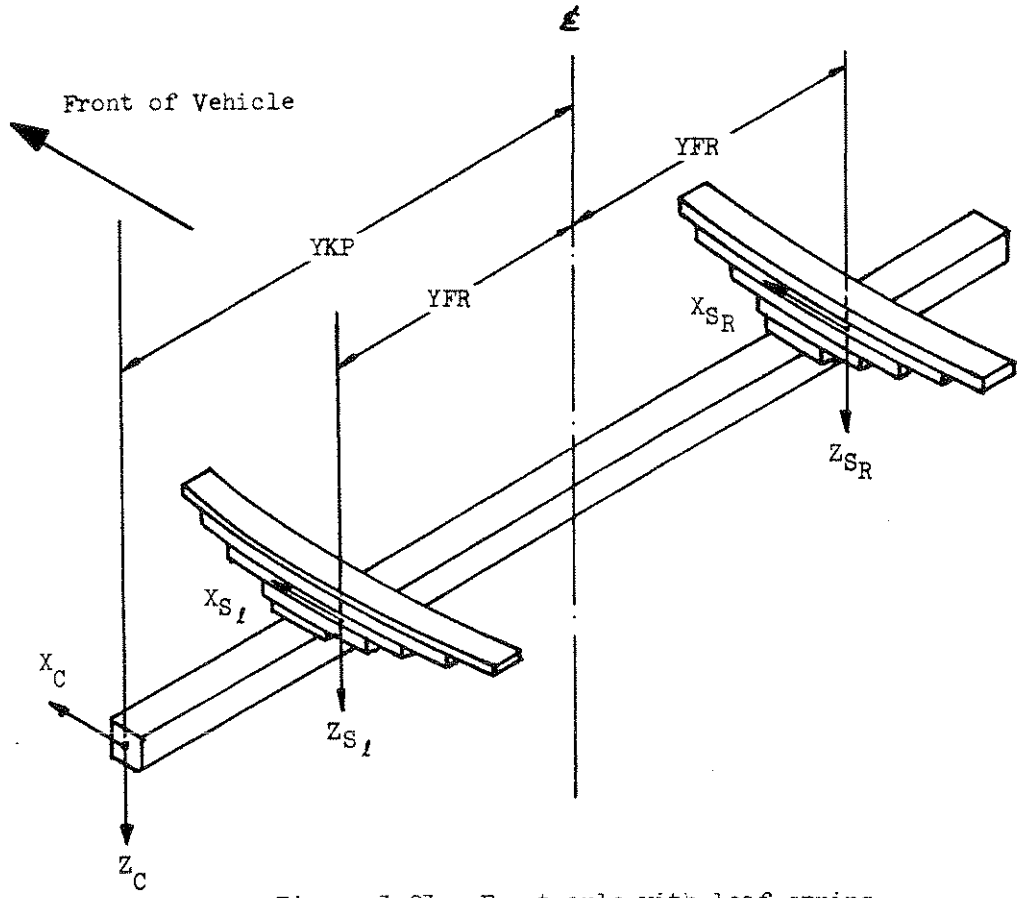

Figure 3-23. Front axle with leaf spring

with the aid of Equation (3-66), Equation (3-70) yields

$$X_c = C_{XZ} Z_c \tag{3-71}$$

The quantities X_c and Z_c may be considered as the components of the differential motion, $\bar{c}$, (ignoring the very small component of $\bar{c}$ in the y direction). That is

$$\bar{c} = \bar{c}(X_c, Z_c) \tag{3-72}$$

and from (3-68)

$$\bar{c} = \bar{c}(C_{XZ}Z_c, Z_c) \tag{3-73}$$

Thus $\bar{c}$ is a function of Z_c only, viz.,

$$\bar{c} = f_4(Z_c) \tag{3-74}$$

Combining Equation (3-65) and (3-74) yields

$$\Delta\delta 1 = \Delta\delta 2 = f_3[f_4(Z_c), \delta T1] \tag{3-75}$$

$$\Delta\delta 1 = \Delta\delta 2 = f(Z_c, \delta T1) \tag{3-76}$$

Measurements conducted in the laboratory, on the two test vehicles indicated that for a particular $\delta T1$, the relationship of Equation (3-76) may be approximated by a linear function of Z_c. That is

$$\Delta\delta 1 = \Delta\delta 2 = C_\delta Z_c \tag{3-77}$$

where

$$C_\delta = g(\delta T1) \tag{3-78}$$

The variable Z_c is the vertical displacement of the left king pin relative to the vehicle frame. Defining Z_{cA} as the vertical motion in inertial space of point C, attached to the axle, and Z_{cS} as the vertical motion in inertial space of an imaginary coincident point attached to the sprung mass, Z_c can be written as

$$Z_c = Z_{cA} - Z_{cS} \tag{3-79}$$

where positive values of Z_c indicate extension of the left front spring.

From Equation (2-10)

$$Z_{cS} = A1 \cdot A(1,3) - YKP \cdot A(2,3) + DELTA\ 1 \cdot A(3,3) + ZN \tag{3-80}$$

where

AL is the static horizontal distance from the sprung mass center to the front axle

DELTA1 is the static vertical distance from the sprung mass center to the front axle

ZN is the change in vertical position of the sprung mass center

The vertical motion, Z_{ca}, can be expressed as

$$Z_{ca} = ZA1 - YKP \cdot \Phi A1 \tag{3-81}$$

where

ZA1 is the deflection of the axle center downward from static equilibrium

ΦA1 is the roll angle of the axle

In the simulation programs, the following series of events occur at each time step:

(1) Equation (3-78) is solved by subroutine TABLE acting on the user input data.
(2) Equation (3-79) through (3-81) are solved for the value of Z_c.
(3) This value of Z_c is used in Equation (3-77) to determine the differential steer angles which are used to modify the driver-commanded steer angle.

To make use of this steering system option, the user must input the commanded steer angles using either the single- or two-table input options. The user must also input an additional table consisting of C_δ versus δT1 data. During a simulation run, Equation (3-78) will be solved through a linear interpolation on this tabulated input.

Although it is permissible to use the roll, pitch and bounce steer option with single table input of commanded steer angle, this practice is not recommended. The approximation introduced by using an average value front wheel steer angle would tend to negate any increased accuracy gained by considering steering caused by the kinematics of the suspension and the steering mechanism.

If the roll, pitch and bounce steer option is used, the axle roll steer option (see previous section) may not be used. (Use of the axle roll steer option implies that all other steer effects are accounted for in the tabular input data.)

The reader is referred to Section 5.3.2 for a description of a test technique which may be used to obtain C_δ.

3.4.6 STEERING SYSTEM COMPLIANCE. The steering mechanisms employed in motor vehicles utilize mechanical components that possess inertial, compliance, and damping properties. For the typical heavy vehicle, these distributed properties can be effectively lumped as shown in Figure 3-24.

An examination of the steer angles and steering wheel angle as measured on two vehicles during testing indicated no dynamic relationship between these two variables. Consequently, it was concluded that the simplified model of Figure 3-25 would suffice to represent steering system compliance. The torsional spring constants SK1 and SK2 are related to SK1' and SK2' and the steering system geometry and they may be determined in the laboratory. The differential steer angles, $\Delta\delta 1$ and $\Delta\delta 2$, about the nominal steer angle result from the deflection of springs SK1 and SK2 under the effect of the tire aligning moments, MZ1 and MZ2.

The equations for the differential steer angles may be derived with reference to Figure 3-25, viz.,

$$\Delta\delta 1 = (MZ1 + MZ2)/SK1 \qquad (3\text{-}82)$$

$$\Delta\delta 2 = \Delta\delta 1 + MZ2/SK2 \qquad (3\text{-}83)$$

The steering system compliance model may be used with either the single or two table steer angle input options. Further, it may be used concurrently with the roll-, pitch- and bounce-steer option, but this model is not allowed if the axle roll steer option has been selected. (Note that the use of the axle roll steer option implies that all other steer effects are accounted for in the tabular input data.) Additional input data are required and a technique for obtaining SK1 and SK2 is described in Section 5.3.3.

It should be noted that brake force application has an important effect on steer angle due to leaf spring wrap-up and king pin offset. These effects are not

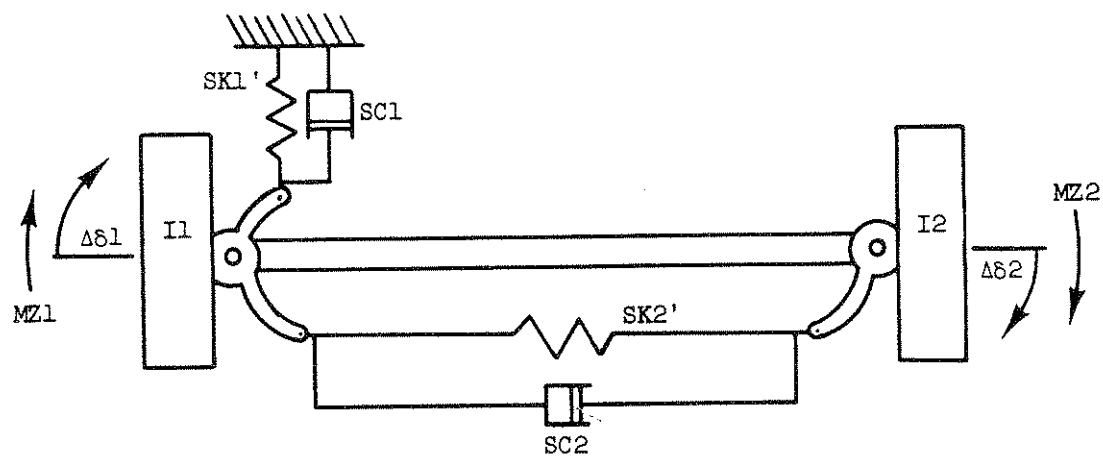

Figure 3-24. Steering system model with inertia, compliance, and damping

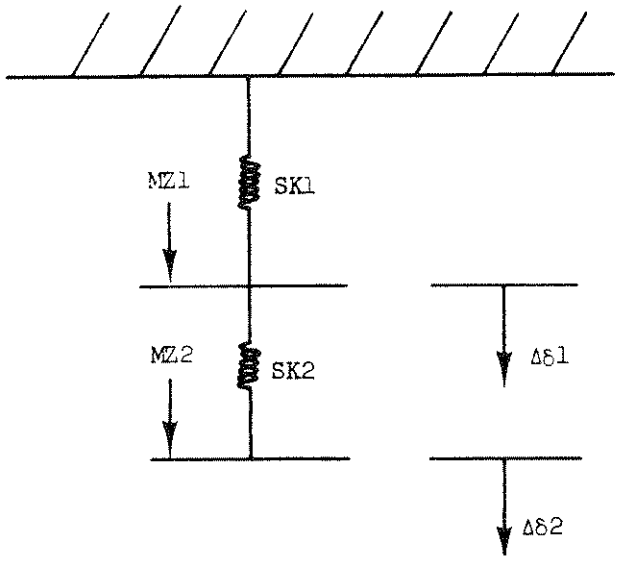

Figure 3-25. Simplified steering system compliance model

modeled here. Consequently, this model is most applicable in turning maneuvers which do not involve braking.

3.5 THE FIFTH WHEEL

The analysis of the mechanics of the fifth wheel, as presented here, departs radically from previous analyses, most notably that of Leucht [6] and Mikulcik [7]. It will be beneficial at this juncture to briefly review their work.

The vehicle model of Leucht entails four degrees of freedom, namely, the yaw plane coordinates X and Y and yaw angle ψ of the tractor, and the articulation angle of the trailer relative to the tractor. It was assumed that the fifth wheel could transmit a yaw moment (due to friction) but no pitch or roll moment. The lateral transfer of wheel loads experienced by the tractor is calculated on the basis of quasi-static considerations with the aid of an input parameter described as the roll rate distribution.* Since roll moments cannot be transferred by the fifth wheel, the roll moments on the trailer are balanced entirely by the lateral transfer of load on the tires of the trailer.

The vehicle model of Mikulcik entails eight degrees of freedom, namely, three coordinate and three rotational degrees of freedom for the sprung mass of the tractor, and two rotational degrees of freedom for the sprung mass of the trailer. The fifth wheel constraint is quite carefully conceived mathematically. When the tractor and semitrailer are in line, the respective roll angles are constrained to be equal, and the appropriate adjustments are made in the presence of an articulation angle. The roll moment transmitted by the fifth wheel is precisely that moment required by the geometric constraint.

Both of the above models could constitute a reasonable simulation of braking and/or handling maneuvers if the dynamics of the unsprung masses are not important, as is the case for vehicles without tandem axles operating on smooth roads, and if the accelerations are reasonably small such that it is not crucial to predict lateral load transfer as carefully as possible. However, to expand the valid range of the simulation, it was felt that a radical departure from the traditional work was called for. In the analysis to be presented herein, the tractor and semitrailer each have six degrees of freedom—there is no geometric constraint at the fifth wheel. There is rather a force and moment constraint in which tractor and trailer are subject to equal and opposite forces and moments dependent on the difference

*Note that, since roll is not included in the model, the system is statically indeterminate and thus requires this additional parameter.

in the fifth wheel position and orientation as measured on the tractor and the semitrailer.

There are benefits to this new formulation:

(1) Fifth wheel constraint results very similar to the models of either Leucht or Mikulcik may be simulated by proper choice of fifth wheel constraint parameters.

(2) The forces and moments being transmitted across the fifth wheel are easily computed. These are summarized on the computer output page entitled "Fifth Wheel Summary."

(3) Since the dynamic coupling caused by a rigid fifth wheel constraint has been removed, no matrix inversion is required to solve for the accelerations. There are, however, more equations to integrate due to the added degrees of freedom.

3.5.1 THE FORCE TRANSMITTED AT THE FIFTH WHEEL. Initially, the fifth wheel position of the tractor and the semitrailer are assumed to be identical. As the simulation run proceeds, however, forces developed at the tire-road interface will cause disparate paths for the fifth wheel position of the tractor and the semitrailer; a distance δ will develop between them. A linear spring and dashpot are the assumed connection at the fifth wheel as is shown in Figure 3-26. The force transmitted is then

$$\bar{F} = KFW \cdot \delta + CFW\,\dot{\delta} \qquad (3\text{-}84)$$

where KFW and CFW are constants describing the spring rate and dissipation.

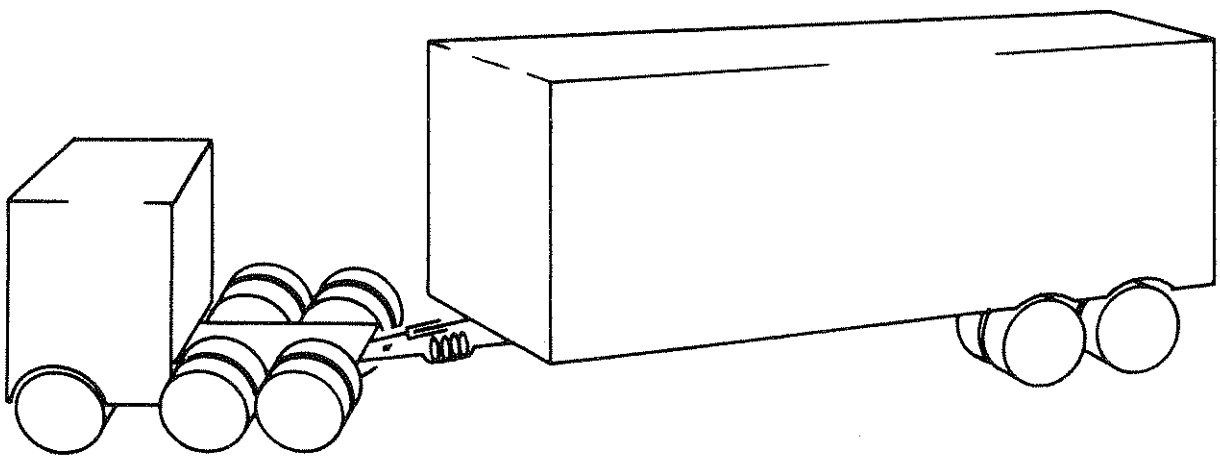

Figure 3-26. Fifth wheel coupling model

The direction of $\bar{F}$ is assumed to be along a line through the fifth wheel location of the tractor and semitrailer. The computation of δ and $\dot{\delta}$, while straightforward, are quite lengthy and thus are left to Appendix C.

Note there is no requirement that the parameters KFW and CFW relate to the actual mechanics of the fifth wheel; they must only prevent large displacement between tractor and semitrailer at the fifth wheel. The following are the requirements for the model:

(a) δ must remain small

(b) KFW and/or CFW cannot be large enough to cause natural frequencies above 10 Hz in the dynamic system (and thus necessitate shortening the integration time step Δt).

The spring rate KFW has been chosen such that, in a hypothetical straight line braking maneuver in which the vehicle is decelerated at 32.2 ft/sec^2 via action of the tractor braking system only, the spring may be expected to deflect less than

1 inch. This criterion is met by setting

$$KFW = (W1 + WS) \text{ lbs/in} \tag{3-85}$$

where

W1 is the sprung weight of the trailer

WS is the unsprung weight of the trailer.

This formulation leads to K values which may be expected to be well within an acceptable range as far as natural frequences are concerned. (Note that the total spring rate of the tires on the tractor rear axles may be much higher.)

The damping CFW is chosen in the following fashion. Consider the simplified articulated vehicle of Figure 3-27, again in a straight line maneuver. For the situation with no trailer braking, the equation of longitudinal motion of the trailer may be written

$$\frac{(W1 + WS)}{g}\ddot{y} + (KFW)y + (CFW)\dot{y} = KX + C\dot{X} \tag{3-86}$$

where W1 + WS is the total weight of the trailer sprung and unsprung masses. Considering the tractor motion as an independent function of time, Equation (3-86) may be rewritten

$$\ddot{y} + 2\zeta\omega_n y + \omega_n^2 \dot{y} = f(t) \tag{3-87}$$

where

$$\zeta = \frac{CFW}{2[\frac{KFW}{g}(W1 + WS)]^{1/2}} \tag{3-88}$$

CFW is chosen such that the dimensionless damping ratio ζ in Equation (3-87) is set to 0.5. In this fashion, unrealistic transients due to the non-rigid fifth wheel coupling are virtually eliminated.

These methods for the choice of KFW and CFW are non-rigorous and, it would seem, may be susceptible to give erroneous results for some range of vehicle parameters. However, this model has proven very satisfactory in the vehicles already simulated. To give the user some assurance that his results from this model are reasonable, the value of $|\delta|$ is printed out on the fifth wheel summary page.

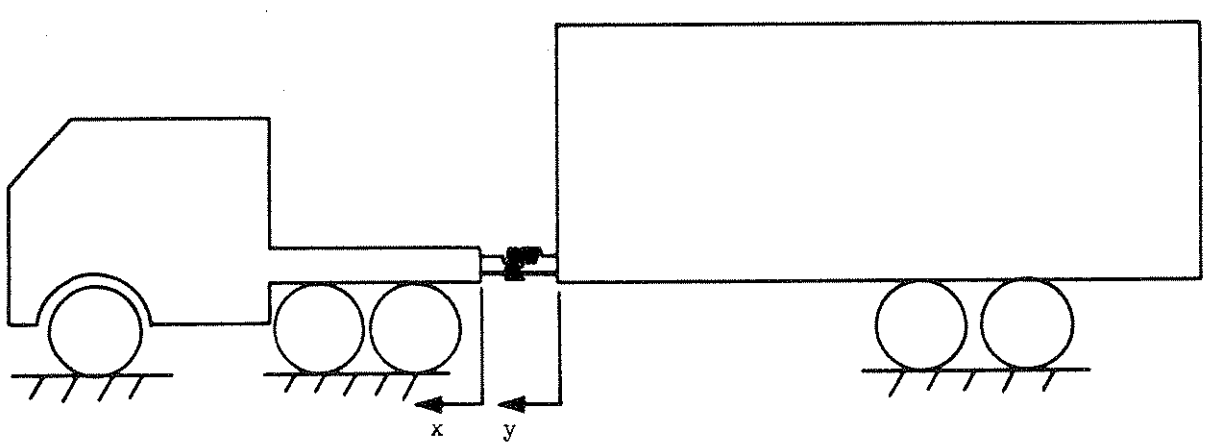

Figure 3-27. Simplified articulated vehicle

Large values of $|\delta|$ would certainly be cause to question the methods of calculation of KFW and CFW given here.

3.5.2 THE MOMENT TRANSMITTED THROUGH THE FIFTH WHEEL. Only a roll moment may be transmitted by the fifth wheel model; the yaw moment due to coulomb friction or anti-jackknife devices at the fifth wheel are neglected. (These may easily be added by the user.) The roll moment, which is assumed to be the product of constant KRM and the difference in roll angles Φ and Φ_t of the tractor and semitrailer fifth wheel, is applied along a line in the $\hat{x}1$ direction (i.e., along the longitudinal axis of the tractor). This is an approximation since Φ and Φ_t are not measured about the same axis; however, quite reasonable roll moments should be expected for reasonable articulation angles. (Note, a large articulation angle would imply that pitch angles would also be a measure of the roll moment, and thus the present analysis would require modification. It is not, however, the goal of this simulation to deal with large articulation angles; to carefully model the jackknife phenomena to its conclusion requires more sophisticated tire model and fifth wheel model than have been considered in any previous work or will be considered here.)

The restoring moment constant KRM is entirely different in purpose from the "spring rate" KFW. The measure of the "proper" operation of KFW is that $|\delta|$ be small; it seems clear that only the proper fifth wheel force can effect that end. The predicted difference in roll angles between tractor and semitrailer will be quite small, however, independent of the choice of KRM. The value of KRM is chosen not to keep the difference between the roll angles small; rather it is chosen to transmit the proper roll moment across the fifth wheel. Thus this constant has been determined experimentally as explained in Section 5.4. (Note that to approximate the fifth wheel model of Mikulcik, as large a value as possible* for KRM would be chosen.)

3.6 THE INCLINED ROADWAY

There is good reason to wish to simulate vehicle performance on real roads. Careful simulation of an actual site could provide insight into the effects of the surface, grade, superrelevation and curvature on vehicle performance, and the combinations of vehicle and roadway factors which simulation shows to be causes for loss of control might be compared with the accident data from that site. However, there are serious difficulties to contend with before such a simulation is feasible.

The first, and perhaps most serious, difficulty is the necessity to "close the loop" if a real road is to be simulated, i.e., to calculate the steer angles during the course of the simulation such that the vehicle model will follow the roadway, rather than to give an input set of steer and braking data and calculate the path of the vehicle model. Simple closed loop models have been attempted for trucks and articulated vehicles by various investigators (for example, [8], [9], [10]). However, it is the belief of the authors of this work that the simulation of an actual driver is a complex task beyond the capabilities of such simplified techniques, and that a simple model might, in some cases, hide meaningful results available from open loop simulation. The user may, however, elect to "close the loop" himself, since a driver model such as those given in [9] and [10] may be easily added to the simulation.**

*Again, limited only by the 10 Hz upper bound on frequency of oscillation.

**The steer model given in [8] is different conceptually from those considered here. The front wheel steer and the braking are degrees of freedom in this model, and the desired trajectory is the input function of time.

In lieu of a driver model, one might wish to specify a realistic terrain and try to gain insight through the analysis of open loop vehicle simulation on such a terrain. This work has been accomplished successfully by McHenry and Deleys for an automobile [11]. The equations of motion, however, are much more complicated than those presented herein, and it was felt that such additional complications would not be in the overall user interest in the case of the present model.*

In view of these considerations, it was decided to use a roadway model in which the normal forces at the tire-road interface are assumed to have only a $\hat{z}n$ component. Thus the model may be thought of as a planar surface, possibly inclined, extending as far as is necessary in the XN and YN directions. It is not, however, assumed that this road surface is smooth. Road profile data in functional or coordinate form may be introduced. But since the normal forces at the tire-road interface do not vary in direction, the fore-aft or lateral forces that might be expected due to surface undulations will not be predicted by the model.

3.6.1 THE EQUATIONS OF THE INCLINED ROADWAY. The initial speed in the longitudinal direction is a user input variable; all other initial conditions are set to zero. Thus, initially, on a level surface the suspension forces add up to the weight of the sprung mass and the moment of the suspension forces about any point is identically zero. The normal forces at the tire-road interface add up to the gross vehicle weight.

This choice of initial conditions, together with the assumption that the vertical suspension forces do not change direction as a function of the orientation of the sprung mass, allow an important simplification of the equations of motion if the roadway is not inclined. In the summation of forces on the sprung mass, only the change in load in the suspensions need be considered, since the static loads will always be equal and opposite the weight of the sprung mass. Thus this choice of coordinates allows consideration of the sprung and unsprung mass equations of motion without any consideration of the force of the weight of the sprung and unsprung masses.

The problem becomes slightly more complicated if the roadway is inclined, since the suspension forces and normal forces remain normal to the road rather than opposite in direction to the gravitational forces. The following is the procedure for adjusting the equations of motion to accommodate an inclined roadway:

(1) The [X1, Y1, Z1] and [XN, YN, ZN] systems (the unsprung mass system and the inertial system, respectively) are again taken to be colinear initially. The direction of $\hat{x}1$ and $\hat{y}1$ will, of course, change in time with the vehicle yaw angle. Note that $\hat{x}n$ and $\hat{y}n$ are in the road plane and $\hat{z}n$ is perpendicular to the road.

(2) The gravity force field, whose direction will be defined by the unit vector $\hat{g}$, may be at an angle with $\hat{z}n$. The user input variables are g1 and g2 where

$$\hat{g} = g1\,\hat{x}n + g2\,\hat{y}n + g3\,\hat{z}n \qquad (3\text{-}89)$$

and

$$g3 = \sqrt{1 - g1^2 - g2^2}$$

Thus the components of the vector $\hat{g}$ define the direction of gravitational forces, or, from a different point of view, the orientation of the "road." A few few examples may be helpful

*These complications would be especially serious in the present work since each of the suspension options would require special treatment.

(a) $$g1 = g2 = 0 \tag{3-90}$$

The gravitational field vector $\hat{g}$ has no component in the $\hat{x}1$ or $\hat{y}1$ directions. Therefore, this surface has no inclindation angle.

(b) $$g1 = .05 \quad g2 = 0 \tag{3-91}$$

The cosine of the angle between $\hat{g}$ and $\hat{x}n$ is 0.05. Thus the XN axis inclines downward as shown in Figure 3-28. The included angle β may be found to be

$$\beta = 90° - \cos^{-1}(.05) \cong 3° \tag{3-92}$$

This corresponds to an initial orientation of the vehicle as facing directly downhill on a 5% grade.

(c) $$g1 = 0, \quad g2 = .05 \tag{3-93}$$

The cosine of the angle between $\hat{g}$ and $\hat{y}n$ is 0.05. Thus the YN axis inclines downward as shown in Figure 3-29. The angle labelled β is about 3°.

The choice of non-zero g1 or g2 or both implies that the gravitational forces applied to the sprung and unsprung masses are not opposite in direction to the suspension forces and the normal forces at the tire-road interface. The appropriate adjustments, however, may be made in a straightforward manner. The initial position of the vehicle will be chosen to be the trim position of the vehicle whether or not the vehicle is on a flat surface. Thus, just as in the case of the flat surface, all initial conditions except the initial speed are zero. As a result, the sprung and unsprung masses cannot be in equilibrium initially unless g1 and g2 are zero.

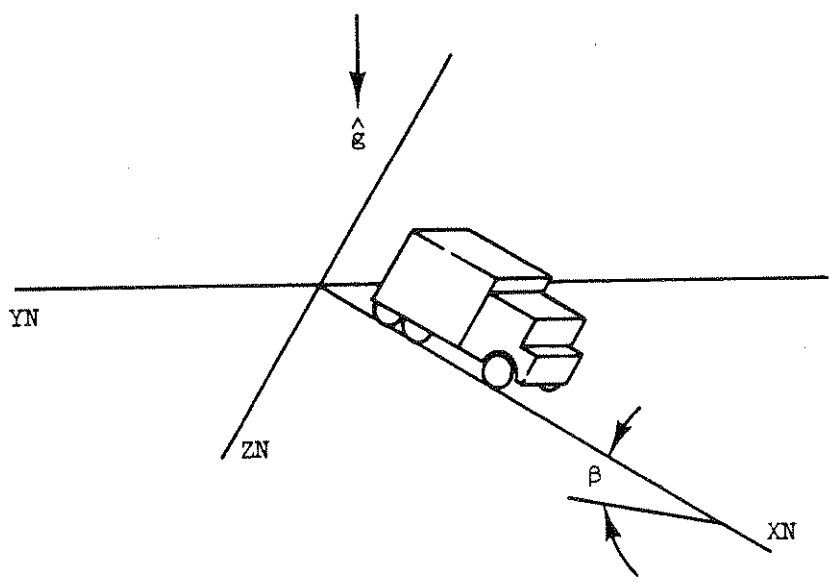

Figure 3-28. The inclined roadway: g1 = .05, g2 = 0.0

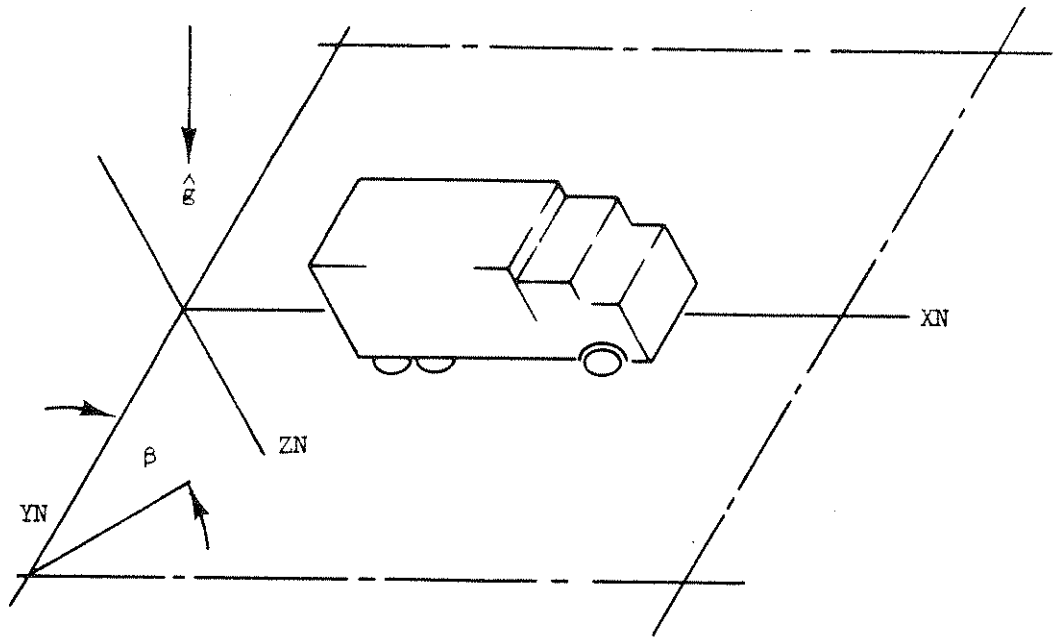

Figure 3-29. The inclined roadway: g1 = 0.0, g2 = 0.05

In the case of non-zero g1 and g2, initially there must be a force imbalance on both the sprung and unsprung masses. On the sprung mass the combination of the suspension forces and the weight may be written

$$\sum\bar{F} = (\sum SF)\hat{z}n + W[g1\ \hat{x}n + g2\ \hat{y}n + g3\ \hat{z}n] \qquad (3\text{-}94)$$

where the first term on the right side is the total suspension force and the second is the sprung weight. Note that, since initially the SF have no net moment about the sprung mass center, there is no moment imbalance.

Equation (3-94) may be rewritten

$$\sum\bar{F} = (\sum SF + W)\hat{z}n + W[g1\ \hat{x}n + g2\ \hat{y}n + (g3-1)\hat{z}n] \qquad (3\text{-}95)$$

The first term in Equation (3-95) is calculated by the algorithm used for a level surface and the second, which is constant, is an additional force applied at the sprung mass center.

The same analysis may be done in the case of the unsprung masses. At each unsprung mass center the force

$$\bar{F} = MS \cdot g[g1\ \hat{x}n + g2\ \hat{y}n + (g3-1)\hat{z}n] \qquad (3\text{-}96)$$

where MS is the appropriate mass, and g is the gravitation constant, may be applied, with the calculation of normal forces and slip angles taking place in the usual way.

3.7 WIND LOADING

The possible modes of application of the wind loading are many and varied. While analytical work has been done (for example, [12]) and has offered insight into the problem, a purely theoretical base on which one might draw in order to write equations suitable for use in vehicle simulation is by no means complete,

thus it is clear that empirical data will, in many cases, be necessary in the simulation. Therefore, the approach taken herein is to supply a subroutine in which the user may program as simple or elaborate a model as seems justified. The basic equations of this subroutine and some sample results are given below.

3.7.1 SUBROUTINE WIND. If the forces and moments due to wind loading are to be simulated, subroutine WIND is called from subroutine FCT at the beginning of each integration time step. Subroutine WIND should return to subroutine FCT the components of the wind forces and their moments about the sprung mass centers in the $\hat{x}1$, $\hat{y}1$ and $\hat{z}1$ directions, i.e., in the longitudinal, lateral and vertical directions. The forces and moments have been called WFORCE(3) and WMOM(3), respectively. Since the common block of subroutine WIND contains virtually all the variables of interest, wind loading as a function of vehicle orientation, velocity and time may be simulated. Note that drag forces as well as side loading may conveniently be modeled.

3.7.2 AN EXAMPLE RUN. In a simulation run of the empty straight truck initially at 30 mph it was desired to simulate a side wind loading at the mass center rising to 500 pounds and decreasing to zero in the course of one second. Below ENTRY WIND in subroutine output the following equations were entered.

```
      DO 10 I = 1,3
      WFORCE(I) = 0.
   10 WMOM(I) = 0.
IF (X .GT. 1.0) GO TO 11
WFORCE(2) = 500.*SIN(3.14*X)
   11 CONTINUE
```

The resulting trajectory is shown in Figure 3-30. Note that the simulated vehicle response is a positive yaw angle, an understeer response.

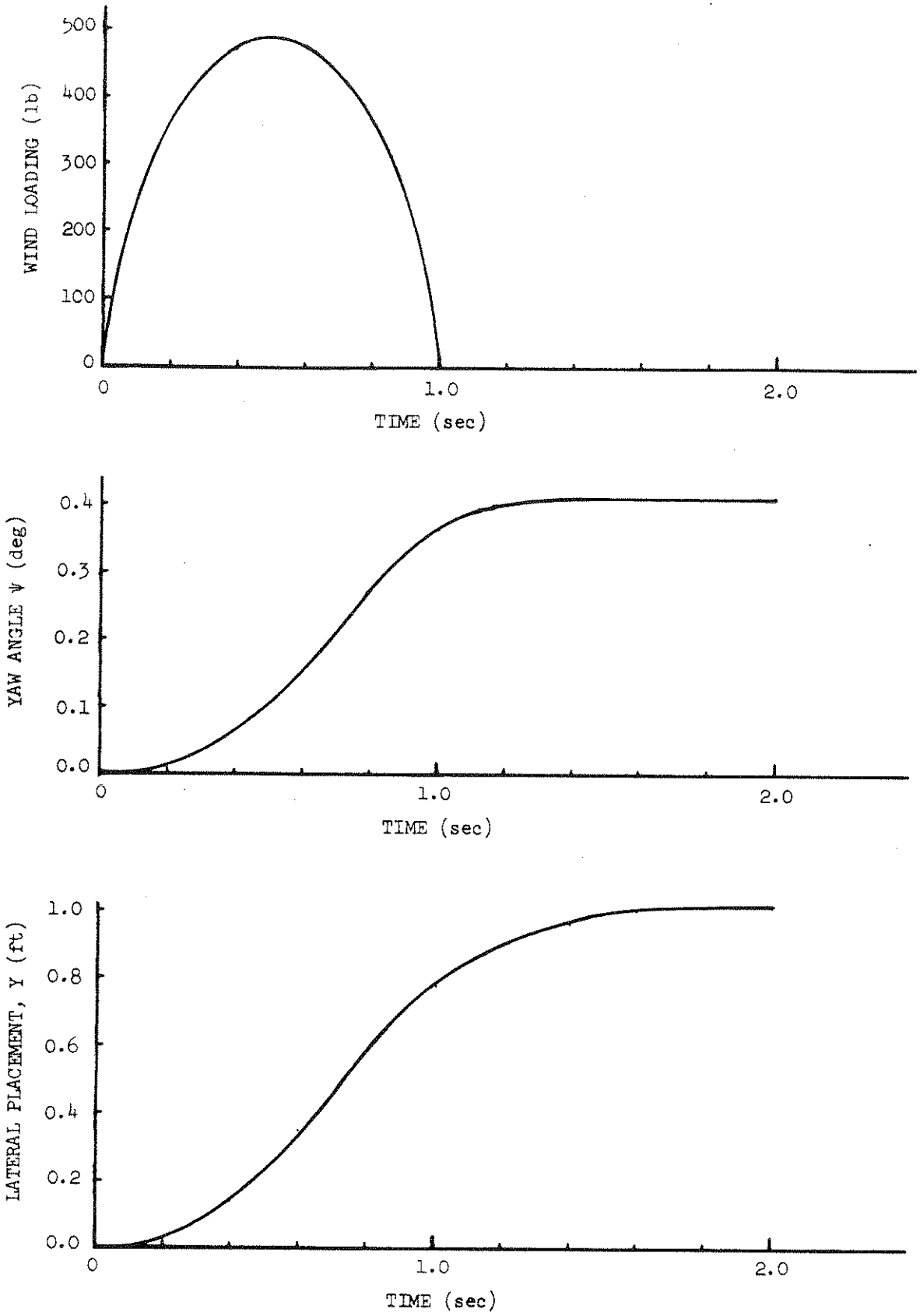

Figure 3-30. Results of wind loading example run

4.0 THE SIMULATION PROGRAMS

4.1 PROGRAM SPECIFICATIONS

The entire program has been written in Fortran IV. The core storage requirements for the articulated vehicle and the straight truck programs, and the integration routine, HPCG, on MTS* are as follows:

Articulated Vehicle	127,976	BYTES
Straight Truck	180,224	BYTES
HPCG	1,382	BYTES

4.2 PROGRAM STRUCTURE

An overview of the program is given in Figure 4-1. With the exception of HPCG, which is an IBM system subroutine, the flow diagrams for each separate subroutine are given in Appendix E. For an explanation of HPCG, the user should consult the HPCG list.

Most algebra is in its most expanded form, and comment cards are used frequently to explain tedious computations. Thus, even a casual Fortran user should be able to follow the logic of all the separate small algorithms that make up the whole. Therefore, changes may easily be made; more variables may be ouput and certain algorithms may be modified.

Certain aspects of the program, however, should be handled with extreme care as inadvised changes may result in errors which may prove difficult to detect and debug. These are listed below:

(a) The integration time step, PRMT(3). This has been carefully chosen based on the physics of the system. While the increase in PRMT(3) from its set value of .0025 may save computer time, it would entail danger of numerical instability and thus incorrect results.

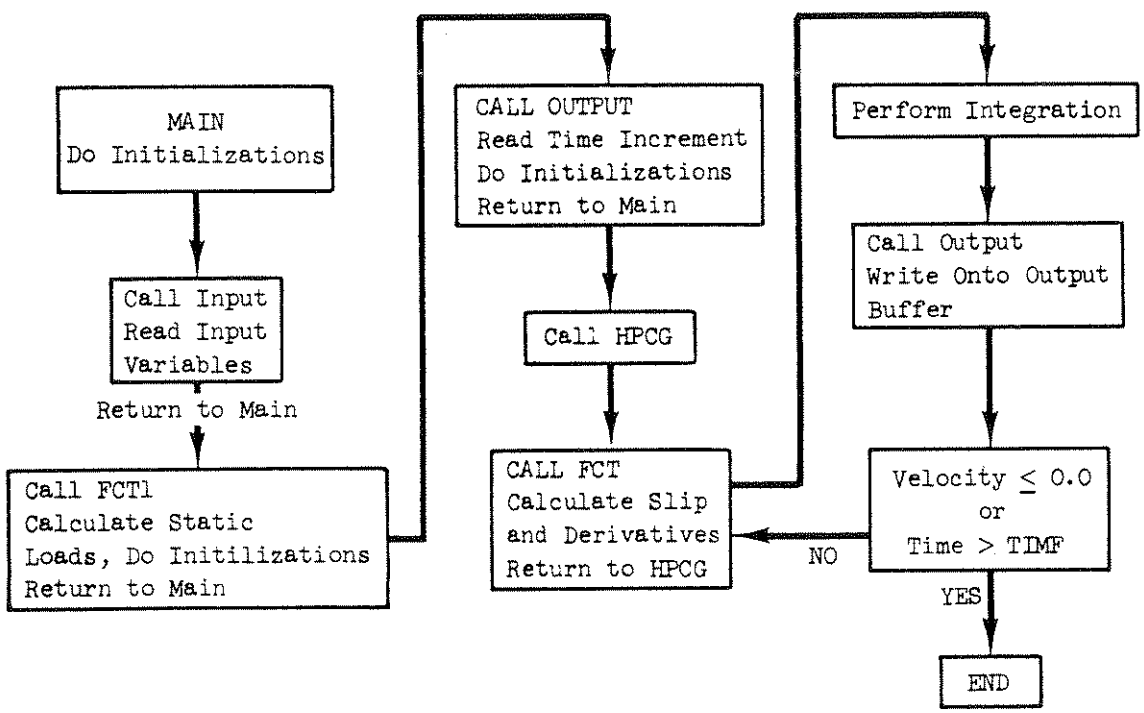

Figure 4-1. Simplified flow diagram, braking and handling performance program

*MTS stands for Michigan Terminal System which is implemented on the IBM 360/67 at The University of Michigan.

Preceding page blank

(b) The slip loop (do loop 5 in subroutine FCT1). The wheel rotational equations of motion are solved to produce wheel velocities and accelerations and brake forces. Any changes should be made only after careful reference to Section 2.4.1 of Reference 1.

(c) The initializations in the beginning of subroutine OUTPUT and FCT1. A false step in this section may result in seemingly correct results which, in fact, are seriously in error.

4.3 SIMULATION COSTS

The cost of the computations will, of course, depend on the options utilized in a particular run. If the most time-consuming options of the articulated vehicle are utilized, the run costs are less than seven dollars per simulated second on MTS. The straight truck runs for about four and one half dollars per simulated second.

5.0 MEASUREMENT OF VEHICLE PARAMETERS

5.1 INTRODUCTION

The parameters necessary for describing the vehicles whose braking and handling performance is to be simulated can be separated into six different categories:

1. Vehicle geometry
2. Suspension and steering system characteristics
3. Inertial properties of vehicle and payload
4. Tire properties and tire-road interface characteristics
5. Brake and brake system characteristics
6. Roll resistance characteristics of the fifth wheel for articulated vehicles.

Extensive parameter measurements were made for the two vehicles tested in this program.* Where it was feasible, parameters were calculated or estimated from design drawings and specifications.

Test procedures used to determine those parameters which are necessary for simulation in the pitch plane were described in the Reference 1. These include suspension spring rates, vertical and longitudinal center of gravity position, pitch moment of inertia of the sprung mass, the rolling moment of inertia of the unsprung mass, and brake system characteristics. These descriptions will not be repeated here.

Measured properties for a wide variety of truck tires are given in Appendix G. The methods used to model these tires are given in some detail in Sections 3.2.2 and 6.3.

The following paragraphs describe the test procedures used to determine the remaining vehicle parameters required as input data for the simulation.

5.2 INERTIAL PARAMETERS

In addition to the inertial properties which were discussed in the Reference 1, the braking and handling simulations require as input data:

1. Yaw moment of inertia of the sprung mass
2. Roll moment of inertia of the sprung mass
3. Yaw moment of inertia of the unsprung masses
4. Roll moment of inertia of the unsprung masses

Inertial properties of the unsprung masses were measured directly (see Section 5.2.3). Then the inertial properties of the sprung masses of the two powered vehicles were determined by (1) measuring the inertial properties for the total vehicle (for the truck, the bare-frame vehicle was measured), and (2) calculating the properties of the sprung masses from the known inertial properties of the unsprung masses and the total vehicle.** The additional effect of the truck body was determined by calculation. Sections 5.2.1 through 5.2.3 describe the test procedures used to measure total vehicle and unsprung mass properties.

The moments of inertia of the trailer were obtained by computing the moments of inertia of each important component part about its own mass center, and then using the parallel axis theorem to find the inertias about the sprung mass center.

---

*The two vehicles tested were: a 50,000 lb gvw Diamond Reo straight truck and a tractor-trailer consisting of a 6 x 4 COE White tractor and a 40 ft Fruehauf van trailer. Vehicle specifications are given in Section 6.

**The appropriate calculations are indicated in [1].

5.2.1 TOTAL VEHICLE YAW MOMENT OF INERTIA.* Figures 5-1 and 5-2 illustrate the technique used to determine the yaw moment of inertia of the bare-frame truck and the tractor. With the suspensions constrained to their static positions by cables, the vehicle is primarily supported at a pivot point, consisting of a 3/4-inch ball bearing in partial spherical seats. This pivot point is located slightly aft of the vehicle c.g., leaving only a small portion of the vehicle weight (a few hundred pounds) to be supported by the front wheels. Under each of the front wheels are placed two steel plates separated by a number of ball bearings. Thus, the front wheels are free to move about on a horizontal plane. A grounded coil spring is attached at right angles to the vehicle at some distance, ℓ_s, from the pivot point. With this arrangement, a small oscillation in yaw may be introduced and the period of oscillation, τ, determined. Using the notation of Figure 5-1 the yaw moment of inertia of the vehicle, I_{zz}, may be determined using Equation (5-1).

$$I_{zz} = \frac{K\ell_s^2\tau^2}{4\pi^2} - \frac{W}{g}\ell_{cg}^2 \qquad (5\text{-}1)$$

Under certain conditions, unwanted oscillations tend to appear during yaw inertia testing. A tendency for the vehicle to oscillate slightly in roll was noted. As it is supported during testing, the vehicle may roll about an axis passing through the ball bearing at the pivot point and the front tire contact point. (The front suspension is effectively rigid due to the constraining cables, and therefore roll can occur only through tire deflection.) This axis is shown by the dashed line in Figure 5-2. To minimize the excitation of roll oscillations, the coil spring was anchored to the vehicle as close to this roll axis as possible. Furthermore, the spring constant, K, and the length, ℓ_s, were chosen such that the natural yaw frequency of the system was considerably different from the roll frequency, thus reducing the tendency for yaw oscillations to excite roll oscillations.

An additional mode of oscillation was observed during yaw inertia tests. The construction of commercial vehicles typically results in considerable torsional compliance of the frame. Consequently, the vehicles showed a tendency to oscillate in a twisting manner along the length of their frames. This problem was effectively reduced by locating the spring near the horizontal centerline of the frame rails, thus reducing the moment resulting from the spring force which was passed into the frame.

5.2.2 ROLL MOMENT OF INERTIA. The pendulum swing shown in Figure 5-3 was used to determine the roll inertia of the test vehicles in their bare-frame condition. The swing is of welded, tubular frame construction and weighs approximately 1800 pounds. This type of construction allows the swing to be strong enough to accept vehicles of up to 25,000 pounds test weight but remain light enough for use with much smaller vehicles.

Two- or three-axle vehicles may be tested. The cross members on which the wheels of the vehicle rest are adjustable along the length of the lower rail of the side members, thus accomodating vehicles of various wheel bases.

During testing, the entire assemble rests on knife edges placed below the center of the "arch" members and atop the supporting pedestals. These arch

*A more detailed discussion of this test method and the associated testing equipment is given in Reference [13].

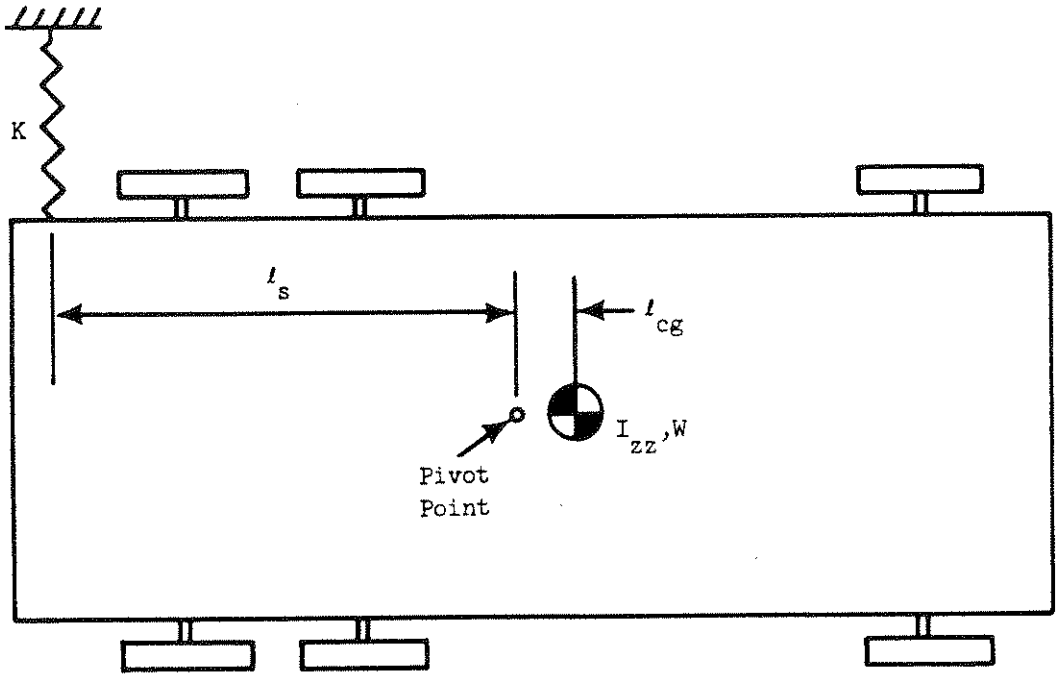

Figure 5-1. Plan view, yaw inertia test

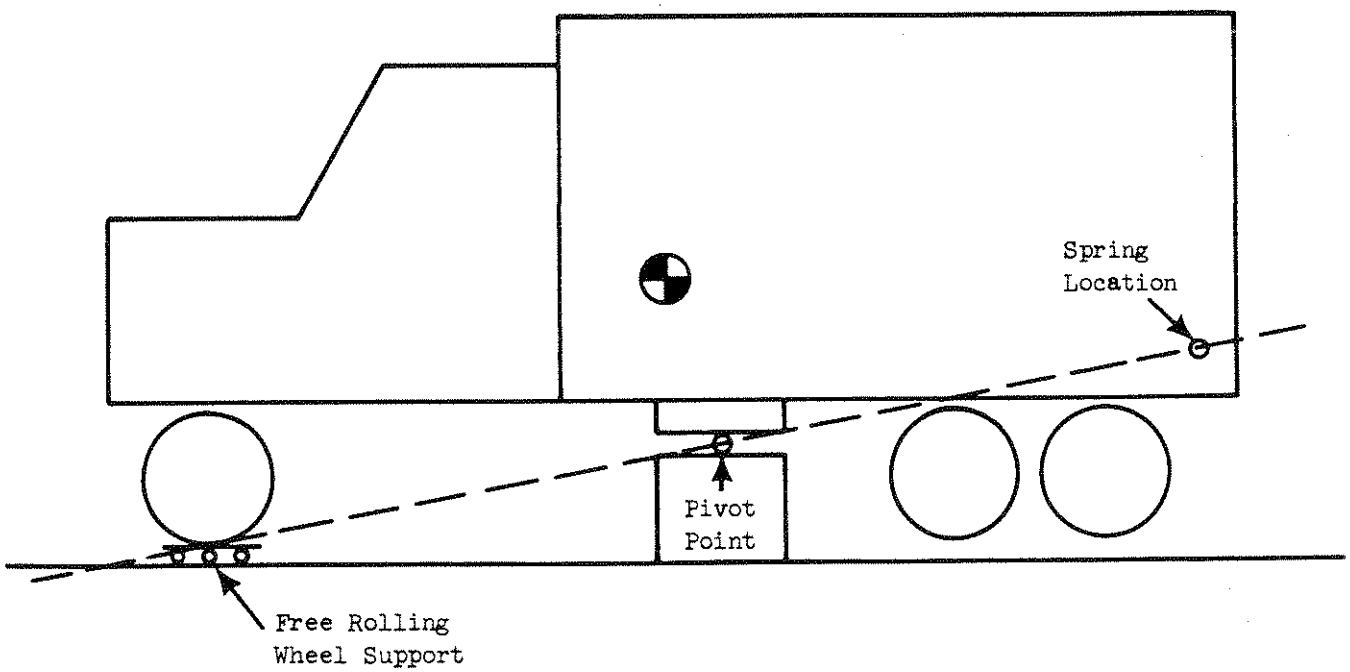

Figure 5-2. Side view, yaw inertia test

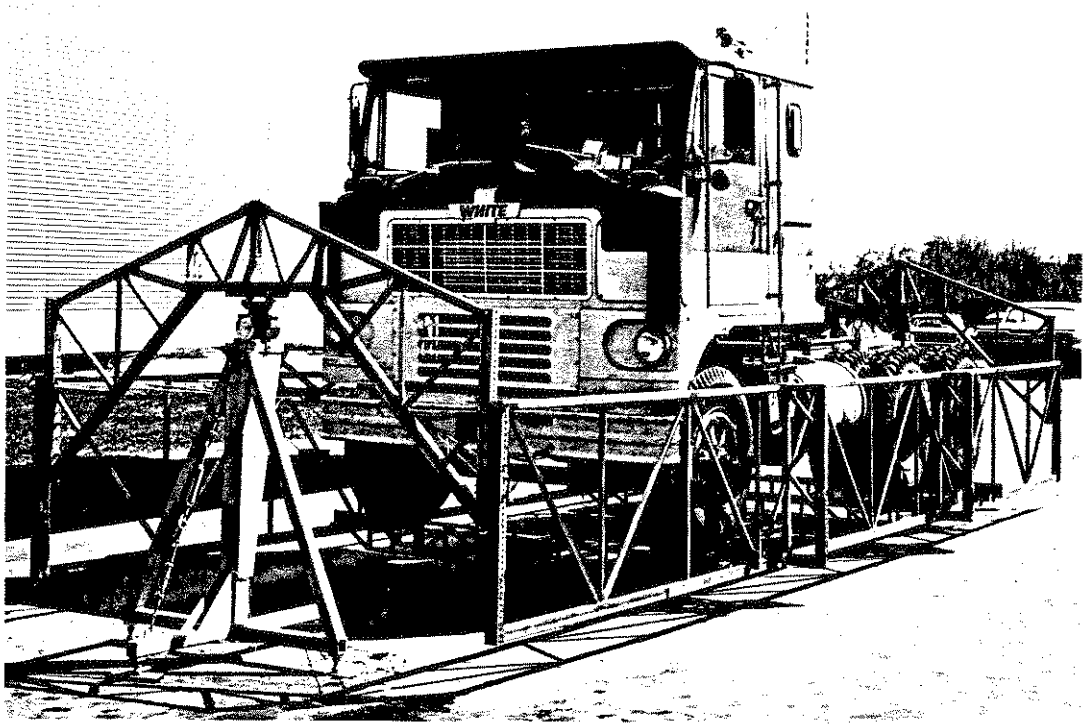

This page is reproduced at the back of the report by a different reproduction method to provide better detail.

Figure 5-3. Roll inertia testing

members may be adjusted to various heights depending on the vertical c.g. position of the test vehicle.

As seen in Figure 5-3, in the roll inertia test mode the arch members are located at either end of the swing with the knife edges placed longitudinally. The swing may also be used to measure pitch moment of inertia, in which case the arch members are located along the side of the swing and the knife edges are placed laterally.

In either case, a small oscillation is introduced and the period of the oscillation, τ, is determined. Using the notation of Figure 5-4, the appropriate moment of inertia is calculated from the following equation

$$I_{ii} = W\ell_o \left[\frac{\tau^2}{4\pi^2} - \frac{\ell_o}{g}\right] + \frac{W_s \ell_s}{4\pi^2}\left[\tau^2 - \tau_s^2\right] \qquad (5\text{-}2)$$

where the subscript i may signify x (roll moment of inertia) or y (pitch moment of inertia), and τ_s is the period of oscillation of the swing along.

5.2.3 MOMENT OF INERTIA OF THE UNSPRUNG MASSES. Roll moment of inertia was measured for the front axle and trailing tandem axle assemblies of each of the powered vehicles. It was assumed that the yaw moment of inertia of an axle assembly was equal to roll moment of inertia of that assembly. It was also assumed that the moments of inertia of the leading tandem axle assemblies were equal to those of the trailing tandem axle assemblies.

The test technique used is illustrated in Figure 5-5. As shown in this figure the axle assembly was suspended on a three-cable, torsional pendulum. A small rotational oscillation was introduced and the period determined.

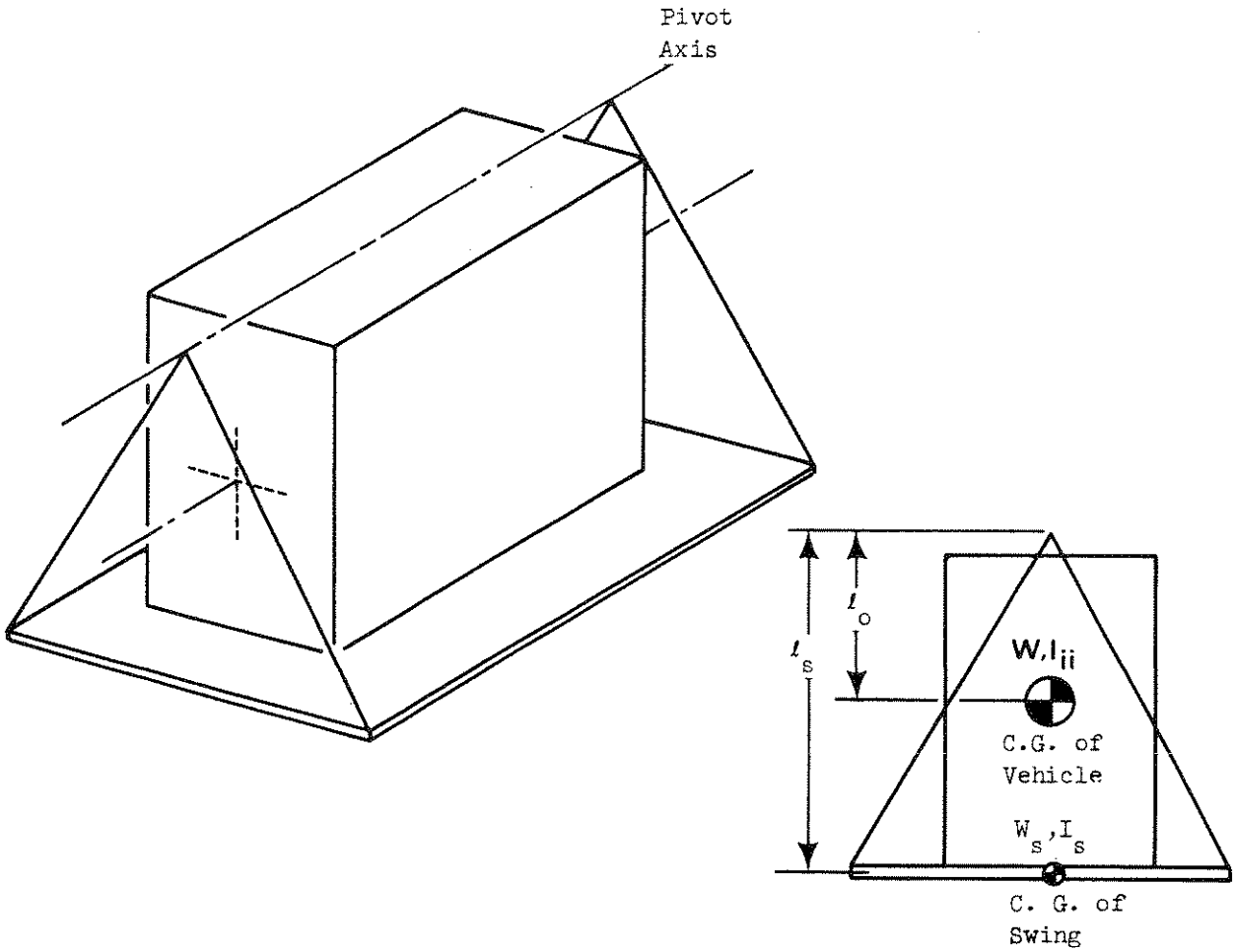

Figure 5-4. Schematic diagram: inertia test device

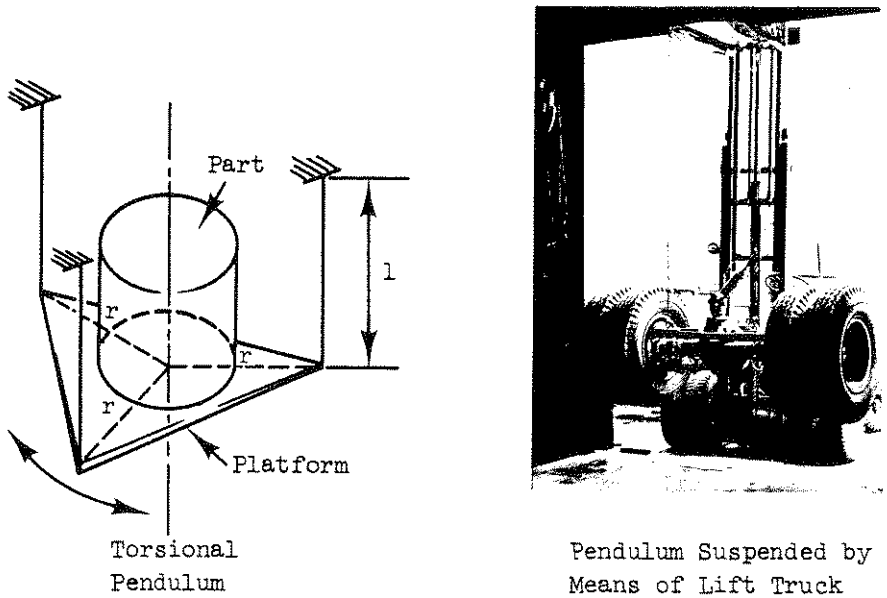

Figure 5-5. Apparatus for measuring moments of inertia of unsprung masses

The equation for calculating the roll moment of inertia, I_{xx}, about the c.g. of the assemblies is

$$I_{xx} = \frac{Wr^2\tau^2}{4\pi^2\ell} + \frac{W_b r^2}{4\pi^2\ell}(\tau^2 - \tau_o^2) \qquad (5\text{-}3)$$

where

W = test weight of the assembly

W_b = weight of the supporting platform

ℓ = length of the supporting cables

r = horizontal distance from center of platform to supporting cables

τ = period of oscillation of platform plus assembly

τ_o = period of oscillation of platform only.

5.3 SUSPENSION AND STEERING SYSTEM PROPERTIES

Measurement techniques used to determine the spring rates and coulomb friction of the various suspension systems were described in [1]. In addition to these spring rates, various parameters of the suspension and steering systems which affect the steer angles of the wheels may be input to the braking and handling simulation.* These include:

(1) Axle roll steer coefficient of each axle

(2) Deflection steer coefficient of the front suspension/steering system

(3) Torsional compliance steer coefficient of the steering system.

The following paragraphs describe the techniques which were used in this study to determine these coefficients.

5.3.1 AXLE ROLL STEER COEFFICIENT. Many common suspensions exhibit roll steer properties. This phenomenon occurs because the axle locating mechanism may cause the axle to move along some curved path, rather than vertically, in the course of suspension bounce and rebound. As the vehicle rolls, this action will impart some steer angle to the axle (see Figure 5-6.)

Due to the beam axle construction of both the steering and the non steering suspensions, this phenomenon is basically the same, although the axle locating mechanisms are quite different, for the three suspension system types considered in this study (single axle front suspensions, and four-spring and walking-beam tandem suspensions). Consequently, the test methods for each of the suspension systems were quite similar in concept.

As shown conceptually in Figure 5-7, the test method consists of deflecting the suspension of interest in bounce and rebound and measuring the path of motion of the axle with respect to the vehicle frame by recording the values of x_ℓ, z_ℓ, x_r, and z_r. (Figure 5-7 illustrates a single axle suspension in which the leaf spring is the axle locating member. Other suspension types with different locating mechanisms are treated similarly.) In pure bounce and rebound, the path of motion of the axle ends will be identical to the paths of the axle at the lateral position of the locating members. That is, in Figure 5-7 paths a, b, c, and d are identical in the x-z plane.

*Section 3.4 describes the steering system models in which these parameters are employed.

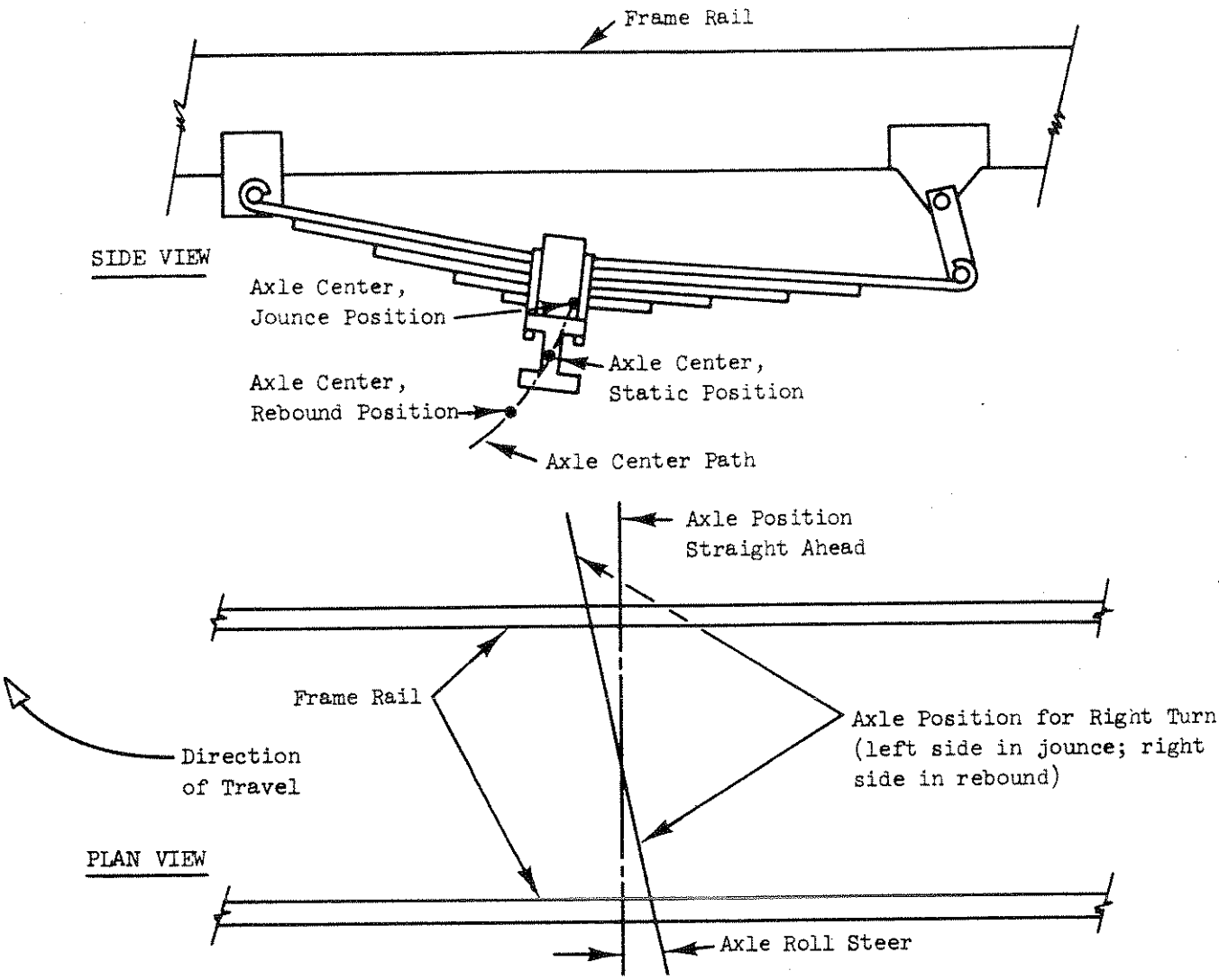

Figure 5-6. Schematic diagram: axle roll steer

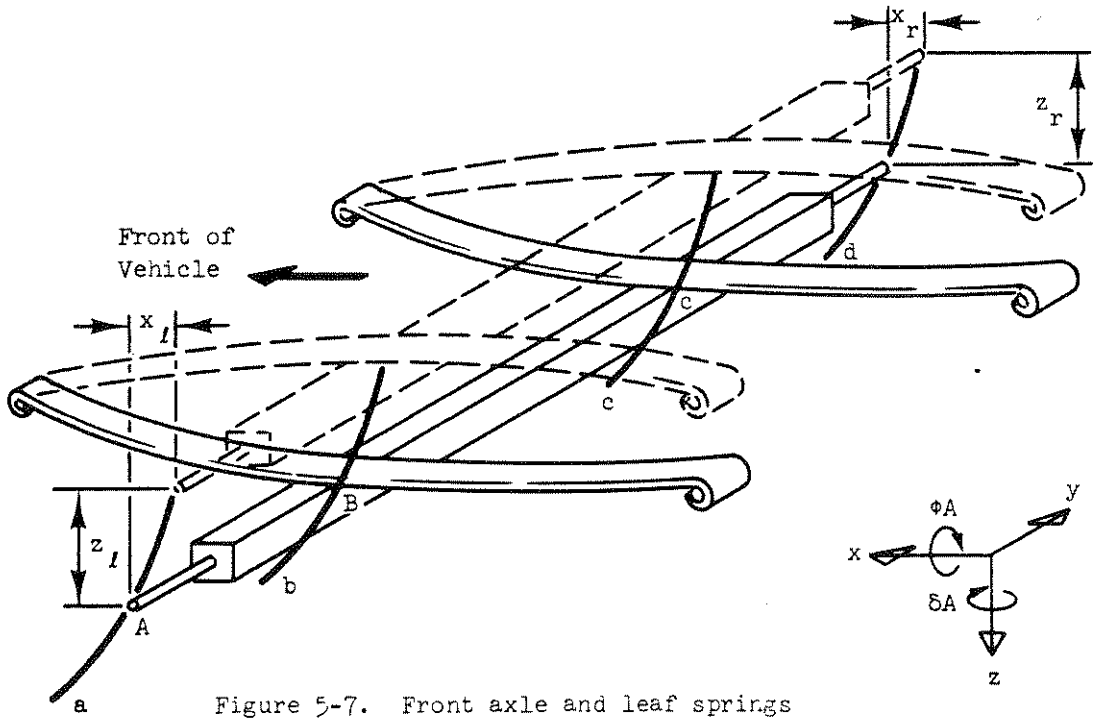

Figure 5-7. Front axle and leaf springs

The following assumptions are reasonable and lead to a useful method of computation of roll steer. In the notation of Figure 5-7:

(1) Points B and C will lie on b and c, respectively, for all axle motions.

(2) In the x-z plane, either of paths a, b, c, or d can be respresented as

$$x = (RSC) \cdot z \tag{5-4}$$

where RSC is some constant.

(3) The body roll angle θ, the axle roll angle, θA, and the axle roll-steer angle, δA, are small.

Using these assumptions, it can be shown that

$$\delta A = (RSC)(\phi - \phi A) \tag{5-5}$$

The quantity RSC is then, by definition, the axle roll-steer coefficient and can be deduced directly from the test data through the use of Equation 5-4 rewritten in the following form*

$$RSC = \frac{x}{z} \tag{5-6}$$

In practice, the tests for the axle roll-steer coefficients were conducted concurrently with those for suspension spring rates and coulomb friction. The technique used to apply load to the suspensions, thus inducing suspension deflections, is described in Reference 1. Measurement of the vertical and longitudinal components of the axle motion was accomplished with the aid of the apparatus shown in Figure 5-8. A pointer, indicating the axle centerline and extending out beyond the body of the vehicle, was attached to each wheel hub of the test suspension. A V-shaped reference frame was rigidly attached to the vehicle body. As the suspension was deflected incrementally, vertical and longitudinal motions of the pointer relative to the frame were measured using adjustable parallels and caliper.

When testing front suspensions, in order to insure that motion of the pointers was the same as the motion of the axle, the steering system drag link was disconnected from the left steering knuckle and the wheels were fixed in position at a nominally zero steer angle.

For each suspension tested, pointer motion was recorded at each wheel. The average deflection characteristics of each of five suspensions tested are illustrated in Figures 5-9 through 5-13. Linearizing the data and applying it to Equation 5-6 yields the roll-steer coefficients given in Table 5-1.

TABLE 5-1
Roll-Steer Coefficients

Straight Truck		Tractor		Trailer
Front	Rear	Front	Rear	
0.26	-0.02	0.27	0.14	0.12

*The proper sign of the axle roll-steer coefficient is arrived at by observing the sign conversions of x and z in Figure 5-7. Axle motion as shown in the figure, i.e., the axle moves rearward with bounce, results in a positive value of RSC. A positive coefficient indicates nominal roll understeer for a front axle or oversteer for a rear axle.

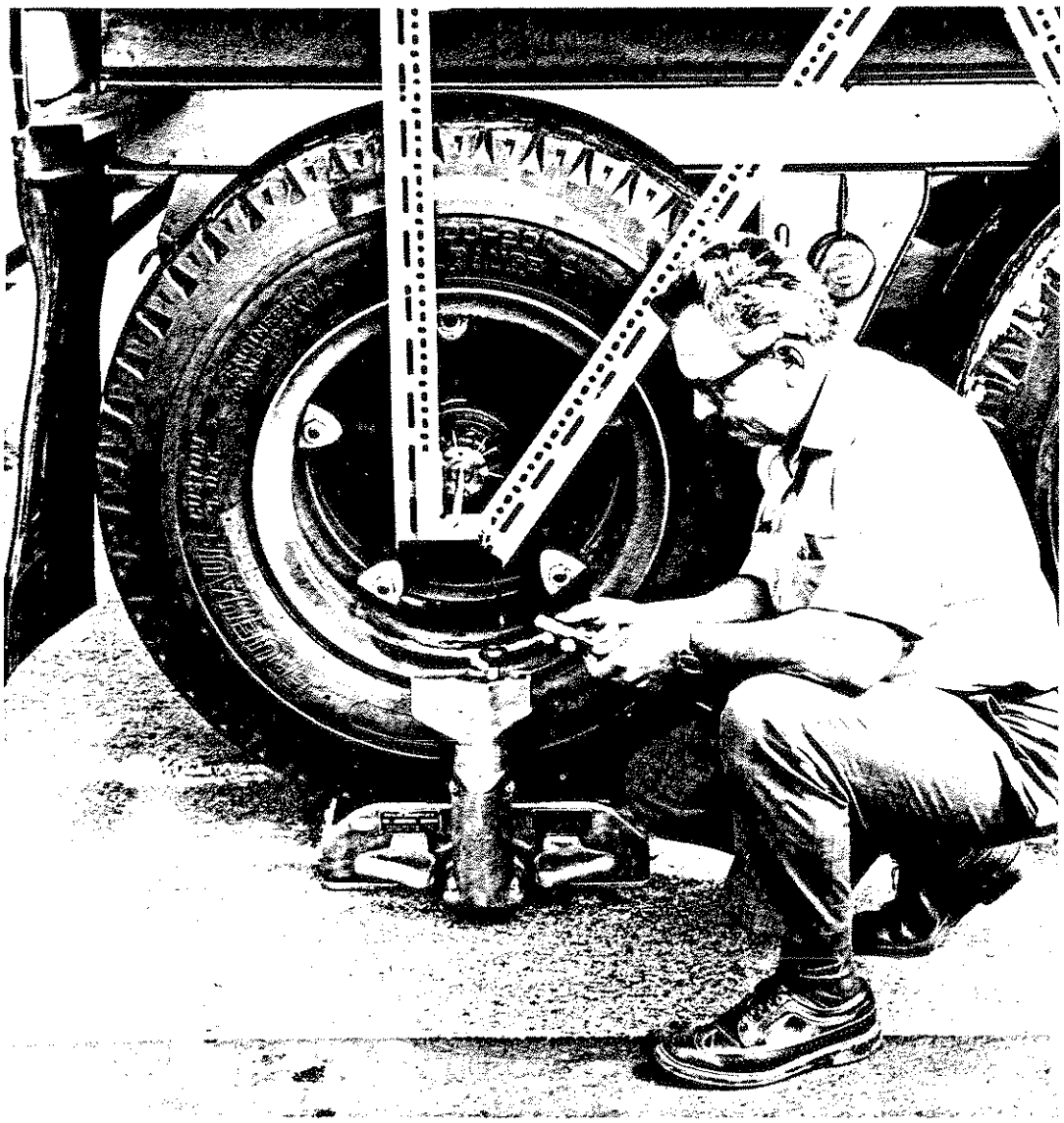

Figure 5-8. Axle displacement measurement

5.3.2 ROLL, PITCH, AND BOUNCE STEER COEFFICIENT. As discussed in Section 3.4.6, C_δ, the deflection steer coefficient of the front suspension/steering system, is a linear coefficient which relates the differential steer angle of the front wheels to the vertical deflection of the left kingping for a given nominal attempted steer angle. The simulation program allows input of a table of C_δ values versus attempted left wheel steer angle.

The test method used to obtain C_δ utilizes the pointer and reference frame apparatus discussed in Section 5.3.1 (see Figure 5-8), at each front wheel with the addition of another reference frame spaced further out on the pointer, as illustrated in Figure 5-14.

Prior to the test, the vehicle steering wheel is locked into position corresponding to the attempted left wheel steer angle which is desired. The front axle is then incrementally deflected in bounce and rebound during which the vertical displacements of each pointer, at lateral positions corresponding to the position of the two reference frame (see Figure 5-15) are recorded.

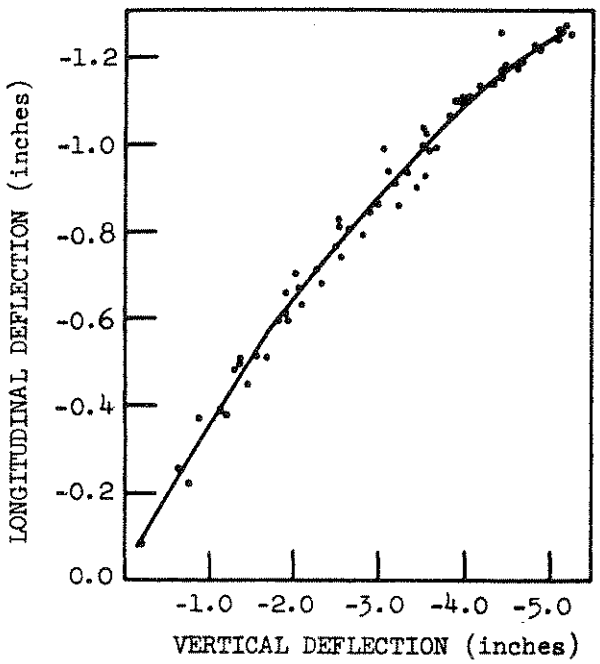

Figure 5-9.
Average deflection characteristics, truck front suspension

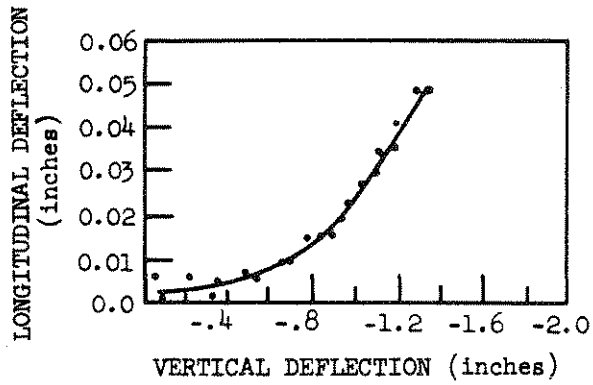

Figure 5-10.
Average deflection characteristics, truck walking beam suspension

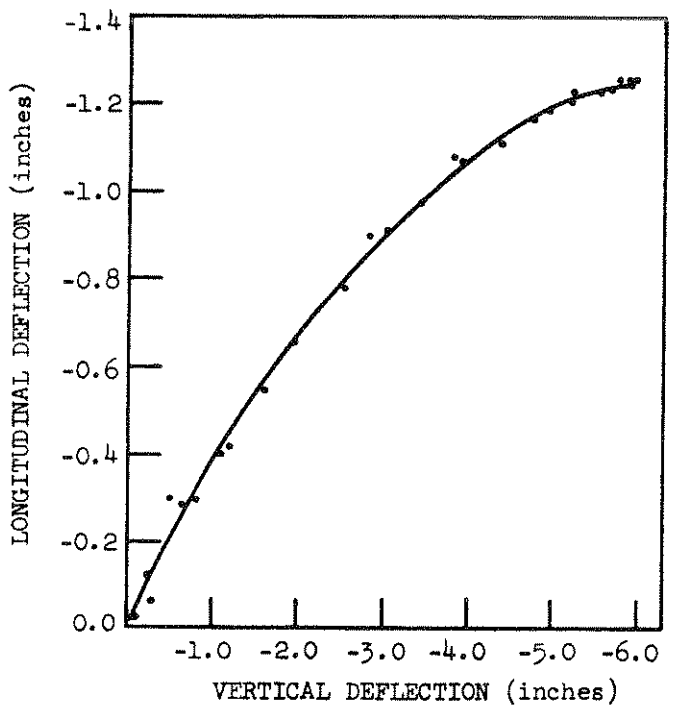

Figure 5-11. Average deflection characteristics, tractor front suspension

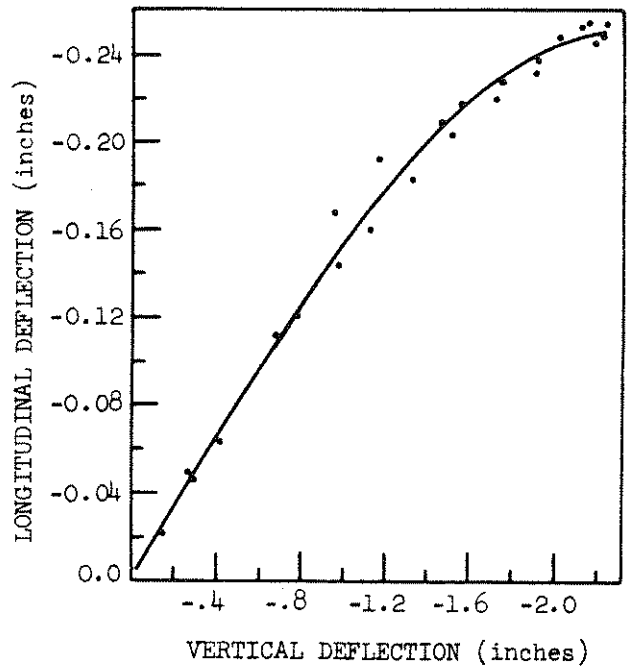

Figure 5-12. Average deflection characteristics, tractor four spring suspension

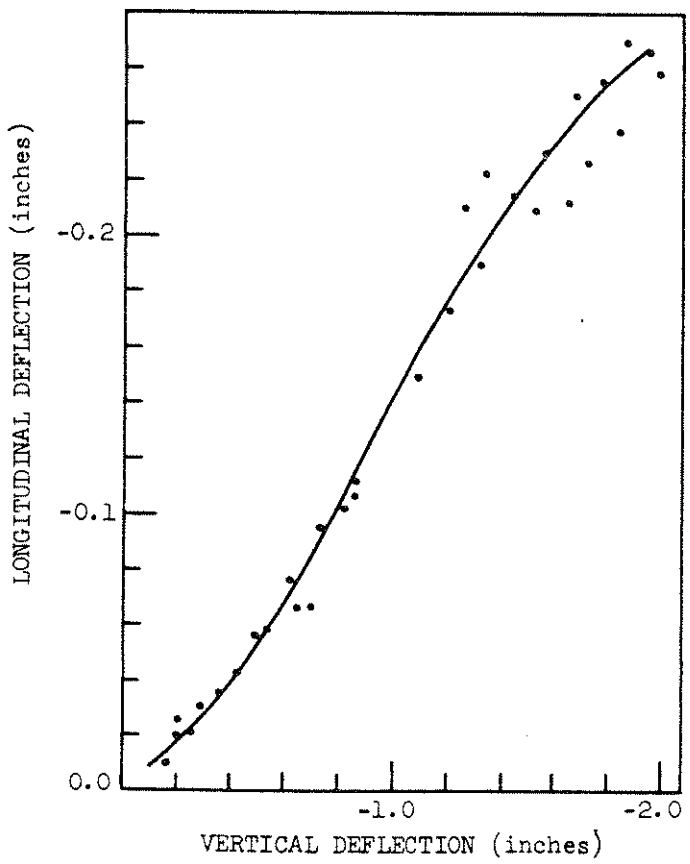

Figure 5-13. Average deflection characteristics, trailer four spring suspension

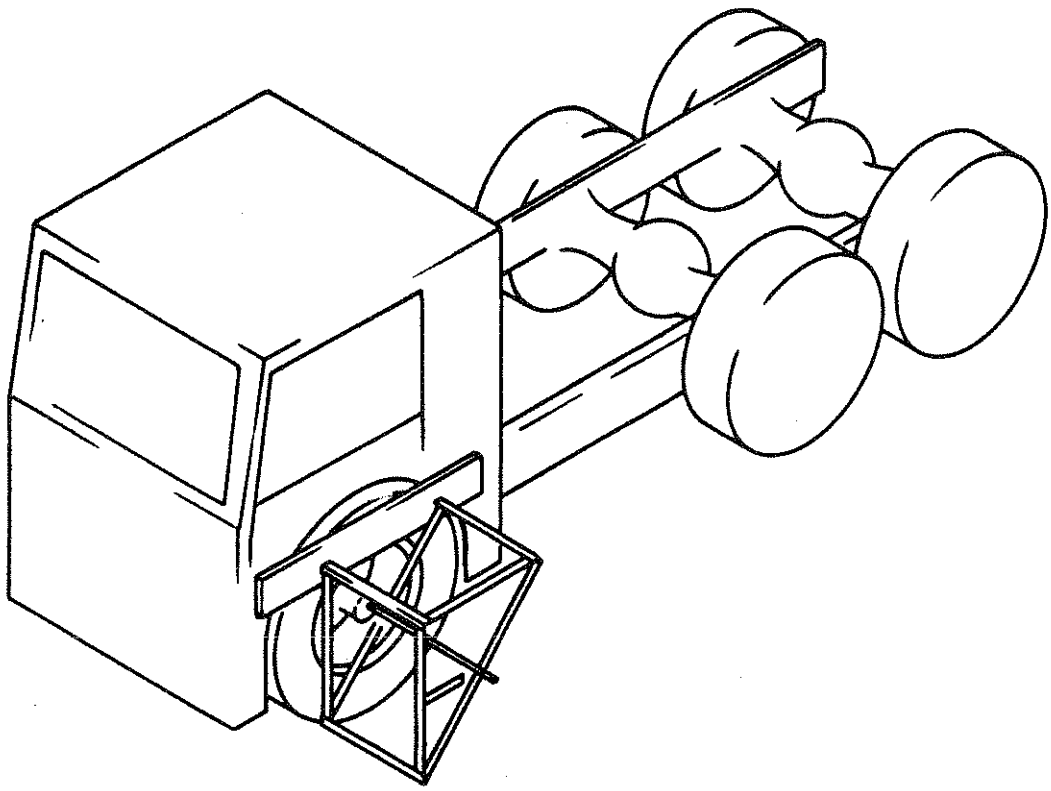

Figure 5-14. Deflection steer measurement device

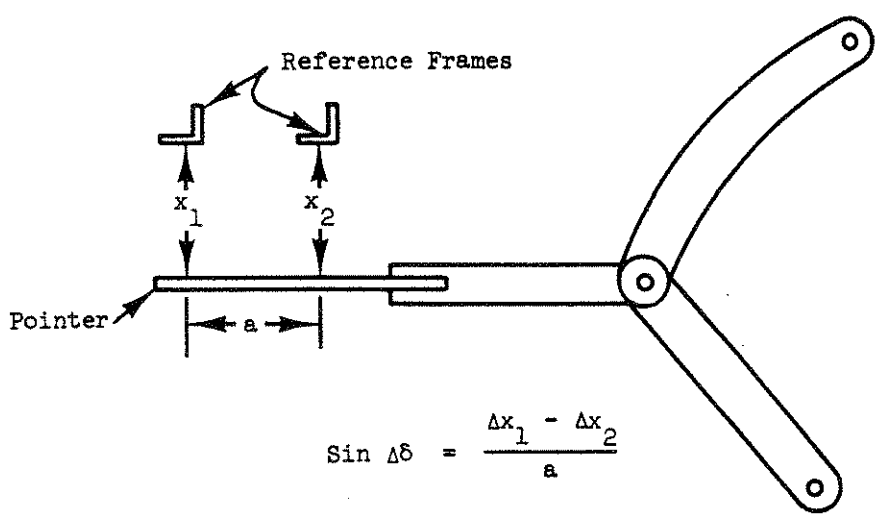

Figure 5-15. Measurement scheme for deflection steer coefficient tests

Using the notation of Figure 5-15, the steer angle of the left wheel is

$$\delta 1 = \sin^{-1} \frac{x_2 - x_1}{a} \tag{5-7}$$

The differential steer angle is then

$$\Delta\delta 1 = \delta 1 - \delta 1A \tag{5-8}$$

where $\delta 1A$ is the attempted left steer angle. Similar equations hold for the right wheel.

The results of the test and the calculations indicated by Equations (5-7) and (5-8) are presented in a plot of averaged left and right side differential steer angle vs. vertical deflection of the wheel pointer. The slope of this plot at the origin is C_δ. The sign convention of C_δ is determined by the body axis system assumed throughout this study. Since steer angles to the right are positive and vertical motion is positive downward, C_δ is positive for a steering system which produces differential steer angles to the right due to axle rebound.

Plots of average differential steer angle vs. vertical deflection at an attempted zero steer angle are presented for the two powered test vehicles in Figures 5-16 and 5-17.

5.3.3 STEERING SYSTEM COMPLIANCE PARAMETERS. The steering system compliance option outlined in Section 3.4.6 requires input of two steering system compliance parameters SK1 and SK2. The test method used to obtain these parameters is illustrated in Figure 5-18.

During this test the vehicle is supported such that the front wheels are not in contact with the ground, however, the front suspension is held in its static loaded position by the load application equipment used in the front suspension spring rate tests. (Details of this test are given in Reference 1.) The steering wheel of the vehicle was locked in the straight ahead position. The steer angle measurement equipment, including wheel pointers and reference frames described in Section 5.3.2, are used to measure differential steer angles, $\Delta\delta 1$ and $\Delta\delta 2$.

As shown in Figure 5-18, a moment of magnitude $a \cdot F$ is applied to the right front wheel by tightening the turnbuckle of the cable-pulley arrangement [15]. Tensile force in the cable, F, is measured through the use of a load cell.

Referring to the steering system compliance model of Section 3.4.7, the torsional spring constants, SK1, SK2, can be obtained from the results of this test through the use of the following equations:

$$SK1 = \frac{a \cdot F}{\Delta\delta 1} \tag{5-9}$$

$$SK2 = \frac{a \cdot F}{\Delta\delta 2 - \Delta\delta 1} \tag{5-10}$$

Plots of moment $(a \cdot F)$ vs. $\Delta\delta 1$ and $\Delta\delta 2 - \Delta\delta 1$ for the two powered test vehicles appear in Figures 5-19 and 5-20. The data clearly indicate that hysteresis and lash, as well as compliance, exists in the steering system. The simulation model considers only the effect of compliance, however. The values of SK1 and SK2 are derived from the slope of those portions of the curves in which the absolute value of moment is rising, since this will generally be the condition during simulated maneuvers. The values derived in this manner appear in Table 5-2.

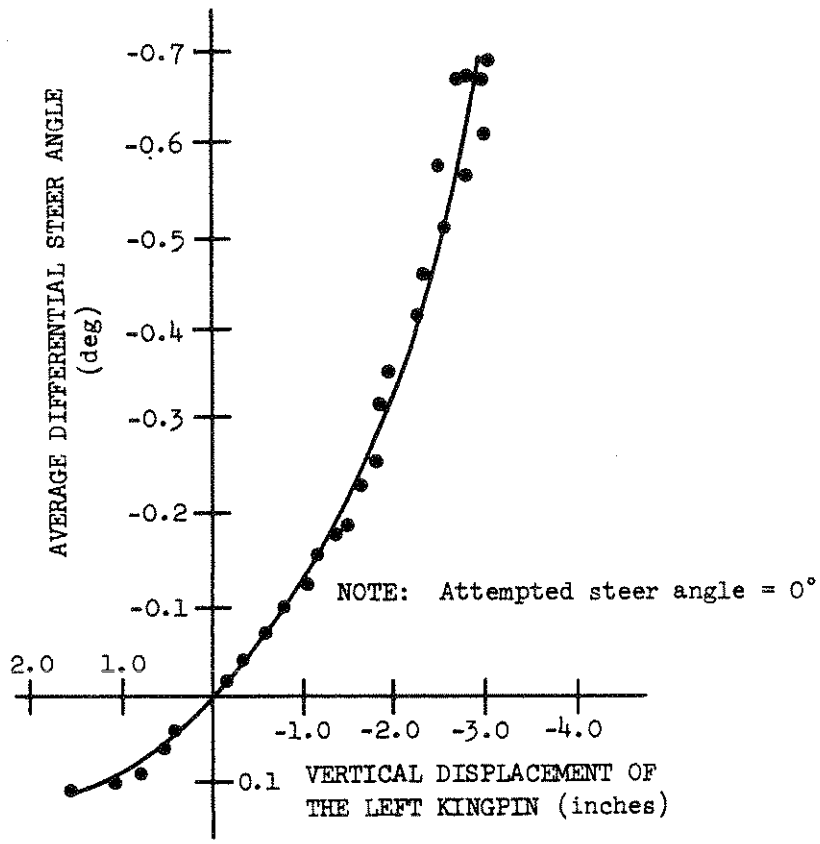

Figure 5-16. Deflection steer data for the truck

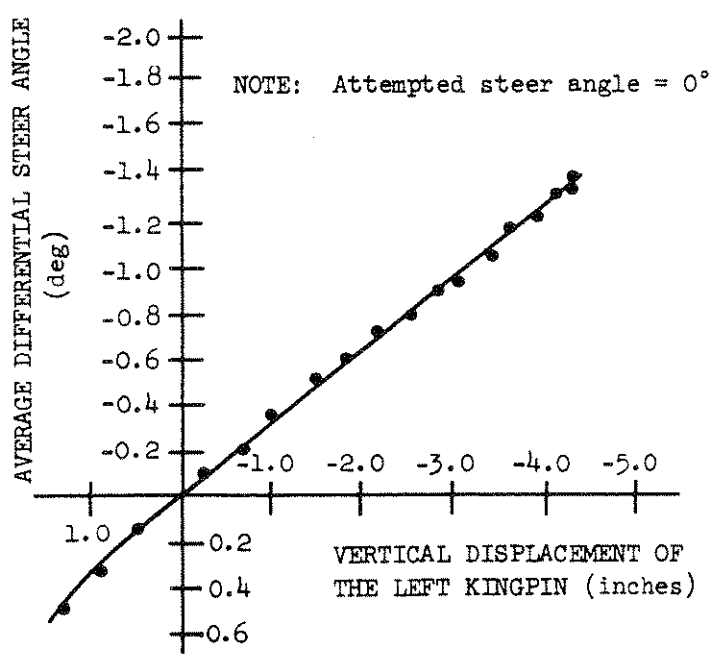

Figure 5-17. Deflection steer data for the tractor

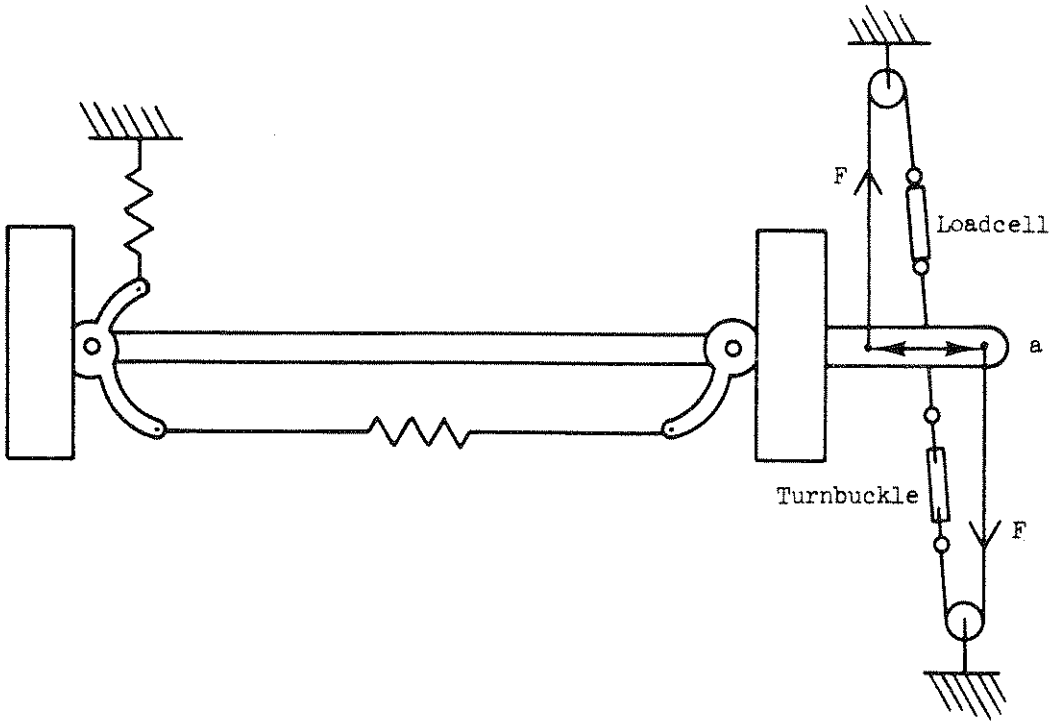

Figure 5-18. Scnematic diagram of steering system compliance measurement

TABLE 5-2
Steering System Compliance Parameters (in.-lb/deg)

Straight Truck		Tractor	
SK1	SK2	SK1	SK2
17,000	24,000	8,400	18,200

5.4 FIFTH WHEEL ROLL SPRING CONSTANT

The static model, on which the test method for determining the torsional roll spring constant of the fifth wheel connection point is based, is shown in Figure 5-21. As shown in this figure, during the test, a roll moment, T, is applied to the trailer. This moment is balanced by the three couples, a·T, b·T, and c·T where:

$$a + b + c = 1 \qquad (5\text{-}11)$$

The spring rates KΦF, KΦR, and KΦT are functions of the suspension geometry, suspension spring rates, and tire vertical spring rates. Referring to the notation of Figure 5-22, illustrating a front suspension system, KΦF for small suspension deflections may be expressed:

$$K\Phi F = \frac{2}{\frac{1}{K1(YFR1)^2} + \frac{1}{KT1(TRA1)^2}} \qquad (5\text{-}12)$$

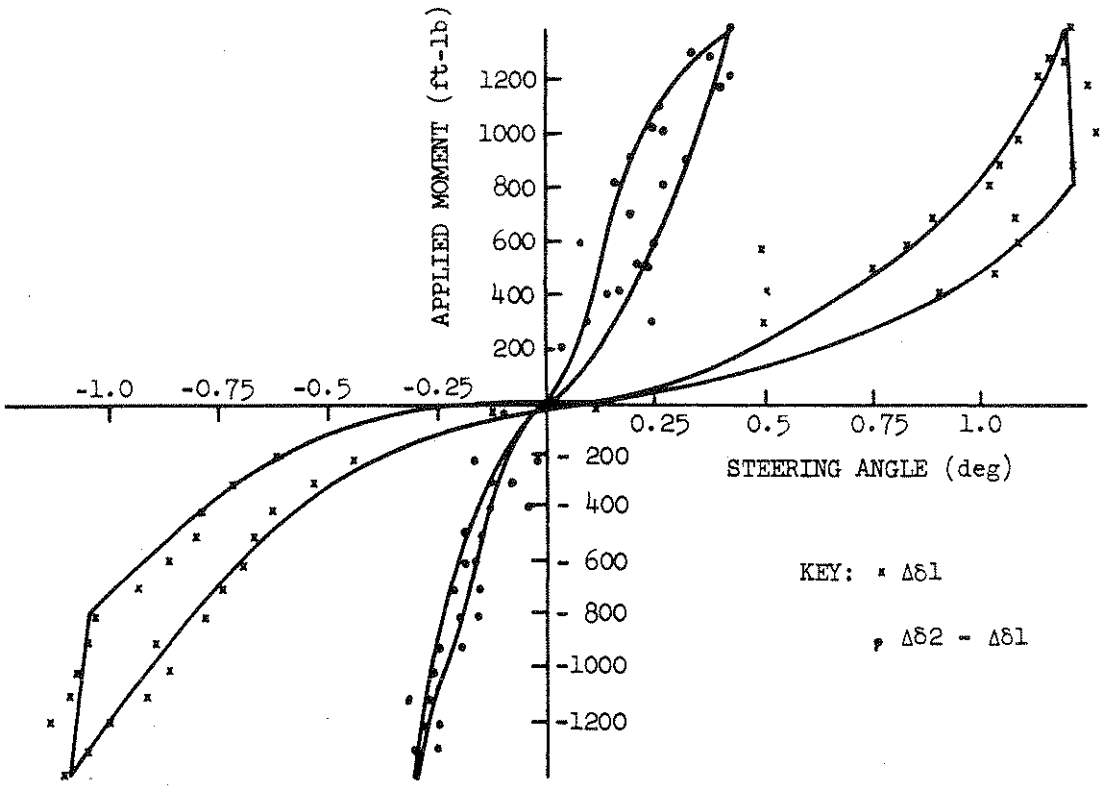

Figure 5-19. Steering system compliance properties of the truck

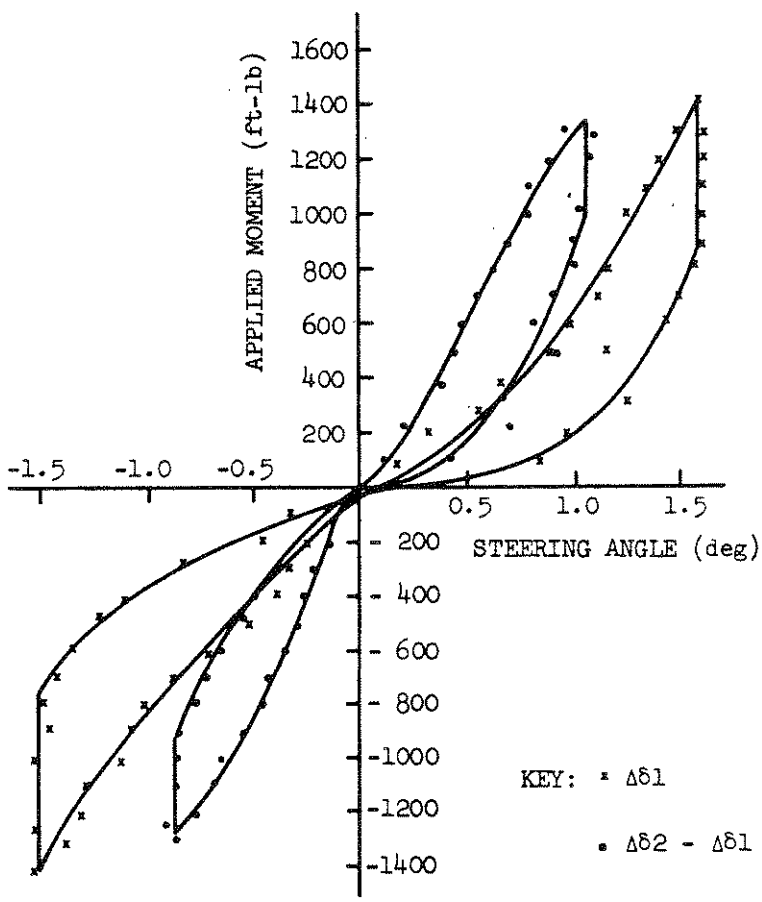

Figure 5-20. Steering system compliance properties of the tractor

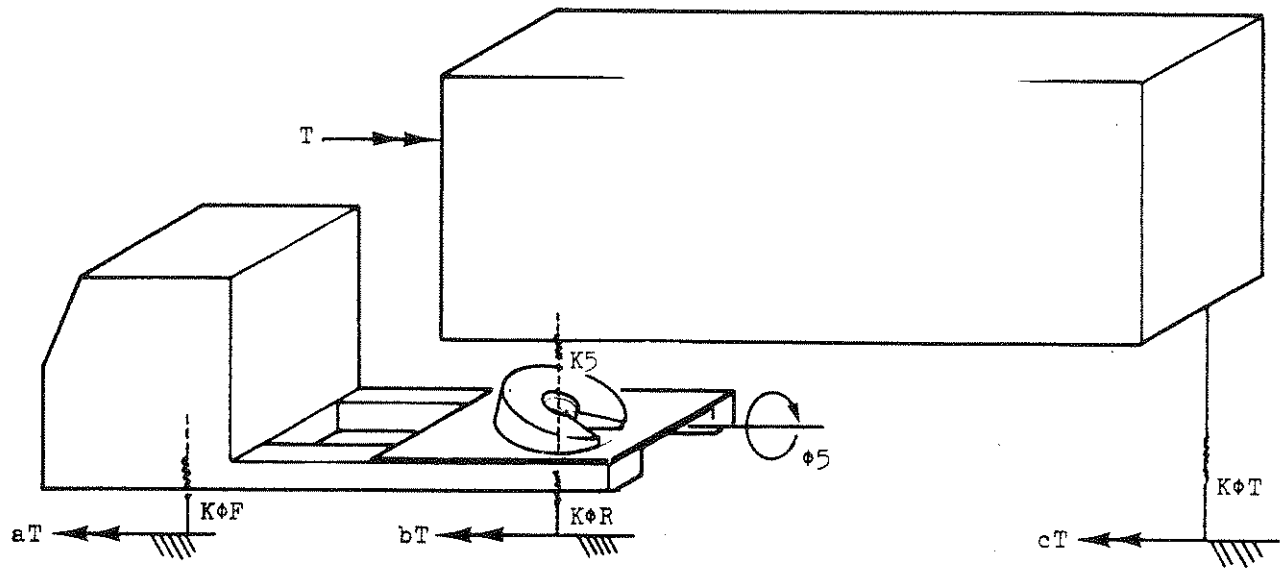

Figure 5-21. Schematic diagram: fiftn wneel roll spring test

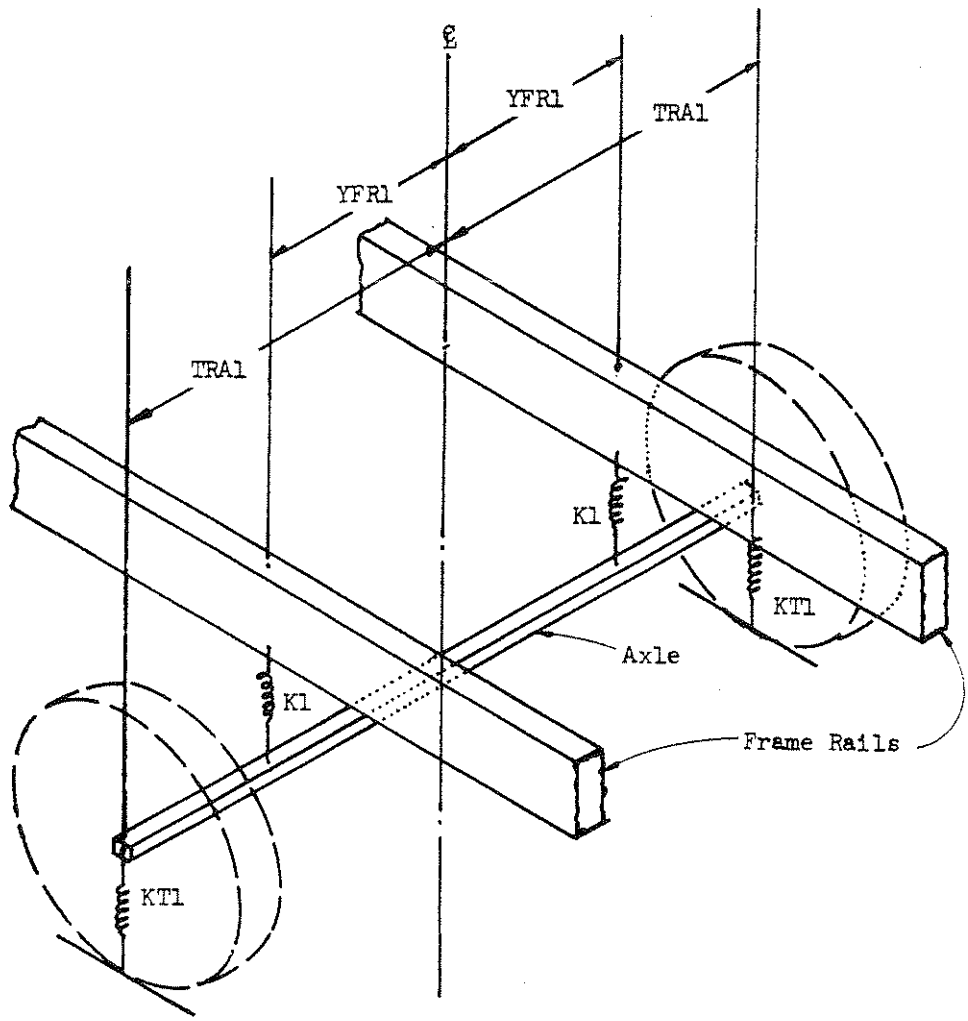

Figure 5-22. Front suspension system

The roll spring rate of the rear suspension, $K\Phi R$, and the trailer suspension, $K\Phi T$, may be calculated from a similar expression. If either suspension is tandem, the roll spring rate is the sum of the roll spring rates of the two axles.

With an equivalent torsional spring rate $K\Phi TR$ defined as:

$$K\Phi TR = K\Phi R + K\Phi F \tag{5-13}$$

the model of Figure 5-21 may be simplified to that of Figure 5-23 in which $K\Phi TR$ represents the roll resistance of the entire tractor as seen from the fifth wheel. The following two equations may be derived using the model of Figure 5-23.

$$cT = \Phi T \cdot K\Phi T \tag{5-14}$$

$$(a + b)T = \Phi T \frac{1}{\frac{1}{K5} + \frac{1}{K\Phi TR}} \tag{5-15}$$

From Equations (5-11), (5-14), and (5-15), the following expression may be derived for the fifth wheel roll spring rate:

$$K5 = \frac{K\Phi T}{\frac{c}{1-c} - \frac{K\Phi T}{K\Phi TR}} \tag{5-16}$$

The roll spring constant of the fifth wheel may be calculated from Equation (5-16) where the quantity c is obtained from test data.

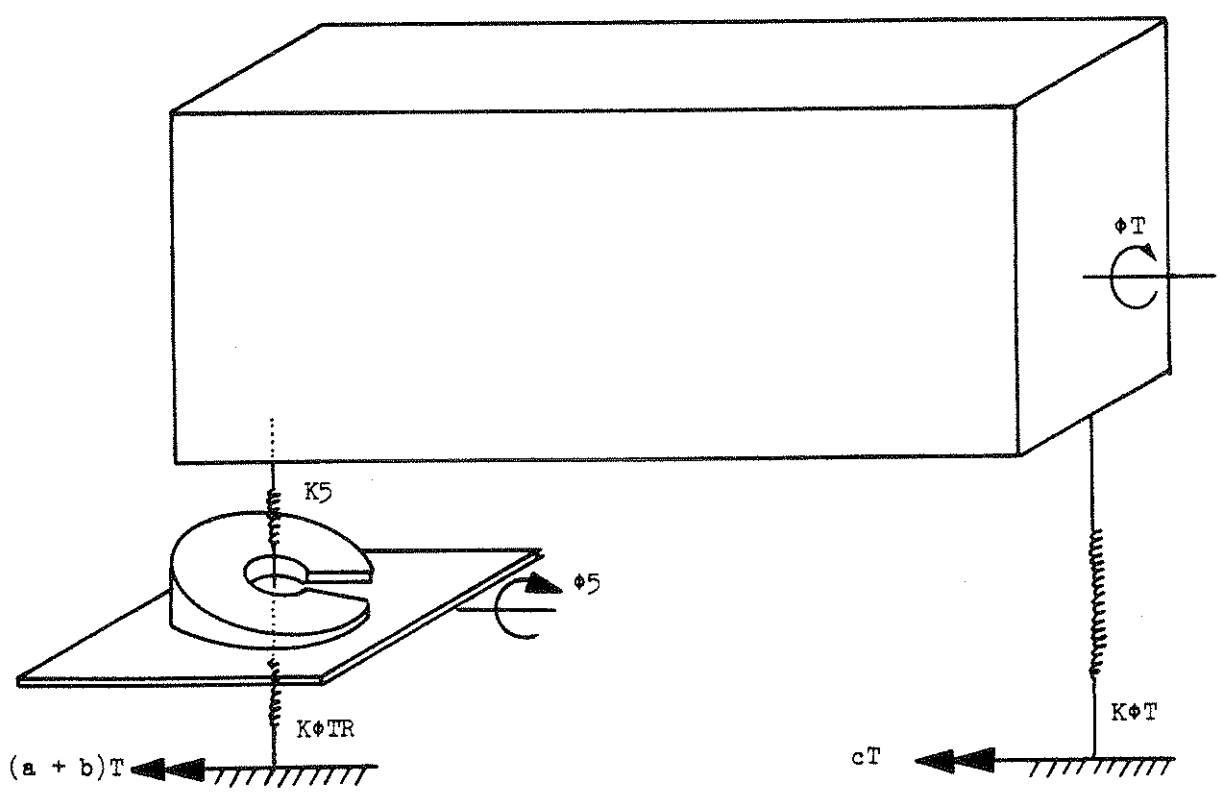

Figure 5-23. Simplified schematic diagram: fifth wheel rod spring test

Figure 5-24 illustrates the testing procedure used to determine the value of c. As shown in the figure, a long beam was rigidly attached to the trailer such that, by applying a vertical force, F, to the end of the beam, a roll moment,

$$T = \ell \cdot F \tag{5-17}$$

was applied to the trailer. The introduction of T and F causes changes in the tire normal forces. These differential forces are designated ΔF1 through ΔF10 in Figure 5-24. During the test, F was measured through the use of a load cell, and ΔF7 through ΔF10 were measured using load scales. ΔF1 through ΔF6 were not measured.

The quantity c is the proportion of the applied roll moment absorbed by the trailer suspension. Thus,

$$c = \frac{(\Delta F7 + \Delta F8 + \Delta F9 + \Delta F10)TRA3}{\ell \cdot F} \tag{5-18}$$

A number of tests were run on the empty tractor-trailer. In these tests, F was varied incrementally such that T varied from a minimum of zero to a maximum of 116,000 in.-lb, and back to zero. This cycle was repeated four times. Two cycles were conducted with the torque applied 18 ft. aft of the king pin, or approximately equidistant between the king pin and the rear suspension centerline, while two others were conducted with the beam located five inches aft of the king pin. The test yielded results as indicated in Table 5-3.

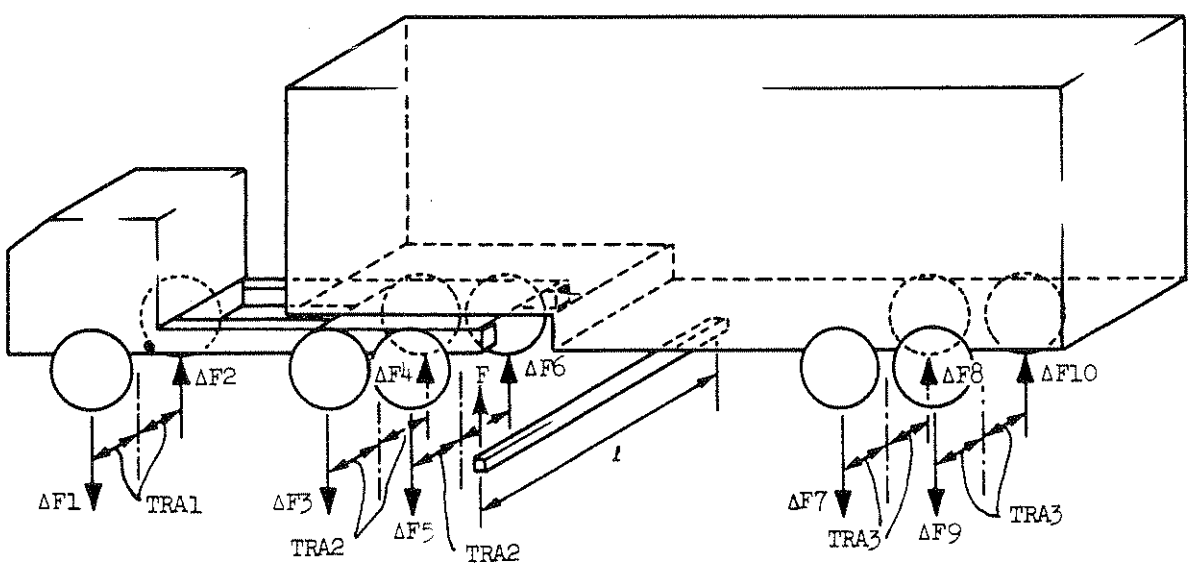

Figure 5-24. Roll moment applied to articulated vehicle

TABLE 5-3
Fifth Wheel Roll Spring Test Results

Longitudinal Position of Torque Application Aft of Kingpin	Average c	Minimum c	Maximum c
18 ft	.697	.573	.783
5 in	.651	.593	.704
Average for both positions	.674		

Using c = 0.674 in Equation (5-16) yields

$$K5 = 258{,}000 \text{ in.-lb/deg}$$

As indicated by the data shown in Table 5-3, the value of c was not greatly affected by the change in the locations of torque application. For other types of trailers, particularly flat beds, this may not be the case. For some trailers it may be necessary to devise new tests to determine how trailer flexibility may be accounted for.

6.0 VEHICLE TESTS AND VALIDATIONS FOR THE STRAIGHT TRUCK

6.1 INTRODUCTION

In this section the results of the steady turn and braking-in-a-turn tests of the straight truck, and the steady turn results for the bobtail tractor are compared with results from the simulation programs. (Braking-in-a-turn tests were not run with the bobtail tractor.) Descriptions of the test vehicles are given in Section 6.2. The test procedures are described in Section 6.3. The measurement techniques used to find the parameters needed for predicting braking performance are presented in Reference 1; these include parameters descriptive of the brake system and the suspensions. The measurement of those additional parameters necessary to simulate handling maneuvers is considered in Section 5. In addition, since the tests were not run on the same surface as that documented extensively in [1], it is necessary to choose new parameters to characterize the tire-road interface. This process is described in Section 6.4. The complete set of tire-road interface parameters used in the simulation runs is given in Appendix F.

In Section 6.5 a time history of the straight truck in a braking-in-a-turn maneuver is considered in some detail. Plots of simulated and measured yaw rate, longitudinal acceleration and lateral acceleration versus time are given as well as the simulated vehicle trajectory.

6.2 A DESCRIPTION OF THE TEST VEHICLES

In order to provide experimental data suitable for verification of the simulation program, a straight truck and tractor-trailer combination were subjected to a series of performance tests. Steady-state turning and braking-in-a-turn maneuvers on high and low coefficient of friction surfaces were performed.

The straight truck, a 4 x 6, 50,000 lb GVW vehicle with a 190 in. wheelbase and equipped with a walking beam suspension, is shown in Figure 6.1. It was fitted with a dump-type body for the test program. Vehicle specifications are given in Table 6-1.

Handling tests were conducted with the truck in the empty condition (i.e., with the dump body empty) and in the low c.g. loaded condition (i.e., with the dump body loaded with gravel). Static axle loads and center of gravity positions for the two loading conditions are listed in Table 6.2.

Since the truck was a new vehicle, a minimum amount of preparation was required to prepare the vehicle for testing. O.E. tires were replaced with those tires specified for testing and the dump body was installed. The vehicle was fitted with a brake pedal stop which could be adjusted for a given brake line pressure prior to testing, thus allowing open loop application of a quasi-step brake line pressure input. The steering column was also fitted with a stop allowing a preset level of steer angle input to be applied in an open loop, limited ramp manner.

The instrumentation installed in the vehicle is listed in Table 6-3.

The tractor (see Figure 7-1), a 4 x 6, 142 in. wheelbase, C.O.E., was tested in the bobtail condition. Preparation of the vehicle was similar to that described for the truck. Vehicle specifications, axle weight and c.g. position data appear in Table 6-4. A listing of instrumentation used in the vehicle appears in Table 6-5.

All tests were conducted on the skid pad at the Bendix Automotive Development Center at New Carlisle, Indiana. Tests were made on both high coefficient (dry jennite) and low coefficient (wet jennite) surfaces.

Prior to testing, brake burnishing was accomplished according to SAE J880. The new tires installed for testing were worn in during this process and on the trip from HSRI to the test site.

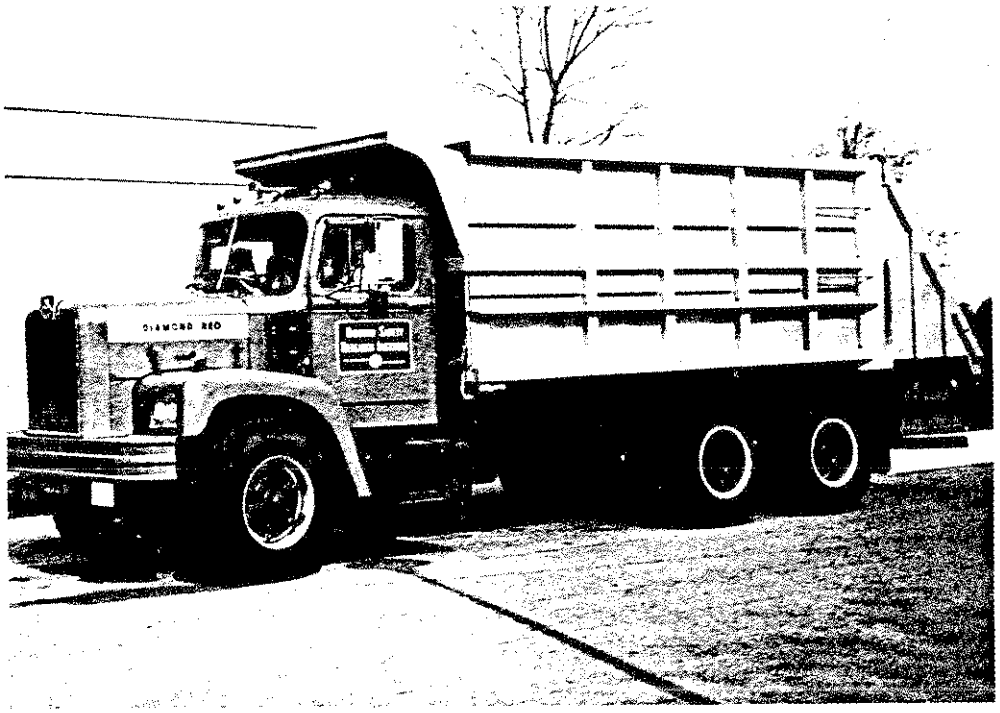

Figure 6-1. Test vehicle. Straight truck

TABLE 6-1
Vehicle Specifications, Straight Truck

General	4x6, 50,000 lb gvw, straight truck, 190 in. wheelbase	
Engine	V8-210	
Transmission	5 speed forward, 1 reverse with 4 speed auxiliary spicer	
Rear Axles	34,000 rated load with 7.8 ratio	
Steering Gear	19:24:19, hydraulic power	
Wheels	cast spoke	
Brakes	Front—dual chamber wedge type	Rear—dual chamber wedge type
Air chamber	type 9	type 12
Wedge angle	12°	12°
Size	15 x 5	15 x 6
Linings	RM-MA-417A	ABB-693-551-D
Lining area	314 sq in.	752 sq in.
Parking-emerg.	---	single swedge, spring actuated, 4 rear wheels
Axles	16,000 lb	34,000 lb
Suspension	leaf springs, 11 leaves, 7000 lb	rubber springs, RSA-340, 34,000 lb, aluminimum walking beam
Tires		
Size	highway tread, tubeless 15-22.5	highway tread, tube type 10.00-20
Load Range	H	F

TABLE 6-2
Loading Conditions for the Straight Truck

Loading Condition	State Axle Loads		
	front lb	rear lb	total lb
Empty	8,700	12,700	21,400
Loaded	13,000	32,200	45,200

Total Vehicle C.G. Position

Loading Condition	Inches Aft of Front Axle	Inches Above Ground
Empty	116	46
Loaded	137	55

TABLE 6-3
Instrumentation

Variable	Instrumentation
Left front steering angle, δ_L	Markite, Type 3595 Potentiometer, 5 K ohms
Right front steering angle, δ_r	Markite, Type 3595 Potentiometer, 5 K ohms
Steering wheel angle, δ_s	Amphenol Model 2101B Potentiometer, 10 K ohms
Brake line pressure at foot valve, P_f	CEC Type 4-237 Strain Gage Pressure Transducer
Brake line pressure at front axle, P_1	Dynisco Model APT136 Strain Gage Pressure Transducer
Brake line pressure at middle axle, P_2	Dynisco Model APT136 Strain Gage Pressure Transducer
Brake line pressure at rear axle, P_3	Dynisco Model APT136 Strain Gage Pressure Transducer
Parking brake air pressure, P_p	Dynisco Model APT136 Strain Gage Pressure Transducer
Yaw rate, ψ, pitch, θ, roll, ϕ, longitudinal acceleration, A_x, lateral acceleration, A_y	Humphry Inc. Stabilized Platform Unit CF 18-0109-1
Wheel rotation, lock-up for each of six wheels, LU_{1-6}	Enwell Bicycle Generators for go/no-go indication
Vehicle velocity, V_x	Tracktest Fifth Wheel
Brake lining temperature for each of six wheels, T_{1-6}	Serve-Rite, Iron-Constantan Thermocouple

Recorders: (1) Honeywell Visicorder, Model 2206, 14 Channel, light beam oscillograph
(2) Clevite-Brush, Model 2310, 16 Channel, light beam oscillograph

TABLE 6-4

Vehicle Specifications, Tractor

Model	4x6, 46,000 lb gvw, 142-in. wheelbase, COE (sleeper type)	
Engine	V-8, 335	
Transmission	5 speed forward, 1 reverse, 2 speed auxiliary spicer	
Rear Axle	34,000 with 4.11 ratio	
Steering Gear	28:1 constant ratio, lock to lock	
Wheels	Cast spoke	
Brakes	Front—dual chamber wedge type	Rear—dual chamber wedge type
Special equip.	limiting and quick release valve	relay valve and quick release valve
Air chamber	type 12	Type 12
Wedge angle	12°	12°
Size	15 x 4	15 x 7
Linings	RM-MR-417A	RM-MA-417A
Parking-emer.	---	single wedge, spring actuated, 4 rear wheels
Axles	12,000 lb	34,000 lb
Suspension	leaf spring	4 spring
Tires	highway tread, tube type	deep lug, tube type
Size	10.00-20	10.00-20
Load Range	F	F
Axle Weights		
Bobtail	8100 lb	6800 lb
Total Vehicle C.G.		
Position, Bobtail	67 inches aft of front axle 40 inches above ground level	

TABLE 6-5
Instrumentation, Tractor

Variable	Instrumentation
Left front steering angle, δ_L	Markite, Type 3595 Potentiometer, 5 K ohms
Right front steering angle, δ_r	Markite, Type 3595 Potentiometer, 5 K ohms
Steering wheel angle, δ_s	Amphenol Model 2101B Potentiometer, 10 K ohms
Brake line pressure at foot valve, P_f	CEC Type 4-327 Strain Gage Pressure Transducer
Brake line pressure at front axle, P_1	Dynisco Model APT136 Strain Gage Pressure Transducer
Brake line pressure at tractor rear axle, P_2	Dynisco Model APT136 Strain Gage Pressure Transducer
Brake line pressure at trailer rear axle, P_3	Dynisco Model APT136 Strain Gage Pressure Transducer
Tractor pitch, Θ, roll, Φ, longitudinal acceleration, A_x, latteral acceleration, A_y	Humphry Inc. Stabilized Platform Unit SA07-0114-1
Yaw rate, $\dot{\psi}$, of tractor	Daystrom Pacific Rate Gyro Model R59B90-1
Wheel rotation/lock-up for each of six wheels, LU_{1-6}	Enwell Bicycle Generators for go/no-go indication
Vehicle velocity, V_x	Tracktest Fifth Wheel
Brake lining temperature for each of six wheels, T_{1-6}	Serve-Rite, Iron-Constantan Thermocouple

Recorders: Two Honeywell Visicorders, Model 2206, 14 Channel, light beam oscillograph

6.3 TEST PROCEDURES

Tests conducted for the purpose of providing data for validation of the braking and handling performance simulation program included steady-state turning and braking-in-a-turn tests. These tests were run on both high and low coefficient surfaces, in the empty and loaded condition, and from various speeds. A list of signals recorded during the tests is given in Table 6-6.

6.3.1 STEADY-STATE TURNING. With the vehicle initially traveling in a straight line at the specified test speed, a limited ramp steer angle was input to the vehicle. Prior to the test, the steering column block was adjusted for the desired maximum steering wheel angle in order that this input could be applied in an open loop fashion. Constant vehicle speed was maintained until a steady-state vehicle response was obtained and recorded.

Tests were conducted at nominal speeds of 25 and 30 mph. Steer angles yielding steady-state lateral accelerations of 25, 50, 75, and 100% of the maximum value

TABLE 6-6
Test Measurements

Variable*	Steady-State Turning	Braking-in-a-Turn
δ_L, δ_r, δ_s	R	R
P_f, P_1, P_2, P_3	---	R
P_p	---	---
$\dot{\psi}$	R	R
θ	---	R
ϕ	R	R
A_x	---	R
A_y	R	R
V_x	R	R
LU_{1-6}	---	R
T_{1-6}	---	Mon

Key: R—Record continuously during test
Mon—Monitor before and after test

*Refer to Table 6-3 for variable definitions.

considered safe for the particular load configuration were used. (Maximum safe steady-state lateral deceleration levels were deemed to be 20 ft/sec^2 for the empty configuration and 16 ft/sec^2 for the loaded configuration.)

6.3.2 BRAKING-IN-A-TURN. Braking-in-a-turn tests were begun in the same manner as described for the steady-state turn tests. However, once the vehicle obtained a steady-state lateral acceleration, a quasi-step brake application was made, in which the brake line pressure level was determined by the preset condition of the brake pedal stop. The steer angle was held fixed until the vehicle came to rest or until the vehicle was in danger of leaving the test area. Tests were conducted from initial velocities of 25 and 30 mph and with initial brake temperatures of 200°F or less. Steer angles and brake line pressures were chosen to cover a broad range of lateral and longitudinal decelerations with the aim of establishing performance limits at which one or more wheels lock.

6.4 TIRE PARAMETERS FOR VALIDATION

Extensive tire test data, taken on the HSRI flat bed test machine [4] was available for new tires of the same model as those used in the experimental work. (The tire test data is given in Appendix G.) It was, of course, necessary to modify some of this data to fit the speed and surface conditions of the tests. This was done in a slightly different fashion for the dry and the wet surface as will be shown below.

6.4.1 TIRE PARAMETERS FOR THE DRY SURFACE. The tire model was used to match tire data taken from the flat bed tire test machine as closely as possible. The speed sensitivity parameter, FA, was set to zero to model flat bed test, and μ_o was chosen from an examination of the tire test data at low load and high slip angle. The curve fit parameters $\bar{\alpha}$ and KF were chosen by trial and error through the use of the algorithm given in Appendix H. This process, as well as some

illustrations of the interaction between longitudinal and lateral slip to produce brake force and cornering force predicted by the tire model, is given in Section 3.2.2 for the 10 x 20F tire, which was used on the tandem axles of the straight truck.

The values for μ_o and FA for the dry surface simulation were chosen in the following way: with FA chosen to be .005 (a reasonable value based on past experience in the pitch plane modeling) and using the values of C_α from the tire test data and the curve fit parameters as explained above, a few preliminary steady turn simulations were run. It was immediately apparent from the dry surface runs that any reasonable μ_o would lead to good steady turn results when μ_o was set to the same value for front and rear tires. Further preliminary runs, this time simulating braking-in-a-turn, led to the choice of μ_o = .85 for all the tires.

The values of the longitudinal stiffness, C_s, were taken directly from the flat bed tire test data. Since C_s varies widely with the normal load, the table lookup mechanism was used as explained in Section 3.2.1 It should be again noted here that, in addition to being a basic parameter in any maneuver involving braking, the longitudinal stiffness is important in a steady turn analysis since a yaw moment results from the longitudinal slip gradient of dual tires traversing a curved path.

The aligning torque, MZ, arising from the operation of a single tire at a sideslip angle was also included in the simulations. The data from the flat bed tire test machine was used directly. Since MZ is a function of both normal load and sideslip angle, the table lookup mechanism is slightly more complicated than the lookup for C_α and C_s. An explanation is given in Section 3.2.3.

6.4.2 TIRE PARAMETERS FOR THE WET SURFACE. To choose values for μ_o and FA for use in the wet surface validation, the following procedure was used. Using the C_α, $\bar{\alpha}$, and KF chosen for the dry surface simulations, and with FA chosen to be .01 (a reasonable value for the wet surface based on past experience in pitch plane modeling), a few preliminary steady turn simulations were run. It became obvious from these runs that a minimum μ_o value of at least .55 on the front tires was required to negotiate the turns at lateral acceleration levels commonly encountered in the tests and, in addition, that a higher nominal friction coefficient was required on the rear tires to maintain yaw rates comparable to those found experimentally. (This is reasonable in view of the fact that the rear tires, especially those on the trailing tandem, are subject to quite different surface conditions than the front tires which encounter only the undisturbed water on the jennite surface.) From these preliminary runs, the rear tire μ_o values were fixed 0.65.

In the matter of the aligning torque, some speculation is necessarily involved. It seems reasonable to assume that, since the cornering forces at any given normal load and slip angle are lower on the wet surface than on the dry surface, the aligning torque at any slip angle and load would be less on the wet surface than on the dry surface.* The values used in the simulation were chosen to be the values used in the dry surface runs scaled down by the ratio of (μ_o wet)/(μ_o dry). The aligning torque data for the front tires was therefore scaled down by the ratio $\frac{.55}{.85}$. In the wet surface testing, in which the truck was run in the empty condition, the tandem tires were operating at such small normal loads that the aligning torque was considered negligible.

*This may not be true at very small slip angles. However, the aligning torque becomes negligibly small for very small slip angles.

It should be noted at this point that, as has been pointed out by Ervin, et al. in [15], water depth variations on the order of 0.07 inches have a "profound influence on tire-road friction properties." Since variations in water depth of at least this magnitude were encountered in the experimental work, it should be expected that the simulation of vehicle maneuvers on such a surface should prove a speculative undertaking. Thus, while a comparison between the simulation and the experimental work on the wet surface indicates good agreement, it should not be inferred that wet surface simulation will, in general, lead to such good results. In contrast to simulation of maneuvers on a dry surface, from which one might expect reasonably repeatable experimental results, wet surface maneuvers cannot be simulated accurately without detailed knowledge of the actual test site at the time of the tests.

6.5 A COMPARISON BETWEEN TEST DATA AND THE SIMULATION RUNS

6.5.1 STEADY TURNS. Steady turn data was taken for the straight truck in the empty and loaded condition on the dry surface and in the empty condition on the wet surface. In addition, the bobtail tractor was tested in steady turns on the dry surface. The testing procedure has been explained in Section 6.3; the parameters necessary to describe the vehicles are given in Appendix F.

With the input data obtained as described above, the entire series of steady turn tests conducted on the straight truck was simulated. The results of the simulation are superimposed on the experimental results in Figures 6-2 through 6-8. A comparison of the simulated runs with the appropriate empirical data is given in Table 6-7.

At this point, certain differences between the experimental procedure and the simulated procedure should be noted. The steady turn experimental results were taken at a steady speed; whatever drive torque necessary to maintain that speed was applied. In the simulation, on the other hand, no drive torque was applied. Thus the simulated vehicle speed drops during the course of the run as a result of the longitudinal component of the side force of the steered front wheels. Therefore, the initial condition of vehicle speed was chosen slightly higher than the speed for which the results were desired; the vehicle model would reach a quasi-steady turn condition in which it would gradually lose speed. When the speed dropped to the test speed, the simulated yaw rate and lateral acceleration predictions were noted. These values are plotted in Figures 6-2 through 6-7 for the straight truck and in Figure 6-8 for the bobtail tractor.

Another slight difficulty is that the test data was taken at speeds slightly different than the "nominal speed" desired for the test. To facilitate the meaningful superposition of simulated and experimental results on the figures, the average speed of the empirical results was used as the speed at which the data was taken from the simulation. The actual speed at which the tests were run is included in the list of results given in Table 6.7.

It should also be noted that the measured steer angles were used in the simulation. These were, as one might expect, significantly different from side to side. (Since all the empirical results and simulation runs were left turns, the left steer angle was always larger than the right.) For the purposes of Figures 6-2 through 6-8 average steer angles were plotted. The measured steer angles are given in Table 6-7.

With very few exceptions, the measured results and the predicted results are in very close agreement. In all the steady turn figures, the simulated yaw rate

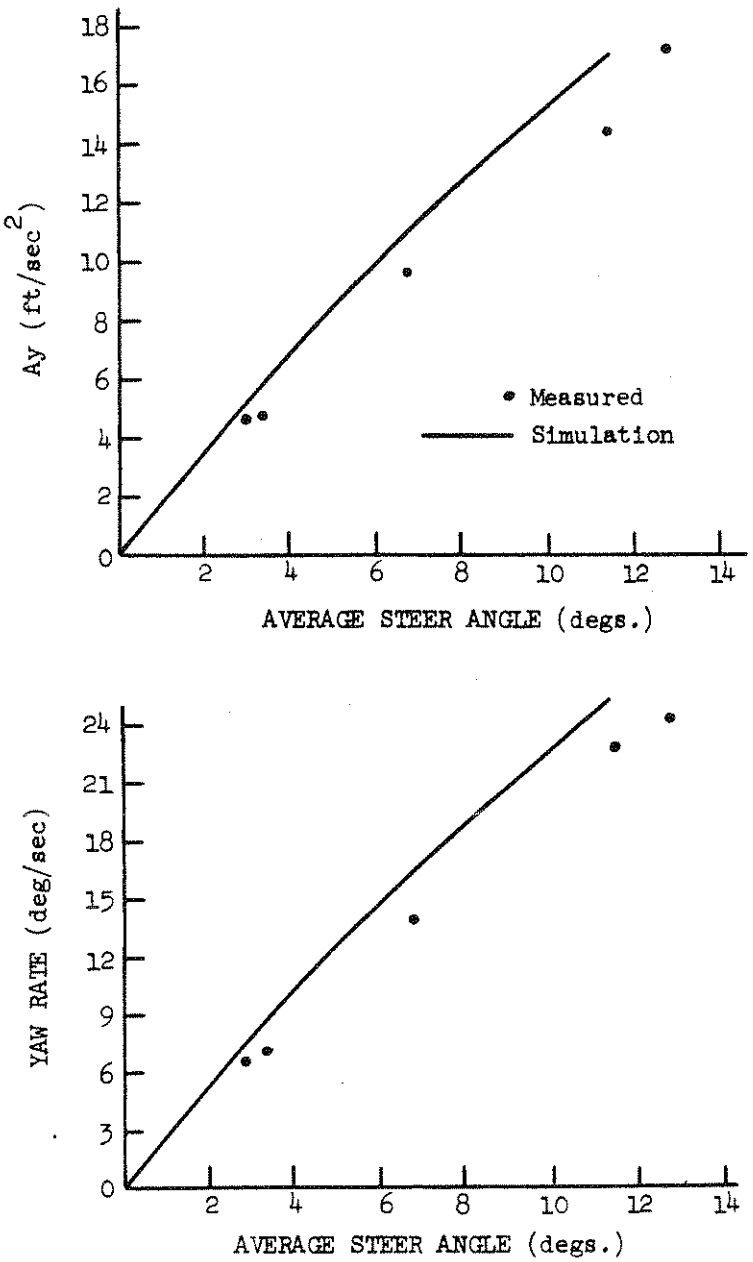

Figure 6-2. Steady turn, empty, dry, 39.5 ft/sec

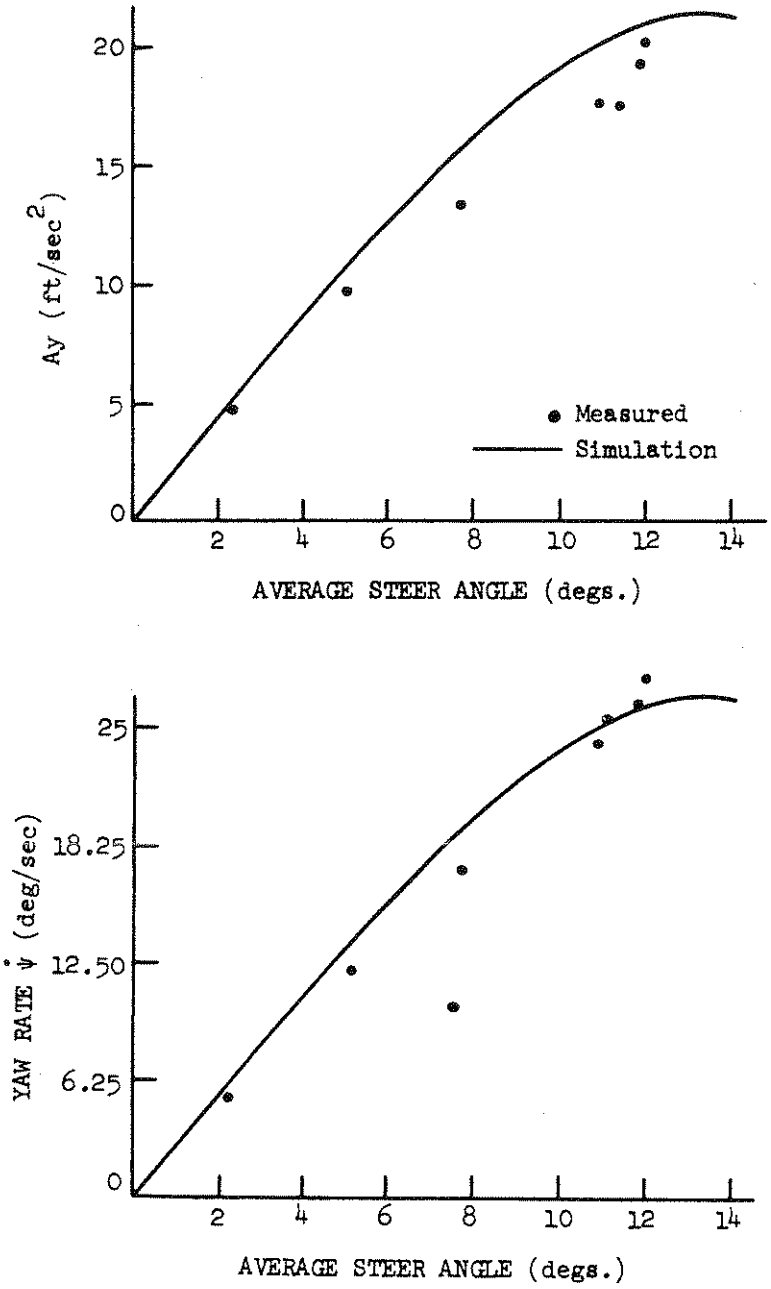

Figure 6-3. Steady turn, empty, dry, 47 ft/sec

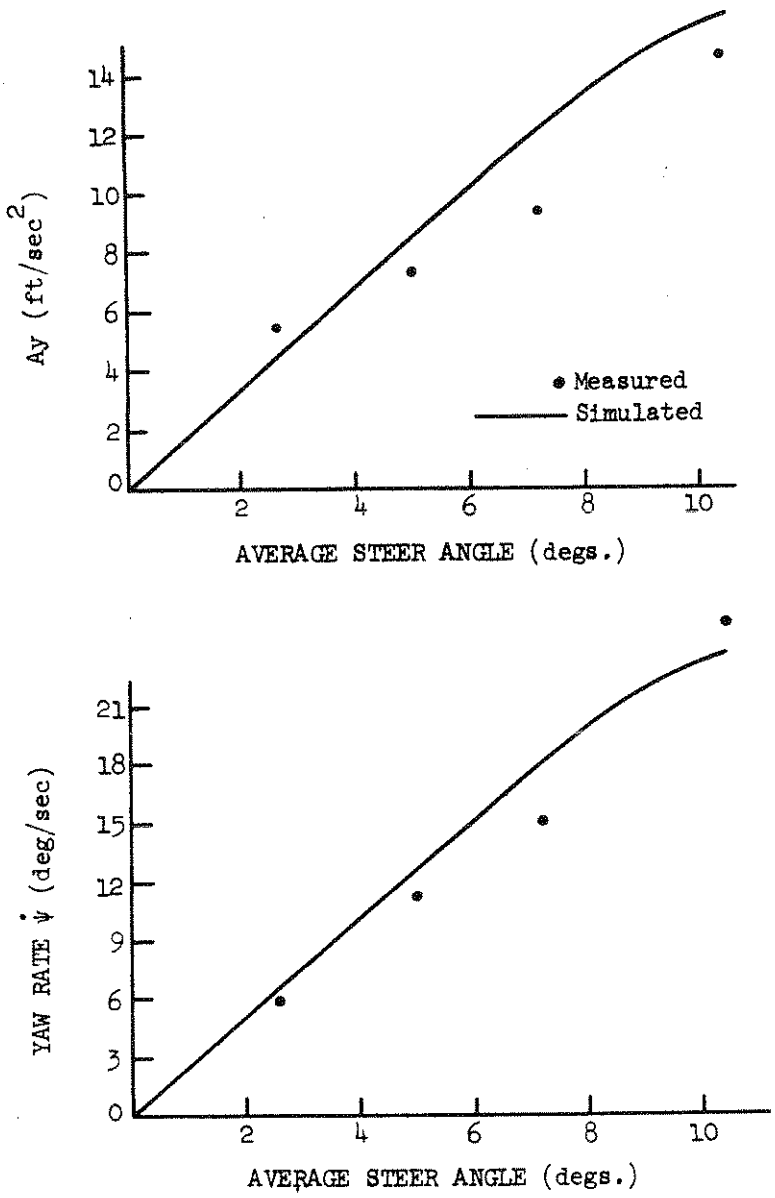

Figure 6-4. Steady turn, low c.g. load, dry, 39.1 ft/sec

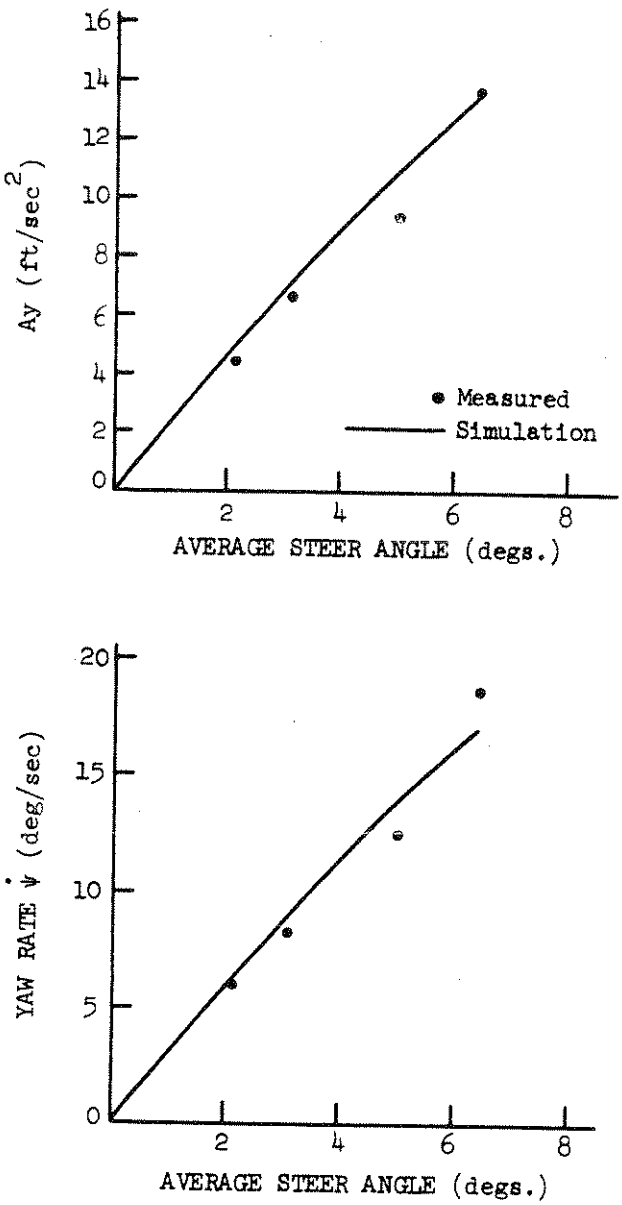

Figure 6-5. Steady turn, low c.g. load, dry, 45.6 ft/sec

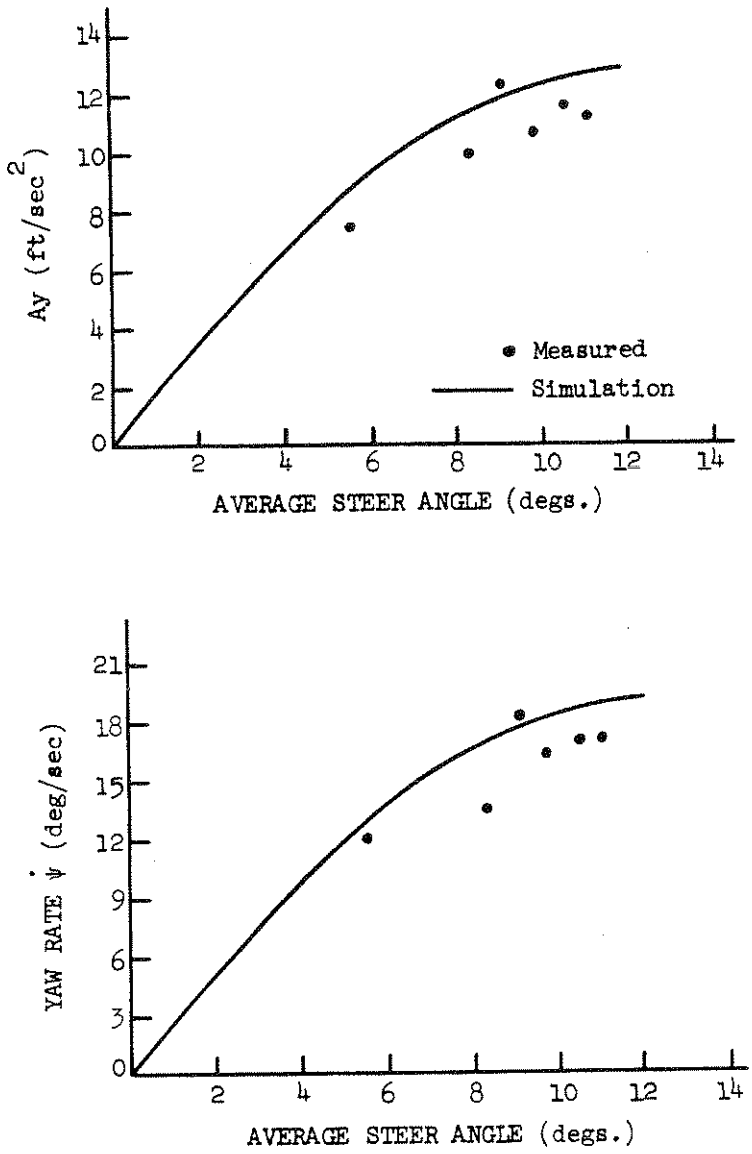

Figure 6-6. Steady turn, empty, wet, 39 ft/sec

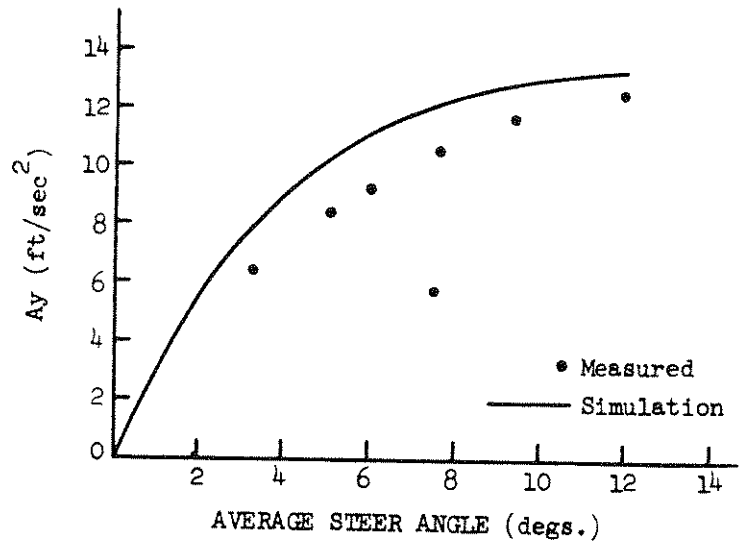

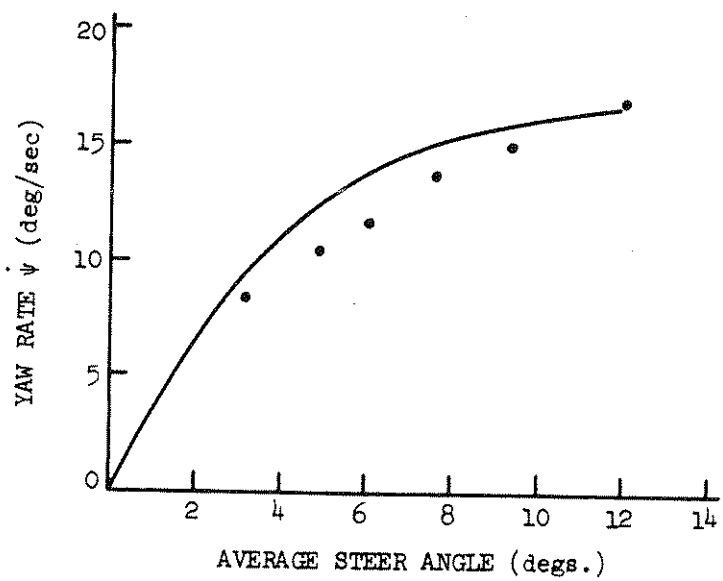

Figure 6-7. Steady turn, empty, wet, 46.8 ft/sec

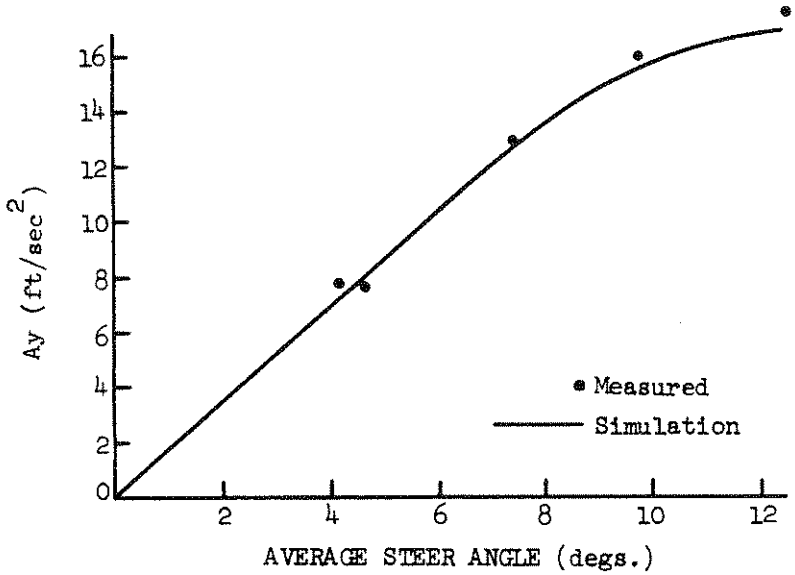

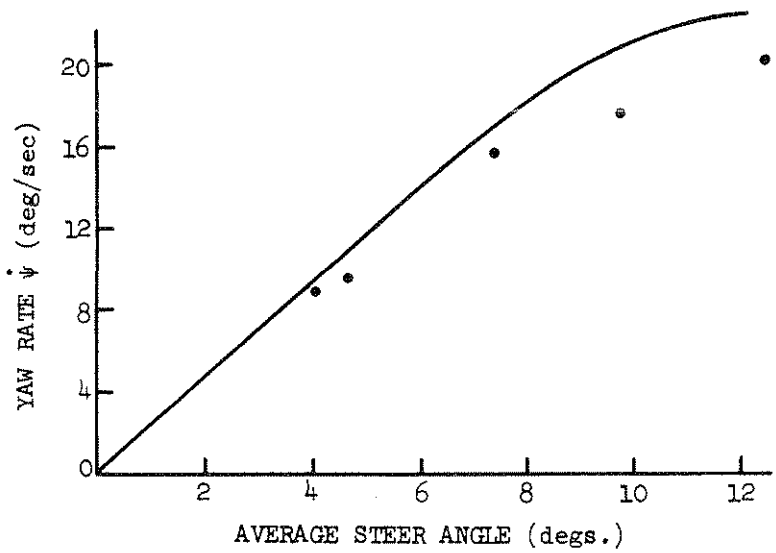

Figure 6-8. Steady turn, bobtail tractor; dry, 43 ft/sec

TABLE 6-7
Steady Turns, Straight Truck

δ_r (deg)	δ_l (deg)	$V_{measured}$ (ft/sec)	A_y (ft/sec^2) measured	A_y (ft/sec^2) simulated	$\dot{\psi}$ (deg/sec) measured	$\dot{\psi}$ (deg/sec) simulated
(a) Empty, dry surface Simulated speed: 39.5 ft/sec						
11.8	13.6	39.7	17.0	18.0	24.0	26.0
10.5	12.5	39.6	14.5	16.8	22.6	24.3
6.1	7.4	40.6	9.6	10.6	13.7	15.2
2.9	3.7	39.0	4.83	4.85	6.6	7.0
2.7	3.2	38.7	4.35	4.71	6.2	6.8
(b) Empty, dry surface Simulation speed: 46.75 ft/sec						
10.8	12.9	44.5	19.32	21.0	26.2	25.6
10.2	12.5	47.0	17.7	20.8	25.3	25.0
7.1	8.5	47.5	13.2	16.2	17.7	19.4
4.76	5.7	46.6	9.66	10.3	12.2	12.5
2.03	2.52	47.5	4.7	5.05	5.2	6.1
(c) Low center of gravity, dry surface Simulation speed: 39.1 ft/sec						
9.3	11.4	38.7	14.8	15.7	25.2	24.0
7.25	8.20	39.7	9.46	13.1	16.1	18.8
4.54	5.38	38.7	7.3	8.1	11.3	11.8
2.28	2.92	39.3	5.4	4.2	5.9	6.2
(d) Low center of gravity, dry surface Simulation speed: 45.6 ft/sec						
5.64	7.23	45.6	13.5	14.0	18.6	17.9
4.6	5.4	46.6	9.35	10.9	12.5	14.0
2.65	3.4	44.46	6.75	6.62	8.4	8.2
1.94	2.35	45.6	4.5	4.7	5.8	5.8
(e) Empty, wet surface Simulation speed: 39 ft/sec						
10.2	12.1	38.8	11.0	12.7	17.0	18.0
9.4	11.6	38.4	11.3	12.2	17.0	18.0
8.8	10.5	38.4	11.0	12.2	16.4	17.3
7.70	8.80	39.0	9.8	11.5	14.4	16.4
5.0	6.1	37.8	7.4	8.2	10.6	12.0

TABLE 6-7 (Concluded)

δ_r (deg)	δ_1 (deg)	$V_{measured}$ (ft/sec)	A_y (ft/sec^2) measured	A_y (ft/sec^2) simulated	$\dot{\psi}$ (deg/sec) measured	$\dot{\psi}$ (deg/sec) simulated
(f) Empty, wet surface Simulation speed: 46.8 ft/sec						
10.8	13.0	45.2	12.5	13.4	17.3	16.2
8.5	10.2	47.5	11.6	12.8	14.9	14.9
6.6	7.9	47.5	10.5	12.1	13.6	14.2
5.4	6.6	47.5	9.15	11.3	11.6	13.6
4.7	5.6	46.6	8.35	10.4	10.6	12.6
3.0	3.74	47.5	6.44	7.1	8.2	8.7
(g) Bobtail tractor, dry surface Simulation speed: 45 ft/sec						
11.5	13.4	46.2	17.7	17.1	20.2	23.1
9.12	10.43	46.2	16.1	15.8	17.8	20.5
3.9	4.3	44.4	7.74	7.85	9.0	10.2
3.25	3.76	44.9	6.02	5.92	7.6	7.85

and the simulated lateral acceleration may appear to be different only by a scale factor. This should be expected since, in the simulated "steady" turns

$$AY \cong u \cdot \dot{\psi} \qquad (6\text{-}1)$$

where

Ay is the lateral acceleration

u is the longitudinal velocity

$\dot{\psi}$ is the yaw rate

The yaw rate and the lateral acceleration were measured independently, however; thus, the empirical results conform to Equation (6-1) only within the limits of accuracy of the instrumentation.

6.5.2 BRAKING-IN-A-TURN. The experimental procedure for the braking-in-a-turn tests has been explained in Section 6.3.2. Some results from these tests are plotted in Figures 6-9 and 6-10. In these figures, steady-state lateral acceleration before the application of the brakes is plotted versus maximum longitudinal decelerations after the application of the brakes. The incidence of wheel lockup may be inferred from the manner of plotting of the point. It should be noted that, since the properties of the tire-road interface may be expected to be quite similar at the nominal test speeds of 25 and 30 mph, both 25 and 30 mph data is included in Figures 6-9 and 6-10.

In the simulation runs, the actual steer and brake pressure data from the braking-in-a-turn tests was not used; rather, the simulation was used to predict the maximum longitudinal deceleration possible without wheel lockup when starting from a steady turn. Thus, for points in the area of the figures above the simulation line, the simulation will predict wheel lockup, and in the area below the

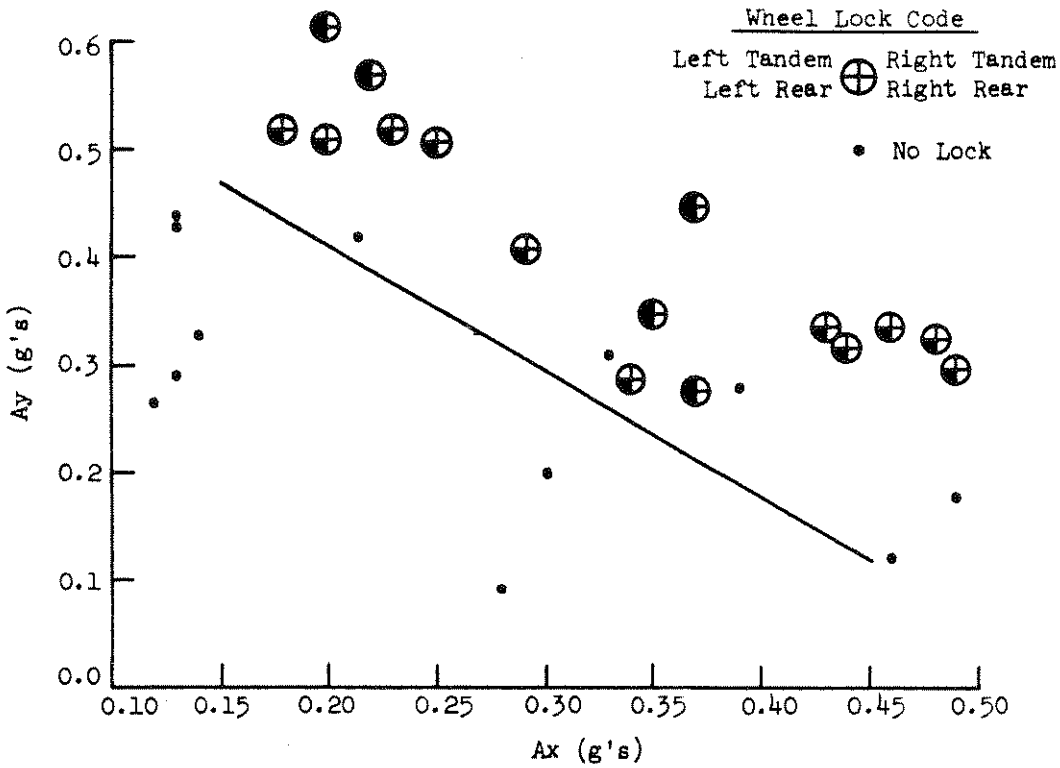

Figure 6-9. Braking-in-a-turn; empty, dry

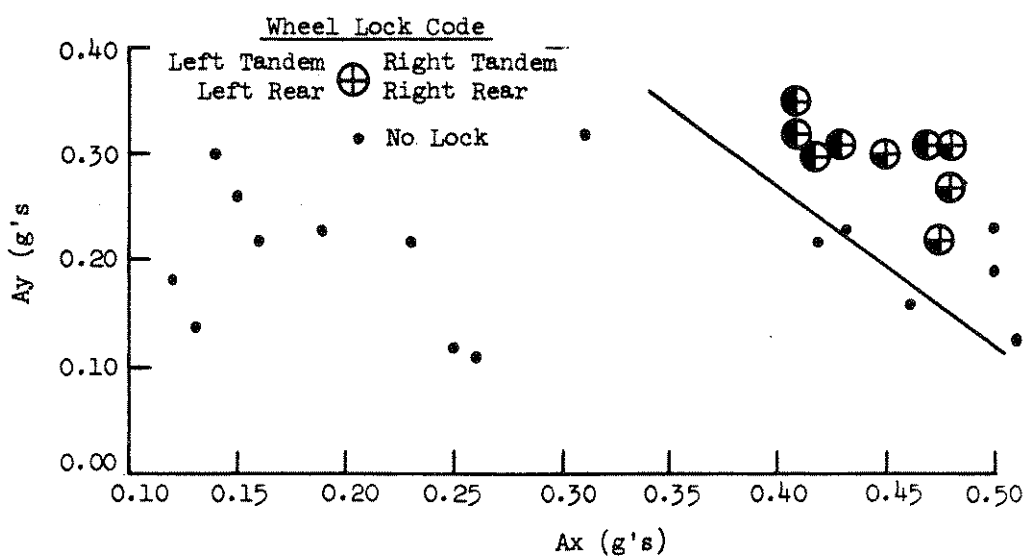

Figure 6-10. Braking-in-a-turn; low c.g. load, dry

simulation line, the simulation will predict that no wheels will lock. The simulated result splits the empirical data quite accurately; with few exceptions, the locked wheel empirical results fall above the simulation line and the unlocked results below the simulation line. In the next section, in which a single braking-in-a-turn run is considered in detail, further evidence is given of the reliability of the straight truck simulation.

6.5.3 DETAILED SIMULATED AND EMPIRICAL RESULTS OF A BRAKING-IN-A-TURN MANEUVER. Time histories of the important dynamic variables describing a braking-in-a-turn maneuver are given in Figure 6-11. In this maneuver, after entering a "steady" right turn, brakes were applied at time t = 2 seconds, and held until the vehicle stopped. Points taken directly from the empirical data were entered in the simulation for (1) the steer angle (right side steady-state 8.5°, left side steady-state, 7.0°), and (2) the applied brake pressure at the foot valve. At the time of brake application, simulated and measured speed were 36.4 ft/sec. Lateral acceleration, A_y, longitudinal acceleration, A_x, and yaw rate, $\dot{\psi}$, are plotted versus time. In this case, as in the majority of the straight truck runs, the correspondence between the empirical results and the predicted results are remarkably good.

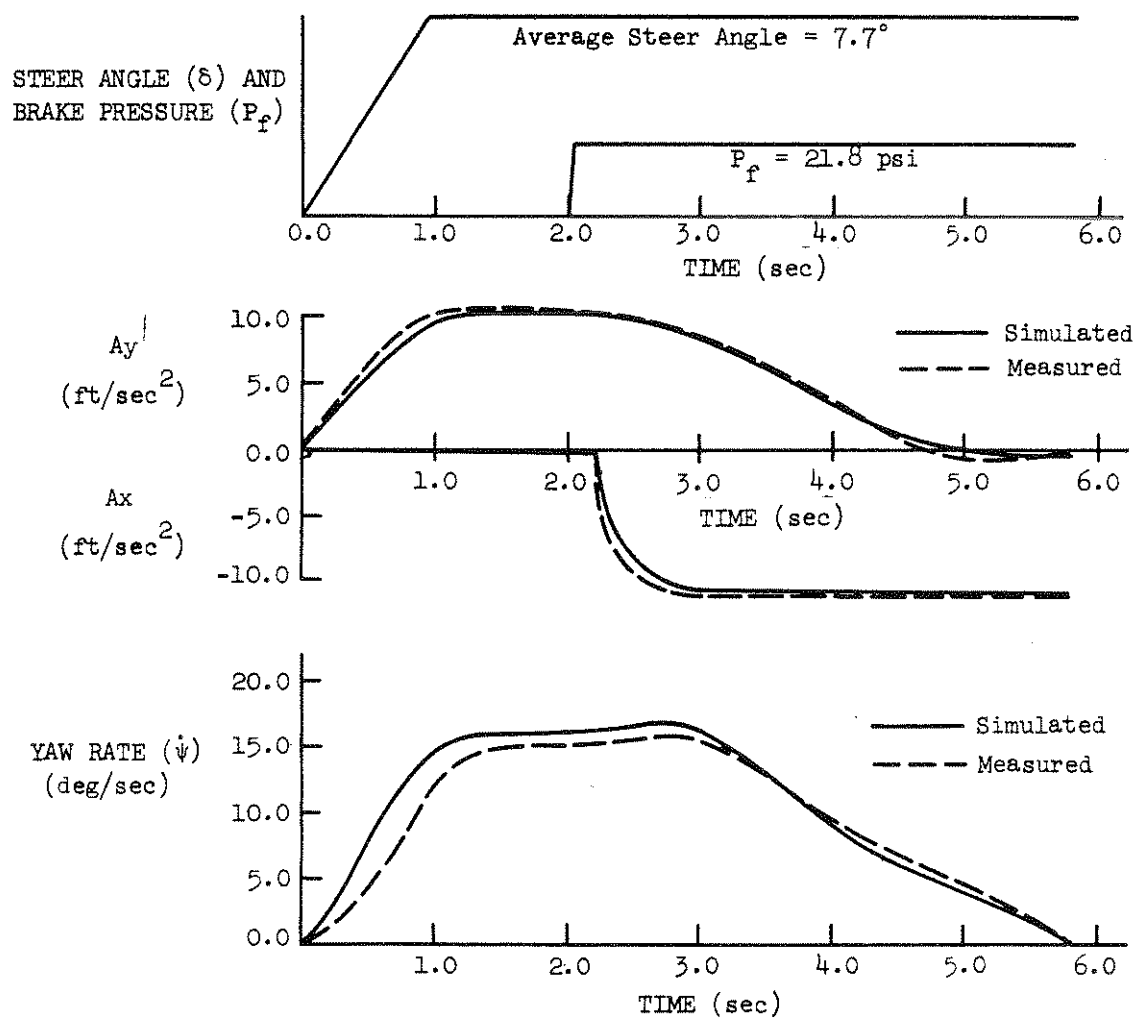

Figure 6-11. A time history of a braking-in-a-turn maneuver

7.0 VEHICLE TESTS AND VALIDATIONS FOR THE ARTICULATED VEHICLE

7.1 INTRODUCTION

In this section the results of the steady turn and braking-in-a-turn tests of the articulated vehicle are compared with results from the simulation programs. A description of the tractor is given in Section 6.2, and a description of the trailer is given in 7.2. The test procedures are described in Section 7.3. The measurement techniques used to find the parameters needed for predicting braking performance are presented in Reference 1; these include parameters descriptive of the brake system and the suspensions. The measurement of those additional parameters necessary to simulate handling maneuvers is considered in Section 5. In addition, since the tests were not run on the same surface as that documented extensively in [1], it was necessary to choose new parameters to characterize the tire-road interface. This process is described in Section 7.4. The complete set of tire-road interface parameters used in the simulation runs is given in Appendix F.

In Section 7.5 certain interesting measured time histories are compared with the corresponding simulation results. Both a stable braking-in-a-turn maneuver and a straight line maneuver resulting in a jackknife are considered.

7.2 A DESCRIPTION OF THE TEST VEHICLE

In order to provide experimental data for the verification of the braking and handling simulation program for articulated vehicles, the tractor-trailer combination shown in Figure 7-1 was subjected to a series of handling performance tests. These tests included steady-state turning, braking-in-a-turn, and jackknife tests.

The test tractor was a 4 x 6, 46,000 lb GVW, COE on a 142-inch wheel base and was equipped with a four-spring suspension with load leveler. Specifications for the tractor were given previously in Table 6-4. The trailer used for testing was

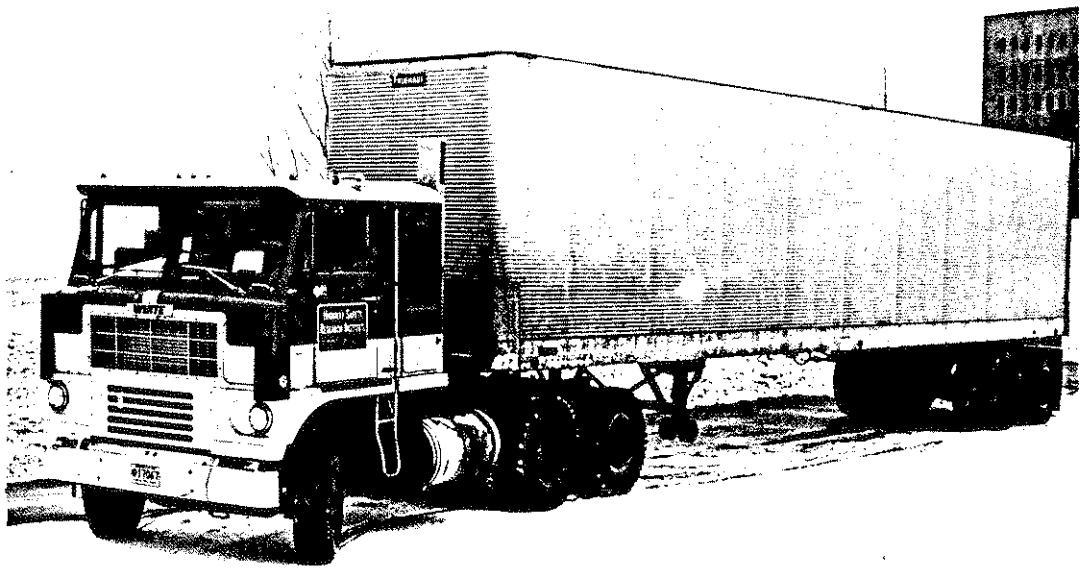

Figure 7-1. Articulated vehicle

a 40-ft van type. This vehicle also was equipped with a four-spring suspension with load leveler rated for a 34,000-lb gross load. Other specifications for this trailer are given in Table 7-1.

TABLE 7-1
Trailer Specifications

Model	40 ft, van type, 2 axle, semitrailer
Suspension	4 spring (3 leaf)
Axles	34,000 lb
Brakes	S-cam, leading-trailing
Air chambers	type 30
Slack adjusters	6-inch length
Size	16-1/2 x 7
Linings	SAE friction code "EE"
Tires	highway tread, tube type
Size	10.00 x 20
Load range	F

Tests were conducted on the tractor-trailer combination with the vehicle in both the empty and loaded conditions. (Load for the trailer consisted of 46,800 lb of containerized gravel.) Axle weights and center of gravity positions for the vehicle in both load configurations is given in Table 7-2.

TABLE 7-2
Loading Conditions for the Articulated Vehicle

Loading Condition	Static Axle Load (lb)			
	Front	Rear	Trailer	Total
Empty	8,900	10,500	7,800	27,200
Loaded	10,500	32,000	31,800	74,300

Loading Condition	C.G. Position			
	Tractor		Trailer	
	Aft of front axle(in.)	Height (in.)	Aft of Kingpin(in.)	Height (in.)
Empty	67	40	265	56
Loaded	67	40	218	66

In addition to the vehicle preparation previously described for the tractor in Section 6-2, the articulation angle limiter shown in Figure 7-2 was fitted to the tractor. This device limits the articulation angle of the combination vehicle to a nominal value of ±15°. In addition, the OEM tires on the trailer were replaced with the tires specified for testing.

Instrumentation installed on the tractor-trailer combination is listed in Table 7-3.

The steady turn tests and the braking-in-a-turn tests were conducted on the skid pad at the Bendix Automotive Development Center (BADC) at New Carlisle, Indiana. Tests were made on both high coefficient (dry jennite) and low coefficient (wet jennite) surfaces. High speed jackknife tests were conducted on dry asphalt on the oval track at the BADC.

TABLE 7-3
Instrumentation, Tractor-Trailer Combination

Variable	Instrumentation
Left front steering angle, δ_L	Markite, Type 3595 Potentiometer, 5 K ohms
Right front steering angle, δ_r	Markite, Type 3595 Potentiometer, 5 K ohms
Steering wheel angle, δ_s	Amphenol Model 2101B Potentiometer, 10 K ohms
Brake line pressure at foot valve, P_f	CEC Type 4-327 Strain Guage Pressure Transducer
Brake line pressure at front axle, P_1	Dynisco Model APT136 Strain Guage Pressure Transducer
Brake line pressure at tractor rear axle, P_2	Dynisco Model APT136 Strain Guage Pressure Transducer
Brake line pressure at trailer rear axle, P_3	Dynisco Model APT136 Strain Guage Pressure Transducer
Tractor pitch, θ, roll, ϕ, Longitudinal acceleration, A_x, Lateral acceleration, A_y	Hymphry Inc., Stabilized Platform Unit SA07-0114-1
Yaw rate, $\dot{\psi}$, of tractor	Daystrom Pacific rate Gyro Model R59B90-1
Articulation angle between tractor and trailer, ψ-ψ1	Beckman Helipot Mod 3301, 1 K
Wheel rotation/lock-up for each of ten wheels, LU_{1-10}	Enwell Bicycle Generators for go/no-go indication
Vehicle velocity, V_x	Tracktest Fifth Wheel
Brake lining temperature for each of ten wheels, T_{1-10}	Serve-Rite, Iron-Constantan Thermocouple

Recorders: Two Honeywell Visicorders, Model 2206, 14 Channel, light beam oscillograph

Figure 7-2. Articulation angle limiter

Prior to testing, brake burnishing was accomplished according to SAE J880. The new tires installed for testing were worn in during this process and on the trip from HSRI to the test site.

7.3 TEST PROCEDURES

Tests conducted for the purpose of providing data for validation of the articulated vehicle braking and handling performance simulation program included steady-state turning, braking-in-a-turn and high speed jackknife tests. These tests were run on both high and low coefficient surfaces, in the empty and loaded condition, and from various speeds. A list of signals recorded during the tests is given in Table 7-4.

7.3.1 STEADY-STATE TURNING. With the vehicle initially traveling in a straight line at the specified test speed, a limited ramp steer angle was input to the vehicle. Prior to the test, the steering column block was adjusted for the desired maximum steering wheel angle in order that this input could be applied in an open loop fashion. Constant vehicle speed was maintained until a steady-state vehicle response was obtained and recorded.

Tests were conducted at a nominal speed of 27 mph. Steer angles yielding steady-state lateral accelerations of 25, 50, 75, and 100% of the maximum value considered safe for the particular load configuration were used.

7.3.2 BRAKING-IN-A-TURN. Braking-in-a-turn tests were begun in the same manner as described for the steady-state turn tests. However, once the vehicle obtained a steady-state lateral acceleration, a quasi-step brake application was made, in which the brake line pressure was determined by the preset condition of the brake pedal stop. The steer angle was held fixed until the vehicle came to rest or until the vehicle was in danger of leaving the test area. Tests were

TABLE 7-4
Test Measurements

Variable	Steady-State Turning	Jackknife and Braking-in-a-Turn
ε_L, ε_r, ε_s	R	R
P_f, P_1, P_2, P_3	--	R
P_p	--	--
$\dot{\psi}$	R	R
θ	--	R
ϕ	R	R
A_x	--	R
A_y	R	R
V_x	R	R
LU_{1-6}	--	R
T_{1-6}	--	Mon

Key: R—Record Continuously During Test
Mon—Monitor Before and After Test

conducted from an initial velocity of 27 mph and with initial brake temperatures of 200° F or less. Steer angles and brake line pressures were chosen to cover a broad range of lateral and longitudinal decelerations with the aim of establishing performance limits at which one or more wheels lock.

7.3.3 HIGH SPEED JACKKNIFE TESTS. With the empty vehicle initially traveling in a straight line at 60 mph on the dry surface, a high level step brake application was made. The level of brake line air pressure attained, which was determined by the preset position of the brake pedal stop, was high enough to produce wheel lock of at least all four tractor rear wheels. This condition leads to the tendency for the vehicle to respond in an unstable, jackknife mode. When such response was imminent, the driver was allowed to introduce steering input in an effort to avoid jackknife, but the level of brake application was maintained until the vehicle came to rest. This procedure produced two runs resulting in jackknife response.

7.4 TIRE PARAMETERS FOR VALIDATION

Extensive tire test data, taken on the HSRI flat bed test machine [4] was available for new tires of the same model as those used in the experimental work. (The tire test data is given in Appendix G.) It was, of course, necessary to modify some of this data to fit the speed and surface conditions of the tests. This was done in a slightly different fashion for the dry and the wet surface as will be shown below.

7.4.1 TIRE PARAMETERS FOR THE DRY SURFACE. The 10 x 20 F tire, which was used on the tractor front axle as well as the trailer axles, has been considered in detail in Sections 6.4.2 and 3.2.2.

The drive axles were equipped with 10 x 20 F deep lug tires. With FA chosen to be .005 (a reasonable value based on past experience in the pitch plane modeling),

a few preliminary steady turn simulations were run. Based on these results, μ_0 for the tractor drive axles was chosen to be .85.

7.4.2 TIRE PARAMETERS FOR THE WET SURFACE. The simulations of the straight truck gave some insight into the 10 x 20 F tire on the wet jennite. Based on the experience gained in this work, FA = .01 was again used, with μ_0 = .55 on the front tractor tires and μ_0 = .65 on the trailer tires.

To choose μ_0 for the deep lug tires on the wet jennite a few preliminary steady turn simulations were run with FA set to .01. Based on these runs μ_0 was chosen to be .75 for the tractor drive wheels. (Such a high value is perhaps justified in view of the open tread pattern. For more details about this tire including photographs, see Reference 16.)

7.5 A COMPARISON BETWEEN TEST DATA AND THE SIMULATION RUNS

7.5.1 STEADY TURNS. Steady turn data was taken for the articulated vehicle in the empty and loaded condition on the dry surface and in the empty condition on the wet surface. The testing procedure has been explained in Section 7.3; the parameters necessary to describe the vehicle are given in Appendix F.

With the input data obtained as described above, the series of steady turn tests conducted on the straight truck was simulated. The results of the simulation are superimposed on the experimental results in Figures 7-3 through 7-5. A comparison of the predicted results and the numerical data is given in Table 7-5.

As in the case of the straight truck, certain differences between the experimental procedure and the simulated procedure should be noted. The steady turn experimental results were taken at a steady speed; whatever drive torque necessary to maintain that speed was applied. In the simulation, on the other hand, no drive torque was applied. Thus the simulated vehicle speed drops during the course of the run as a result of the longitudinal component of the side force of the steered front wheels. Therefore, the initial condition of vehicle speed was chosen slightly higher than the speed for which the results were desired; the vehicle model would reach a quasi-steady turn condition in which it would gradually lose speed. When the speed dropped to the test speed, the simulated yaw rate and lateral acceleration predictions were noted. These values are plotted in Figures 7-3 through 7-5.

Another slight difficulty is that the test data was taken at speeds slightly different than the "nominal speed" desired for the test. To facilitate the meaningful superposition of simulated and experimental results on the figures, the average speed of the empirical results is used as the speed at which the data was taken from the simulation. The actual speed at which the tests were run is included in the list of results given in Table 7-5.

It should also be noted that the measured steer angles were used in the simulation. These were, as one might expect, significantly different from side to side. (Since all the empirical results and simulation runs were right turns, the right steer angle was always larger than the left.) For the purposes of Figures 7-1 through 7-3, average steer angles were plotted. The measured steer angles are given in Table 7-5.

The measured results and the predicted results are in very close agreement for the empty trailer runs, but in the case of the loaded vehicle, a marked difference is apparent between the experimental and simulated results, since even at low lateral accelerations the simulation predicts higher lateral acceleration than the measured values. The reasons for this difference are not clear; the experimental data seems smooth and quite repeatable, yet the simulation has proven quite accurate, especially for low lateral accelerations. (A simplified purely analytical analysis based on the work of Jindra [17] verifies the result of the simulation.)

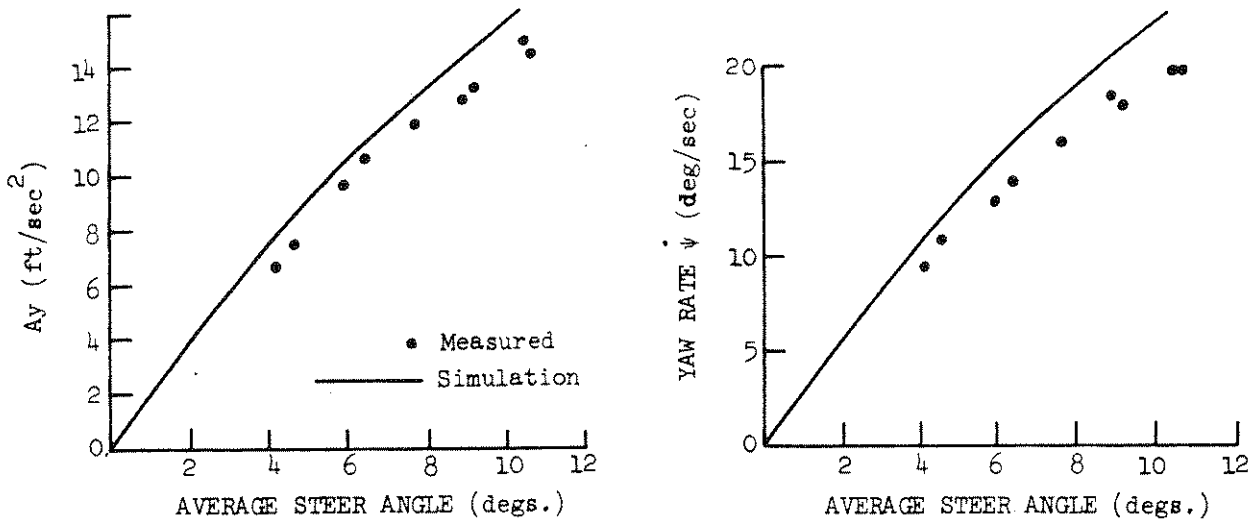

Figure 7-3. Steady turn

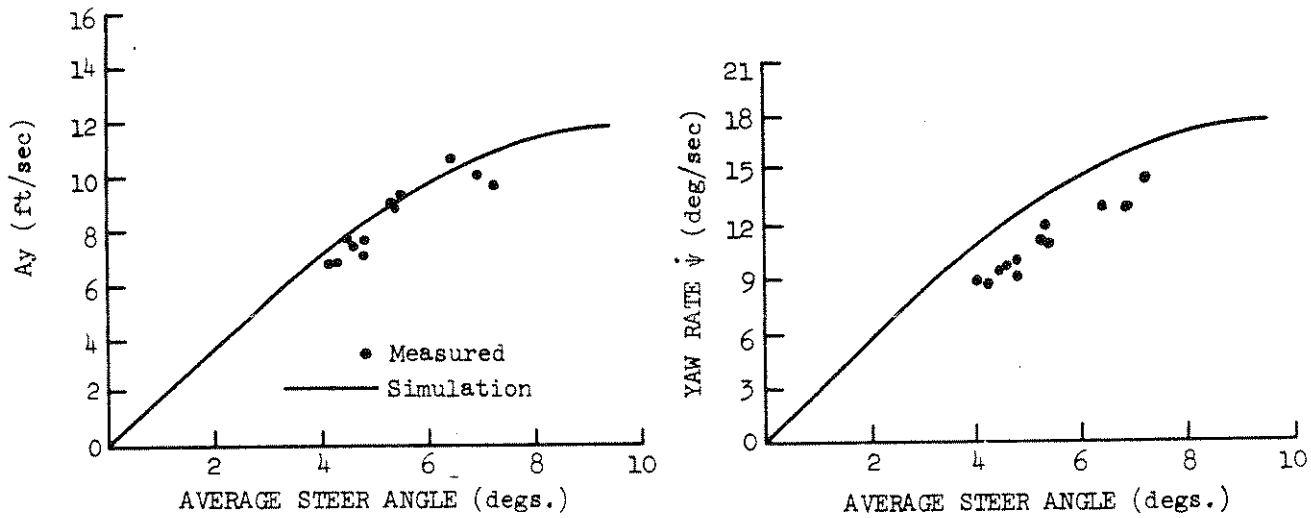

Figure 7-4. Steady turn

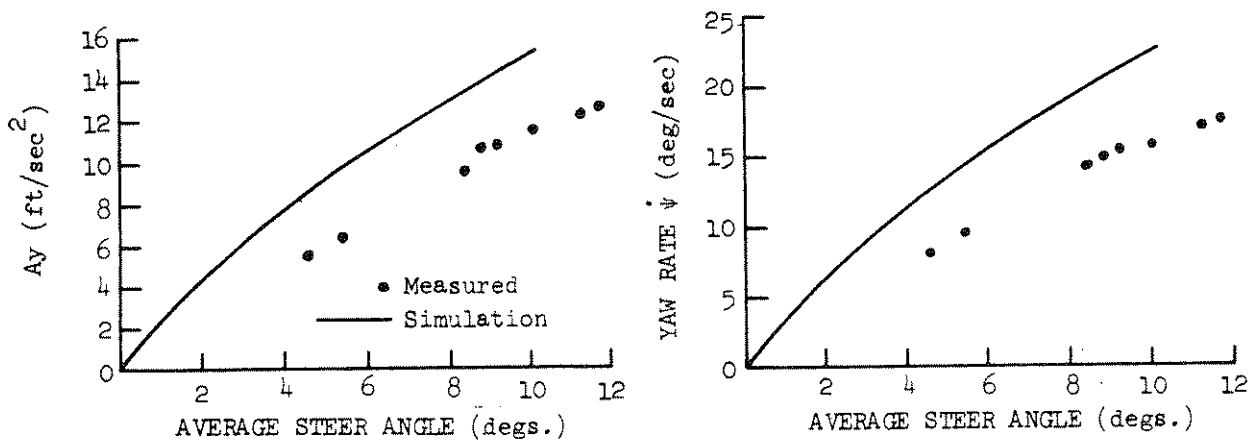

Figure 7-5. Steady turn

TABLE 7-5
Steady Turn Tractor-Trailer

ε_r (deg)	ε_ℓ (deg)	$V_{measured}$ (ft/sec)	A_y (ft/sec^2) measured	A_y (ft/sec^2) simulated	$\dot{\psi}$ (deg/sec) measured	$\dot{\psi}$ (deg/sec) simulated
(a) Empty, dry surface Simulation speed: 40.0 ft/sec						
9.67	11.18	38.1	14.50	15.00	19.8	21.8
9.67	11.07	38.1	14.80	15.80	19.8	21.8
8.56	9.78	38.1	13.20	14.60	17.7	20.7
8.36	9.46	39.6	12.80	14.30	17.9	20.0
7.34	8.38	40.1	11.90	12.90	15.9	18.2
6.23	7.09	40.5	10.30	11.40	14.1	16.1
5.67	6.24	40.5	9.60	10.7	13.2	15.0
4.00	4.40	40.5	6.50	7.90	9.3	11.0
4.47	4.73	40.5	7.74	8.00	10.5	11.1
(b) Empty, wet surface Simulation speed: 40.0 ft/sec						
6.60	7.84	39.5	9.60	9.80	14.3	16.1
5.86	6.98	39.5	10.40	10.00	12.9	14.3
5.86	6.77	40.3	9.35	9.00	12.7	14.1
5.20	5.90	39.5	9.35	9.40	10.8	13.5
5.02	5.70	39.5	9.20	9.20	11.6	12.8
4.46	5.16	40.2	7.65	7.75	10.0	12.0
4.93	4.73	40.3	7.10	7.60	9.0	11.0
4.28	4.94	40.3	7.40	7.90	9.5	11.2
4.19	4.84	40.3	7.75	7.75	9.4	11.8
4.09	4.51	40.3	6.70	7.20	8.9	10.5
3.90	4.40	40.3	6.70	7.00	8.8	10.3
(c) Loaded, dry surface Simulation speed: 39.0 ft/sec						
11.07	12.36	38.8	12.90	16.60	17.8	23.0
10.69	11.93	38.8	12.20	16.20	17.1	22.7
9.58	10.54	39.0	11.50	15.30	15.9	22.4
8.74	9.56	38.9	10.90	14.00	15.4	22.0
8.37	9.25	39.0	10.00	13.50	15.0	21.7
7.90	8.70	39.0	9.60	13.50	14.3	19.9
5.20	5.60	39.0	6.70	9.50	9.7	14.2
4.56	4.62	39.3	5.50	8.40	7.6	12.3

Simple explanations such as geometric errors in the description of the vehicle or errors in the tire description seem at this stage untenable, but it is still expected that, through the course of future use of the simulation and further experimental work, the reasons for this discrepancy will become apparent.

7.5.2 BRAKING-IN-A-TURN. The experimental procedure for the braking-in-a-turn tests has been explained in Section 7.3.2. Some results from these tests are plotted in Figures 7-6 and 7-7. In these figures, steady-state lateral acceleration before the application of the brakes is plotted vs. maximum longitudinal deceleration after the application of the brakes. The incidence of wheel lockup may be inferred from the manner of plotting of the point. It should be noted that the properties of the tire-road interface may be expected to be quite similar at the nominal test speeds of 25 and 30 mph, thus, both 25 and 30 mph data is included in Figures 7-6 and 7-7.

In the simulation runs, the measured steer and brake pressure data from the braking-in-a-turn tests was not used; rather, the simulation was used to predict the maximum longitudinal deceleration possible without wheel lockup when starting from a steady turn. Thus, for points in the area of the figures above the simulation line, the simulation will predict wheel lockup, and in the area below the simulation line, the simulation will predict that no wheels will lock. The simulated results split the empirical data quite accurately; with few exceptions, the locked wheel empirical results fall above the simulation line and the unlocked results below the simulation line. In the next section, in which a single braking-in-a-turn run is considered in detail, further evidence is given of the reliability of the articulated vehicle simulation.

7.5.3 DETAILED SIMULATED AND EMPIRICAL RESULTS OF A BRAKING-IN-A-TURN MANEUVER. Time histories of the important dynamic variables describing a braking-in-a-turn maneuver are given in Figure 7-8a and 7-8b. In this maneuver, a left turn with brakes applied at time $t = 2.15$ seconds, points taken directly from the strip chart data on board the articulated vehicle were entered in the simulation for (1) the steer angle (right side steady-state 4.73, left side steady-state 4.47) and (2) the applied brake pressure at the foot valve. Lateral acceleration A_y, longitudinal acceleration A_x, yaw rate $\dot{\psi}$, and the articulation angle Γ are plotted vs. time, and the simulated trajectory is given. Predicted and measured incidence of wheel lockup are shown on the right side of the lead trailer tandem axle. In this case, as in the majority of the articulated vehicle runs, the correspondence between empirical results and the predicted results is remarkably good.

7.5.4 DETAILED RESULTS FOR HIGH SPEED JACKKNIFE TESTS. Time histories of the important dynamic variables describing a high speed jackknife test are given in Figures 7-9a and 7-9b. In this maneuver, which starts with an initial longitudinal velocity of 60 mph, a step input is applied at the foot valve, causing line pressure to rise almost immediately to 88 psi. This was sufficient to lock all the tractor and trailer wheels in the test; this result was also predicted by the simulation. The empirical and simulated results prior to impact with the articulation angle limiter are given in Figures 7-9a and 7-9b. It should be noted that, although the driver tried to maintain stability through the application of the steering maneuver shown in the figure, that simulated steer angle was held to zero. The fact that the driver steer correction was largely ineffective can be inferred by the relatively close agreement between the simulation and the empirical result.

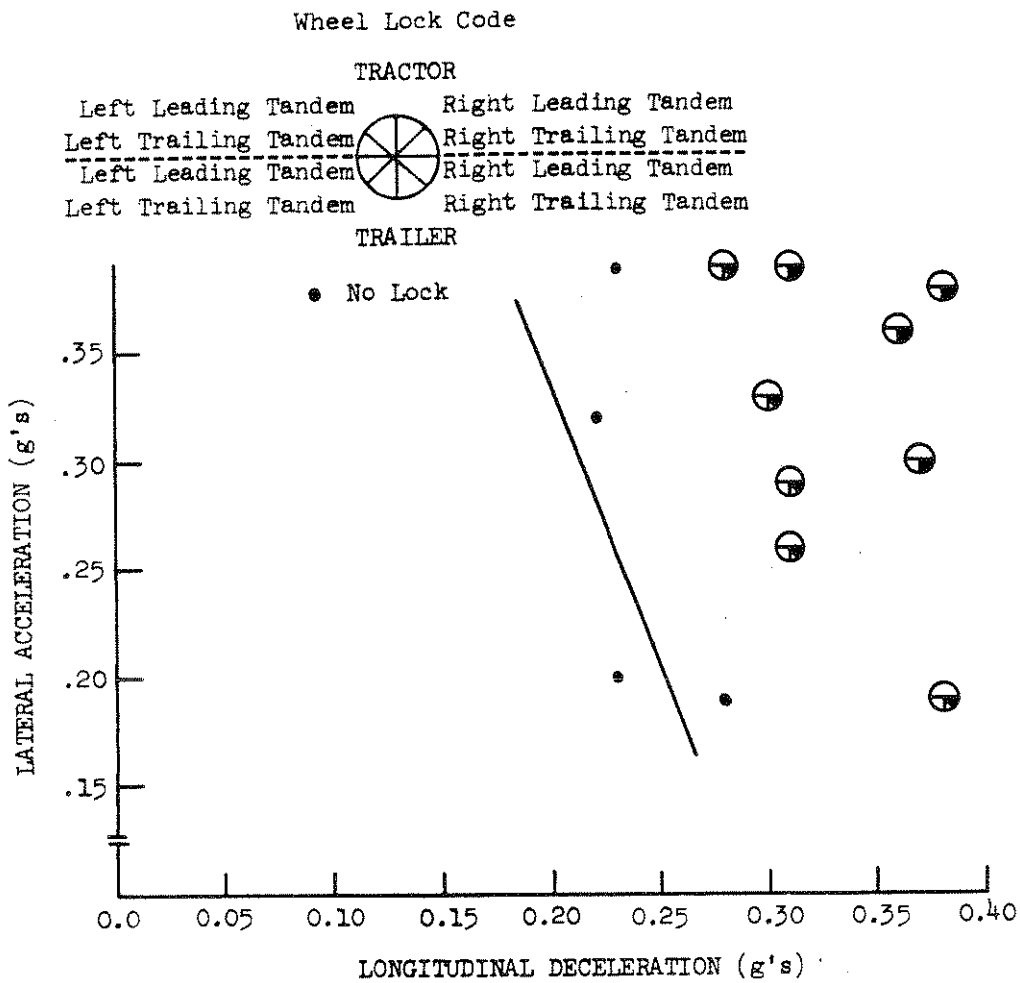

Figure 7-6. Braking-in-a-turn; dry, empty

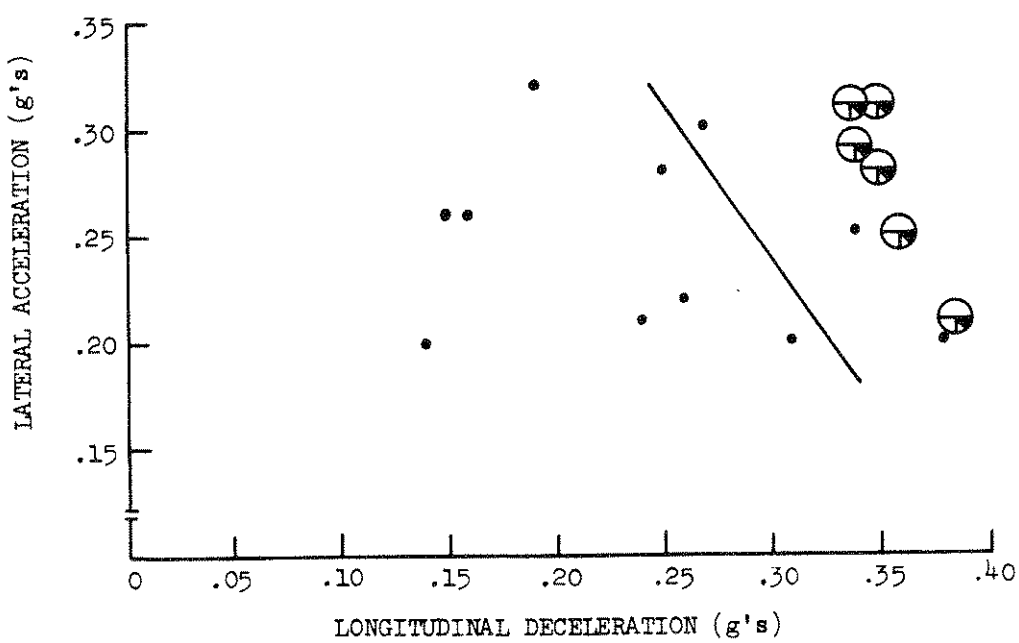

Figure 7-7. Braking-in-a-turn; dry, loaded

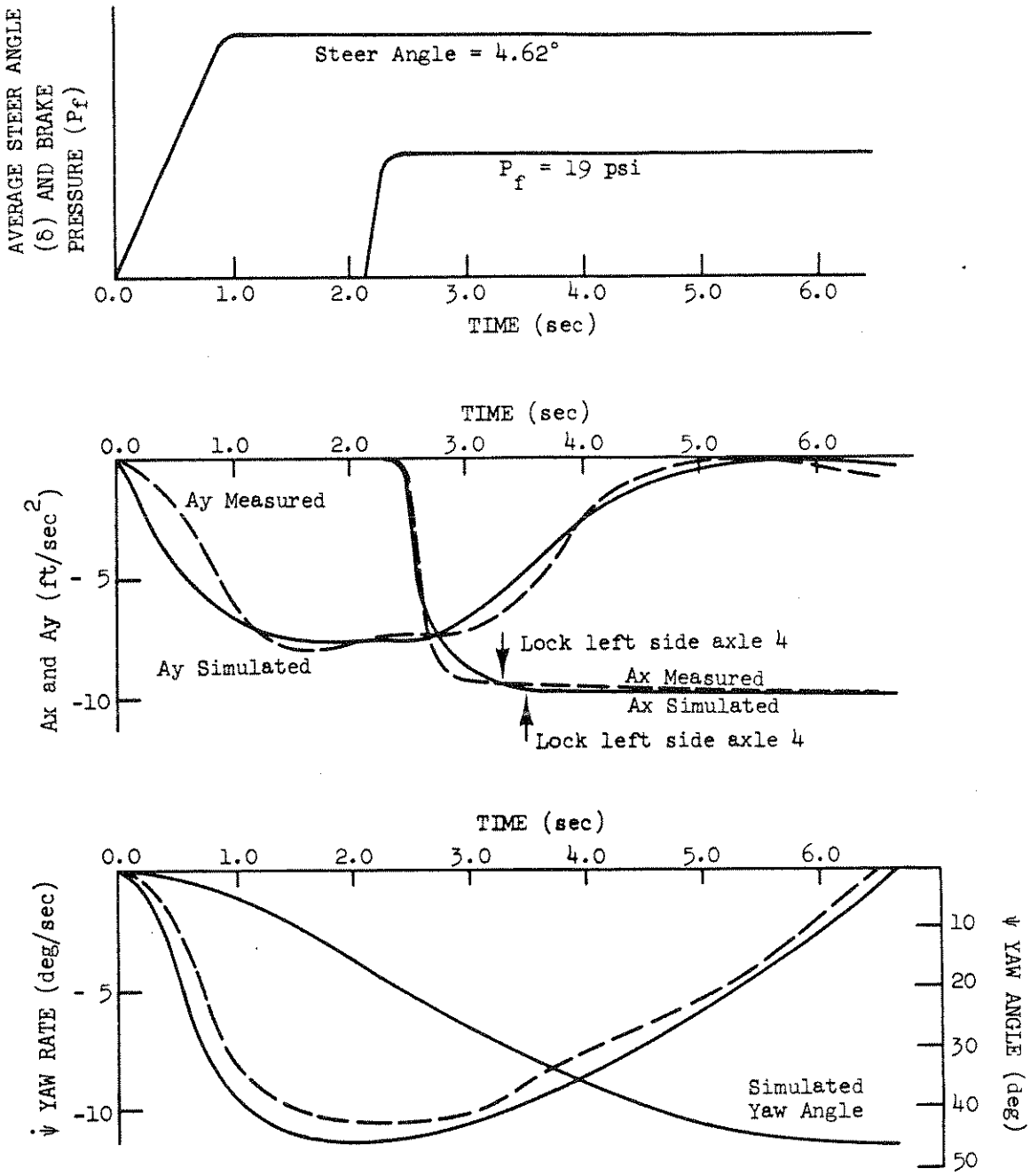

Figure 7-8a. Time history of a braking-in-a-turn maneuver

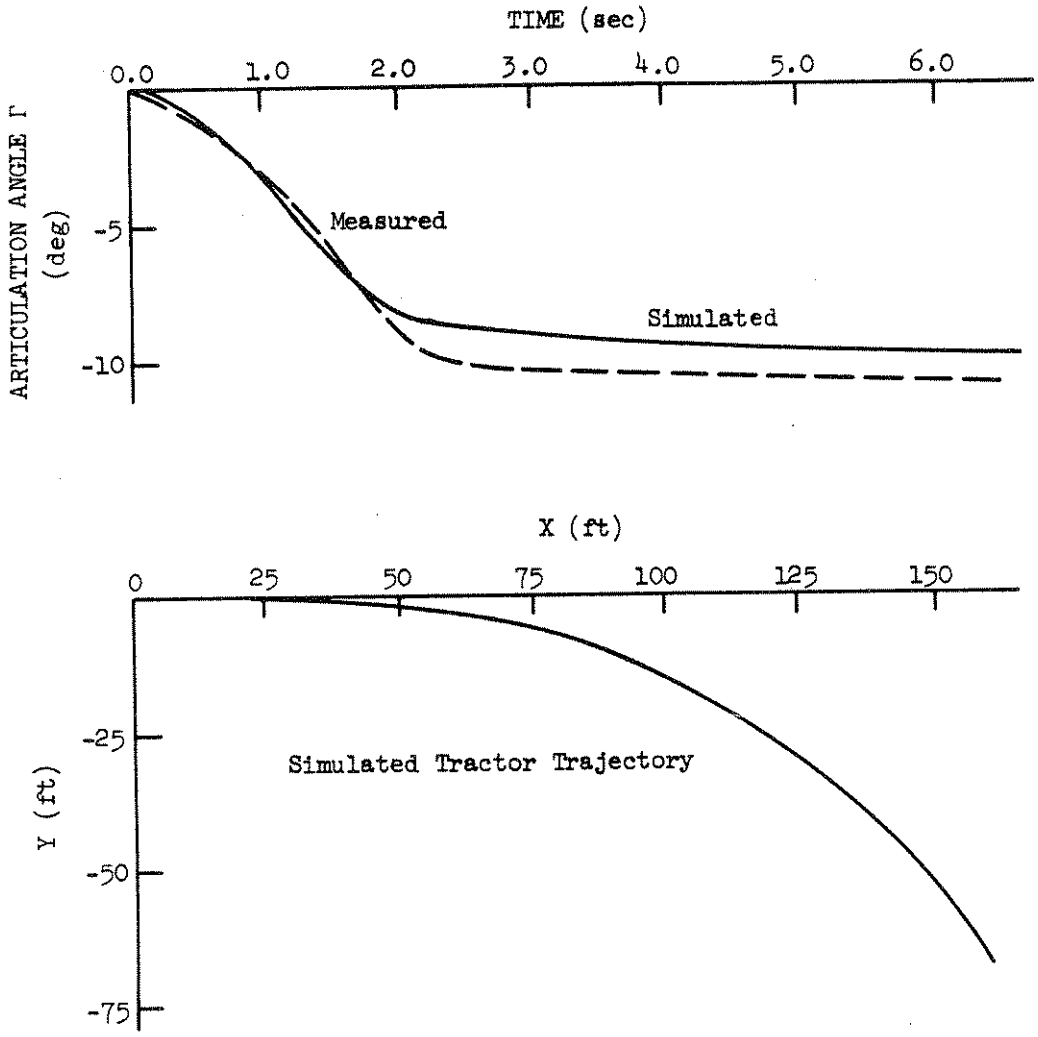

Figure 7-8b. Time history of a braking-in-a-turn maneuver

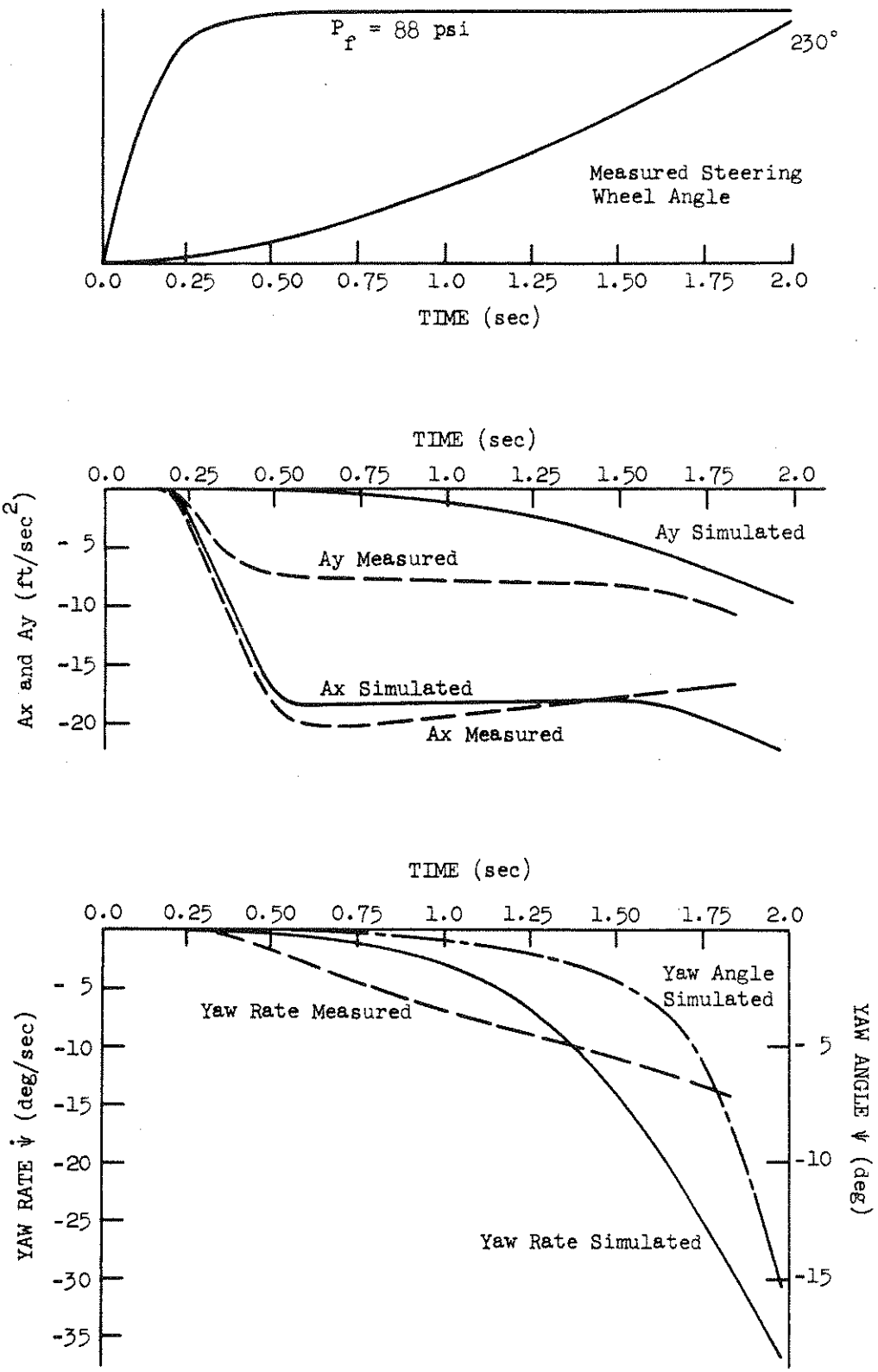

Figure 7-9a. Time history of a jackknife maneuver

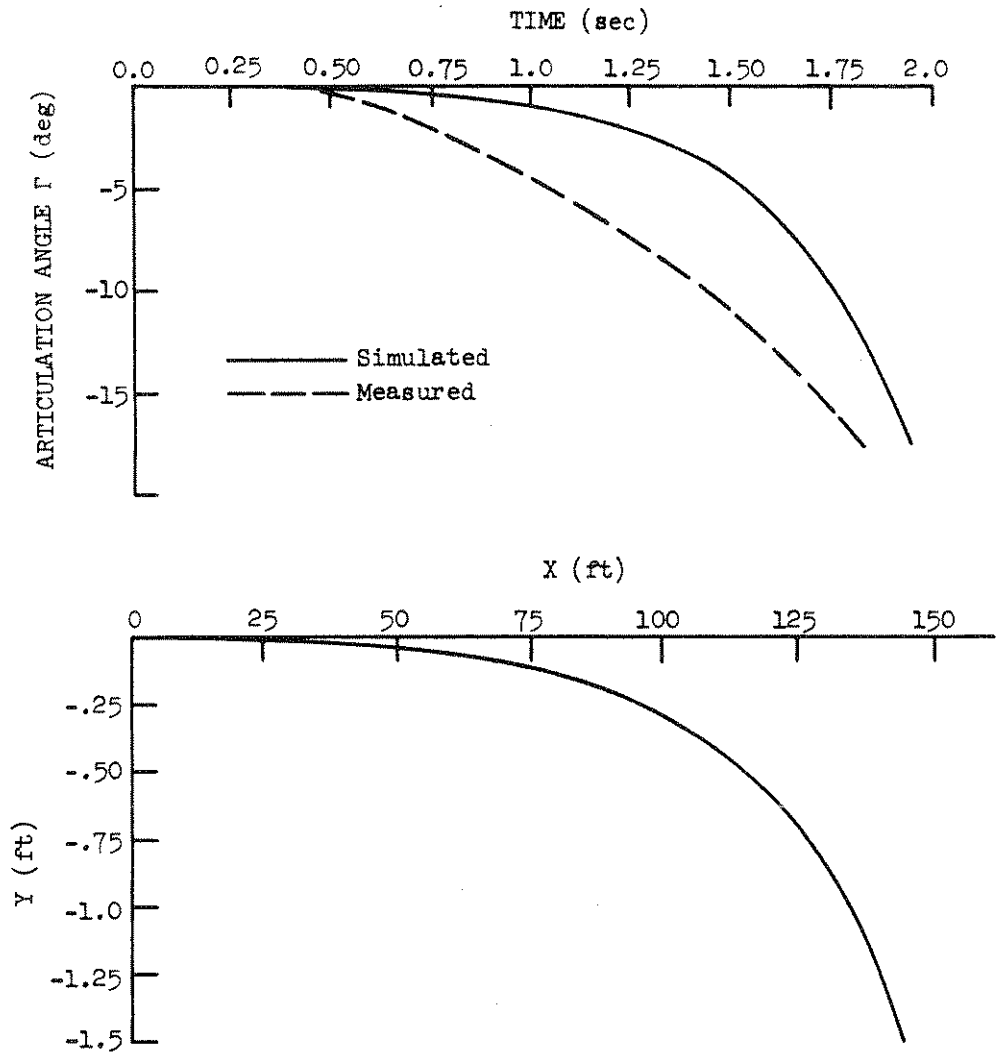

Figure 7-9b. Time history of a jackknife maneuver

8.0 SUMMARY AND CONCLUSIONS

The primary objective of the Phase II study was to develop a simulation program for predicting the steering and combined steering and braking performance of trucks and tractor-trailers. This objective has been fulfilled. The results from the simulation compare favorably with the data from vehicle tests.

The problem of developing a simulation tool for predicting the directional response of an articulated vehicle is an immense, complex undertaking. To complete this undertaking, it was necessary to begin with the pitch plane model developed in Phase I [1], and perform the following additional tasks:

(1) Select appropriate axis systems and write equations describing the vehicle motion in terms of dynamic variables defined relative to these axis systems.

(2) Program and refine a semi-empirical mathematical model for representing measured tire shear force characteristics, and, in addition, consider aligning torque and special effects due to dual tires.

(3) Develop techniques for computing forces and moments of constraint between sprung and unsprung masses.

(4) Model the fifth wheel coupling between tractor and trailer.

(5) Include deflection and compliance steer characteristics as well as side-to-side differences in steer angle.

(6) Develop, refine, and use equipment and techniques for measuring vehicle inertial properties, axle roll steer, fifth wheel roll spring rate, and tire shear force characteristics.

(7) Perform full scale vehicle tests consisting of steady turns, braking-in-a-turn maneuvers, and jackknife maneuvers.

(8) Simulate the maneuvers listed in (7) and compare the predicted results with measured results to verify the validity of the simulations.

A detailed technical discussion of the work done on these eight tasks has been presented in this report.

The braking and handling program has been written to be efficient and easy to use. Nevertheless, calculation of articulated vehicle response to braking and steering inputs is, necessarily, a very complex problem. Consequently, the users of this program must know a great deal about the components of the vehicle (or projected vehicle) to be able to supply the needed parametric data. In addition, since almost any conceivable open loop steering and braking maneuver can be simulated, the user will be forced to carefully consider which combinations of steering and braking inputs will give him the most useful information. While computer costs may run as high as $7.00/second simulated time,* it seems clear that, with a judicious choice of simulated maneuvers, the simulations may be used in a very cost effective manner to aid in the solution of vehicle design problems.

*For the five axle articulated vehicle, this figure related to the MTS system (see Section 4). The costs will vary for other systems.

APPENDIX A

List of Symbols

Appendix A

The following list includes input parameters to the program, the parameters which are computed in the program, and the variables of motion. The dimensions of the input parameters are in [inch, pound, second]. These are converted to the [slug, foot, second] system immediately after they are read into the program by subroutine INPUT. Thus, the equations of motion and all the auxiliary computations in subroutine FCT1 are written in terms of variables in the [slug, foot, second] system.

To avoid confusion, parameters which are read in are labelled with an (R), parameters which are calculated rather than input are labelled with a (C), and the variables of motion are labelled with a (V).

For the walking beam; straight truck or tractor...

AA1	horizontal distance from walking beam pin to front tandem axle (in.) (R)
AA2	horizontal distance from walking beam pin to rear tandem axle (in.) (R)
AA3	horizontal distance from walking beam pin to walking beam mass center (ft.) (C)
AA4	vertical distance from axle to walking beam (in.) (R)
AA5	vertical distance from axle to torque rod (in.) (R)
AA6	horizontal distance from front tandem axle to walking beam mass center (ft.) (C)
AA7	horizontal distance from rear tandem axle to walking beam mass center (ft.) (C)

For the 4 sping suspension; straight truck or tractor...

AA1	horizontal distance from front leaf-frame contact to axle center (in.) (R)
AA2	horizontal distance from rear leaf-frame contact to axle center (in.) (R)
AA4	horizontal distance from front leaf contact to load leveler "pin" (in.) (R)
AA5	horizontal distance from rear leaf contact to load leveler "pin" (in.) (R)
AA6	vertical distance from axle down to torque rod (in.) (R)
AA7	angle between torque rod and horizontal (deg.) (R)
AA8	horizontal distance from axle center forward to torque rod (in.) (R)
ARM1	perpendicular distnace from line of action of TR2 (TR3) to forward (rear) tandem axle center (ft.) (C)
ARM2	horizontal distance from sprung mass c.g. to forward tandem axle center (ft.) (C)
ARM3	horizontal distance from sprung mass c.g. to rear tandem axle center (ft.) (C)

For walking beam; trailer...

AA9	horizontal distance from walking beam pin to front tandem axle (in.) (R)
AA10	horizontal distance from walking beam pin to rear tandem axle (in.) (R)
AA11	horizontal distance from walking beam pin to walking beam mass mass center (ft.) (C)

AA13	vertical distance from axle to torque rods (in.) (R)
AA14	horizontal distance from front tandem axle to walking beam mass center (ft.) (C)
AA15	horizontal distance from rear tandem axle to walking beam mass center (ft.) (C)

For the 4 spring suspension; trailer...

AA9	horizontal distance from front lear-frame contact to axle center (in.) (R)
AA10	horizontal distance from rear leaf-frame contact to axle center (in.) (R)
AA12	horizontal distance from front leaf contact to load leveler "pin" (in.) (R)
AA13	vertical distance from rear leaf contact to load leveler "pin" (in.) (R)
AA14	vertical distance from axle down to torque rod (in.) (R)
AA15	angle between torque rod and horizontal (deg.) (R)
AA16	horizontal distance from axle center forward to torque rod (in.) (R)
ARM4	perpendicular distance from line of action of TR4 (TR5) to forward (rear) tandem axle center (ft.) (C)
ARM5	horizontal distance from sprung mass c.g. to forward tandem axle center (ft.) (C)
ARM6	horizontal distance from sprung mass c.g. to rear tandem axle center (ft.) (C)

For all vehicles...

A	transformation matrix from truck (tractor) inertia axis to body axis (C)
A1	horizontal distance from truck (tractor) CG to center of truck (tractor) front suspension (in.) (R)
A2	horizontal distance from truck (tractor) CG to center of truck (tractor) rear suspension (in.) (R)
A3	horizontal distance from trailer CG to 5th wheel (in.) (R)
A4	horizontal distance from trailer CG to center of trailer suspension (in.) (R)
ALPHA1	static distance, truck (tractor) front axle to ground (in.) (R)
ALPHA2	static distance, truck (tractor) rear axle(s) to ground (in.) (R)
ALPHA3	static distance, trailer axle(s) to ground (in.) (R)
AT	transformation matrix from trailer inertia axis to body axis (C)
BB	horizontal distance from 5th wheel to midpoint of tractor rear suspension (in.) (R)
BZ	transformation matrix from truck (tractor) unsprung axis to body axis (C)
BZT	transformation matrix from trailer unsprung axis to body axis (C)
C1	viscous damping: jounce on truck (tractor) front suspension (lb.-sec./in.) (R)
C2	viscous damping: rebound on truck (tractor) front suspension (lb.-sec./in.) (R)
C3	viscous damping: jounce on truck (tractor) rear suspension (lb.-sec./in.) (R)
C4	viscous damping: rebound on truck (tractor) rear suspension (lb.-sec./in.) (R)

C5	viscous damping: jounce on trailer suspension (lb.-sec./in.) (R)
C6	viscous damping: rebound on trailer suspension (lb.-sec./in.) (R)
CALF(I,JI)	lateral stiffness, tires at wheel I,JI (lbs./deg.) (R)
CF1	maximum coulomb friction, truck (tractor) front suspension (lb.) (R)
CF2	maximum coulomb friction, truck (tractor) rear suspension (lb.) (R)
CF3	maximum coulomb friction, trailer suspension (lb.) (R)
CFP1(I)	curve fit parameter No. 1, axle I (R)
CFP2(I)	curve fit parameter No. 2, axle I (deg.) (R)
CS(I,JI)	longitudinal stiffness, wheel I,JI (lbs.) (R)
CT(I)	tire-road interface vertical damping, axle I (lb.-sec./ft.) (C)
D	vertical distance from 5th wheel to tractor CG (in.) (R)
D1	vertical distance from 5th wheel to trailer CG (in.) (R)
DEL1-DEL3	coulomb friction "break points" (ft./sec.) (C)
DELTA	relative displacement at the 5th wheel (in.) (C)
DELTA1	static vertical distance, truck (tractor) CG to truck (tractor) front axle (in.) (R)
DELTA2	static vertical distance, truck (tractor) CG to truck (tractor) rear axle(s) (ft.) (C)
DELTA3	static vertical distance, trailer CG to trailer rear axle(s) (in.) (R)
DT2	distance between dual tires, truck (tractor) rear suspension (in.) (R)
DT3	distance between dual tires, trailer suspension (in.) (R)
FA(I)	tire/road friction reduction parameter, axle I (sec./ft.) (R)
G1	gravity x component (R)
G2	gravity y component (R)
G3	gravity z component (C)
GAMMA	articulation angle (deg.) (C)
IXX	truck (tractor) sprung mass roll moment of inertia (in.-lb.-sec.**2) (R)
IYY	truck (tractor) sprung mass pitch moment of inertia (in.-lb.-sec.**2) (R)
IZZ	truck (tractor) yaw moment of inertia (in.-lb.-sec.**2) (R)
IXZ	truck (tractor) pitch plane cross moment (in.-lb.-sec.**2) (R)
ITXX	trailer sprung mass roll moment of inertia (in.-lb.-sec.**2) (R)
ITYY	trailer sprung mass pitch moment of inertia (in.-lb.-sec.**2) (R)
ITZZ	trailer yaw moment of inertia (in.-lb.-sec.**2) (R)
ITXZ	trailer pitch plane cross moment (in.-lb.-sec.**2) (R)
IWIND	wind key; 0 implies no wind, 1 implies a wind (R)
JA1	roll moment of truck (tractor) front axle (in.-lb.-sec.**2) (R)
JA2	roll moment of truck (tractor) rear axle(s) (in.-lb.-sec.**2) (R)
JA3	roll moment of trailer axle(s) (in.-lb.-sec.**2) (R)
JS(I)	polar moment of inertia, wheels at axle I (in.-lb.-sec.**2) (R)
K1	spring rate, truck (tractor) front suspension (lb./in.) (R)
K2	spring rate, truck (tractor) rear suspension (lb./in.) (R)
K3	spring rate, trailer suspension (lb./in.) (R)
KAXLE	number of axles on vehicle (C)
KEY	truck axle key — 0 for single axle
KEY(1)	tractor axle key — 1 for walking beam
KEY(2)	trailer axle key — 2 for four spring suspension

KROAD	road key (R)
KT(I)	spring rate of tires, axle I (lb/in.) (R)
M1	sprung mass of truck (tractor) (slugs) (C)
M2	sprung mass of trailer (slugs) (C)
MS(I)	mass of suspension axle and wheel, axle I (slugs) (C)
MC5	moment across the 5th wheel (in.-lbs./deg.) (R)
MUZERO(I)	coefficient of friction, tires, axle I (C)
MZ	aligning torque (in.-lbs.) (C)
NS(I)	total static load on tires, axle I (lbs.) (C)
OMEGAD(I,JI)	wheel angular acceleration (rad./sec.^{2}) (V)
P	rotation rate about "body x" axis (rad./sec.) (C)
P1	truck (tractor) walking beam interaxle load transfer parameter (C)
PERCNT	percent effectiveness of truck torque rods (R)
PERCNT(1)	percent effectiveness of tractor torque rods (R)
PERCNT(2)	percent effectiveness of trailer torque rods (R)
PIN	5th wheel spring rate (C)
PINX	force on the tractor from the 5th wheel in the X1 direction (C)
PINY	force on the tractor from the 5th wheel in the Y1 direction (C)
PINZ	force on the tractor from the 5th wheel in the Z1 direction (C)
PJ1	roll moment of inertia of payload (in.-lb.-sec.**2) (R)
PJ2	pitch moment of inertia of payload (in.-lb.-sec.**2) (R)
PJ3	yaw moment of inertia of payload (in.-lb.-sec.**2) (R)
PX	horizontal distance from midpoint of truck rear (trailer) suspension to payload mass center (in.) (R)
PW	weight of payload (lb.) (R)
PZ	vertical distance from ground to payload mass center (in.) (R)
Q	rotation rate about "body y" axis (rad./sec.) (C)
R	rotation rate about "body z" axis (rad./sec.) (C)
RCH1	roll center height, truck (tractor) front suspension (in.) (R)
RCH2	roll center height, truck (tractor) rear suspension (in.) (R)
RCH3	roll center height, trailer suspension (in.) (R)
ROADZ(I)	vertical coordinate of road, axle I...up is positive (in.) (R)
RR(I,JI)	rolling radius, tires on wheel I,JI (ft.) (C)
RS1	compliance steer (deg./in.) (R)
RSC1	roll steer coefficient, truck (tractor) front suspension (R)
RSC2	roll steer coefficient, truck (tractor) rear suspension (R)
RSC3	roll steer coefficient, trailer suspension (R)
S(I,JI)	extension of suspension at wheel I,JI (ft.) (C)
SD	velocity of suspension extension (ft./sec.) (C)
SF(I,JI)	total load minus static load in the suspension, axle I (tension is positive) (lbs.) (V)
SLIP(I,JI)	wheel slip, wheel I,JI (V)
SMY(I)	lateral constraint force at axle I (C)
SY1	horizontal distance from truck (tractor) body x-axis to truck (tractor) front suspension (in.) (R)
SY2	horizontal distance from truck (tractor) body x-axis to truck (tractor) rear suspension (in.) (R)
SY3	horizontal distance from trailer body x-axis to trailer suspension (in.) (R)
T(I,JI)	attempted brake torque, wheel I,JI (in.lbs.) (R)

TIMF	maximum real time for simulation (sec.) (R)
TN1-TN4	contact force between tractor leaf springs and frame (lb) (V)
TP1	trailer walking beam interaxle load transfer parameter (C)
TQ(I,JI,1)	line pressure time lag, wheel I,JI (sec.) (R)
TQ(1,JI,2)	line pressure rise time characteristic, wheel I,JI (sec.) (R)
TRA1	half track, truck (tractor) front axle (in.)
TRA2	half track, truck (tractor) rear axle(s) (in.)
TRA3	half track, trailer axle(s) (in.)
TRUCK	exit key (R): TRUCK = 1.0, another data set follows TRUCK = 0.0, call exit
TR2-TR5	tensile forces in torque rods at appropriate axle (lb.) (C)
TT(I,JI)	actual brake torque, wheel I,JI (ft.lbs.) (V)
TTN1-TTN4	contact forces between trailer leaf spring and frame (lb.) (V)
TXDD(I)	longitudinal acceleration of trailer axle I (ft./sec.**2) (V)
TYDD(I)	lateral acceleration of trailer axle I (ft./sec.**2) (V)
TXX	static load on trailer walking beam pin (lb.) (C)
U	speed in the "body x" direction (ft./sec.) (C)
V	speed in the "body y" direction (ft./sec.) (C)
VEL	initial velocity (ft./sec.) (R)
W	speed in the "body z" direction (ft./sec.) (C)
W1	sprung weight of truck (tractor) (lb.) (R)
W2	sprung weight of trailer (lb.) (R)
WFORCE	force of wind applied to mass center (C)
WMOM	moment of wind about an axis through the mass center (C)
WS(I)	weight of suspension, axle, and wheel; axle I (lb.) (R)
XDD(I)	longitudinal acceleration of truck (tractor) axle (I) (ft./sec.**2) (V)
XDOT(I,JI)	longitudinal velocity of wheel I,JI (ft./sec.) (V)
XS(I,JI)	body x coordinate of suspension I,JI (ft.) (C)
XU(I)	body x coordinate of center of axis I (ft.) (C)
XXX	static load on tractor walking beam pin (lb.) (C)
YDD(I)	lateral acceleration of truck (tractor) axle I (ft./sec.**2) (V)
YS(I,JI)	body y coordinate of suspension I,JI (ft.) (C)
YT(I,JI)	tire position, wheel I,JI (ft.) (V)
YTD(I,JI)	tire velocity, wheel I,JI (ft./sec.) (V)
YU(I,JI)	body y coordinate of center of wheel I,JI (ft.) (C)
Z1-Z3	static suspension deflection computed in look-up for nonlinear spring (ft.) (C)

For brake module at wheel I,JI...

AB(I,JI)	distance from horizontal centerline of drum to parallel line through shoe contact (in.) (R)
AC(I,JI)	brake chamber area (sq. in.) (R)
ALPH1(I,JI)	acute angle between a diametrical line through a shoe pin and a diametrical line through the top (see figure 2-31, Reference 1) drum/lining contact point of the same shoe (deg.) (R)
ALPH3(I,JI)	ALPHO(I) + 2*ALPH1(I) (deg.) (R)
ALPHO(I,JI)	lining contact angle (deg.) (R)
ALPHW(I,JI)	wedge angle (deg.) (R)
ALPRIM(I,JI)	radial distance from center of drum to shoe pin (in.)
BETA(I,JI)	lining offset angle (deg.) (R)
C2(I,JI)	distance from horizontal centerline of drum to parallel line through point of actuating force (in.) (R)

EM(I,JI)	mechanical efficiency (R)
FRAY(I,JI)	brake fade coefficient (R)
HB(I,JI)	distance from horizontal centerline through shoe pin to parallel line through connector contact point (in.) (R)
IBRT(I,JI)	brake type (R) 0 for no brakes 1 for s-cam brake 2 for 2-wedge brake 3 for 1-wedge brake 4 for DSSA 5 for duplex brake 6 for disc brake
OH(I,JI)	distance from vertical centerline of drum to parallel line through shoe contact point (in.) (R)
PO(I,JI)	pushout pressure (p.s.i.) (R)
RC(I,JI)	cam radius (in.) (R)
RD(I,JI)	drum radius (in.) (R)
SAL(I,JI)	slack adjuster length (in.) (R)
ULH(I,JI)	lining friction coefficient, high (R)
ULL(I,JI)	lining friction coefficient, low (R)

For all vehicles...The following are the integration variables sent to subroutine HPCG

Y(1)	Z (inertial)
Y(2)	W
Y(3)	THETA
Y(4)	Q
Y(5)	X (inertial)
Y(6)	U
Y(7)	YT(1,1)
Y(8)	d/dt(ZA1)
Y(9)	YT(1,2)
YT(10)	d/dt(THETAA1)

For a single rear axle tractor...

Y(11)	YT(2,1)
Y(12)	d/dt(ZA2)
Y(13)	YT(2,2)
Y(14)	d/dt(THETAA2)
Y(15)	0
Y(16)	0
Y(17)	0
Y(18)	0

For the four leaf tandem tractor...

Y(11)	YT(2,1)
Y(12)	d/dt(ZA2)
Y(13)	YT(2,2)
Y(14)	d/dt(THETAA2)
Y(15)	YT(3,1)
Y(16)	d/dt(ZA3)
Y(18)	d/dt(THETAA3)

For the walking beam tractor...

Y(11)	YT(2,1)
Y(12)	d/dt(ZS(3,1))
Y(13)	YT(2,2)
Y(14)	d/dt(THETAT1)
Y(15)	YT(3,1)
Y(16)	d/dt(ZS(3,2))
Y(17)	YT(3,2)
Y(18)	d/dt(THETAT2)
Y(19)	PHI
Y(20)	P
Y(21)	PSI
Y(22)	R
Y(23)	Y (inertial)
Y(24)	V
Y(25)	XT
Y(26)	UT
Y(27)	YT
Y(28)	VT
Y(29)	ZT
Y(30)	WT
Y(31)	PHIT
Y(32)	PT
Y(33)	THETAT
Y(34)	QT
Y(35)	PSIT
Y(36)	RT

For a single rear axle trailer...

Y(37)	YT(4,1)
Y(38)	d/dt(ZA4)
Y(39)	YT(4,2)
Y(40)	d/dt(THETAA4)
Y(41)	0
Y(42)	0
Y(43)	0
Y(44)	0

For the four leaf tandem trailer...

Y(37)	YT(4,1)
Y(38)	d/dt(ZA4)
Y(39)	YT(4,2)
Y(40)	d/dt(THETAA4)
Y(41)	YT(5,1)
Y(42)	d/dt(ZA5)
Y(43)	YT(5,2)
Y(44)	d/dt(THETAA5)

For the walking beam trailer...

Y(37)	YT(4,1)
Y(38)	d/dt(ZS(4,1))
Y(39)	YT(4,1)

Y(40)	d/dt(THETAT3)
Y(41)	YT(5,1)
Y(42)	d/dt(ZS(5,2))
Y(43)	YT(5,2)
Y(44)	d/dt(THETAT4)

APPENDIX B

Euler Angles and Axis Systems

Appendix B

In the truck and tractor-trailer simulation models Euler angles are used to specify the orientation of the body axes of the vehicle with respect to a fixed set of axes (inertial axes). Since the Euler angles for describing the trailer orientation are analogous to the Euler angles for the tractor (or straight truck), it is sufficient to discuss the equations for computing the tractor orientation. Similar equations apply to the trailer.

The angles selected for this program are:

(1) ψ, a yaw angle measured in a plane perpendicular to the inertial system vertical unit vector $\hat{z}n$,

(2) θ, a pitch angle measured in a plane perpendicular to the unsprung mass lateral unit vector $\hat{y}1$,

and

(3) ϕ, a roll angle measured in a plane perpendicular to the sprung mass forward unit vector $\hat{x}b$.

The angles ψ, θ, and ϕ are shown in Figure B-1. In this discussion four sets of axis systems are used. These axis systems are specified by the following sets of unit vectors:

(1) $[\hat{x}n, \hat{y}n, \hat{z}n]$ the inertial set of unit vectors

(2) $[\hat{x}1, \hat{y}1, \hat{z}1]$ the unsprung mass set of unit vectors

(3) $[\hat{x}2, \hat{y}2, \hat{z}2]$ an auxiliary set of unit vectors

(4) $[xb, yb, zb]$ the sprung mass set of unit vectors

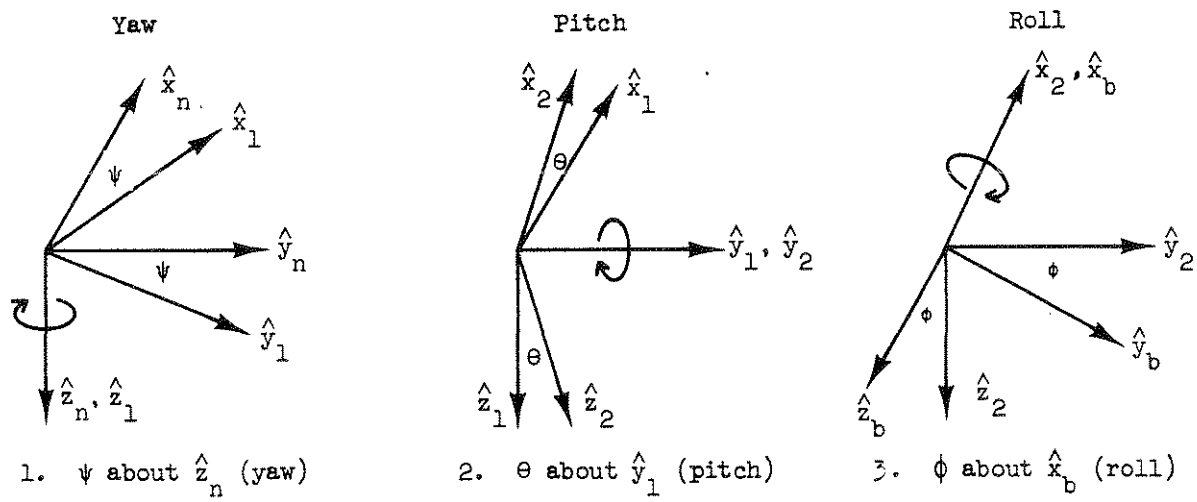

Figure B-1. Euler angles

See Figure B-1 for an illustration of these unit vectors. The $[\hat{x}b, \hat{y}b, \hat{z}b]$ unit vectors can be expressed in terms of the $[\hat{x}n, \hat{y}n, \hat{z}n]$ unit vectors by three rotations through the angles ψ, θ, and ϕ consecutively. Consider these roations one at a time. For ψ, a rotation about the $\hat{z}n$ unit vector, as shown in Figure B-1:

$$\begin{aligned} \hat{x}1 &= \cos\psi\,\hat{x}n + \sin\psi\,\hat{y}n \\ \hat{y}1 &= -\sin\psi\,\hat{x}n + \cos\psi\,\hat{y}n \\ \hat{z}1 &= \hat{z}n \end{aligned} \tag{B1}$$

(Note that $[\hat{x}1, \hat{y}1, \hat{z}1]$ are the unit vectors used in deriving the unsprung mass equations of motion.) For θ, a rotation about the $\hat{y}1$ axis:

$$\begin{aligned} \hat{x}2 &= \hat{x}1 \cos\theta - \hat{z}1 \sin\theta \\ \hat{y}2 &= \hat{y}1 \\ \hat{z}2 &= \hat{x}1 \sin\theta + \hat{z}1 \cos\theta \end{aligned} \tag{B2}$$

and for ϕ, a rotation about the $\hat{x}2$ axis:

$$\begin{aligned} \hat{x}b &= \hat{x}2 \\ \hat{y}b &= \hat{y}2 \cos\phi + \hat{z}2 \sin\phi \\ \hat{z}b &= -\hat{y}2 \sin\phi + \hat{z}2 \cos\phi \end{aligned} \tag{B3}$$

(Note that $\hat{x}2 = \hat{x}b$ where $\hat{x}b$ is the forward body axis of the sprung mass.)

At this point it is convenient to express Equations (B1), (B2), and (B3) in matrix notation. For example, Equation (B1) can be written as:

$$\begin{aligned} [\hat{x}1, \hat{y}1, \hat{z}1] &= [\hat{x}n, \hat{y}n, \hat{z}n] \begin{bmatrix} \cos\psi & -\sin\psi & 0 \\ \sin\psi & \cos\psi & 0 \\ 0 & 0 & 1 \end{bmatrix} \\ &= [\hat{x}n, \hat{y}n, \hat{z}n] \quad (C^{n1}) \end{aligned} \tag{B4}$$

where (C^{n1}) is equal to the matrix used to express the $[\hat{x}1, \hat{y}1, \hat{z}1]$ unit vectors in terms of the $[\hat{x}n, \hat{y}n, \hat{z}n]$ unit vectors. Similarly, Equations (B2) and (B3) may expressed as:

$$[\hat{x}2, \hat{y}2, \hat{z}2] = [\hat{x}1, \hat{y}1, \hat{z}1] \quad (C^{12}) \tag{B5}$$

where

$$(C^{12}) = \begin{bmatrix} \cos\theta & 0 & \sin\theta \\ 0 & 1 & 0 \\ -\sin\theta & 0 & \cos\theta \end{bmatrix}$$

and

$$[\hat{z}b, \hat{y}b, \hat{z}b] = [\hat{x}2, \hat{y}2, \hat{z}2] \quad (C^{2b}) \tag{B6}$$

where

$$(C^{2b}) = \begin{bmatrix} 1 & 0 & 0 \\ 0 & \cos\phi & -\sin\phi \\ 0 & \sin\phi & \cos\phi \end{bmatrix}$$

Using (B5) to substitute for $[\hat{x}2, \hat{y}2, \hat{z}2]$ in (B6),

$$[\hat{x}b,\ \hat{y}b,\ \hat{z}b] = [\hat{x}1,\ \hat{y}1,\ \hat{z}1] \quad (C^{12})(C^{2b}) \tag{B7}$$

where $(C^{12})(C^{2b})$ can be evaluated by matrix multiplication, that is,

$$(C^{12})(C^{2b}) = \begin{bmatrix} \cos\theta & \sin\theta\sin\phi & \sin\theta\cos\phi \\ 0 & \cos & -\sin\phi \\ -\sin\theta & \cos\theta\sin\phi & \cos\theta\cos\phi \end{bmatrix} = (b_{ji}) \tag{B8}$$

(Note that $(C^{12})(C^{2b}) = (b_{ji})$ where (b_{ji}) is used in Equation (2-5b) of the text. Also note that (b_{ij}) is the matrix obtained by transposing the horizontal rows of (B8) with the vertical columns of (B8).)

Now proceeding to substitute for $[\hat{x}1,\ \hat{y}1,\ \hat{z}1]$ using Equation (B4), the following expression is obtained:

$$[\hat{x}b,\ \hat{y}b,\ \hat{z}b] = [\hat{x}n,\ \hat{y}n,\ \hat{z}n]\ (C^{n1})(C^{12})(C^{2b})$$

The matrix product, $(C^{n1})(C^{12})(C^{2b})$, is equal to the matrix for the transformation (a_{ji}) which is used in Equation (2-1b) of the text. Thus,

$$[\hat{x}b,\ \hat{y}b,\ \hat{z}b] = [\hat{x}n,\ \hat{y}n,\ \hat{z}n]\ (a_{ji}) \tag{B9}$$

Carrying out the indicated multiplication (i.e., using Equations (B4) and (B8)),

$$(a_{ji}) = \begin{bmatrix} \cos\psi\cos\theta & \cos\psi\sin\theta\sin\phi-\sin\psi\cos\phi & \cos\psi\sin\theta\cos\phi+\sin\psi\sin\phi \\ \sin\psi\cos\theta & \sin\psi\sin\theta\sin\phi+\cos\psi\cos\phi & \sin\psi\sin\theta\cos\phi-\cos\psi\sin\phi \\ -\sin\theta & \cos\theta\sin\phi & \cos\theta\cos\phi \end{bmatrix} \tag{B10}$$

and transposing (a_{ji}) one obtains

$$(a_{ij}) = \begin{bmatrix} \cos\psi\cos\theta & \sin\psi\cos\theta & -\sin\theta \\ \cos\psi\sin\theta\sin\phi-\sin\psi\cos\phi & \sin\psi\sin\theta\sin\phi+\cos\psi\cos\phi & \cos\theta\sin\phi \\ \cos\psi\sin\theta\cos\phi+\sin\psi\sin\phi & \sin\psi\sin\theta\cos\phi-\cos\psi\sin\phi & \cos\theta\cos\phi \end{bmatrix} \tag{B11}$$

In summary, if the Euler angles are known, the matrix (a_{ji}) can be used to obtain the inertial axis components of a vector whose body axis components are given. To illustrate the statement above, consider the sprung mass velocity vector which is expressed, in body axis coordinates, as

$$\overline{V} = [\hat{x}b,\ \hat{y}b,\ \hat{z}b] \begin{bmatrix} u \\ v \\ w \end{bmatrix} \tag{B12}$$

and, in inertial coordinates, as

$$\overline{V} = [\hat{x}n,\ \hat{y}n,\ \hat{z}n] \begin{bmatrix} XNDOT \\ YNDOT \\ ZNDOT \end{bmatrix} \tag{B13}$$

Using Equation (B9) in (B12), one obtains

$$\overline{V} = [\hat{x}n,\ \hat{y}n,\ \hat{z}n]\ (a_{ji}) \begin{bmatrix} u \\ v \\ w \end{bmatrix} \tag{B15}$$

Equating the components of $\overline{V}$ in Equations (B13) and (B14), one obtains

$$\begin{bmatrix} XNDOT \\ YNDOT \\ ZNDOT \end{bmatrix} = (a_{ji}) \begin{bmatrix} u \\ v \\ w \end{bmatrix} \tag{B15}$$

Thus the inertial components of the velocity fector, $\overline{V}$, can be calculated from the body axis components of $\overline{V}$ and the matrix, (a_{ji}), which is a function of ψ, θ, and ϕ.

Since the body axes of the sprung mass are rotating with the sprung mass, the Euler angles are changing with time during a vehicle maneuver. In the following discussion the differential equations for the time rates of change of the Euler angles are derived. In the computer simulation the Euler anges are found by integrating these equations.

The time rates of change of the Euler angles are $\dot{\psi}$, $\dot{\theta}$, and $\dot{\phi}$. These angular rates can be represented by the vectors $\dot{\psi}\hat{z}n$, $\dot{\theta}\hat{y}1$, and $\dot{\phi}\hat{x}b$ (see reference [18] for an explanation of treating angular rates as vectors). The angular rotation vector of the sprung mass, $\overline{\omega}$, is the sum of these rates, that is,

$$\overline{\omega} = \dot{\psi}\hat{z}n + \dot{\theta}\hat{y}1 + \dot{\phi}\hat{x}b \tag{B16}$$

In Equation (2-14) $\overline{\omega}$ was defined by:

$$\overline{\omega} = p\,\hat{x}b + q\,\hat{y}b + r\,\hat{z}b \tag{B17}$$

Thus, since (B16) and (B17) are two expressions for the same vector,

$$p\,\hat{x}b + q\,\hat{y}b + r\,\hat{z}b = \dot{\psi}\hat{z}n + \dot{\theta}\hat{y}1 + \dot{\phi}\hat{x}b \tag{B18}$$

Now consider expressing $\hat{z}n$ and $\hat{y}1$ in the body axis system. From Figure B-1 it can be seen that

$$\hat{y}1 = \hat{y}2 = \hat{y}b\cos\phi - \hat{z}b\sin\phi \tag{B19}$$

(This result could also be derived from the matrix (b_{ij}).) It is not easy to visualize $\hat{z}n$ and thus $\hat{z}n$ is more readily obtained from the expression $[\hat{x}n, \hat{y}n, \hat{z}n] = [\hat{x}b, \hat{y}b, \hat{z}b]\,(a_{ij})$. The answer is

$$\hat{z}n = -\sin\theta\,\hat{x}b + \cos\theta\sin\phi\,\hat{y}b + \cos\theta\cos\phi\,\hat{z}b \tag{B20}$$

Using (B19) and (B20) in (B18) and equating the $\hat{x}b$, $\hat{y}b$, $\hat{z}b$ components, the following set of equations are obtained:

$$\left.\begin{aligned} p &= \dot{\phi} - \sin\theta\,\dot{\psi} \\ q &= \dot{\psi}\cos\theta\sin\phi + \dot{\theta}\cos\phi \\ r &= -\dot{\theta}\sin\phi + \dot{\psi}\cos\theta\cos\phi \end{aligned}\right\} \tag{B21}$$

Solving (B21) for $\dot{\psi}$, $\dot{\theta}$, and $\dot{\phi}$, yields

$$\left.\begin{aligned} \dot{\psi} &= \left(\frac{(q \sin\phi + r \cos\phi)}{\cos\theta}\right) \\ \dot{\theta} &= q \cos\phi - r \sin\phi \\ \dot{\phi} &= p + \dot{\psi} \sin\theta \end{aligned}\right\} \qquad \text{(B22)}$$

In conclusion, equations (B22) are integrated in the simulation to find ψ, θ, and ϕ which are used throughout the computer program to convert vector components from one axis system to another.

APPENDIX C

Equations of Motion

C.1. INTRODUCTION

The equations of motion of the articulated vehicle are given below. The straight truck equations may be derived by setting kingpin forces and moments equal to zero in the tractor equations.

Equations are given in the following order:

a) Equations concerning the tires
b) Equations concerning the suspensions
c) Equations concerning the sprung masses

In many areas, a detailed explanation of the equations under consideration will have been given in the body of this report or in Reference 1. In that case, only a short summary of the equations will be given in this appendix and the interested reader will be referred to the appropriate documentation. To avoid confusion, subscripts indicating axle number or right or left side are dropped unless they are necessary for clarity.

C.2. EQUATIONS CONCERNING THE TIRES

For further details, see Section 3.2 of this report.

Normal Forces at the Tire/Road Interface:

$$N = KT \cdot YT + CT \cdot YTD \tag{C1}$$

Shear Forces at the Tire/Road Interface:

$$\alpha = \tan^{-1}\frac{v_i}{u_i} - \delta \tag{C2}$$

$$S = 1 - \frac{RR \cdot \Omega}{u_w} \tag{C3}$$

where

$$u_w = u \cos\delta + u \sin\delta \tag{C4}$$

$$V_s = u_w[S^2 + \tan^2\alpha]^{1/2} \tag{C5}$$

$$\mu = \mu_o(1 - FA \cdot V_s) \tag{C6}$$

$$\lambda = \frac{1}{2}\mu F_z(1-S)[(C_s S)^2 + (C_\alpha \tan\alpha)^2]^{1/2} \tag{C7}$$

$$f(\lambda) = (2\lambda) \cdot \lambda \qquad \text{for } \lambda < 1 \tag{C7a}$$

$$f(\lambda) = 1 \qquad \text{for } \lambda \geq 1 \tag{C7b}$$

$$FXW = \frac{-C_s \cdot S}{1-S} f(\lambda) \tag{C8}$$

$$FYW = \frac{-C_\alpha \tan\alpha}{1-S} f(\lambda) \tag{C9}$$

C.3. EQUATIONS CONCERNING THE SUSPENSIONS

(For more details see Section 3.3.2 of this report.)

a) Single Axle

$$SF = K \cdot \Delta + C \cdot \frac{d}{dt}(\Delta) + CF \tag{C10}$$

where

Δ is the change in suspension length from static equilibrium (extension is positive), and CF is the coulomb friction. For details of the coulomb friction model see Reference 1, Section 2.3.

$$MS \cdot \dot{Z}\dot{S} = \sum_{I=1}^{2} \{SF(I) + FZ(I)\} \tag{C11}$$

$$JA \cdot \dot{\phi}\dot{A} = (FZ(2) - FZ(1))TRA + (S(1) - S(2))FRY - SMY \cdot d \tag{C12}$$

where d is the vertical distance from the roll center to the sprung mass center, and where a 1 indicates the left side and 2 indicates the right side.

$$SMY = FY(1) + FY(2) - MS \cdot (VD1 + \ddot{\psi} \cdot XU) \tag{C13}$$

$$RX1 + RX2 = FX1 + FX2 - MS(UDI - \dot{\psi}^2 XU) \tag{C14}$$

$$RX2 - RX1 = \frac{1}{FRY}\{(FX2-FX1) \cdot TRA - JA \cdot \ddot{\psi}\} \tag{C15}$$

where UD1, VD1 and $\ddot{\psi}$ may be found through the methods of Figure 3-13.

b) The Four Spring Suspension

(For more details see Section 3.3.3 of this report and Section 2.3.7 of Reference 1.) In the equations in this section, the initial subscript indicates the axle, the second indicates right side or left side. A tractor force spring tandem is considered here, hence the use of axle subscripts 2 and 3.

For each side,

$$SF(2,JI) = KK \cdot \Delta(JI) + CF \tag{C16}$$

where Δ is the average of the change of suspension length for axles 2 and 3, KK is the sum of the leaf spring rates, and CF is the coulomb friction.

For both axles,

$$TR(I,JI) = RX(I,JI)/\cos AA7 \tag{C17}$$

and for each side

$$TN1(J) \cdot AA1 - TN2(J) \cdot AA2 = JS(2) \cdot \dot{\Omega}(2,J) + TR(2,J) \cdot ARM1 + FX(2,J) \cdot RR(2,J) \tag{C18}$$

$$TN3(J) \cdot AA1 - TN4(J) \cdot AA2 = JS(3) \cdot \dot{\Omega}(3,J) + TR(3,J) \cdot ARM1 + FX(3,J) \cdot RR(3,J) \tag{C19}$$

$$TN2(J) \cdot AA4 = TN3(J) \cdot AA5 \tag{C20}$$

$$TN1(J) + TN2(J) + TN3(J) + TN4(J) = -SF(3,J) + TN1S + TN2S + TN3S + TN4S \tag{C21}$$

c) The Walking Beam Suspension

(For more details see Section 3.3.4 of this report and Sections 2.3.6 of Reference 1.)

For each side

$$SF(2,JI) = K \cdot \Delta + CF \tag{C22}$$

where Δ is the change in suspension length and CF is the coulomb friction.

For each axle

$$TR(I) = \frac{TT(I,1) + TT(I,2) - AA4(MS(I) \cdot UD1(I) - FX(I,1) - FX(I,2))}{AA4 + (1 + P1)AA5} \tag{C23}$$

$$VA(2) = TR(2) \cdot P1 \cdot AA5 \tag{C24}$$

$$VA(3) = TR(3) \cdot P1 \cdot AA5 \tag{C25}$$

For each side

$$AA8 \cdot \dot{\theta}\dot{T}(J) = N(2,J) \cdot AA6 - N(3,J) \cdot AA7 - (VA(2) + VA(3))/2 + (SF(2,J) - XXX) \cdot AA3 \tag{C26}$$

where XXX is the static load on the walking beam pin.

C.4. EQUATIONS CONCERNING THE SPRUNG MASSES

Many kinematic details are given in Section 2 of this report.

THE FIFTH WHEEL FORCES AND MOMENTS. (For more details see Section 3.5 of this report.)

Let the position of the tractor fifth wheel be written

$$\overline{FW} = \overline{R} + XKP(1)\hat{x}b + XKP(3)\hat{z}b \tag{C27}$$

where $\overline{R}$ is a vector from a fixed point τ to the tractor sprung mass center. Similarly, the position of the trailer fifth wheel may be written

$$\overline{TFW} = \overline{TR} + TXKP(1)t\hat{x}b + TXKP(3)t\hat{z}b \tag{C28}$$

where $\overline{TR}$ is a vector from ρ to the trailer sprung mass center. We are interested in the vector $\overline{\delta}$

$$\overline{\delta} = \overline{FW} - \overline{TFW} - \overline{C} \tag{C29}$$

where $\overline{C}$ is a constant vector which may be chosen to set

$$\overline{\delta} = 0 \tag{C30}$$

for the initial condition. Since, we have chosen all zero initial conditions (with the exception of forward velocity u)

$$\bar{R} = \overline{TR} \tag{C31}$$

In addition, at time zero

$$\hat{x}b = t\hat{x}b = \hat{x}n \tag{C32a}$$

$$\hat{z}b = t\hat{x}b = \hat{z}n \tag{C32b}$$

thus the vector $\bar{C}$ may be found to be

$$\bar{C} = (TXKP(1) - XKP(1))\hat{x}n + (TZKP(3) - ZKP(3))\hat{z}n \tag{C33}$$

The vector $\bar{\delta}$ may now be written

$$\begin{aligned}\bar{\delta} = \bar{R} - \overline{TR} &+ XKP\{(A(1,1)-1)\hat{x}n + A(1,2)\hat{y}n + A(1,3)\hat{z}n\} \\ &+ ZKP\{A(3,1)\hat{x}n + A(3,2)\hat{y}n + (A(3,3)-1)\hat{z}n\} \\ &+ TXKP\{(AT(1,1)-1)\hat{x}n + AT(1,2)\hat{y}n + AT(1,3)\hat{z}n\} \\ &+ TZKP\{AT(3,1)\hat{x}n + AT(3,2)\hat{y}n + (AT(3,3)-1)\hat{z}n\}\end{aligned} \tag{C34}$$

Now since $\bar{R} - \overline{TR}$ is just the vector difference between the sprung mass center positions, the components of $\bar{\delta}$ may easily be calculated from Equation (C34).

The relative velocity at the fifth wheel may be calculated by a straightforward differentiation of $\bar{\delta}$ as given in Equation (C34). Referring to Equation (B11) for the A(I,J) and dropping the high order products of small terms yields

$$\begin{aligned}\dot{\bar{\delta}} = \dot{\bar{R}} - \dot{\overline{TR}} &+ XKP\{\dot{\psi}(-\sin\psi\ \hat{x}n + \cos\psi\ \hat{y}n) - \dot{\theta}\ \hat{z}n\} \\ &+ ZKP\{(\dot{\theta}\cos\psi + \dot{\phi}\sin\psi)\hat{x}n + (\dot{\theta}\sin\psi - \dot{\phi}\sin\psi)\hat{y}n\} \\ &+ TXKP\{\dot{\psi}T(-\sin\psi T\ \hat{x}n + \cos\psi T\ \hat{y}n - \dot{\theta}T\ \hat{z}n\} \\ &+ TZKP\{(\dot{\theta}T\cos\psi T + \dot{\phi}T\sin\psi T)\hat{x}n + (\dot{\theta}T\sin\psi T - \dot{\phi}T\cos\psi T)\hat{y}n\}\end{aligned} \tag{C35}$$

Now the force transmitted through the fifth wheel may be easily computed.

$$\bar{F} = KFW \cdot \bar{\delta} + CFW \cdot \dot{\bar{\delta}} \tag{C36}$$

This force may be written for convenience in the yaw axis components for both tractor and trailer:

$$\begin{aligned}\bar{F} &= PINX\ \hat{x}1 + PINY\ \hat{y}1 + PINZ\ \hat{z}1 \\ &= TPINX\ t\hat{x}1 + TPINY\ t\hat{y}1 + TPINZ\ t\hat{z}1\end{aligned} \tag{C37}$$

The roll moment transmitted through the fifth wheel is assumed a function only of the roll angles of the tractor and semitrailer (the effects of pitch

rotation and the articulation angle are neglected). Thus

$$XMOM = \{MC5 \cdot (\Phi - \Phi T) + CC5 \cdot (\dot{\Phi} - \dot{\Phi}_t)\}\hat{x}1 \tag{C38}$$

C.5. THE EQUATIONS OF MOTION OF THE SPRUNG MASSES

Only the tractor will be considered here. The equations of trailer sprung mass motion are directly analogous to the tractor equations.

Due to the way the suspension equations are written, the forces and moments on the sprung mass may be written most conveniently in the [X1, Y1, Z1] system. In the following equations, I is the axle number; J = 1 indicates the left side and J = 2 indicates the right side. The total number of tractor axles is KAXLE.

The total force on the sprung mass may be written

$$\overline{F} = F(1)\,\hat{x}1 + F(2)\,\hat{y}1 + F(3)\,\hat{z}1 \tag{C39}$$

where

$$F(1) = PINX + \sum_{I=1}^{KAXLE} \sum_{J=1}^{2} RX(I,J) \tag{C40a}$$

$$F(2) = PINY + \sum_{I=1}^{KAXLE} SMY(I) \tag{C40b}$$

$$F(3) = PINZ + \sum_{I=1}^{KAXLE} \sum_{J=1}^{2} SF(I,JI) \tag{C40c}$$

These may then be rotated into body position and used to calculate the accelerations:

$$\dot{u} = rv - qw + \frac{1}{M1} \sum_{K=1}^{3} B(1,K) \cdot F(K) \tag{C41a}$$

$$\dot{v} = p \cdot w - r \cdot u + \frac{1}{M1} \sum_{K=1}^{3} B(2,K) \cdot F(K) \tag{C41b}$$

$$\dot{w} = q \cdot u - p \cdot v + \frac{1}{M1} \sum_{K=1}^{3} B(3,K) \cdot F(K) \tag{C41c}$$

The computation of the total moment on the sprung mass depends on the fifth wheel forces and roll couple, the forces of constraint at the suspensions, and the brake torque. We will assume a single rear axle here; note that in the case of a walking beam or four spring suspension, slightly more complicated moments in the $\hat{y}1$ direction result. These added terms are carefully derived in Sections 2.3.6 and 2.3.7 of Reference 1. The total moment on the tractor sprung mass of a single rear axle vehicle may be defined as

$$\overline{T} = MOM(1)\hat{x}1 + MOM(2)\hat{y}1 + MOM(3)\hat{z}1 \tag{C42}$$

where

$$MOM(1) = -PINY \cdot ZKP + \sum_{I=1}^{2} \{(SF(I,2) - SF(I,1)) \cdot FRY - SMY(I) \cdot d(I)\} \tag{C43a}$$

$$MOM(2) = PINX \cdot ZKP + PINZ \cdot XKP - \sum_{J=1}^{2} \sum_{I=1}^{2} \{TT(I,J) + RX(I,J)(ALPHA(I) + DELTA(I) - Z) - SF(I,J) \cdot XS(I)\} \tag{C43b}$$

$$MOM(3) = PINY \cdot XKP + \sum_{I=1}^{2} \{(RX(I,1) - RX(I,2)) \cdot FRY(I) + SMY(I) \cdot XS(I)\} \tag{C43c}$$

These may then be rotated into body position and used to calculate the angular accelerations:

$$\dot{p} = \frac{1}{I_{xx}} \{(I_{yy} - I_{zz}) \cdot q \cdot r + I_{xz}(\dot{r} + p \cdot q) + \sum_{K=1}^{3} MOM(K) \cdot BZ(1,K)\} \tag{C44a}$$

where $\dot{r}$ is estimated as shown in Figure 3-13.

$$\dot{q} = \frac{1}{I_{yy}} \{(I_{zz} - I_{xx}) \cdot p \cdot r + I_{xz}(r^2 - p^2) + \sum_{K=1}^{3} MOM(K) \cdot BZ(2,K)\} \tag{C44b}$$

$$\dot{r} = \frac{1}{I_{zz}} \{(I_{xx} - I_{yy}) \cdot p \cdot q + I_{xz}(\dot{p} - q \cdot r) + \sum_{K=1}^{3} MOM(K) \cdot BZ(3,K)\} \tag{C44c}$$

APPENDIX D

Program Manipulation

Appendix D

D-1. INTRODUCTION

The purpose of this appendix is to facilitate use of the program. Initially, the most straightforward options are presented. Note there is one parameter per record except where a two coordinate relationship is appropriate; i.e., pressure-torque tables, etc. Integer variables are in I2 format. Real variables are in F15.3 format. Pairs of numbers are entered in 2F10.3 format.

D-2. INPUT INSTRUCTIONS FOR THE STRAIGHT TRUCK PROGRAM

In this section, the most straightforward options of the straight truck program are presented. Data List D-1 gives the order of data input for a single rear axle vehicle with dynamometer tables.

In the case of tandem rear axles, there will be several changes from the sequence in Data List D-1. Data List D-2 and D-3 give the order of the input data for the walking beam and the four spring tandem axles, respectively.

D-3. INPUT INSTRUCTIONS FOR THE ARTICULATED VEHICLE

In this section, the most straightforward options of the articulated vehicle are given. Data List D-4 gives the order of the input data for a three-axle vehicle.

In the case of tandem axles, there will be several changes from the sequence shown in Data List D-4. Data List D-5 gives the input sequence for a four spring tandem axle tractor with a four spring tandem axle trailer. The input sequence for the walking beam tandem axle tractor with a walking beam tandem axle trailer differs from Data List D-5 by the absence of AA6, AA7, AA8, AA14, AA15, and AA16. PERCNT(1) and PERCNT(2) are to be inserted after MUZERO(5).

D-4. THE BRAKE TABLES - INPUT INSTRUCTIONS

The brake tables allow user input time varying pressure at the foot valve and dynamometer curves for each wheel. Table 1 is the time vs. pressure table. Tables 2 through 2*KAXLE + 1 are the pressure vs. torque tables. (Note KAXLE is the total number of axles. Thus, there is one pressure vs. torque table for each wheel.) Each table may contain up to 25 coordinate pairs entered in 2F10.3 format. The actual number of pairs in the a table is always the first entry for that table. The time vs. pressure table must always be entered. The pressure vs. torque tables must be entered unless the brake modules are to be used.

D-5. STEER TABLE LOOK-UP

There are two time vs. steer angle tables. The first one is for the left front wheel, the second is for the right front wheel. Each table may contain up to 25 coordinate pairs entered in 2F10.3 format. The first of the two numbers is the time value, the second is the corresponding steer angle. Preceding each table is a data card containing in I2 format the actual number of pairs in that table.

Both steer tables must always be entered and are placed after the brake tables or the brake modules and after the force deflection tables and the aligning torque tables if either of these are used.

D-6. INPUT INSTRUCTIONS FOR VARIOUS OPTIONS

To use the following program options, special action by the user is required. Input instructions for the various options are explained below:

ROUGH ROAD

A data card containing a -1 (I2 format) must be inserted after the 80-character title data card and before KEY or KEY(1). This signals the program to call subroutine ROAD at the proper time and place. Subroutine ROAD contains a

user input function or series of points for road height coordinate data. An examination of the subroutine ROAD list will clearly indicate how and where to insert the road profile.

THE BRAKE MODULES

To use the brake subroutine, insert a -1 or a -2 (I2 format) immediately after the time vs. pressure table. This will cause a call to subroutine BRAKE. The parameters needed for the brake calculations will then be read. A -1 indicates side-to-side equality of brakes. Thus one brake type and its related parameters must be entered for each axle. A -2 indicates side-to-side inequality of brakes. Thus one brake type and its related parameters must be entered for each wheel. If you are using the brake modules omit the pressure vs. torque tables. (See Data List D-6 for a list of brake types and their related parameters.)

ALIGNING TORQUE TABLE LOOK-UP

The data cards for aligning torque are placed immediately before the steer tables. There is one set of tables for each axle. The first data card should be a -1 (I2 format) to signal that aligning torque is to be used and more data follows. There may be 5 or less vertical load entries for each axle and 5 or less sideslip angle, aligning torque pairs for each vertical load entry. The aligning torque values are for one tire. Refer to section 3.2.3 for further details.

Following is an example of the aligning torque tables for one axle (in particular the front axle of the tractor-trailer). A similar set of data cards should be entered for each axle.

```
  03    (NO. OF VERTICAL LOAD ENTRIES FOR THIS AXLE IN I2 FORMAT)
2800.    05    (FIRST VERTICAL LOAD ENTRY, NO. OF SIDESLIP ANGLE VS. ALIGNING
                TORQUE PAIRS IN F10.3, I2 FORMAT)
   0.0    0.0  (SIDESLIP ANGLE, ALIGNING TORQUE) (2F10.3 FORMAT)
   2.0   80.
   4.0  108.
   8.0   81.
  16.0   24.
5430.    05    (SECOND VERTICAL LOAD ENTRY, NO. OF SIDESLIP ANGLE VS. ALIGNING
                TORQUE PAIRS IN F10.3, I2 FORMAT)
   0.0    0.0  (SIDESLIP ANGLE, ALIGNING TORQUE) (2F10.3 FORMAT)
   2.0  182.
   4.0  274.
   8.0  263.
  16.0  132.
9200.    05    (THIRD VERTICAL LOAD ENTRY, NO. OF SIDESLIP ANGLE VS. ALIGNING
                TORQUE PAIRS IN F10.3, I2 FORMAT)
   0.0    0.0  (SIDESLIP ANGLE, ALIGNING TORQUE) (2F10.3 FORMAT)
   2.0  323.
   4.0  533.
   8.0  618.
  12.0  561.
```

LATERAL STIFFNESS TABLE LOOK-UP

The user sets a flag for lateral stiffness table look-up by setting CALF1 to a negative value. There is one table for each axle. (NOTE: There is a CALF table look-up for either all or none of the axles.) Each table may contain up to 25 coordinate pairs entered in 2F10.3 format. The first of the two numbers is a vertical load value. The second is the corresponding lateral stiffness value. Preceding each table is a data card containing in I2 format the actual number of pairs in that table.

The lateral stiffness tables are placed after the steer tables. (See Data List D-7.)

LONGITUDINAL STIFFNESS TABLE LOOK-UP

The user set a flag for longitudinal stiffness table look-up by setting CS1 to a negative value. There is one table for each axle. (NOTE: There is a CS table look-up for either all or none of the axles.) Each table may contain up to 25 coordinate pairs entered in 2F10.3 format. The first of the two numbers is a vertical load value. The second is the corresponding longitudinal stiffness value. Preceding each table is a data card containing in I2 format the actual number of pairs in that table.

The longitudinal stiffness tables are placed after the lateral stiffness tables if they are used, otherwise after the steer tables. (See Data List D-8.)

DATA LIST D-1
SINGLE REAR AXLE VEHICLE

80 Character Title (20A4 format)
0
A1 (F14.4 format)
A2
ALPHA1
ALPHA2
C1*
C2*
C3*
C4*
CALF1**
CALF2**
CF1*
CF2*
CFP11
CFP12
CFP21
CFP22
CS1**
CS2**
DELTA1
DT2
FA1
FA2
IXX
IYY
IZZ
IXZ
JA1
JA2
JS1
JS2
K1
K2
KT1**
KT2**
MUZERO1
MUZERO2
PW
PJ1***
PJ2***
PJ3***
PX***
PZ***
RCH1
RCH2
RS1
RSC1
RSC2

SY1
SY2
TIMF
TRA1
TRA2
VEL
W
WS1
WS2
TQ(1,1,1) TQ(1,1,2) (2F10.3 FORMAT)
TQ(1,2,1) TQ(1,2,2)
TQ(2,1,1) TQ(2,1,2)
TQ(2,2,1) TQ(2,2,2)
NO. OF PAIRS IN TIME VS. PRESSURE TABLE (I2 FORMAT)
TIME PRESSURE (UP TO 25 PAIRS IN 2F10.3 FORMAT)
. .
. .
TIME PRESSURE
NO. OF PAIRS IN PRESSURE VS. TORQUE TO AXLE 1 (I2 FORMAT)
PRESSURE TORQUE (UP TO 25 PAIRS IN 2F10.3 FORMAT)
. .
. .
PRESSURE TORQUE
NO. OF PAIRS IN PRESSURE VS. TORQUE TO AXLE 2 (I2 FORMAT)
PRESSURE TORQUE
. .
. .
PRESSURE TORQUE
NO. OF PAIRS IN TIME VS. LEFT FRONT STEER ANGLE TABLE (I2 FORMAT)
TIME STEER ANGLE (UP TO 25 PAIRS IN 2F10.3 FORMAT)
. .
. .
TIME STEER ANGLE
NO. OF PAIRS IN TIME VS. RIGHT FRONT STEER ANGLE TABLE (I2 FORMAT)
TIME STEER ANGLE (UP TO 25 PAIRS IN 2F10.3 FORMAT)
. .
. .
TIME STEER ANGLE
G1
G2
IWIND (I2 FORMAT)
TINC
TRUCK

* One side value
** Value for one tire
***Omit if PW = 0.0

DATA LIST D-2
WALKING BEAM SUSPENSION, STRAIGHT TRUCK

80 Character Title (20A4 format)
01
AA1 (F14.4 format)
AA2
AA4
AA5
ALPHA1
ALPHA2
C1*
C2*
C3*
C4*
CALF1**
CALF2**
CALF3**
CF1*
CF2*
CFP11
CFP12
CFP13
CFP21
CFP22
CFP23
CS1**
CS2**
CS3**
DELTA1
DT2
FA1
FA2
FA3
IXX
IYY
IZZ
IXZ
JA1
JA2
JS1
JS2
JS3
K1
K2
KT1**
KT2**
KT3**
MUZERO1
MUZERO2
MUZERO3
PERCNT
PW

```
PJ1***
PJ2***
PJ3***
PX***
PZ***
RCH1
RCH2
RS1
RSC1
RSC2
SY1
SY2
TIMF
TRA1
TRA2
VEL
W
WS1
WS2
WS3
TQ(1,1,1) TQ(1,1,2) (2F10.3 FORMAT)
TQ(1,2,1) TQ(1,2,2)
TQ(2,1,1) TQ(2,1,2)
TQ(2,2,1) TQ(2,2,2)
TQ(3,1,1) TQ(3,1,2)
TQ(3,2,1) TQ(3,2,2)
NO. OF PAIRS IN TIME VS. PRESSURE TABLE (I2 FORMAT)
TIME PRESSURE (UP TO 25 PAIRS IN 2F10.3 FORMAT)
 .      .
 .      .
TIME PRESSURE
NO. OF PAIRS IN PRESSURE VS. TORQUE TO AXLE 1 (I2 FORMAT)
PRESSURE TORQUE (UP TO 25 PAIRS IN 2F10.3 FORMAT)
   .      .
   .      .
PRESSURE TORQUE
NO. OF PAIRS IN PRESSURE VS. TORQUE TO AXLE 2 (I2 FORMAT)
PRESSURE TORQUE (UP TO 25 PAIRS IN 2F10.3 FORMAT)
   .      .
   .      .
PRESSURE TORQUE
NO. OF PAIRS IN PRESSURE VS. TORQUE TO AXLE 3 (I2 FORMAT)
PRESSURE TORQUE (UP TO 25 PAIRS IN 2F10.3 FORMAT)
   .      .
   .      .
PRESSURE TORQUE
NO. OF PAIRS IN TIME VS. LEFT FRONT STEER ANGLE TABLE (I2 FORMAT)
TIME STEER ANGLE (UP TO 25 PAIRS IN 2F10.3 FORMAT)
 .      .
 .      .
TIME STEER ANGLE
```

DATA LIST D-2 (Continued)

NO. OF PAIRS IN TIME VS. RIGHT FRONT STEER ANGLE (I2 FORMAT)
TIME STEER ANGLE (UP TO 25 PAIRS IN 2F10.3 FORMAT)

. .

. .

TIME STEER ANGLE
G1
G2
IWIND (I2 FORMAT)
TINC
TRUCK

* One side value
** Value for one tire
*** Omit if PW = 0.0

DATA LIST D-3

FOUR SPRING SUSPENSION, STRAIGHT TRUCK

80 Character Title (20A4 format)
02
AA1
AA2
AA4
AA5
AA6
AA7
AA8
A1
A2
C1*
C2*
C3*
C4*
CALF1**
CALF2**
CALF3**
CF1*
CF2*
CFP11
CFP12
CFP13
CFP21
CFP22
CFP23
CS1**
CS2**
CS3**
DELTA1
DT2
FA1
FA2
FA3
IXX
IYY
IZZ
IXZ
JA1
JA2
JS1
JS2
JS3
K1
K2
KT1**
KT2**
KT3**

```
MUZERO1
MUZERO2
MUZERO3
PW
PJ1***
PJ2***
PJ3***
PX***
PZ***
RCH1
RCH2
RS1
RSC1
RSC2
SY1
SY2
TIMF
TRA1
TRA2
VEL
W
WS1
WS2
WS3
TQ(1,1,1) TQ(1,1,2) (2F10.3 FORMAT)
TQ(1,2,1) TQ(1,2,2)
TQ(2,1,1) TQ(2,1,2)
TQ(2,2,1) TQ(2,2,2)
TQ(3,1,1) TQ(3,1,2)
TQ(3,2,1) TQ(3,2,2)
NO. OF PAIRS IN TIME VS. PRESSURE TABLE (I2 FORMAT)
TIME PRESSURE (UP TO 25 PAIRS IN 2F10.3 FORMAT)
  .      .
  .      .
TIME PRESSURE
NO. OF PAIRS IN PRESSURE VS. TORQUE TO AXLE 1 (I2 FORMAT)
PRESSURE TORQUE (UP TO 25 PAIRS IN 2F10.3 FORMAT)
    .      .
    .      .
PRESSURE TORQUE
NO. OF PAIRS IN PRESSURE VS. TORQUE TO AXLE 2 (I2 FORMAT)
PRESSURE TORQUE (UP TO 25 PAIRS IN 2F10.3 FORMAT)
    .      .
    .      .
PRESSURE TORQUE
NO. OF PAIRS IN PRESSURE VS. TORQUE TO AXLE 3 (I2 FORMAT)
PRESSURE TORQUE (UP TO 25 PAIRS IN I2 FORMAT)
    .      .
    .      .
PRESSURE TORQUE
```

DATA LIST D-3 (Continued)

NO. OF PAIRS IN TIME VS. LEFT FRONT STEER ANGLE TABLE (I2 FORMAT)
TIME STEER ANGLE (UP TO 25 PAIRS IN I2 FORMAT)

. .
. .

TIME STEER ANGLE
NO. OF PAIRS IN TIME VS. RIGHT FRONT STEER ANGLE TABLE (I2 FORMAT)
TIME STEER ANGLE (UP TO 25 PAIRS IN I2 FORMAT)

. .
. .

TIME STEER ANGLE
G1
G2
IWIND (I2 FORMAT)
TINC
TRUCK

* Value for one side
** Value for one tire
*** Omit if PW = 0.0

DATA LIST D-4
TRACTOR-TRAILER SINGLE AXLE VEHICLE

80 Character Title (20A4 format)
0
0
A1 (F14.4 format)
A2
A3
A4
ALPHA1
ALPHA2
ALPHA3
BB
C1*
C2*
C3*
C4*
C5*
C6*
CALF1**
CALF2**
CALF3**
CF1*
CF2*
CF3*
CFP11
CFP12
CFP13
CFP21
CFP22
CFP23
CS1**
CS2**
CS3**
D
DELTA1
DELTA3
DT2
DT3
FA1
FA2
FA3
IXX
IYY
IZZ
IXZ
ITXX
ITYY
ITZZ
ITXZ

JA1
JA2
JA3
JS1
JS2
JS3
K1
K2
K3
KT1**
KT2**
KT3**
MC5
MUZERO1
MUZERO2
MUZERO3
PW
PJ1***
PJ2***
PJ3***
PX***
PZ***
RCH1
RCH2
RCH3
RS1
RSC1
RSC2
RSC3
SY1
SY2
SY3
TIMF
TRA1
TRA2
TRA3
VEL
W1
W2
WS1
WS2
WS3
TQ(1,1,1) TQ(1,1,2) (2F10.3 FORMAT)
TQ(1,2,1) TQ(1,2,2)
TQ(2,1,1) TQ(2,1,2)
TQ(2,2,1) TQ(2,2,2)
TQ(3,1,1) TQ(3,1,2)
TQ(3,2,1) TQ(3,2,2)

NO. OF PAIRS IN TIME VS. PRESSURE TABLE (I2 FORMAT)
TIME PRESSURE (UP TO 25 PAIRS IN 2F10.3 FORMAT)

. .
. .

TIME PRESSURE
NO. OF PAIRS IN THE PRESSURE VS. TOTAL TORQUE TO AXLE 1 (I2 FORMAT)
PRESSURE TORQUE (UP TO 25 PAIRS IN 2F10.3 FORMAT)

. .
. .

PRESSURE TORQUE
NO. OF PAIRS IN THE PRESSURE VS. TOTAL TORQUE TO AXLE 2 (I2 FORMAT)
PRESSURE TORQUE (UP TO 25 PAIRS IN 2F10.3 FORMAT)

. .
. .

PRESSURE TORQUE
NO. OF PAIRS IN THE PRESSURE VS. TOTAL TORQUE TO AXLE 3 (I2 FORMAT)
PRESSURE TORQUE

. .
. .

PRESSURE TORQUE
NO. OF PAIRS IN TIME VS. LEFT FRONT STEER ANGLE TABLE (I2 FORMAT)
TIME STEER ANGLE (UP TO 25 PAIRS IN 2F10.3 FORMAT)

. .
. .

TIME STEER ANGLE
NO. OF PAIRS IN TIME VS. RIGHT FRONT STEER ANGLE TABLE (I2 FORMAT)
TIME STEER ANGLE (UP TO 25 PAIRS IN 2F10.3 FORMAT)

. .
. .

TIME STEER ANGLE
G1
G2
IWIND (I2 FORMAT)
TINC
TRUCK

---

* One side value
** Value for one tire
***Omit if PW = 0.0

DATA LIST D-5
TRACTOR-TRAILER FOUR SPRING

80 Character Title (20A4 format)
KEY(1) (I2 format)
KEY(2)
AA1 (F14.4 format)
AA2
AA4
AA5
AA6
AA7
AA8
AA9
AA10
AA12
AA13
AA14
AA15
AA16
A1
A2
A3
A4
ALPHA1
ALPHA2
ALPHA3
BB
C1*
C2*
C3*
C4*
C5*
C6*
CALF1**
CALF2**
CALF3**
CALF4**
CALF5**
CF1*
CF2*
CF3*
CFP11
CFP12
CFP13
CFP14
CFP15
CFP21
CFP22
CFP23
CFP24
CFP25

CS1**
CS2**
CS3**
CS4**
CS5**
D
DELTA1
DELTA3
DT2
DT3
FA1
FA2
FA3
FA4
FA5
IXX
IYY
IZZ
IXZ
ITXX
ITYY
ITZZ
ITXZ
JA1
JA2
JA3
JS1
JS2
JS3
JS4
JS5
K1
K2
K3
KT1**
KT2**
KT3**
KT4**
KT5**
MC5
MUZER01
MUZER02
MUZER03
MUZER04
MUZER05
PW
PJ1***
PJ2***
PJ3***
PX***
PZ***

```
RCH1
RCH2
RCH3
RS1
RSC1
RSC2
RSC3
SY1
SY2
SY3
TIMF
TRA1
TRA2
TRA3
VEL
W1
W2
WS1
WS2
WS3
WS4
WS5
TQ(1,1,1) TQ(1,1,2) (2F10.3 FORMAT)
TQ(1,2,1) TQ(1,2,2)
TQ(2,1,1) TQ(2,1,2)
TQ(2,2,1) TQ(2,2,2)
TQ(3,1,1) TQ(3,1,2)
TQ(3,2,1) TQ(3,2,2)
TQ(4,1,1) TQ(4,1,2)
TQ(4,2,1) TQ(4,2,2)
TQ(5,1,1) TQ(5,1,2)
TQ(5,2,1) TQ(5,2,2)
NO. OF PAIRS IN TIME VS. PRESSURE TABLE (I2 FORMAT)
TIME PRESSURE (UP TO 25 PAIRS IN 2F10.3 FORMAT)
 .      .
 .      .
TIME PRESSURE
NO. OF PAIRS IN PRESSURE VS. TOTAL TORQUE TO AXLE 1 (I2 FORMAT)
PRESSURE TORQUE (UP TO 25 PAIRS IN 2F10.3 FORMAT)
   .      .
   .      .
PRESSURE TORQUE
NO. OF PAIRS IN PRESSURE VS. TOTAL TORQUE TO AXLE 2 (I2 FORMAT)
PRESSURE TORQUE (UP TO 25 PAIRS IN 2F10.3 FORMAT)
   .      .
   .      .
PRESSURE TORQUE
```

DATA LIST D-5 (Continued)

NO. OF PAIRS IN PRESSURE VS. TOTAL TORQUE TO AXLE 3 (I2 FORMAT)
PRESSURE TORQUE (UP TO 25 PAIRS IN 2F10.3 FORMAT)

. .

. .

PRESSURE TORQUE
NO. OF PAIRS IN PRESSURE VS. TOTAL TORQUE TO AXLE 4 (I2 FORMAT)
PRESSURE TORQUE (UP TO 25 PAIRS IN 2F10.3 FORMAT)

. .

. .

PRESSURE TORQUE
NO. OF PAIRS IN PRESSURE VS. TOTAL TORQUE TO AXLE 5 (I2 FORMAT)
PRESSURE TORQUE (UP TO 25 PAIRS IN 2F10.3 FORMAT)

. .

. .

PRESSURE TORQUE
NO. OF PAIRS IN TIME VS. LEFT FRONT STEER ANGLE TABLE (I2 FORMAT)
TIME STEER ANGLE (UP TO 25 PAIRS IN 2F10.3 FORMAT)

. .

. .

TIME STEER ANGLE
NO. OF PAIRS IN TIME VS. RIGHT FRONT STEER ANGLE TABLE (I2 FORMAT)
TIME STEER ANGLE (UP TO 25 PAIRS IN 2F10.3 FORMAT)

. .

. .

TIME STEER ANGLE
G1
G2
IWIND (I2 FORMAT)
TINC
TRUCK

* One side value
** Value for one tire
***Omit if PW = 0.0

DATA LIST D-6
BRAKE MODULES

0 NO BRAKES (I1 format)
1 S-CAM BRAKE (I1 format)
AC
EM
FRAY
PO
RD
ULH
ULL
ALPHO
ALPH3
APRIM
HB
RC
SAL
2 2-WEDGE BRAKE (I1 format)
AC
EM
FRAY
PO
RD
ULH
ULL
AB
ALPHO
ALHPW
BETA
C2
OH
3 1-WEDGE (I1 format)
AC
EM
FRAY
PO
RD
ULH
ULL
ALPHO
ALPHW
ALPH3
APRIM
HB
4 DSSA (I1 format)
AC
EM
FRAY
PO
RD
ULH
ULL

AB
ALPHO
ALPHW
ALPH3
APRIM
BETA
C2
HB
OH
5 DUPLEX BRAKES (I1 format)
AC
EM
FRAY
PO
RD
ULH
ULL
AB
ALPHO
ALPHW
BETA
C2
OH
6 DISC BRAKES (I1 format)
AC
EM
FRAY
PO
RD
ULH
ULL

DATA LIST D-7

LATERAL STIFFNESS TABLE LOOK-UP

```
NO. OF PAIRS IN VERTICAL LOAD VS. LATERAL STIFFNESS TABLE AXLE 1 (I2)
VERTICAL LOAD  LATERAL STIFFNESS  (UP TO 25 PAIRS IN 2F10.3 FORMAT)
      .                .
      .                .
VERTICAL LOAD  LATERAL STIFFNESS
NO. OF PAIRS IN VERTICAL LOAD VS. LATERAL STIFFNESS TABLE, AXLE 2 (I2)
VERTICAL LOAD  LATERAL STIFFNESS  (UP TO 25 PAIRS IN 2F10.3 FORMAT)
      .                .
      .                .
VERTICAL LOAD  LATERAL STIFFNESS
             .
             .
             .
NO. of PAIRS IN VERTICAL LOAD VS. LATERAL STIFFNESS TABLE, LAST AXLE (I2)
VERTICAL LOAD  LATERAL STIFFNESS  (UP TO 25 PAIRS IN 2F10.3 FORMAT)
      .                .
      .                .
VERTICAL LOAD  LATERAL STIFFNESS
```

DATA LIST D-8

LONGITUDINAL STIFFNESS TABLE LOOK-UP

```
NO. OF PAIRS IN VERTICAL LOAD VS. LONG. STIFFNESS TABLE, AXLE 1 (I2)
VERTICAL LOAD  LONG. STIFFNESS  (UP TO 25 PAIRS IN 2F10.3 FORMAT)
      .              .
      .              .
VERTICAL LOAD  LONG. STIFFNESS
NO. OF PAIRS IN VERTICAL LOAD VS. LONG. STIFFNESS TABLE, AXLE 2 (I2)
VERTICAL LOAD  LONG. STIFFNESS  (UP TO 25 PAIRS IN 2F10.3 FORMAT)
      .              .
      .              .
VERTICAL LOAD  LONG. STIFFNESS
             .
             .
             .
NO. OF PAIRS IN VERTICAL LOAD VS. LONG. STIFFNESS TABLE, LAST AXLE (I2)
VERTICAL LOAD  LONG. STIFFNESS  (UP TO 25 PAIRS IN 2F10.3 FORMAT)
      .              .
      .              .
VERTICAL LOAD  LONG. STIFFNESS
```

APPENDIX E

Flowcharts

Preceding page blank

Main

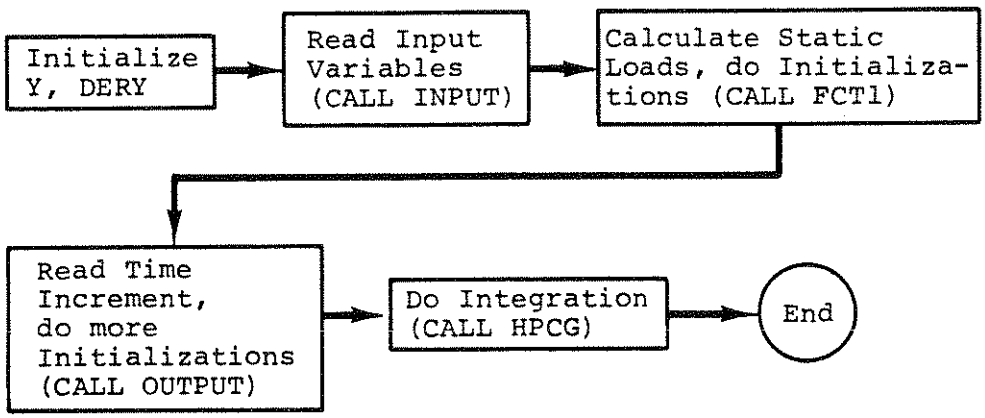
Initialize Y, DERY
Read Input Variables (CALL INPUT)
Calculate Static Loads, do Initializations (CALL FCT1)
Read Time Increment, do more Initializations (CALL OUTPUT)
Do Integration (CALL HPCG)
End

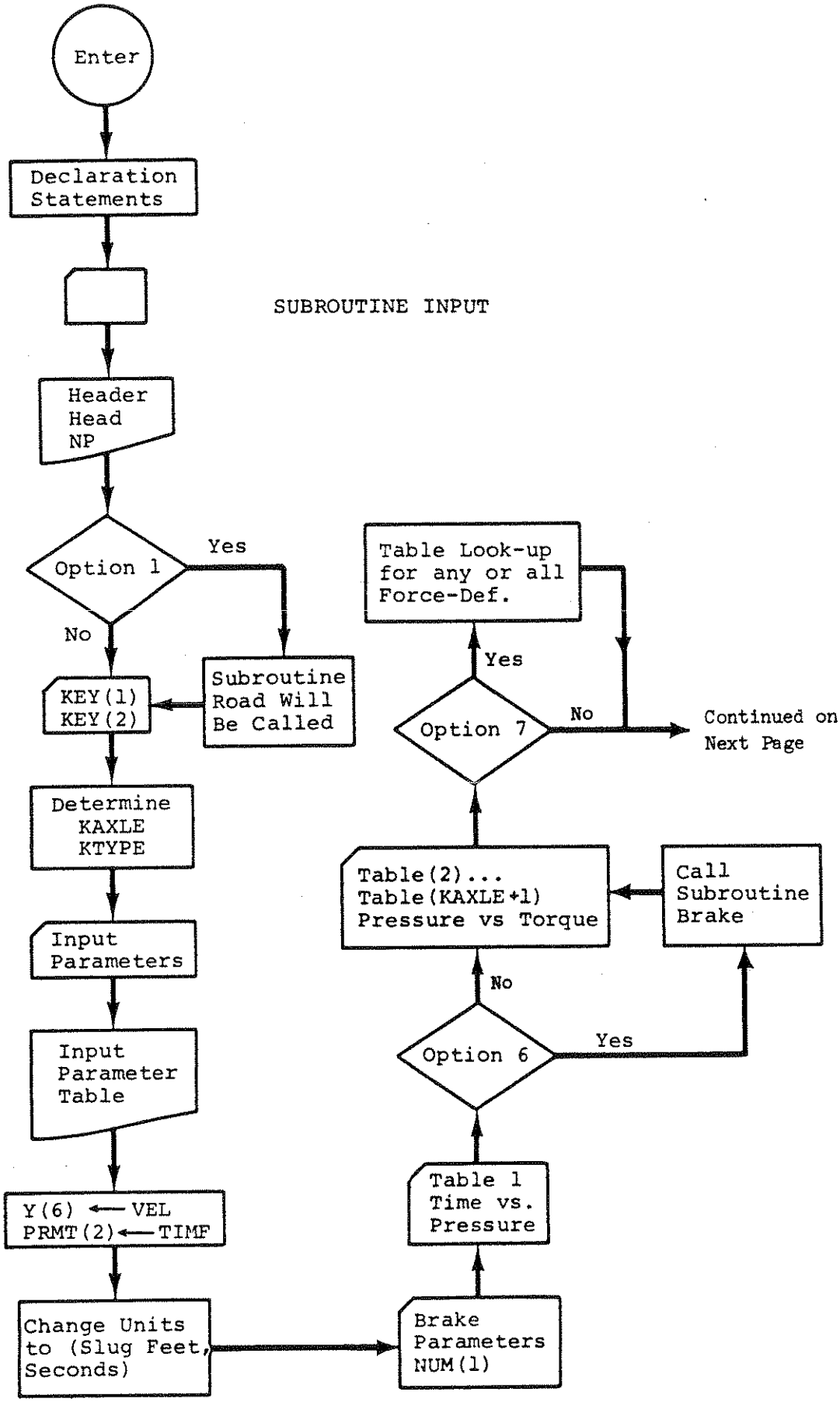
Enter
Declaration Statements
SUBROUTINE INPUT
Header Head NP
Option 1
Yes
No
Subroutine Road Will Be Called
KEY(1) KEY(2)
Determine KAXLE KTYPE
Input Parameters
Input Parameter Table
Y(6) ← VEL
PRMT(2) ← TIMF
Change Units to (Slug Feet, Seconds)
Brake Parameters NUM(1)
Table 1 Time vs. Pressure
Option 6
Yes
No
Table(2)... Table(KAXLE+1) Pressure vs Torque
Call Subroutine Brake
Option 7
Yes
No
Table Look-up for any or all Force-Def.
Continued on Next Page

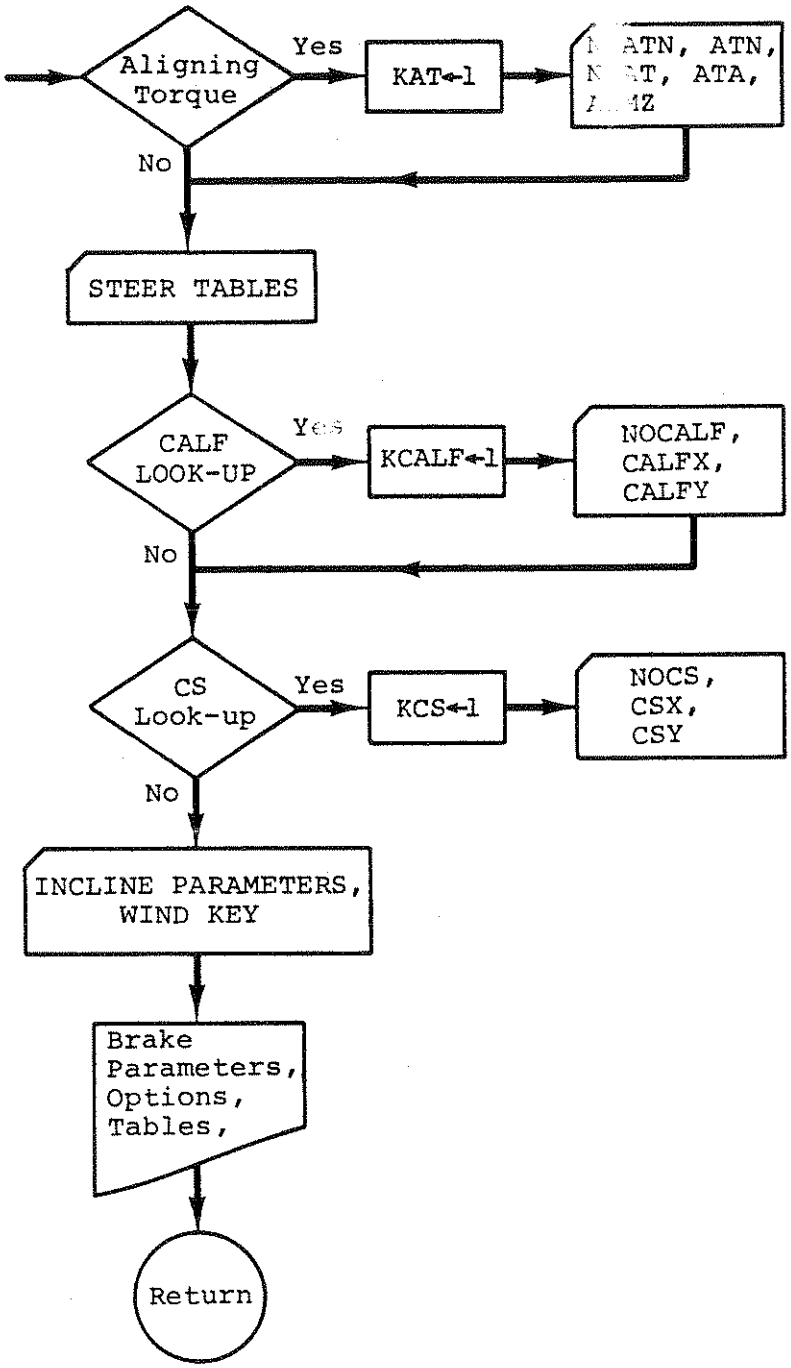
Aligning Torque
Yes
KAT←1
ATN, ATN,
T, ATA,
Z
No
STEER TABLES
CALF LOOK-UP
Yes
KCALF←1
NOCALF, CALFX, CALFY
No
CS Look-up
Yes
KCS←1
NOCS, CSX, CSY
No
INCLINE PARAMETERS, WIND KEY
Brake Parameters, Options, Tables,
Return

SUBROUTINE FCT1

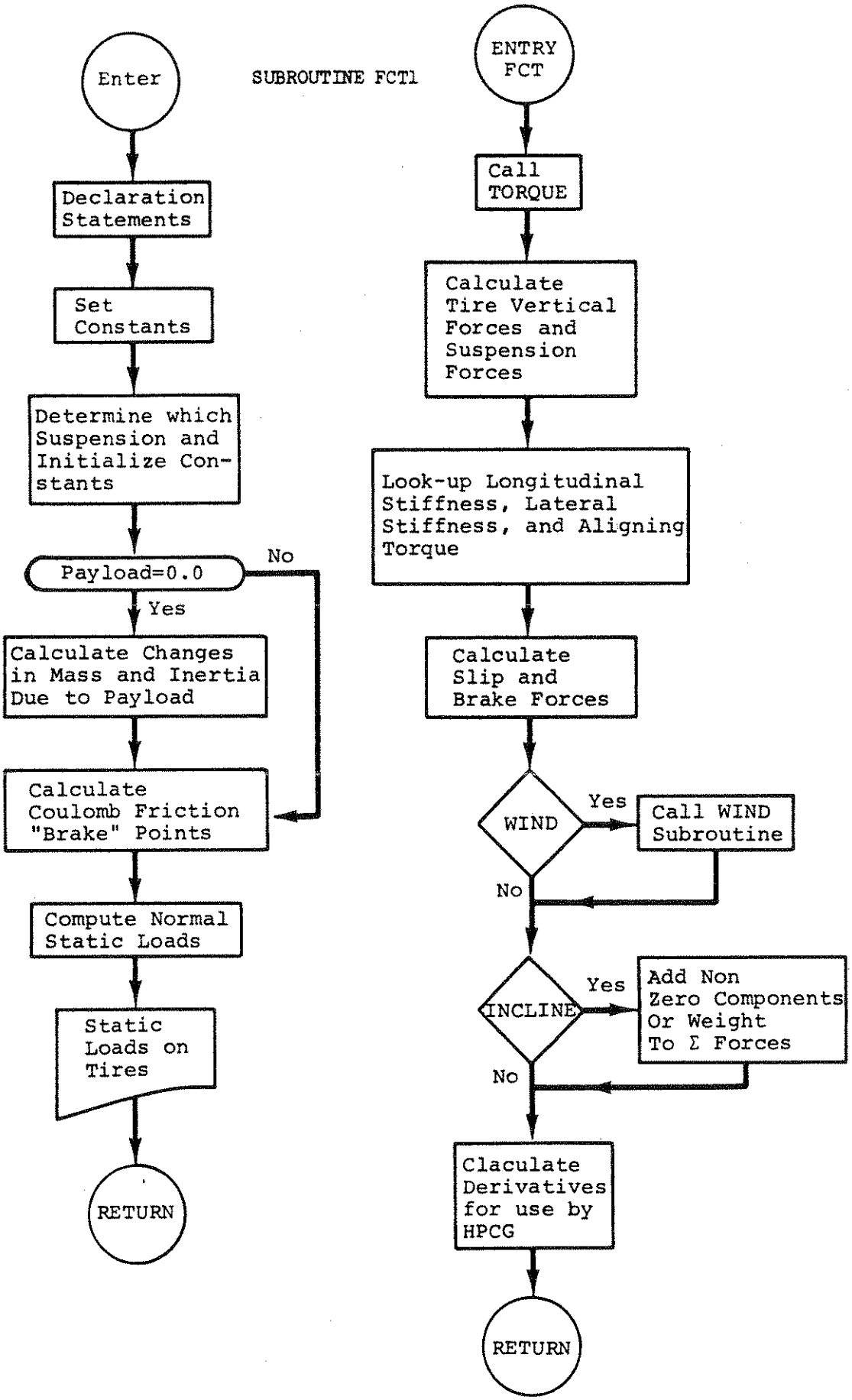

SUBROUTINE OUTPUT

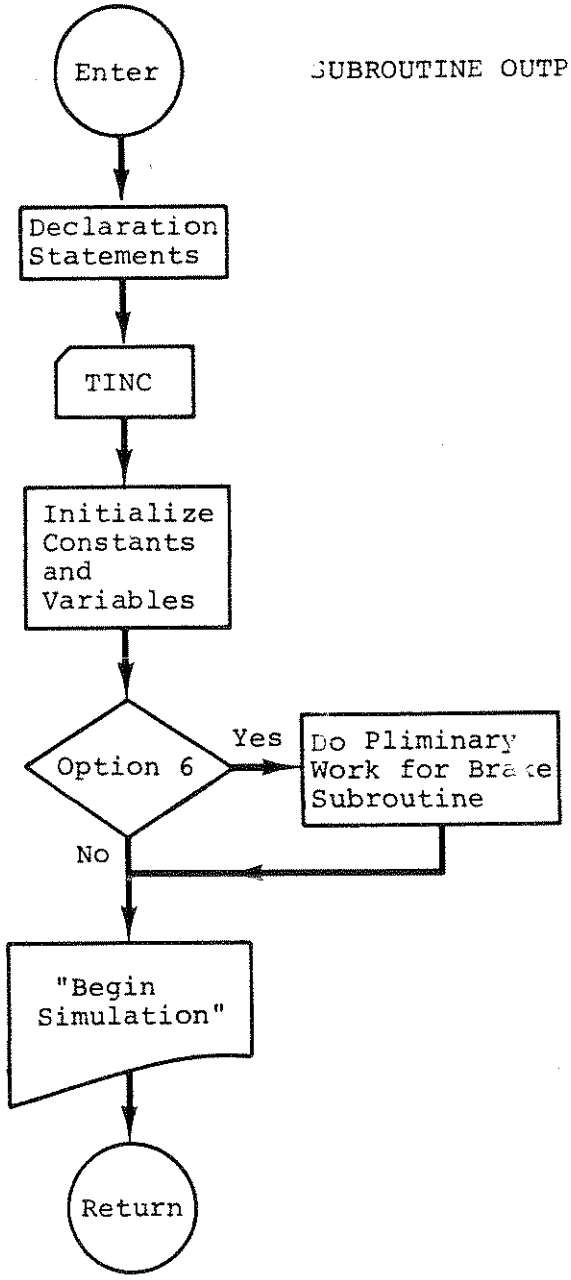

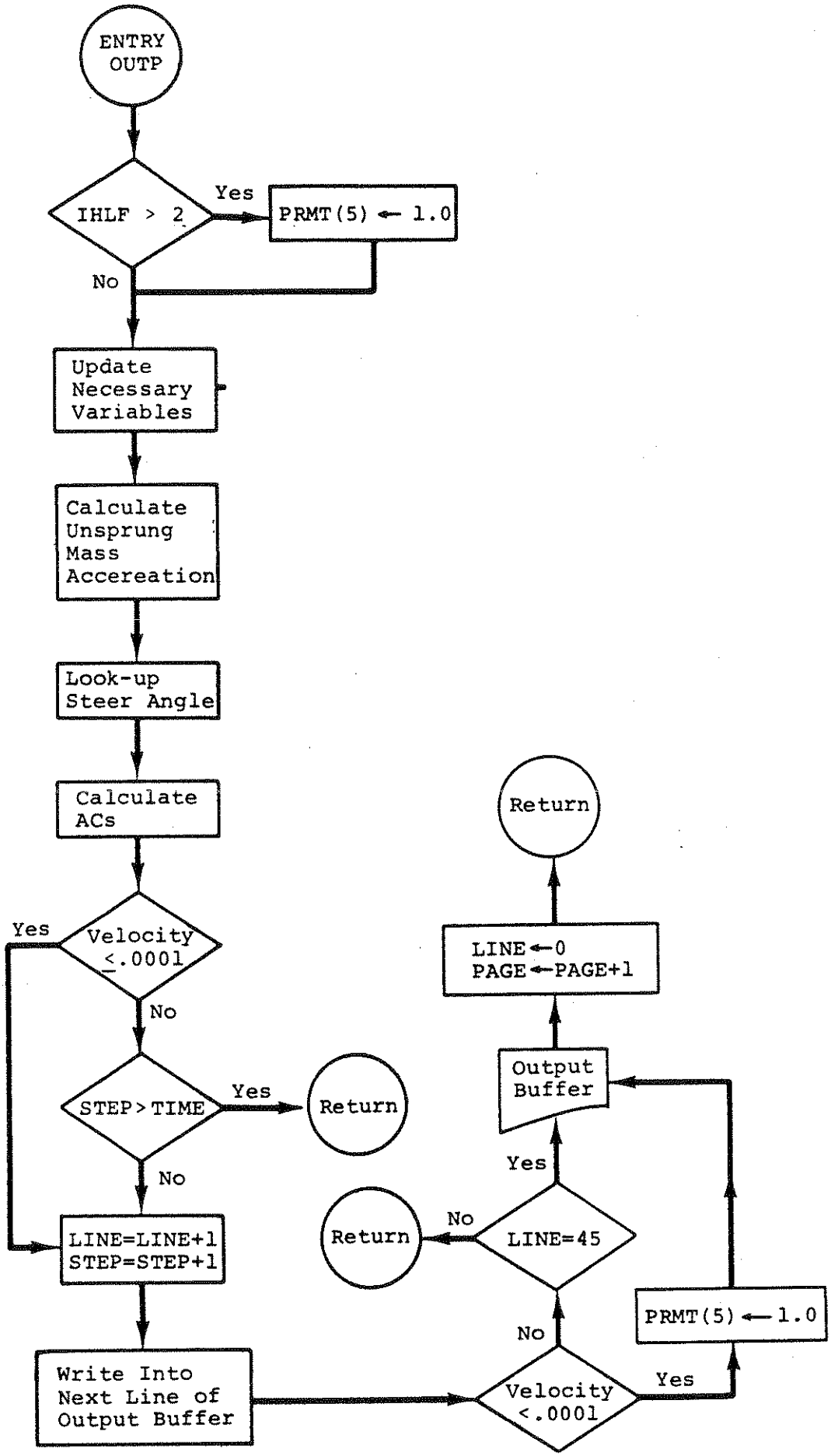
ENTRY OUTP
IHLF > 2
Yes
PRMT(5) ← 1.0
No
Update Necessary Variables
Calculate Unsprung Mass Accereation
Look-up Steer Angle
Calculate ACs
Yes
Velocity ≤.0001
No
STEP > TIME
Yes
Return
No
LINE=LINE+1
STEP=STEP+1
Write Into Next Line of Output Buffer
Velocity <.0001
No
Yes
PRMT(5) ← 1.0
LINE=45
No
Return
Yes
Output Buffer
LINE ← 0
PAGE ← PAGE+1
Return

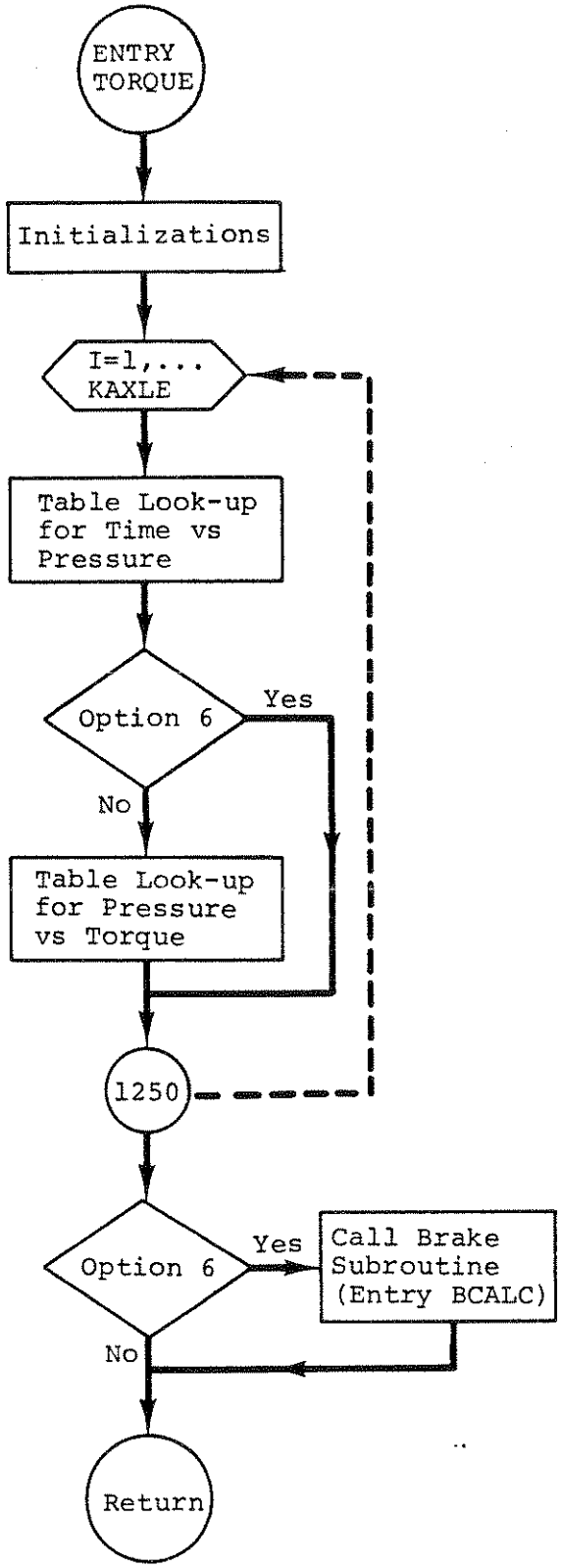
ENTRY
TORQUE
Initializations
I=1,...
KAXLE
Table Look-up
for Time vs
Pressure
Option 6
Yes
No
Table Look-up
for Pressure
vs Torque
1250
Option 6
Yes
Call Brake
Subroutine
(Entry BCALC)
No
Return

APPENDIX F

Validation Data

TABLE F-1
INPUT PARAMETERS, STRAIGHT TRUCK

SYMBOL	DESCRIPTION	VALUE FOR ALL CONDITIONS	SPECIAL CONDITION	SPECIAL VALUE
	*****Vehicle Parameters*****			
KEY	Axle Key: Set to 0 for Single Axle 1 for Walking Beam 2 for Elliptic Leaf	1		
AA1	Horizontal Dist. From Walking Beam Pin to Front Axle (in)	24.00		
AA2	Horizontal Dist. From Walking Beam Pin to Rear Axle (in)	26.00		
AA4	Vertical Dist. From Axle to W.B. (in)	8.00		
AA5	Vertical Dist. From Axle to Torque Rod (in)	18.00		
A1	Horizontal Distance From CG to Midpoint of Front Suspension (in)*	49.50		
A2	Horizontal Distance From CG to Midpoint of Rear Suspension (in)*	140.50		
ALPHA1	Static Distance, Front Axle to Ground (in)	19.95		
ALPHA2	Static Distance, Rear Axle(s) to Ground (in)	20.00		
C1	Viscous Damping: Jounce on Front Axle (lb-sec/in)	4.16		
C2	Viscous Damping: Rebound on Front Axle (lb-sec/in)	8.33		
C3	Viscous Damping: Jounce on Rear Axle(s) (lb-sec/in)	0.0		
C4	Viscous Damping: Rebound on Rear Axle(s) (lb-sec/in)	0.0		
CALF1	Lateral Stiffness, Front Tires (lbs/deg)	-1.000**		
CALF2	Lateral Stiffness, Front Tandem Tires (lbs/deg)	-1.00**		
CALF3	Lateral Stiffness, Rear Tandem Tires (lbs/deg)	-1.00**		
CF1	Max. Coulomb Friction, Front Suspension (lb)	1100.00		
CF2	Max. Coulomb Friction, Rear Suspension (lb)	2200.00		
CFP11	Curve Fit Parameter No. 1, Front Axle	2.30		
CFP12	Curve Fit Parameter No. 1, Front Tandem Axle	1.70		
CFP13	Curve Fit Parameter No. 1, Rear Tandem Axle	1.70		
CFP21	Curve Fit Parameter No. 2, Front Axle (deg)	6.00		
CFP22	Curve Fit Parameter No. 2, Front Tandem Axle (deg)	9.00		
CFP23	Curve Fit Parameter No. 2, Rear Tandem Axle (deg)	9.00		
CS1	Longitudinal Stiffness, Front Tires (lbs)	-1.00**		
CS2	Longitudinal Stiffness, Front Tandem Tires (lbs)	-1.00**		
CS3	Longitudinal Stiffness, Rear Tandem Tires (lbs)	-1.00**		
DELTA1	Static Vertical Distance, Front Axle to Tractor CG (in)	22.00		
DT2	Distance Between Dual Tires, Front Tandem Axle (in)	13.00		

*For empty vehicle, body was considered as payload. For loaded vehicles, body was considered as part of truck.

**Table look up.

TABLE F-1 (Continued)

SYMBOL	DESCRIPTION	VALUE FOR ALL CONDITIONS	SPECIAL CONDITION	SPECIAL VALUE
FA1	Friction Reduction Parameter on Front Tires	0.0055		
FA2	Friction Reduction Parameter on Front Tandem Tires	0.0055		
FA3	Friction Reduction Parameter on Rear Tandem Tires	0.0055		
IXX	Sprung Mass Roll Moment of Inertia (in-lb-sec**2)	51746.00		
IYY	Sprung Mass Pitch Moment of Inertia (in-lb-sec**2)	103492.00		
IZZ	Yaw Moment of Inertia (in-lb-sec**2)	155238.00		
IXZ	Pitch Plane Cross Moment (in-lb-sec**2)	0.0		
JA1	Roll Moment of Front Axle (in-lb-sec**2)	3000.00		
JA2	Roll Moment of Front Tandem Axle (in-lb-sec**2)	4000.00		
JS1	Polar Moment of Front Wheels (in-lb-sec**2)	326.00		
JS2	Polar Moment of Front Tandem Wheels (in-lb-sec**2)	410.00		
JS3	Polar Moment of Rear Tandem Wheels (in-lb-sec**2)	410.00		
K1	Spring Rate, Front Suspension (lb/in)	2800.00		
K2	Spring Rate, Rear Suspension (lb/in)	15000.00		
KT1	Spring Rate, Front Tires (lb/in)	4700.00		
KT2	Spring Rate, Front Tandem Tires (lb/in)	4700.00		
KT3	Spring Rate, Rear Tandem Tires (lb/in)	4700.00		
MUZERO1	Coefficient of Friction, Front Wheels		Dry Road	0.85
			Wet Road	0.55
MUZERO2	Coefficient of Friction, Front Tandem Wheels		Dry Road	0.85
			Wet Road	0.65
MUZERO3	Coefficient of Friction, Rear Tandem Wheels		Dry Road	0.85
			Wet Road	0.65
PERCNT	Percent Effectiveness of Torque Rods	100.00		
PW	Weight of Payload (lbs)*	7390.00		
PJ1	Roll Moment of Inertia of Payload (in-lb-sec**2)*		Empty	34990.00
			Loaded	39800.00
PJ2	Pitch Moment of Inertia of Payload (in-lb-sec**2)*		Empty	112051.00
			Loaded	170000.00
PJ3	Yaw Moment of Inertia of Payload (in-lb-sec**2)*		Empty	129120.00
			Loaded	203000.00
PX	Horizontal Distance From Midpoint of Rear Suspension to Mass Center (in)*	22.00		
PZ	Vertical Distance From Ground to Paylaod Center of Mass (in)*	72.00		
RCH1	Roll Center Height, Front Suspension (in)	33.00		
RCH2	Ro-l Center Height, Rear Suspension (in)	25.00		
RS1	Compliance Steer (deg/in)	0.0		
RSC1	Roll Steer Coefficient, Front Axle	0.26		
RSC2	Roll Steer Coefficient, Rear Suspension	0.26		
SY1	Horizontal Distance from Body X-Axis to Front Suspension (in)	16.40		
SY2	Horizontal Distance from Body Y-Axis to Rear Suspension (in)	17.00		
TIMF	Max. Real Time for Simulation	**		
TRA1	Half Track of Front Axle (in)	40.000		
TRA2	Half Track of Front Tandem Axle (in)	36.00		
VEL	Initial Velocity (fps)	**		
W	Sprung Weight of Truck (lbs)*	8190.00		

*For empty vehicle, body was considered as payload. For loaded vehicles, body was considered part of truck.

**Varies with expected duration of stop.

TABLE F-1 (Continued)

SYMBOL	DESCRIPTION	VALUE FOR ALL CONDITIONS	SPECIAL CONDITION	SPECIAL VALUE
WS1	Weight of Front Suspension (lbs)	1742.00		
WS2	Weight of Tandem Front (lbs)	2078.00		
WS3	Weight of Rear Tandem (lbs)	1972.00		
	*****Braking Parameters*****			
TQ(1,1,1)		0.032		
TQ(1,1,2)		0.296		
TQ(1,2,1)		0.032		
TQ(1,2,2)		0.296		
TQ(2,1,1)		0.070		
TQ(2,1,2)		0.181		
TQ(2,2,1)		0.070		
TQ(2,2,2)		0.181		
TQ(3,1,1)		0.073		
TQ(3,1,2)		0.276		
TQ(3,2,1)		0.073		
TQ(3,2,2)		0.276		
FRAY	Brake Fade Coefficient	0.0120		
	Axle 1, Left Side			
IBRT	Brake Type	2-Wedge		
AC	Brake Chamber Area (sq.in)	9.000		
EM	Mechanical Efficiency	0.880		
PO	Pushout Pressure (PSI)	8.000		
RD	Drum Radius (in)	7.500		
ULH	Mu Lining, High	0.500		
ULL	Mu Lining, Low	0.350		
AB	Distance From Horizontal Centerline of Drum to Parallel Line Through Shoe Contact Point (in)	5.560		
ALPHO	Lining Contact Angle (deg)	127.197		
ALPHW	Wedge Angle (deg)	12.548		
BETA	Lining Offset Angle (deg)	0.573		
C2	Distance from Horizontal Centerline of Drum Parallel Line Through Point of Actuating Force (in)	5.310		
OH	Distance From Vertical Centerline of Drum to Parallel Line Through Shoe Contact Point (in)	3.160		
	Axle 2, Left Side			
IBRT	Brake Type	2-Wedge		
AC	Brake Chamber Area (sq in)	12.000		
EM	Mechanical Efficiency	0.880		
PO	Pushout Pressure (PSI)	7.500		
RD	Drum Radius (in)	7.500		
ULH	Mu Lining, High	0.540		
ULL	Mu Lining, Low	0.370		
AB	Distance From Horizontal Centerline of Drum to Parallel Line Through Shoe Contact Point (in)	5.310		
ALPHO	Lining Contact Angle (deg)	126.051		
ALPHW	Wedge Angle (deg)	12.548		
BETA	Lining Offset Angle (deg)	0.573		
C2	Distance From Horizontal Centerline of Drum Parallel Line Through Point of Actuating Force (in)	5.440		
OH	Distance From Vertical Centerline of Drum to Parallel Line Through Shoe Contact Point (in)	3.050		
	Axle 3, Left Side			
IBRT	Brake Type	2-Wedge		
AC	Brake Chamber Area (sq. in)	12.000		
EM	Mechanical Efficiency	0.880		
PO	Pushout Pressure (PSI)	7.500		
RD	Drum Radius (in)	7.500		
ULH	Mu Lining, High	0.540		
ULL	Mu Lining, Low	0.370		
AB	Distance From Horizontal Centerline of Drum to Parallel Line Through Shoe Contact Point (in)	5.310		
ALPHO	Lining Contact Angle (deg)	126.051		
ALPHW	Wedge Angle (deg)	12.548		

SYMBOL	DESCRIPTION	VALUE FOR ALL CONDITIONS	SPECIAL CONDITION	SPECIAL VALUE
BETA	Lining Offset Angle (deg)	0.573		
C2	Distance From Horizontal Centerline of Drum Parallel Line Through Point of Actuating Force (in)	5.440		
OH	Distance From Vertical Centerline of Drum to Parallel Line Through Shoe Contact Point (in)	3.050		

TABLE F-2
INPUT PARAMETERS, TRACTOR TRAILER

SYMBOL	DESCRIPTION	VALUE FOR ALL CONDITIONS	SPECIAL CONDITION	SPECIAL VALUE
	*****Vehicle Parameters*****			
KEY(1)	Tractor Axle Key: 0 for Single Axle 1 for Walking Beam 2 for 4 Elliptic Leaf	2		
KEY(2)	Trailer Axle Key	2		
AA1	Horizontal Distance From Tractor Front Leaf-Frame Contact to Axle Center (in)	21.60		
AA2	Horizontal Distance From Tractor Rear Leaf-Frame Contact to Axle Center (in)	19.25		
AA4	Horizontal Distance From Tractor Front Leaf-Frame Contact to Load Leveler Pin (in)	6.75		
AA5	Horizontal Distance From Tractor Rear Leaf-Frame Contact to Load Leveler Pin (in)	6.75		
AA6	Vertical Distance From Axle Down to Tractor Torque Rod (in)	7.00		
AA7	Angle Between Tractor Torque Rod and Horizontal (deg)	13.00		
AA8	Horizontal Distance From Axle Center Forward to Tractor Torque Rod (in)	-1.00		
AA9	Horizontal Distance From Trailer Front Leaf-Frame Contact to Axle Center (in)	18.50		
AA10	Horizontal Distance From Trailer Rear Leaf-Frame Contact to Axle Center (in)	18.50		
AA12	Horizontal Distance From Trailer Front Leaf-Frame Contact to Load Leveler Pin (in)	6.00		
AA13	Horizontal Distance From Trailer Rear Leaf-Frame Contact to Load Leveler Pin (in)	6.25		
AA14	Vertical Distance From Axle Down to Trailer Torque Rod (in)	7.00		
AA15	Angle Between Trailer Torque Rod and Horizontal (deg)	15.01		
AA16	Horizontal Distance From Axle Center Forward to Trailer Torque Rod (in)	5.50		
A1	Horizontal Distance From Tractor CG to Center of Tractor Front Suspension (in)	35.90		
A2	Horizontal Distance From Tractor CG to Center of Tractor Rear Suspension (in)	106.10		
A3	Horizontal Distance From Trailer CG to 5th Wheel (in)	222.00		
A4	Horizontal Distance From Trailer CG to Center of Trailer Suspension (in)	144.00		
ALPHA1	Static Distance, Tractor Front Axle to Ground (in)	19.20		
ALPHA2	Static Distance, Tractor Rear Axle(s) to Ground (in)	19.50		
ALPHA3	Statis Distance, Trailer Axle(s) to Ground (in)	19.50		
BB	Horizontal Distance From 5th Wheel to Midpoint of Tractor Rear Suspension (in)	0.0		
C1	Viscous Damping: Jounce on Tractor Front Suspension (lb-sec/in)	4.16		
C2	Viscous Damping: Rebound on Tractor Front Suspension (lb-sec/in)	8.33		
C3	Viscous Damping: Jounce on Tractor Rear Suspension (lb-sec/in)	0.0		
C4	Viscous Damping: Rebound on Tractor Rear Suspension (lb-sec/in)	0.0		
C5	Viscous Damping: Jounce on Trailer Suspension (lb-sec/in)	0.0		
C6	Viscous Damping: Rebound on Trailer Suspension (lb-sec/in)	0.0		
CALF1	Lateral Stiffness, Tractor Front Tires (lbs/deg)	-1.00*		
CALF2	Lateral Stiffness, Tractor Front Tandem Tires (lbs/deg)	-1.00*		

*Table look up.

TABLE F-2 (Continued)

SYMBOL	DESCRIPTION	VALUE FOR ALL CONDITIONS	SPECIAL CONDITION	SPECIAL VALUE
CALF3	Lateral Stiffness, Tractor Rear Tandem Tires (lbs/deg)	-1.00*		
CALF4	Lateral Stiffness, Trailer Front Tandem Tires (lbs/deg)	-1.00*		
CALF5	Lateral Stiffness, Trailer Rear Tandem Tires (lbs/deg)	-1.00*		
CF1	Maximum Coulomb Friction, Tractor Front Suspension (lb)	900.00		
CF2	Maximum Coulomb Friction, Tractor Rear Suspension (lb)	4400.00		
CF3	Maximum Coulomb Friction, Trailer Suspension (lb)	3600.00		
CFP11	Curve Fit Parameter No. 1, Tractor Front Axle	1.70		
CFP12	Curve Fit Parameter No. 1, Tractor Front Tandem Axle	4.00		
CFP13	Curve Fit Parameter No. 1, Tractor Rear Tandem Axle	4.00		
CFP14	Curve Fit Parameter No. 1, Trailer Front Tandem Axle	1.70		
CFP15	Curve Fit Parameter No. 1, Trailer Rear Tandem Axle	1.70		
CFP21	Curve Fit Parameter No. 2, Tractor Front Axle (deg)	9.00		
CFP22	Curve Fit Parameter No. 2, Tractor Front Tandem Axle (deg)	2.00		
CFP23	Curve Fit Parameter No. 2, Tractor Rear Tandem Axle (deg)	2.00		
CFP24	Curve Fit Parameter No. 2, Trailer Front Tandem Axle (deg)	9.00		
CFP25	Curve Fit Parameter No. 2, Trailer Rear Tandem Axle (deg)	9.00		
CS1	Longitudinal Stiffness, Tractor Front Tires (lbs)	-1.00*		
CS2	Longitudinal Stiffness, Tractor Front Tandem Tires (lbs)	-1.00*		
CS3	Longitudinal Stiffness, Tractor Rear Tandem Tires (lbs)	-1.00*		
CS4	Longitudinal Stiffness, Trailer Front Tandem Tires (lbs)	-1.00*		
CS5	Longitudinal Stiffness, Trailer Rear Tandem Tires (lbs)	-1.00*		
D	Vertical Distance From 5th Wheel Connection to Tractor CG (in)	-4.50		
DELTA1	Static Vertical Distance, Tractor CG to Tractor Front Axle (in)	33.30		
DELTA3	Static Vertical Distance, Trailer CG to Trailer Axle(s) (in)	49.50		
DT2	Distance Between Dual Tires, Tractor Rear Suspension (in)	13.00		
DT3	Distance Between Dual Tires, Trailer Suspension (in)	13.00		
FA1	Friction Reduction Parameters for Tractor Front Tires		Dry Road Wet Road	0.005 0.010
FA2	Friction Reduction Parameter for Tractor Front Tandem Tires		Dry Road Wet Road	0.005 0.010
FA3	Friction Reduction Parameter for Tractor Rear Tandem Tires		Dry Road Wet Road	0.005 0.010
FA4	Friction Reduction Parameter for Trailer Front Tandem Tires		Dry Road Wet Road	0.005 0.010
FA5	Friction Reduction Parameters for Trailer Rear Tandem Tires		Dry Road Wet Road	0.005 0.010
IXX	Tractor Sprung Mass Roll Moment of Inertia (in-lb-sec**2)	13500.00		
IYY	Tractor Sprung Mass Pitch Moment of Inertia (in-lb-sec**2)	53374.00		

* Table look up.

TABLE F-2 (Continued)

SYMBOL	DESCRIPTION	VALUE FOR ALL CONDITIONS	SPECIAL CONDITION	SPECIAL VALUE
IZ	Tractor Yaw MOment of Inertia (in-lb-sec**2)	119000.00		
IXZ	Tractor Pitch Plane Cross Moment (in-lb-sec**2)	0.0		
ITXX	Trailer Sprung Mass Roll Moment of Inertia (in-lb-sec**2)	51000.00		
ITYY	Trailer Sprung Mass Pitch Moment of Inertia (in-lb-sec**2)	607200.00		
ITZZ	Trailer Yaw Moment of Inertia (in-lb-sec**2)	605000.00		
ITXZ	Trailer Pitch Plane Cross Moment (in-lb-sec**2)	0.0		
JA1	Roll Moment of Tractor Front Axle (in-lb-sec**2)	3719.00		
JA2	Roll Moment of Tractor Front Tandem Axle (in-lb-sec**2)	4458.00		
JA3	Roll Moment of Trailer Front Tandem Axle (in-lb-sec**2)	4100.00		
JS1	Polar Moment of Tractor Front Wheels (in-lb-sec**2)	206.00		
JS2	Polar Moment of Tractor Front Tandem Wheels (in-lb-sec**2)	462.00		
JS3	Polar Moment of Tractor Rear Tandem Wheels (in-lb-sec**2)	462.00		
JS4	Polar Moment of Trailer Front Tandem Wheels (in-lb-sec**2)	462.00		
JS5	Polar Moment of Trailer Rear Tandem Wheels (in-lb-sec**2)	462.00		
K1	Spring Rate, Tractor Front Suspension (lb/in)	2600.00		
K2	Spring Rate, Tractor Rear Suspension (lb/in)	20800.00		
K3	Spring Rate, Trailer Suspension (lb/in)	28000.00		
KT1	Spring Rate, Tractor Front Tires (lb/in)	9400.00		
KT2	Spring Rate, Tractor Front Tandem Tires (lb/in)	18000.00		
KT3	Spring Rate, Tractor Rear Tandem Tires (lb/in)	18000.00		
KT4	Spring Rate, Trailer Front Tandem Tires (lb/in)	18000.00		
KT5	Spring Rate, Trailer Rear Tandem Tires (lb/in)	18000.00		
MC5	Moment Across the Fifth Wheel (in-lbs/deg)	103000.00		
MUZERO1	Coefficient of Friction, Tractor Front Tires		Dry Road	0.85
			Wet Road	0.55
MUZERO2	Coefficient of Friction, Tractor Front Tandem Tires		Dry Road	0.85
			Wet Road	0.75
MUZERO3	Coefficient of Friction, Tractor Rear Tandem Tires		Dry Road	0.85
			Wet Road	0.75
MUZERO4	Coefficient of Friction, Trailer Front Tandem Tires		Dry Road	0.85
			Wet Road	0.75
MUZERO5	Coefficient of Friction, Trailer Rear Tandem Tires		Dry Road	0.85
			Wet Road	0.65
PW	Weight of Payload (lbs)		Empty	0.0
			Loaded	46800.00
PJ1	Poll Moment of Inertia of Payload (in-lb-sec**2)		Empty	not entered
			Loaded	5420000.00
PJ2	Pitch Moment of Inertia of Payload (in-lb-sec**2)		Empty	not entered
			Loaded	5340000.00
PJ3	Yaw Moment of Inertia of Payload (in-lb-sec**2)		Empty	not entered
			Loaded	3000000.00
PX	Horizontal Distance From Midpoint of Rear Suspension to Payload Mass Center (in)		Empty	not entered
			Loaded	183.00
PZ	Vertical Distance From Ground to Payload Mass Center (in)		Empty	not entered
			Loaded	68.25

TABLE F-2 (Continued)

SYMBOL	DESCRIPTION	VALUE FOR ALL CONDITIONS	SPECIAL CONDITION	SPECIAL VALUE
PW	Weight of Payload (lbs)	0.0		
RCH1	Roll Center Height, Tractor Front Suspension (in)	37.70		
RCH2	Roll Center Height, Tractor Rear Suspension (in)	30.30		
RCH3	Roll Center Height, Trailer Suspension (in)	25.60		
RS1	Compliance Steer (deg.in)	0.0		
RSC1	Roll Steer Coefficient, Tractor Front Suspension	0.27		
RSC2	Roll Steer Coefficient, Tractor Rear Suspension	0.14		
RSC3	Roll Steer Coefficient, Trailer Suspension	0.12		
SY1	Horizontal Distance from Tractor Body X-Axis to Tractor Front Suspension (in)	16.30		
SY2	Horizontal Distance from Tractor Body X-Axis to Tractor Rear Suspension (in)	18.50		
SY3	Horizontal Distance from Trailer Body X-Axis to Trailer Suspension (in)	19.00		
TIMF	Maximum Real Time for Simulation (sec)	*		
TRA1	Half Track, Tractor Front Axle (in)	40.00		
TRA2	Half Track, Tractor Rear Axle(s) (in)	36.00		
TRA3	Half Track, Trailer Axle(s) (in)	36.00		
VEL	Initial Velocity (ft/sec)		30 MPH Tests 60 MPH Tests	44.00 88.00
W1	Sprung Weight of Tractor (lbs)	9245.00		
W2	Sprung Weight of Trailer (lbs)	8120.00		
WS1	Weight of Tractor Front Suspension (lbs)	1321.00		
WS2	Weight of Tractor Front Tandem Suspension (lbs)	2330.00		
WS3	Weight of Tractor Rear Tandem Suspension (lbs)	2074.00		
WS4	Weight of Trailer Front Tandem Suspension (lbs)	1520.00		
WS5	Weight of Trailer Rear Tandem Suspension (lbs)	1520.00		
	*****Brake Parameters*****			
TQ(1,1,1)	Brake Timing Parameter	0.050		
TQ(1,1,2)		0.270		
TQ(1,2,1)		0.050		
TQ(1,2,2)		0.270		
TQ(2,1,1)		0.075		
TQ(2,1,2)		0.245		
TQ(2,2,1)		0.075		
TQ(2,2,2)		0.245		
TQ(3,1,1)		0.075		
TQ(3,1,2)		0.245		
TQ(3,2,1)		0.075		
TQ(3,2,2)		0.245)		
TQ(4,1,1)		0.175		
TQ(4,1,2)		0.303		
TQ(4,2,1)		0.175		
TQ(4,2,2)		0.303		
TQ(5,1,1)		0.175		
TQ(5,1,2)		0.303		
TQ(5,2,1)		0.175		
TQ(5,2,2)		0.303		
	Axle 1, Left Side			
IBRT	Brake Type	2-Wedge		
AC	Brake Chamber Area (sq. in)	12.000		
EM	Mechanical Efficiency	0.800		
FRAY	Brake Fade Coefficient		30 MPH Tests 60 MPH Tests	0.0045 0.0080
PO	Pushout Pressure (PSI)	7.500		
RD	Drum Radius (in)	7.500		
ULH	Mu Lining, High	0.400		
ULL	Mu Lining, Low	0.250		
AB	Distance From Horizontal Centerline of Drum to Parallel Line Through Shoe Contact Point (in)	5.400		

*Varies with expected duration of run.

Varies.

TABLE F-2 (Continued)

SYMBOL	DESCRIPTION	VALUE FOR ALL CONDITIONS	SPECIAL CONDITION	SPECIAL VALUE
ALPHO	Lining Contact Angle (deg)	125.000		
ALPHW	Wedge Angle (deg)	12.000		
BETA	Lining Offset Angle (deg)	0.0		
C2	Distance From Horizontal Centerline of Drum Parallel Line Through Point of Actuating Force (in)	5.400		
OH	Distance From Vertical Centerline of Drum to Parallel Line Through Shoe Contact Point (in)	3.000		
	Axle 2, Left Side			
IBRT	Brake Type	2-Wedge		
AC	Brake Chamber Area (sq. in)	12.000		
EM	Mechanical Efficienty	0.800		
FRAY	Brake Fade Coefficient		30 MPH Tests	0.0045
			60 MPH Tests	0.0080
PO	Pushout Pressure (PSI)	7.500		
RD	Drum Radius (in)	7.500		
ULH	Mu Lining, High	0.400		
ULL	Mu Lining, Low	0.300		
AB	Distance From Horizontal Centerline of Drum to Parallel Line Through Shoe Contact Point (in)	5.400		
ALPHO	Lining Contact Angle (deg)	125.000		
ALPHW	Wedge Angle (deg)	12.000		
BETA	Lining Offset Angle (deg)	0.0		
C2	Distance From Horizontal Centerline of Drum Parallel Line Through Point of Actuating Force (in)	5.400		
OH	Distance From Vertical Centerline of Drum to Parallel Line Through Shoe Contact Point (in)	3.000		
	Axle 3, Left Side			
IBRT	Brake Type	2-Wedge		
AC	Brake Chamber Area (sq. in)	12.000		
EM	Mechanical Efficiency	0.800		
FRAY	Brake Fade Coefficient		30 MPH Tests	0.0045
			60 MPH Tests	0.0080
PO	Pushout Pressure (PSI)	7.500		
RD	Drum Radius (in)	7.500		
ULH	Mu Lining, High	0.420		
ULL	Mu Lining, Low	0.300		
AB	Distance From Horizontal Centerline of Drum to Parallel Line Through Shoe Contact Point (in)	5.400		
ALPHO	Lining Contact Angle (deg)	125.000		
ALPHW	Wedge Angle (deg)	12.000		
BETA	Lining Offset Angle (deg)	0.0		
C2	Distance From Horizontal Centerline of Drum Parallel Line Through Point of Actuating Force (in)	5.400		
OH	Distance From Vertical Centerline of Drum to Parallel Line Through Shoe Contact Point (in)	3.000		
	Axle 4, Left Side			
IBRT	Brake Type	S-Cam		
AC	Brake Chamber Area (sq. in)	30.000		
EM	Mechanical Efficiency	0.700		
FRAY	Brake Fade Coefficient		30 MPH Tests	0.0045
			60 MPH Tests	0.0080
PO	Pushout Pressure (PSI)	2.500		
RD	Drum Radius (in)	8.250		
ULH	Mu Lining, High	0.280		
ULL	Mu Lining, Low	0.150		
ALPHO	Lining Contact Angle (deg)	111.000		
ALPH3	ALPHO(4) + 2*ALPH1(4) (deg)	207.000		
APRIM	Radial Distance From Center of Drum to Shoe Pin (in).	6.900		

SYMBOL	DESCRIPTION	VALUE FOR ALL CONDITIONS	SPECIAL CONDITION	SPECIAL VALUE
HB	Distance From Horizontal Centerline Through Shoe Pin to Parallel Line Through Connector Contact Point (in)	12.600		
RC	Cam Radius (in)	0.500		
SAL	Slack Adjuster Length (in)	6.000		
	Axle 5, Left Side			
IBRT	Brake Type	S-Cam		
AC	Brake Chamber Area (sq. in)	30.000		
EM	Mechanical Efficiency	0.700		
FRAY	Brake Fade Coefficient		30 MPH Tests	0.0045
			60 MPH Tests	0.0080
PO	Pushout Pressure (PSI)	2.500		
RD	Drum Radius (in)	8.250		
ULH	Mu Lining, High	0.280		
ULL	Mu Lining, Low	0.150		
ALPH0	Lining Contact Angle (deg)	111.000		
ALPH3	ALPH0(5) + 2*ALPH1(5) (deg)	207.000		
APRIM	Radial Distance From Center of Drum to Shoe Pin (in)	6.900		
HB	Distance From Horizontal Centerline Through Shoe Pin to Parallel Line Through Connector Contact Point (in)	12.600		
RC	Cam Radius (in)	0.500		
SAL	Slack Adjuster Length (in)	8.000		

APPENDIX G

Tire Data

Preceding page blank

APPENDIX G

Tire Data

The data presented in this appendix was measured on the HSRI flat bed tire test machine. For the 10.00-20 tires, lateral force and aligning torque are presented each as a function of normal load and inflation pressure, their longitudinal stiffness and vertical spring rate are given at selected loads and inflation pressures.

Following the 10.00-20 tires, certain other tires are presented. This data is not as extensive as the 10.00-20 data, since the tests were run at only one inflation pressure. Data for particular tires may be located through the use of the following table.

Tire: Highway Tread 10.20/F (New) Rim: 20x7.50

LATERAL FORCE vs SLIP ANGLE AND VERTICAL LOAD

Vertical Load (lbs.)	Inflation Pressure (psi)	Lateral Force at Indicated Slip Angle (degs.)					
		1	2	4	8	12	16
1400	50	245	444	758	1068	1195	1160
	85	214	399	688	971	1050	1115
	100	190	360	681	1088	1218	1309
2800	50	364	687	1209	1865	2211	2347
	85	364	693	1227	1829	2052	2213
	100	333	639	1232	2031	2377	2568
4200	50	388	744	1374	2289	2832	3163
	85	467	897	1612	2490	2881	3187
	100	437	844	1639	2745	3298	3626
5430	50	372	720	1365	2421	3142	3649
	85	523	1009	1830	2917	3458	3994
	100	501	973	1888	3201	3937	4399
6700	50	350	677	1307	2401	3286	3965
	85	550	1066	1962	3237	3994	4604
	100	546	1059	2045	3518	4455	5076
8100	50	332	632	1215	2274	3253	4079
	85	558	1086	2044	3446	4328	5181
	100	565	1109	2116	3744	4859	5468
9200	50	313	594	1129	2106	3060	3856
	85	557	1079	2044	3517	4459	-- *
	100	563	1112	2113	3791	5050	--

ALIGNING TORQUE vs SLIP ANGLE AND VERTICAL LOAD

Vertical Load (lbs.)	Inflation Pressure (psi)	Aligning Torque at Indicated Slip Angle (degs.)					
		1	2	4	8	12	16
1400	50	23	36	41	21	5	0
	85	18	30	36	20	7	4
	100	15	26	38	33	16	5
2800	50	58	99	136	113	73	30
	85	47	80	108	81	47	24
	100	40	69	112	116	76	47
4200	50	91	163	248	243	180	98
	85	77	136	194	170	115	67
	100	66	117	201	228	165	109
5430	50	120	220	351	394	313	198
	85	101	182	274	263	193	132
	100	89	159	281	335	262	180

*—indicates loads beyond the capacity of the load cells

ALIGNING TORQUE vs SLIP ANGLE AND VERTICAL LOAD (Continued)

Vertical Load (lbs.)	Inflation Pressure (psi)	Aligning Torque at Indicated Slip Angle (degs.)					
		1	2	4	8	12	16
	50	147	273	457	[illegible]1	500	348
6700	85	126	229	358	372	313	205
	100	111	201	370	478	384	278
	50	176	329	567	751	715	591
8100	85	153	281	458	504	439	318
	100	135	250	484	636	543	376
	50	194	368	644	896	900	800
9200	85	173	323	533	618	561	--
	100	154	288	580	768	685	--

CIRCUMFERENTIAL STIFFNESS vs SLIP ANGLE AND NORMAL LOAD

Vertical Load (lbs.)	Inflation Pressure (psi)	C_s (lbs.)	Vertical Spring Rate (lbs./in.)
	50		
2800	85	28,000	
	100		
	50	36,000	2943
5430	85	42,000	4700
	100	40,000	4309
	50		
8100	85	42,000	
	100		

Tire: Highway Tread 10-20/G (New) Rim: 20x7.50

LATERAL SOURCE vs SLIP ANGLE AND VERTICAL LOAD

Vertical Load (lbs.)	Inflation Pressure (psi)	Lateral Force at Indicated Slip Angle (degs.)					
		1	2	4	8	12	16
1400	50	261	472	795	1099	1210	1304
	85	252	449	706	1027	1159	1342
	100	210	416	759	1120	1195	1152
2800	50	405	757	1323	1991	2291	2548
	85	444	771	1282	1945	2253	2613
	100	366	727	1356	2083	2294	2242
4200	50	451	859	1562	2510	3033	3459
	85	536	991	1708	2666	3171	3725
	100	479	958	1809	2859	3247	3275
5430	50	447	861	1630	2768	3471	4043
	85	589	1117	1966	3147	3833	4520
	100	552	1102	2068	3374	3932	4034
6700	50	427	833	1572	2848	3733	4447
	85	605	1171	2136	3533	4377	5197
	100	603	1182	2257	3747	4494	4710
8100	50	414	806	1507	2806	3825	4609
	85	611	1193	2233	3813	4838	5785
	100	631	1244	2325	4000	4967	5353
9200	50	405	790	1433	2672	3803	4500
	85	611	1189	2217	3927	--	--
	100	640	1258	2229	4083	5070	--

ALIGNING TORQUE vs SLIP ANGLE AND VERTICAL LOAD

Vertical Load (lbs.)	Inflation Pressure (psi)	Aligning Torque at Indicated Slip Angle (degs.)					
		1	2	4	8	12	16
1400	50	21	36	41	18	3	2
	85	21	32	35	21	7	1
	100	17	29	40	30	8	0
2800	50	58	100	134	101	55	27
	85	56	89	104	82	45	25
	100	42	79	119	97	45	11
4200	50	92	166	246	223	145	93
	85	91	150	196	174	113	72
	100	72	137	217	203	112	49
5430	50	124	223	350	350	258	183
	85	118	200	278	272	186	131
	100	97	188	302	313	191	88

ALIGNING TORQUE vs SLIP ANGLE AND VERTICAL LOAD (Continued)

Vertical Load (lbs.)	Inflation Pressure (psi)	Aligning Torque at Indicated Slip Angle (degs.)					
		1	2	4	8	12	16
6700	50	161	[illegible]	451	522	407	310
	85	148	233	365	383	278	208
	100	120	234	403	443	289	143
8100	50	183	342	561	715	606	406
	85	180	311	463	515	406	311
	100	146	295	471	595	418	222
9200	50	209	395	647	868	768	--
	85	205	353	537	632	--	--
	100	168	335	594	727	468	--

CIRCUMFERENTIAL STIFFNESS vs SLIP ANGLE AND NORMAL LOAD

Vertical Load (lbs.)	Inflation Pressure (psi)	C_s (lbs.)	Vertical Spring Rate (lbs./in.)
5430	50	50,000	2857
	85		4363
	100		5532

Tire: Lug Type 10-20/F (New) Rim: 20x7.50

LATERAL FORCE vs SLIP ANGLE AND VERTICAL LOAD

Vertical Load (lbs.)	Inflation Pressure (psi)	Lateral Force at Indicated Slip Angle (degs.)					
		1	2	4	8	12	16
1400	50	249	464	710	1103	708	1559
	85	195	373	625	946	1149	1380
	100	199	373	664	1067	1205	1213
2800	50	405	771	1262	2017	1294	2892
	85	342	660	1145	1772	2168	2634
	100	349	663	1202	1980	2277	2324
4200	50	474	898	1569	1869	1705	3859
	85	449	873	1561	2444	3021	3677
	100	465	895	1643	2738	3181	3296
5430	50	468	904	1696	2211	1958	4498
	85	516	997	1811	2919	3636	4409
	100	538	1044	1928	3257	3848	4048
6700	50	447	873	1711	2311	2095	4923
	85	546	1062	1958	3294	4138	5049
	100	584	1150	2141	3660	4415	4726
8100	50	435	837	1662	3038	2055	4974
	85	542	1079	2038	3584	4600	5626
	100	609	1217	2302	3966	4921	5373
9200	50	413	783	1576	2184	1947	4752
	85	556	1074	2063	3751	4865	--
	100	623	1238	2341	4145	4992	--

ALIGNING TORQUE vs SLIP ANGLE AND VERTICAL LOAD

Vertical Load (lbs.)	Inflation Pressure (psi)	Aligning Torque at Indicated Slip Angle (degs.)					
		1	2	4	8	12	16
1400	50	22	39	38	30	10	1
	85	19	30	37	35	23	8
	100	16	26	40	37	22	8
2800	50	60	105	126	116	55	37
	85	43	76	104	100	69	43
	100	41	73	109	116	75	32
4200	50	97	174	228	169	108	112
	85	73	130	190	189	146	96
	100	70	124	193	222	153	73
5430	50	128	233	327	277	187	214
	85	97	178	266	278	219	164
	100	94	169	272	323	231	117

ALIGNING TORQUE vs SLIP ANGLE AND VERTICAL LOAD (Continued)

Vertical Load (lbs.)	Inflation Pressure (psi)	Aligning Torque at Indicated Slip Angle (degs.)					
		1	2	4	8	12	16
	50	155	295	431	398	289	371
6700	85	121	226	343	377	313	253
	100	116	215	355	434	326	172
	50	188	353	542	686	435	605
8100	85	140	270	428	495	418	359
	100	139	271	453	567	440	248
	50	213	404	622	639	499	784
9200	85	165	310	497	596	526	--
	100	161	310	524	680	474	--

CIRCUMFERENTIAL STIFFNESS vs SLIP ANGLE AND NORMAL LOAD

Vertical Load (lbs.)	Inflation Pressure (psi)	C_s (lbs.)	Vertical Spring Rate (lbs./in.)
	50		
2800	85	20,000	
	100		
	50		3600
5430	85	28,000	4500
	100		5000
	50		
8100	85	40,000	
	100		

Tire: Competitive Highway Tread 10-20/F (New) Rim: 20x7.50

LATERAL FORCE vs SLIP ANGLE AND VERTICAL LOAD

Vertical Load (lbs.)	Inflation Pressure (psi)	Lateral Force at Indicated Slip Angle (degs.)					
		1	2	4	8	12	16
1400	50	273	475	912	1309	1466	1382
	85	203	378	657	1002	1148	1197
	100	260	384	655	1082	1257	1157
2800	50	403	731	1389	2139	2512	2527
	85	347	655	1170	1835	2162	2300
	100	354	664	1178	2031	2341	2219
4200	50	443	831	1573	2601	3195	3351
	85	440	852	1541	2482	2971	3189
	100	459	876	1578	2762	3233	3101
5430	50	444	849	1600	2761	3531	3752
	85	508	968	1773	2935	3569	3888
	100	524	1014	1845	3235	3887	3790
6700	50	439	849	1519	2643	3508	4173
	85	551	1063	1946	3300	4087	4523
	100	575	1120	2053	3650	4474	4439
8100	50	430	830	1357	2283	3208	4165
	85	595	1131	2084	3608	4570	5149
	100	614	1203	2250	3967	4996	5089
9200	50	399	794	1126	1906	2797	3800
	85	619	1163	2147	3761	4868	5507
	100	635	1253	3292	4111	5281	--

ALIGNING TORQUE vs SLIP ANGLE AND VERTICAL LOAD

Vertical Load (lbs.)	Inflation Pressure (psi)	Aligning Torque at Indicated Slip Angle (degs.)					
		1	2	4	8	12	16
1400	50	29	40	63	42	18	2
	85	17	27	34	28	13	5
	100	12	28	33	33	15	1
2800	50	68	106	183	154	92	36
	85	43	75	108	97	57	28
	100	43	70	100	116	67	24
4200	50	104	170	313	316	225	102
	85	70	123	187	184	120	63
	100	69	119	178	220	139	54
5430	50	134	225	435	500	395	190
	85	92	165	259	277	192	106
	100	90	161	248	321	225	93

ALIGNING TORQUE vs SLIP ANGLE AND VERTICAL LOAD (Continued)

Vertical Load (lbs.)	Inflation Pressure (psi)	Aligning Torque at Indicated Slip Angle (degs.)					
		1	2	[illegible]	8	12	16
6700	50	167	285	551	711	639	378
	85	114	208	334	384	283	171
	100	112	202	320	443	332	144
8100	50	204	349	685	964	956	653
	85	140	253	416	508	405	255
	100	135	248	420	588	481	221
9200	50	232	397	776	1171	1216	900
	85	157	285	483	618	515	336
	100	154	283	468	717	598	--

CIRCUMFERENTIAL STIFFNESS vs SLIP ANGLE AND NORMAL LOAD

Vertical Load (lbs.)	Inflation Pressure (psi)	C_s (lbs.)	Vertical Spring Rate (lbs./in.)
2800	50		
	85	33,000	
	100		
5430	50	70,000	2680
	85	46,000	5032
	100	46,000	5416
8100	50		
	85	53,000	
	100		

Tire: Half Worn Highway Tread 10-20/F Rim: 20x7.50

LATERAL FORCE vs. SLIP ANGLE AND VERTICAL LOAD

Vertical Load (lbs.)	Inflation Pressure (psi)	Lateral Force at Indicated Slip Angle (degs.)					
		1	2	4	8	12	16
1400	85	363	620	965	1278	1633	1835
2800	85	556	1018	1675	2357	3004	3352
4200	85	662	1230	2130	3179	4105	4550
5430	85	691	1321	2368	3728	4833	5408
6700	85	680	1343	2492	4105	5408	6163
8100	85	657	1311	2530	4342	5766	6750
9200	85	628	1266	2499	4430	5892	--

ALIGNING TORQUE vs. SLIP ANGLE AND VERTICAL LOAD

Vertical Load (lbs.)	Inflation Pressure (psi)	Aligning Torque at Indicated Slip Angle (degs.)					
		1	2	4	8	12	16
1400	85	32	43	41	18	15	6
2800	85	81	126	132	85	70	41
4200	85	126	201	251	182	163	101
5430	85	162	269	360	307	269	171
6700	85	197	336	473	448	419	253
8100	85	235	408	599	624	602	374
9200	85	262	463	695	782	768	--

CIRCUMFERENTIAL STIFFNESS vs. SLIP ANGLE AND NORMAL LOAD

Vertical Load (lbs.)	Inflation Pressure (psi)	C_s (lbs.)	Vertical Spring Rate (lbs./in.)
5430	85	52,000	3939

Tire: Fully Worn Highway Tread 10-20/F Rim: 20x7.50

LATERAL FORCE vs. SLIP ANGLE AND VERTICAL LOAD

Vertical Load (lbs.)	Inflation Pressure (psi)	Lateral Force at Indicated Slip Angle (degs.)					
		1	2	4	8	12	16
1400	85	391	769	1169	1426	1529	1649
2800	85	598	1205	2027	2681	2884	3182
4200	85	712	1413	2517	3635	4207	4522
5430	85	772	1464	2681	4192	5049	5488
6700	85	759	1436	2713	4473	5687	--
8100	85	729	1360	2628	4537	--	--
9200	85	699	1280	2505	--	--	--

ALIGNING TORQUE vs. SLIP ANGLE AND VERTICAL LOAD

Vertical Load (lbs.)	Inflation Pressure (psi)	Aligning Torque at Indicated Slip Angle (degs.)					
		1	2	4	8	12	16
1400	85	32	52	45	14	5	2
2800	85	80	148	161	44	37	20
4200	85	126	249	324	123	119	66
5430	85	166	331	479	253	231	122
6700	85	198	409	635	443	378	--
8100	85	233	490	799	686	--	--
9200	85	260	546	920	--	--	--

CIRCUMFERENTIAL STIFFNESS vs. SLIP ANGLE AND NORMAL LOAD

Vertical Load (lbs.)	Inflation Pressure (psi)	C_s (lbs.)	Vertical Spring Rate (lbs./in.)
5430	85	60,000	4600

Tire: Highway Tread 8.25-20/E Rim: 20x7.00

LATERAL FORCE vs SLIP ANGLE AND VERTICAL LOAD

Vertical Load (lbs.)	Inflation Pressure (psi)	Lateral Force at Indicated Slip Angle (degs.)					
		1	2	4	8	12	16
1300	85	188	368	636	969	1137	1001
2700	85	318	631	1137	1814	2189	2076
4050	85	399	770	1404	2340	2934	2865
5400	85	398	807	1550	2662	3455	3530
6500	85	393	807	1546	2765	3719	3931

ALIGNING TORQUE vs SLIP ANGLE AND VERTICAL LOAD

Vertical Load (lbs.)	Inflation Pressure (psi)	Aligning Torque at Indicated Slip Angle (degs.)					
		1	2	4	8	12	16
1300	85	16	30	40	32	17	4
2700	85	42	77	116	116	81	34
4050	85	69	124	196	220	172	87
5400	85	92	175	288	351	296	164
6500	85	112	219	369	468	422	242

CIRCUMFERENTIAL STIFFNESS vs SLIP ANGLE AND NORMAL LOAD

Vertical Load (lbs.)	Inflation Pressure (psi)	C_s (lbs.)	Vertical Spring Rate (lbs./in.)
1300	85	14,000	
4050	85	22,000	3900
6500	85	36,000	

Tire: Highway Tread 9-20/E Rim: 20x7.00

LATERAL FORCE vs SLIP ANGLE AND VERTICAL LOAD

Vertical Load (lbs.)	Inflation Pressure (psi)	Lateral Force at Indicated Slip Angle (degs.)					
		1	2	4	8	12	16
1300	80	216	388	632	911	1026	1048
2700	80	367	687	1187	1791	2081	2181
4160	80	466	868	1535	2441	2937	3162
5400	80	479	926	1696	2812	3478	3828
6500	80	460	924	1771	3026	3807	4314

ALIGNING TORQUE vs SLIP ANGLE AND VERTICAL LOAD

Vertical Load (lbs.)	Inflation Pressure (psi)	Aligning Torque at Indicated Slip Angle (degs.)					
		1	2	4	8	12	16
1300	80	19	29	32	19	8	0
2700	80	52	84	108	88	49	21
4160	80	87	146	202	198	136	70
5400	80	112	196	288	304	223	134
6500	80	134	240	365	410	312	206

CIRCUMFERENTIAL STIFFNESS vs SLIP ANGLE AND NORMAL LOAD

Vertical Load (lbs.)	Inflation Pressure (psi)	C_s (lbs.)	Vertical Spring Rate (lbs./in.)
1300	80	14,000	
4160	80	41,000	3824
6500	80	6,500	

Tire: Highway Tread 9-20/F Rim: 20x7.00

LATERAL FORCE vs SLIP ANGLE AND VERTICAL LOAD

Vertical Load (lbs.)	Inflation Pressure (psi)	Lateral Force at Indicated Slip Angle (degs.)					
		1	2	4	8	12	16
1400	85	238	440	718	1001	1263	1232
2800	85	391	743	1286	1898	2500	2431
4250	85	479	920	1631	2538	3082	3459
5600	85	509	987	1805	2943	3690	4227
6500	85	506	1005	1856	3115	3990	4628

ALIGNING TORQUE vs SLIP ANGLE AND VERTICAL LOAD

Vertical Load (lbs.)	Inflation Pressure (psi)	Aligning Torque at Indicated Slip Angle					
		1	2	4	8	12	16
1400	85	20	33	38	20	6	-3
2800	85	52	89	118	87	49	19
4250	85	84	148	213	187	118	74
5600	85	114	202	306	295	208	139
6500	85	135	250	382	385	279	191

CIRCUMFERENTIAL STIFFNESS vs SLIP ANGLE AND NORMAL LOAD

Vertical Load (lbs.)	Inflation Pressure (psi)	C_s (lbs.)	Vertical Spring Rate (lbs./in.)
1400	85	16,000	
4250	85	41,000	4122
6800	85	50,000	

Tire: Highway Tread 11-22/F Rim: 22x8.00

LATERAL FORCE vs SLIP ANGLE AND VERTICAL LOAD

Vertical Load (lbs.)	Inflation Pressure (psi)	Lateral Force at Indicated Slip Angle (degs.)					
		1	2	4	8	12	16
2100	85	268	508	903	1428	2003	2269
4200	85	434	832	1535	2584	3456	4020
6290	85	543	1034	1916	3310	4474	5308
8200	85	571	1122	2091	3718	5073	6155
9900	85	573	1140	2162	3932	5351	6706

ALIGNING TORQUE vs SLIP ANGLE AND VERTICAL LOAD

Vertical Load (lbs.)	Inflation Pressure (psi)	Aligning Torque at Indicated Slip Angle (degs.)					
		1	2	4	8	12	16
2100	85	31	51	73	73	54	22
4200	85	76	133	205	230	204	131
6290	85	120	215	345	420	400	274
8200	85	156	290	478	607	613	448
9900	85	183	356	598	784	838	639

CIRCUMFERENTIAL STIFFNESS vs SLIP ANGLE AND NORMAL LOAD

Vertical Load (lbs.)	Inflation Pressure (psi)	C_s (lbs.)	Vertical Spring Rate (lbs./in.)
2100	85	21,000	
6290	85	47,000	5578
9800	85	48,000	

Tire: Highway Tread 11-22/G Rim: 22x8.50

LATERAL FORCE vs SLIP ANGLE AND VERTICAL LOAD

Vertical Load (lbs.)	Inflation Pressure (psi)	Lateral Force at Indicated Slip Angle (degs.)					
		1	2	4	8	12	16
2100	90	265	497	973	1636	2017	1927
4200	90	435	828	1550	2807	3510	3577
6140	90	537	1036	1979	3517	4497	4669
8200	90	587	1148	2189	4028	5245	5572
10000	90	601	1183	2236	4163	5633	6137

ALIGNING TORQUE vs SLIP ANGLE AND VERTICAL LOAD

Vertical Load (lbs.)	Inflation Pressure (psi)	Aligning Torque at Indicated Slip Angle (degs.)					
		1	2	4	8	12	16
2100	90	28	46	77	75	46	-5
4200	90	72	124	210	243	183	80
6140	90	112	199	350	428	342	174
8200	90	152	280	509	646	551	271
10000	90	185	345	652	853	766	429

CIRCUMFERENTIAL STIFFNESS vs SLIP ANGLE AND NORMAL LOAD

Vertical Load (lbs.)	Inflation Pressure (psi)	C_s (lbs.)	Vertical Spring Rate (lbs./in.)
2100	90	23,000	
6140	90	51,000	5852
10000	90	60,000	

Tire: Highway Tread 11-22.5/F Rim: 22.5x8.25

LATERAL FORCE vs. SLIP ANGLE AND VERTICAL LOAD

Vertical Load (lbs.)	Inflation Pressure (psi)	Lateral Force at Indicated Slip Angle (degs.)					
		1	2	4	8	12	16
1800	85	197	427	752	1250	1547	1605
3600	85	395	748	1352	2302	2876	3086
5430	85	504	973	1773	3065	3867	4317
7200	85	570	1102	2023	3591	4605	5310
8700	85	625	1159	2166	3883	5047	5930

ALIGNING TORQUE vs. SLIP ANGLE AND VERTICAL LOAD

Vertical Load (lbs.)	Inflation Pressure (psi)	Aligning Torque at Indicated Slip Angle (degs.)					
		1	2	4	8	12	16
1800	85	18	36	48	45	27	10
3600	85	59	101	146	157	125	74
5430	85	96	171	261	310	269	178
7200	85	130	235	374	481	442	315
8700	85	159	293	479	640	623	452

CIRCUMFERENTIAL STIFFNESS vs. SLIP ANGLE AND NORMAL LOAD

Vertical Load (lbs.)	Inflation Pressure (psi)	C_s (lbs.)	Vertical Spring Rate (lbs./in.)
1800	85	18,000	
5430	85	56,000	5700
8700	85	46,000	

Tire: Highway Tread 12-20/G Rim: 20x8.50

LATERAL FORCE vs. SLIP ANGLE AND VERTICAL LOAD

Vertical Load (lbs.)	Inflation Pressure (psi)	Lateral Force at Indicated Slip Angle (degs.)					
		1	2	4	8	12	16
2100	80	391	741	1245	1746	2047	2189
4200	80	590	1144	2041	3063	3681	4002(?)
6140	80	701	1343	2438	3846	4763	5292
8200	80	721	1417	2671	4414	5675	6472
9900	80	729	1440	2672	4695	6195	7197

ALIGNING TORQUE vs. SLIP ANGLE AND VERTICAL LOAD

Vertical Load (lbs.)	Inflation Pressure (psi)	Aligning Torque at Indicated Slip Angle (degs.)					
		1	2	4	8	12	16
2100	80	48	82	104	76	42	16
4200	80	114	203	292	261	177	101
6140	80	170	309	471	467	338	204
8200	80	224	422	659	713	559	369
9900	80	272	512	795	930	770	528

CIRCUMFERENTIAL STIFFNESS vs. SLIP ANGLE AND NORMAL LOAD

Vertical Load (lbs.)	Inflation Pressure (psi)	C_s (lbs.)	Vertical Spring Rate (lbs./in.)
2100	80	23,000	
6140	80	60,000	4800
9900	80	74,000	

Tire: Highway Tread 12-22.5/F Rim: 22.5x8.50

LATERAL FORCE vs SLIP ANGLE AND VERTICAL LOAD

Vertical Load (lbs.)	Inflation Pressure (psi)	Lateral Force at Indicated Slip Angle (degs.)					
		1	2	4	8	12	16
2000	85	313	581	1001	1472	1758	1796
4000	85	502	944	1718	2693	3262	3614(?)
5920	85	621	1132	2090(?)	3436(?)	4299	4682
8000	85	609	1186	2241	3915	5044	5770
10000	85	603	1168	2243	4083	5381	6367

ALIGNING TORQUE vs SLIP ANGLE AND VERTICAL LOAD

Vertical Load (lbs.)	Inflation Pressure (psi)	Aligning Torque at Indicated Slip Angle (degs.)					
		1	2	4	8	12	16
2000	85	35	55	67	40	14	-1
4000	85	89	153	212	180	117	31
5920	85	136	241	362	366	275	151
8000	85	179	331	530	605	520(?)	327(?)
10000	85	220	421	688	858	817	559

CIRCUMFERENTIAL STIFFNESS vs SLIP ANGLE AND NORMAL LOAD

Vertical Load (lbs.)	Inflation Pressure (psi)	C_s (lbs.)	Vertical Spring Rate (lbs./in.)
2000	85	20,000	
5920	85	58,000	4534
10000	85	57,000	

Tire: Highway Tread 12.5-22.5/G Rim: 22.5x8.25

LATERAL FORCE vs SLIP ANGLE AND VERTICAL LOAD

Vertical Load (lbs.)	Inflation Pressure (psi)	Lateral Force at Indicated Slip Angle (degs.)					
		1	2	4	8	12	16
1960	90	284	540	956	1344	1623	1770
3925	90	470	911	1653	2469	3042	3352
5890	90	593	1157	2117	3261	4121	4629
7850	90	649	1261	2370	3844	4945	5658
9800	90	666	1310	2420	4234	5558	6569

ALIGNING TORQUE vs SLIP ANGLE AND VERTICAL LOAD

Vertical Load (lbs.)	Inflation Pressure (psi)	Aligning Torque at Indicated Slip Angle (degs.)					
		1	2	4	8	12	16
1960	90	31	54	77	58	34	13
3925	90	78	140	211	188	130	68
5890	90	126	230	363	353	263	157
7850	90	171	318	530	540	430	270
9800	90	219	417	697	760	636	429

CIRCUMFERENTIAL STIFFNESS vs SLIP ANGLE AND NORMAL LOAD

Vertical Load (lbs.)	Inflation Pressure (psi)	C_s (lbs.)	Vertical Spring Rate (lbs./in.)
1960	90	21,000	
5890	90	62,000	4785
9800	90	50,000	

Tire: Highway Tread 15-22.5/H Rim: 22.5x11.75

LATERAL FORCE vs SLIP ANGLE AND VERTICAL LOAD

Vertical Load (lbs.)	Inflation Pressure (psi)	Lateral Force at Indicated Slip Angle (degs.)					
		1	2	4	8	12	16
2900	90	461	850	1402	2027	2376	2772
5800	90	790	1488	2531	3791	4479	5256
8640	90	1015	1915	3368	5190	6195	7301
10000	90	1041	2012	3583	5628	6860	8119(?)

ALIGNING TORQUE vs SLIP ANGLE AND VERTICAL LOAD

Vertical Load (lbs.)	Inflation Pressure (psi)	Aligning Torque at Indicated Slip Angle (degs.)					
		1	2	4	8	12	16
2900	90	44	71	86	63	29	10
5800	90	124	208	276	223	131	78
8640	90	214	375	515	449	273	161
10000	90	251	449	632	571	347	215

CIRCUMFERENTIAL STIFFNESS vs SLIP ANGLE AND NORMAL LOAD

Vertical Load (lbs.)	Inflation Pressure (psi)	C_s (lbs.)	Vertical Spring Rate (lbs./in.)
2900	90	47,000	
8640	90	85,000	5420
10000	90	76,000	

Tire: Highway Tread 8-22.5/D: Single Rim: 22.5x5.25

LATERAL FORCE vs SLIP ANGLE AND VERTICAL LOAD

Vertical Load (lbs.)	Inflation Pressure (psi)	Lateral Force at Indicated Slip Angle (degs.)					
		1	2	4	8	12	16
900	65	153	292	447	643	712	748
1800	65	259	496	809	1235	1439	1527
2750	65	311	588	1018	1654	2002	2210
3600	65	295	577	1053	1804(?)	2334	2635
4500	65	275	548	1039(?)	1926	2530	2936

ALIGNING TORQUE vs SLIP ANGLE AND VERTICAL LOAD

Vertical Load (lbs.)	Inflation Pressure (psi)	Aligning Torque at Indicated Slip Angle (degs.)					
		1	2	4	8	12	16
900	65	13	22	25	10	3	1
1800	65	35	61	69	52	30	17
2750	65	57	102	141	126	87	53
3600	65	77	144	200	214	163	104
4500	65	100	186	275	322	272	191

CIRCUMFERENTIAL STIFFNESS vs SLIP ANGLE AND NORMAL LOAD

Vertical Load (lbs.)	Inflation Pressure (psi)	C_s (lbs.)	Vertical Spring Rate (lbs./in.)
2750	65	31,000	2690

Tire: Highway Tread 8-22.5/D: Dual Rim: 22.5x5.25

LATERAL FORCE vs SLIP ANGLE AND VERTICAL LOAD

Vertical Load (lbs.)	Inflation Pressure (psi)	Lateral Force at Indicated Slip Angle (degs.)					
		1	2	4	8	12	16
1800	65	294	543	911	1249	1394	1452
3600	65	508	956	1654	2431	2827	3000
5500	65	594	1137	2020	3182	3905	4290
7200	65	570	1127	2096	3485	4521	5151
9800	65	540	1072	2052	3617	4980	6071

ALIGNING TORQUE vs SLIP ANGLE AND VERTICAL LOAD

Vertical Load (lbs.)	Inflation Pressure (psi)	Aligning Torque at Indicated Slip Angle (degs.)					
		1	2	4	8	12	16
1800	65	27	42	49	21	6	-0(?)
3600	65	69	118	152	103	59	31
5500	65	110	197	283	252	172	92
7200	65	141	262	406	423	312	178
9800	65	189	353	580	704	604	429

CIRCUMFERENTIAL STIFFNESS vs SLIP ANGLE AND NORMAL LOAD

Vertical Load (lbs.)	Inflation Pressure (psi)	C_s (lbs.)	Vertical Spring Rate (lbs./in.)
5500	65	54,000	1556

APPENDIX H

A Short Algorithm to Assist in the Choice of the Tire Parameters

APPENDIX H

A Short Algorithm To Assist In The Choice Of Tire Parameters

The purpose of this program is to give the user facility to find out what shear forces the tire model will predict, given any combination of kinematic variables and tire parameters. Thus it is envisioned that this algorithm may be used for "curve fitting" carpet plots, as in Section 3.2.2, or for examining the predicted interaction of longitudinal slip and sideslip to produce shear forces at the tire road interface.

The following examples are given below:

1. Using the rated load of 5430 lbs. for the tire considered in detail in Section 3.2.2, as well as the measured values C_α and C_s, and with FA set to zero (to match tire test machine data) and M_o set to .85, lateral force vs. sideslip angle are computed. Note the correspondence to Figure 3-3c.
2. With the suggested curve fit parameters KF = 1.7, $\bar{\alpha}$ = 9, lateral force vs. sideslip angle is again computed. Note the correspondece to Figure 3-3d.
3. Tire parameters from (2) are again used with one exception; FA is set to .005. Longitudinal slip is set to 0.1. Note the correspondence with Figure 3-5a.
4. A μ-slip curve is calculated with the tire parameters from (3) and with the sideslip angle set to 16°. Note the correspondence with Figure 3-5b.

```
ENTER PARAMETERS IN F-FORMAT
UW=  44.

CS =  42000.

CALPHA =  523.

MUZERO =  .85

FA =  0.

FZ =  5430.

KF  =  0.

ALPHABAR =  0.

 1 UW=        44.00000

 2 CS=     42000.00000

 3 CA=       523.00000

 4 MUO=        0.85000

 5 FA=         0.0

 6 FZ=      5430.00000

 7 KF =        0.0

 8 ALPHABAR =        0.0

***************
```

```
USER OPTIONS-ENTER A 1 FOR FYW VS. ALPHA
             ENTER A 2 FOR FXW VS. SLIP
             ENTER A 3 FOR BOTH OPTIONS
             ENTER A ZERO TO RESTART INPUT

1


FOR FYW CURVE,ENTER SLIP VALUE:  0.

        ALPHA          FYW


         0.0            0.0
         1.00        -523.05
         2.00       -1046.42
         4.00       -2095.40
         8.00       -3350.90
        12.00       -3779.36
        16.00       -3995.69
        20.00       -4127.19

****************

CHANGE VARIABLES: ENTER A 1 TO CHANGE ALL
                  ENTER A 2 TO CHANGE ONLY A FEW INPUT VARIABLES
                  ENTER A 3 TO RETAIN VARIABLE VALUES FOR A FYW
                              VS. ALPHA GRAPH
                  ENTER A 4 TO RETAIN VARIABLE VALUES FOR A FXW
                              VS. SLIP GRAPH
                  ENTER A ZERO TO TERMINATE PROGRAM

2

ENTER NO. OF PARAMETERS TO BE CHANGED
2

ENTER THE IVARIABLE NUMBERS IN I2 FORMAT
SEPARATE BY COMMAS
07,08

ENTER CORRECTIONS:
KF = 1.7
ALPHABAR = 9.

****************

USER OPTIONS-ENTER A 1 FOR FYW VS. ALPHA
             ENTER A 2 FOR FXW VS. SLIP
             ENTER A 3 FOR BOTH OPTIONS
             ENTER A ZERO TO RESTART INPUT

1


FOR FYW CURVE,ENTER SLIP VALUE:  0.
```

```
          ALPHA          FYW


           0.0             0.0
           1.00         -507.53
           2.00         -984.33
           4.00        -1846.73
           8.00        -2957.35
          12.00        -3472.45
          16.00        -3768.19
          20.00        -3947.96

****************

TO CHANGE VARIABLES: ENTER A 1 TO CHANGE ALL
                     ENTER A 2 TO CHANGE ONLY A FEW INPUT VARIABLES
                     ENTER A 3 TO RETAIN VARIABLE VALUES FOR A FYW
                                  VS. ALPHA GRAPH
                     ENTER A 4 TO RETAIN VARIABLE VALUES FOR A FXW
                                  VS. SLIP GRAPH
                     ENTER A ZERO TO TERMINATE PROGRAM

 2

ENTER NO. OF PARAMETERS TO BE CHANGED
 1

ENTER THE IVARIABLE NUMBERS IN I2 FORMAT
 SEPARATE BY COMMAS
 05

ENTER CORRECTIONS:
 FA=  0.005

****************

 USER OPTIONS-ENTER A 1 FOR FYW VS. ALPHA
              ENTER A 2 FOR FXW VS. SLIP
              ENTER A 3 FOR BOTH OPTIONS
              ENTER A ZERO TO RESTART INPUT

 3.


 FOR FYW CURVE,ENTER SLIP VALUE:   .1

          ALPHA          FYW


           0.0             -0.0
           1.00         -411.43
           2.00         -786.77
           4.00        -1409.68
           8.00        -2187.65
          12.00        -2740.65
          16.00        -3122.11
          20.00        -3349.47

 ****************
```

```
FOR FXW CURVE,ENTER ALPHA VALUE: 16.

        SLIP          FXW


         0.05        -1157.00
         0.10        -2086.24
         0.15        -2724.16
         0.20        -3134.20
         0.25        -3393.61
         0.30        -3557.44
         0.35        -3659.98
         0.40        -3722.13
         0.45        -3756.83
         0.50        -3772.27
         0.55        -3773.83
         0.60        -3765.13
         0.65        -3748.68
         0.70        -3726.26
         0.75        -3699.17
         0.80        -3668.34
         0.85        -3634.52
         0.90        -3598.24
         0.95        -3559.95
         1.00        -3519.98

****************

TO CHANGE VARIABLES: ENTER A 1 TO CHANGE ALL
                     ENTER A 2 TO CHANGE ONLY A FEW INPUT VARIABLES
                     ENTER A 3 TO RETAIN VARIABLE VALUES FOR A FYW
                                  VS. ALPHA GRAPH
                     ENTER A 4 TO RETAIN VARIABLE VALUES FOR A FXW
                                  VS. SLIP GRAPH
                     ENTER A ZERO TO TERMINATE PROGRAM
```

REFERENCES

1. R. W. Murphy, J. E. Bernard, and C. B. Winkler, A Computer Based Mathematical Method for Predicting the Braking Performance of Trucks and Tractor-Trailers. Phase I Report, Highway Safety Research Institute, The University of Michigan, September 15, 1972.

2. P. S. Fancher, C. B. Winkler, and J. E. Bernard, Simulation of the Braking and Handling of Trucks and Tractor-Trailers. (To be published by HSRI.)

3. H. Dugoff, P. S. Fancher, and L. Segel, Tire Performance Characteristics Affecting Vehicle Response to Steering and Braking Control Inputs. Final Report for Period May 1968-August 1969 for Contract CST-460, Office of Vehicle Systems Research, National Bureau of Standards, August 1969.

4. H. Dugoff and B. J. Brown, "Measurement of Tire Shear Forces." SAE Paper #700092, January 1970.

5. J. E. Bernard, "A Digital Computer Method for the Prediction of Braking Performance of Trucks and Tractor-Trailers." SAE Paper #730181, January 1973.

6. P. M. Leucht, "The Directional Dynamics of the Commercial Tractor-Semitrailer Vehicle During Braking." SAE Transactions, Vol. 79 (1970), Paper #700371.

7. E. C. Mikulcik, The Dynamics of Tractor-Semitrailer Vehicles: The Jackknifing Problem. Ph.D. Thesis, Cornell University, June 1968.

8. R. L. Eshleman and S. D. Desai, Articulated Vehicle Handling. Final Report, Illinois Institute of Technology, Research Institute, April 1972.

9. A. I. Krauter and R. K. Wilson, "Simulation of Tractor-Semitrailer Handling." SAE Paper #720922, October 1972.

10. V. T. Nicholas and T. R. Comstock, "Predicting Directional Behavior of Tractor-Semitrailers when Anti-Skid Brake Systems are Used." Presented at ASME Winter Annual Meeting, New York, New York, November 1972.

11. R. R. McHenry and N. J. Deleys, Vehicle Dynamics in Single Vehicle Accidents. CAL No. VJ-2251-V-3, December 1968.

12. H. Dugoff, "On the Influence of Aerodynamic Forces and Moments on the Lateral Stability of Articulated Highway Vehicles." Stevens Institute of Technology, Davidson Laboratory, Hoboken, New Jersey.

13. C. B. Winkler, "The Measurement of Inertial Properties and Suspension Parameters of Heavy Highway Vehicles." SAE Paper #730182 presented at SAE International Automotive Engineering Congress, Detroit, January 1973.

14. P. S. Fancher, et al., Limit Handling Performance as Influenced by Degradation of Steering and Suspension Systems. Final Report, Highway Safety Research Institute, The University of Michigan, November 1972.

15. R. D. Ervin, et al., Vehicle Handling Performance. Final Report, Highway Safety Research Institute, The University of Michigan, November 1972.

16. J. T. Tielking, P. S. Fancher, and R. E. Wild, "Mechanical Properties of Truck Tires." Paper #730183 presented at SAE International Automotive Engineering Congress, Detroit, January 1973.

Preceding page blank

REFERENCES (Concluded)

17. F. Jindra, "Tractor and Semi-Trailer Handling." Automobile Engineer, October 1963.

18. H. Goldstein, Classical Mechanics, Addison-Wesley Publishing Company, Inc., Reading, Mass., June 1969.

Reproduced by NTIS

U.S. DEPARTMENT OF COMMERCE
Technology Administration
National Technical Information Service
Springfield, VA 22161 (703) 605-6000

PB221630

BA

BIN: M140 05-06-98
INVOICE: 587705
SHIPTO: 1*258427
PAYMENT: CSH*AORNG